

The Miaoli Tableland in Taiwan: Morphological, sedimentological and geochronological studies of the Quaternary landscape developments



Dissertation

zur Erlangung des akademischen Grades Doktor der Naturwissenschaften (Dr. rer. nat.)

am Fachbereich Geowissenschaften der Freien Universität Berlin

vorgelegt von

Shih-Hung Liu / 劉時宏

Berlin, 2023

First supervisor: Prof. Dr. Margot Böse (Freie Universität Berlin)

Second supervisor: Prof. Dr. Manfred Frechen (Freie Universität Berlin, Leibniz-Institut für Angewandte Geophysik)

First reviewer: Prof. Dr. Margot Böse (Freie Universität Berlin)

Second reviewer: Univ.-Prof. Dr. Anne Bernhardt (Freie Universität Berlin)

Date of defense: 06.12.2023

Acknowledgements

First of all, I would like to thank my supervisor Prof. Dr. Margot Böse for the enormous patience, support and consistently friendly guidance throughout my PhD stage at FU-Berlin. The education encompassed not only the logic and disciplines for conducting good scientific research, but also for a very comprehensive approach to the lifestyle itself, including the most important core values: authenticity and passion.

I would like to thank my second supervisor Prof. Dr. Manfred Frechen for the generous support for all the laboratory assessments and technical trainings within the facilities in LIAG, a great beginning that really helped me to swift acclimate to the new environment and I am profoundly thankful for the atmosphere and logical frameworks I experienced in Hanover.

So many thanks to Dr. Robert Hebenstreit for the amicable help in organizing ideas, data presentation and argument formations, etc. These discussions can always guide me toward uncovering these long-lasting arguments, which are often grounded in very simple and straightforward solutions. Especially most of these arguments are notably fundamental and sometimes with captivating historical context, but unfortunately had been ignored for an extended period of time. A case in this point is the chapter 3 of this work, a section that was inspired by your insightful input.

Many thanks to Dr. Jacob Hardt, your comments and help are always warm and helpful, and introducing me to alternative methods to deal with the challenges throughout my study. Many thanks to Prof. Dr. Christopher Lüthgens for the immense help in the very beginning stage of the field campaign and managing the publication focusing on the OSL results of the Miaoli samples. Handling the Taiwanese samples is very challenging to me, and I truly appreciate that the works would not have been successfully done without your invaluable assistance and expertise. Many thanks to Dr. Dirk Wenske for the assistance provided throughout all the stages of my PhD. Establishing a life in a foreign country is not easy, and finding a suitable and easy solution is always very challenging. I have learned how to recognize the concept of "enough is enough", which is a life-long debate especially when tasks and deadlines rapidly accumulate. Many thanks to Dr. Fabian Becker for the extensive assistance especially during the COVID-19 pandemic. Dr. Becker's insightful suggestion to explore the countryside has provided me with a deeper understanding of the country and local communities.

Many thanks to Dr. Sumiko Tsukamoto, Prof. Dr. Yan Li and all the members in S3-LIAG, the dating analyses are significant endeavors that need perfect cooperation among all the participants. The serious atmosphere maintained in the laboratory, coupled with direct discussions, greatly aided me in solving challenges that I couldn't have overcome without your assistance. Thanks to Prof. Dr. Jiun-Chuan Lin, Prof. Dr. Chia-Han Tseng, Prof. Dr. Chia-Hung Jen and other colleagues from NTU and NKNU for your friendly support for the field campaign of this work.

Many thanks to all the people I met in Beijing, Berlin, Dublin, Gießen, Miaoli, Taipei, Hanover, Schney and Vienna, during all my stays and international meeting participations. I appreciate each of you for the invaluable inspirations that guide me in shaping the ideas.

So many thanks to my family for the unwavering support and understanding throughout these years, and finally, we can announce the long-awaited good news.

In the final section of the acknowledgements, I wish to present my appreciations to all those who engage with this work, I quote the first passage from the most famous classical work of Chinese Literature, *Dream of the Red Chamber* (*Honglou Meng* / 紅樓夢) from Cao, Xueqin / 曹雪芹:

滿紙荒唐言，一把辛酸淚，皆云作者癡，誰解其中味。

A stack of unwiseness passages.

All comprise of facts, thoughts and woes.

A fool faithfully devotes.

Anticipating someone understands.

Shih-Hung Liu / 劉時宏

Berlin, August 2023

Table of Contents

Acknowledgements	1
Glossary of all the abbreviations in this text (in alphabetic order)	6
Abstract	8
Zusammenfassung.....	9
Chapter 1. Introduction	11
1.1 Aims, objectives and research questions of the thesis.....	11
1.2 Structure of the thesis.....	20
Chapter 2. Research area	21
2.1 Location.....	21
2.2 Topography	21
2.3 Geology and tectonics	26
2.4 Climate	33
2.5 The fluvial systems and previous ideas/models of landform evolution developments	36
2.6 Human activities and local history	40
Chapter 3. A historical review of the stratigraphic nomenclature problems of the Quaternary depositions in the Miaoli Tableland	42
3.1 Introduction.....	42
3.2 Historical evolution of the stratigraphic nomenclatures of the Miaoli Tableland's strata.....	43
3.2.1 The Japanese ruling time (1895-1945)	43
3.2.2. Transition from the Japanese system to the Chinese system (1945 to 1949).....	45
3.2.3. The Republic of China since 1949.....	47
3.3 The general remarks of the contemporary stratigraphic nomenclature issues	50
Chapter 4. Methods.....	52
4.1 Methodical approaches of the thesis	52
4.2 Morphological analyses.....	52
4.2.1. Maps and remote sensing data processing	52
4.2.2. Tableland surface mapping	53
4.2.3. Classification of tableland surfaces by calculation of the theoretical linear surface.....	55
4.3 Field works	56
4.4 Sedimentological and stratigraphical analyses.....	58
4.4.1. Particle size analyses	58
4.4.2. Data processing of the borehole data set	59
4.4.3. Cross-section drawing	61

4.5	Geochronological analyses	62
4.5.1.	Principles and settings of optically stimulated luminescence (OSL) dating.....	62
4.5.2.	The measurement of environmental dose-rate	66
4.5.3.	The measurement of equivalent dose by means of the Single-Aliquot-Regenerative dose (SAR) protocol ..	66
4.5.4.	Age model calculations.....	67
4.5.5.	Calculation of the corresponding uplift rates	69
Chapter 5. Paper I — Late Quaternary landform evolution and sedimentary successions in the Miaoli Tableland, northwestern Taiwan.....		71
Chapter 6. An investigation of the Quaternary stratigraphy with borehole data in the Miaoli Tableland		94
6.1	Introduction, material and methods	94
6.1.1	Introduction.....	94
6.1.2	The borehole data set and data coverage	94
6.1.3	Conversion of coordinates and elevations	97
6.1.4	Cross-section mapping based on the borehole logs.....	97
6.2.	Results	100
6.2.1	The cross-section TP (E-W direction).....	100
6.2.2	The cross-section HSR (N-S direction, proximal area)	103
6.2.3	The cross-section M3 (N-S direction, proximal area)	107
6.2.4	The cross-section T61 (N-S direction, distal and coastal areas).....	109
6.2.5	Remarks of the cross sections	111
6.3.	Discussion.....	112
6.3.1	The sedimentary successions	112
6.3.2	Tectonism and its influences on the palaeo-topography	113
6.3.3	The forming of the box shaped valleys and redepositions of the gravels and cobbles in the valley floors, flood plains, coastal areas, and estuaries.....	115
Chapter 7. Paper II — Late Quaternary formation of Miaoli Tableland in northwest Taiwan: an interplay of tectonic uplift and fluvial processes dated by OSL.....		117
Chapter 8. Summarizing discussion		140
8.1	Consistency of new DEM-based surface mapping and the sedimentary succession in the Miaoli Tableland.....	141
8.2	A new chronology of the Miaoli Tableland development and the uplift rates.....	142
8.3	The aeolian deposition as index of ages of topographic surfaces.....	145
8.4	Impacts of base-level change to the tableland morphology	146
8.5	The climate impacts on tableland morphology.....	149
8.6	A proposal of revision of the stratigraphic model based on the international stratigraphic guidelines	151
Chapter 9. Overall conclusions and outlook.....		154
References.....		157

Appendix 1: Academic publications and conference contributions	169
Appendix 2: Curriculum Vitae.....	170
Appendix 3: Eidesstattliche Erklärung	171
Appendix 4: AI-assisted language check disclaimer	172

Glossary of all the abbreviations in this text (in alphabetic order)

2D	two dimension	GIS	geographical information system
^{222}Rn	radon	GPS	Global Positioning System
^{226}Ra	radium	Gy	Gray
^{235}U	uranium	H_2O_2	hydrogen peroxide
^{232}Th	thorium	HCl	hydrochloric acid
3D	three dimension	HF	hydrofluoric acid
^{40}K	potassium	Hs	Hsiangshan Facies
a	annual	IR	infrared
AL	Alluvial and Coastal Plains	IRSL	infrared stimulated luminescence
asl	average sea level	ka	thousand years
ca.	circa	KDE	kernel density estimation
CAM	central age model	km^2	square kilometer
CGS	Central Geological Survey	L	Greyish loam layer
CSB	Coarse sand with stones and boulders (gravels and cobbles) layer	LED	light emission diode
CW-OSL	continuous wavelength - optically stimulated luminescence	LGM	Last Glacial Maximum
D_0	the onset of saturation	LH	Lateritic Highlands
$\delta^{18}\text{O}$	delta O-18, ratio of $^{18}\text{O} / ^{16}\text{O}$	Lk	Lungkang Formation
D_e	equivalent dose	LS	Loamy sand layer
DEM	digital elevation model	LT	Lateritic Terraces
D_r	dose recovery ratio	m^2	square meter
ESR	Electron spin resonance	Ma	million years
FAO	Food and Agriculture Organization of the United Nations	MAM	minimum age model
FT	Fluvial Terraces	mg	milligram
		mGy	milli-Gray
		μm	micrometer

MIS	marine oxygen isotope stages	SL	Sandy loam layer
mm	millimeter	ST	Sedimentary Terraces
NH ₄ OH	ammonia solution	SRTM	Satellite Radar Topography Mission
NTU	National Taiwan University	TWD 67 / 97	Taiwan Datum 1967 / 1997
OD	over-dispersion	TIN	triangulated irregular network
OSL	optically stimulated luminescence	TIU	Taihoku Imperial University
P.R.C.	People's Republic of China	Tks / Tk	Toukoshan Formation
R ²	coefficient of determination	TL/OSL	thermal luminescence / optically stimulated luminescence
R.O.C.	Republic of China (Taiwan)	Ty / Ts	Tûsyo / Tung-Xiao Formation
rpm	round per minute	Tz	Takazan Gravel Bed
sigma _b	common standard deviation	USGS	United States Geological Survey
SAR	single aliquot regenerative protocol	WF	Western Foothills
SH	Sedimentary Highlands (including SH-I and SH-II)	WGS 84	World Geodetic System 1984
SiC	Alternation of greyish silt loam and yellowish silt loam layers	WMTS	Web Map Tile Service
SiL	Silty loamy cover layer	yr	year

(*) outcrops names through the whole thesis are not listed, due to they are the abbreviations of the local names. Model number of the laboratory analyzers and their components are not listed.

Abstract

The Taiwan Island is located at the convergence of the Eurasian and Philippine Sea plates. Dynamic orogeny caused the rapid uplift of the Neogene mountain ranges. The sediments yielded from these Neogene mountain ranges were deposited in the foreland basins, and subsequently uplifted, eroded, and redeposited, progressively toward the west. The sedimentation-uplift-erosion-redeposition cycles resulted in the formation of sedimentary terraces there, which are locally called “tablelands”. Due to methodological restrictions in early studies, the chronological control and corresponding Quaternary environmental change factors are still open for debate. This study focuses on the Miaoli Tableland, where is highly accessible for observing numerous outcrops of the tableland segments. A synthesis of the Miaoli Tableland morphology is proposed based on the analyses of high precision 3D geomorphological mapping, particle size analysis, borehole data interpolation, and OSL dating for depositional ages. The mapping results reveal that the palaeo-topography of alluvial fan(s) covered throughout the Miaoli Tableland area. A new numeral classification of the tableland segments is carried out, with subdivisions based on geometrical properties as Sedimentary Highlands (SH-I/II), and Sedimentary Terraces (ST). Spatial distributions of parallel / dendritic fluvial network developments and corresponding fluvial valley shapes (V-shaped / box-shaped) are identified, roughly bounded at ca. 150m asl. Three sub-types of sedimentary successions are summarized based on the existence and varying thickness of the gravel and cobble bed(s). Spatial distributions of these sub-types correspond to the morphological states of tableland segments. The geometry and morphological state of tableland segment surfaces, the corresponding sub-types of sedimentary successions, and their locations are combined into a 3D model. This 3D model shows that tectonic uplift and successive fluvial dissection caused redepositions of gravels and cobbles from the SH-I through the SH-II and ST to the coastal areas. The cross sections interpolated from the borehole data reveals a spatial pattern of the movement of the gravels and cobbles that corroborates this 3D model. The depositional age estimations provided by OSL dating of the coastal, fluvial and aeolian sediments show that the depositions of gravels and cobbles in the SH-I started during the marine isotope stage (MIS) 5a (approximately 90ka). Those gravels and cobbles were successively redeposited towards the west and north (proximal areas of the SH-II/ST) approximately from the MIS5a to the MIS3. The successive redepositions of gravels and cobbles reached the distal areas by the coast approximately during the MIS2. These depositional phases are correlated with low base level and relative dry climate periods, which are affected by loosened vegetation that provide less protection to the tableland segments during intensive erosion events (e.g. typhoons). The deposition ages among the tablelands surface depositions in western Taiwan shows a pattern that the formation of tablelands in the central to north, including the Miaoli Tableland, are younger than the tablelands in the central to south. A revision of the lithostratigraphy nomenclatures is proposed based on the international stratigraphic guidelines, which reintroduces the original Japanese time stratigraphical terms.

Zusammenfassung

Die Insel Taiwan liegt an der Konvergenz zwischen der eurasischen und der philippinischen Platte. Die dynamische Orogenese führte zu einer raschen Hebung der neogenen Gebirgszüge. Die von diesen neogenen Gebirgszügen stammenden Sedimente wurden in den Vorlandbecken abgelagert und anschließend nach und nach in Richtung Westen angehoben, erodiert und wieder abgelagert. Die Zyklen von Sedimentation, Hebung, Erosion und Wiederablagerung führten dort zur Bildung von Sedimentterrassen, die lokal als "Tablelands" bezeichnet werden. Aufgrund methodischer Einschränkungen in frühen Studien sind die chronologische Kontrolle und die entsprechenden Faktoren für Umweltveränderungen im Quartär noch immer umstritten. Diese Studie konzentriert sich auf das Miaoli Tableland, wo zahlreiche Aufschlüsse der Tableland-Segmente gut zugänglich sind. Auf der Grundlage von Analysen hochpräziser geomorphologischer 3D-Kartierungen, der Analyse der Partikelgröße, der Interpolation von Bohrlochdaten und der OSL-Datierung für das Ablagerungsalter wird eine Synthese der Morphologie des Miaoli-Tablelands vorgeschlagen. Die Kartierungsergebnisse zeigen, dass die Paläo-Topographie der Schwemmfächer das gesamte Gebiet der Miaoli-Tablelands abdeckt. Es wird eine neue numerische Klassifizierung der Tableland-Segmente vorgenommen, mit Unterteilungen auf der Grundlage geometrischer Eigenschaften als Sedimentary Highlands (SH-I/II) und Sedimentary Terraces (ST). Es werden räumliche Verteilungen von parallelen / dendritischen fluvialen Netzwerkentwicklungen und entsprechenden fluvialen Talformen (V-förmig / kastenförmig) identifiziert, die grob auf ca. 150 m ü. NN. Drei Untertypen von Sedimentabfolgen werden auf der Grundlage des Vorhandenseins und der unterschiedlichen Mächtigkeit der Kies- und Geröllschicht(en) zusammengefasst. Die räumliche Verteilung dieser Untertypen entspricht den morphologischen Zuständen der Tableland-Segmente. Die Geometrie und der morphologische Zustand der Oberflächen von Tableland-Segmenten, die entsprechenden Untertypen von Sedimentabfolgen und ihre Standorte werden in einem 3D-Modell kombiniert. Dieses 3D-Modell zeigt, dass die tektonische Hebung und die sukzessive fluviale Zergliederung zu einer Umlagerung von Kiesen und Geröll von SH-I über SH-II und ST bis zu den Küstengebieten geführt haben. Die aus den Bohrlochdaten interpolierten Querschnitte zeigen ein räumliches Muster der Bewegung der Kiese und Gerölle, das dieses 3D-Modell bestätigt. Die durch OSL-Datierungen der küstennahen, fluvialen und äolischen Sedimente gewonnenen Schätzungen des Ablagerungsalters zeigen, dass die Ablagerung der Kiese und Gerölle im SH-I während des marinen Isotopenstadiums (MIS) 5a (ca. 90ka) begann. Diese Kiese und Gerölle wurden etwa ab dem MIS5a bis zum MIS3 sukzessive in Richtung Westen und Norden (proximale Bereiche des SH-II/ST) umgelagert. Die sukzessiven Umlagerungen von Kiesen und Geröll erreichten die distalen Bereiche an der Küste etwa während des MIS2. Diese Ablagerungsphasen korrelieren mit einem niedrigen Meeresspiegel und relativ trockenen Klimaperioden, die durch eine aufgelockerte Vegetation gekennzeichnet sind, die den Tableland-Segmenten bei intensiven Erosionsereignissen (z. B. Taifunen) weniger

Schutz bietet. Das Ablagerungsalter der Tablelands im Westen Taiwans zeigt, dass die Tablelands in der Mitte und im Norden, einschließlich des Miaoli Tableland, jünger sind als die Tablelands in der Mitte und im Süden. Es wird eine Überarbeitung der lithostratigraphischen Nomenklatur auf der Grundlage der internationalen stratigraphischen Richtlinien vorgeschlagen, die die ursprünglichen japanischen stratigraphischen Begriffe wieder einführt.

Chapter 1. Introduction

1.1 Aims, objectives and research questions of the thesis

Taiwan Island is located at the convergence boundary of the Eurasian Plate and the Philippine Sea Plate (Suppe, 1980b, 1981), which is located at the western Pacific (Fig. 1.1 and 1.2). The plate convergence has been assumed to continue for ca. 3 Ma (Suppe, 1980b, 1981), which has caused the forming of mountain ranges in the central part of the island. Four mountain ranges are aligned in parallel with a northeast-southwest direction as the backbone ranges of the island (Ho, 1975, 1988). The orogeny began in the north and moves toward the south, the uplift in the central section of the ranges is more rapidly than other parts, conversely the north of the island is subsiding (Suppe, 1984; Teng, 1990) (Fig. 1.2).

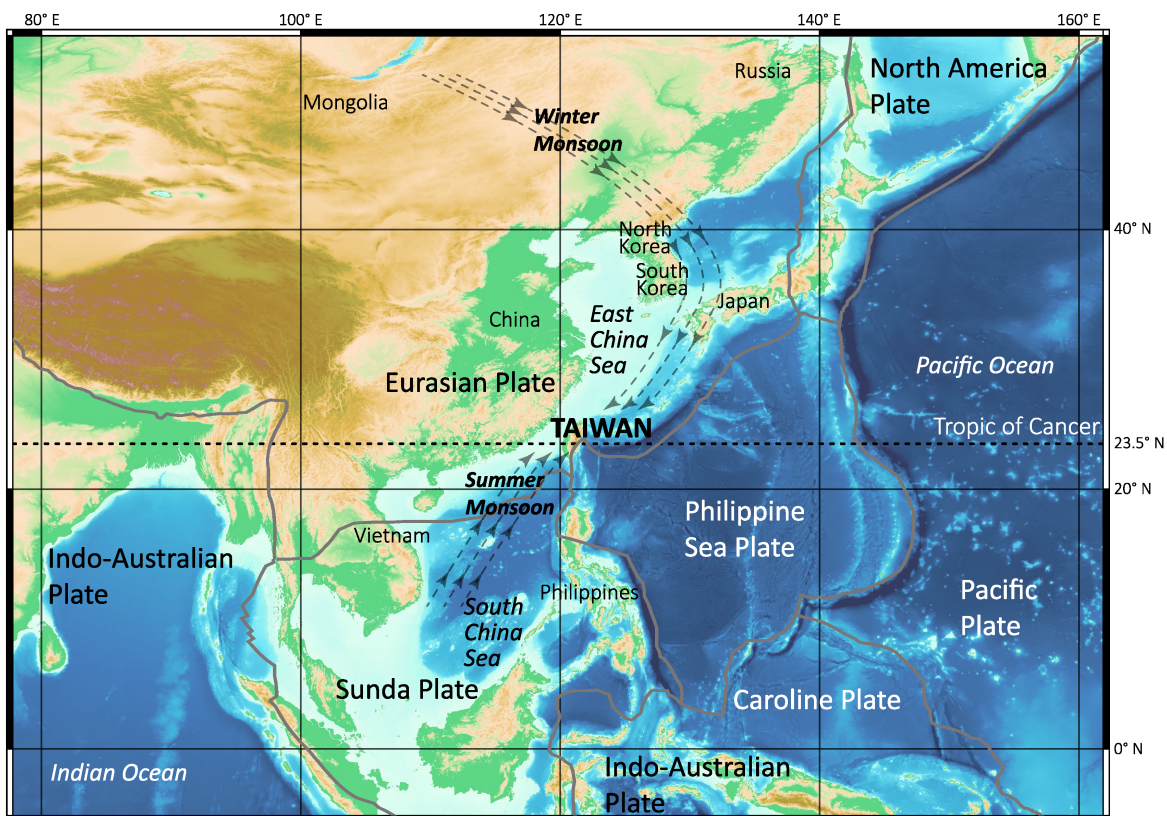


Figure 1.1: Location of Taiwan in the western Pacific region. The elevation was extracted from GEBCO (The General Bathymetric Chart of the Oceans, 2022); the plate boundaries were simplified after Bird (2003). The Taiwan island is located at the convergence belt of the Eurasian plate and the Philippine Sea Plate. The boundary of these two plates is a segment of the western Pacific orogeny belt. The Eurasian Plate side including the eastern China Sea is a huge continental shelf, with its marginal part forming the foreland basin of the orogeny belt. The sub-tropical climate setting of the Taiwan Island is characterized by significant seasonal variations of temperature and precipitations. These variations are strongly influenced by the Eastern Asian Monsoon Belt (marked with dash lines). The monsoons consist of two phases with distinct atmospheric characteristics influenced by the environmental settings of their origins: i). The relative cold and dry winter monsoon from the mid-high latitude interior of the Eurasian Continent (Russia and Mongolia). ii). The relative humid and

warm summer monsoon from the tropical ocean (South China Sea).

The Xueshan Range is the northern part of the backbone range, which includes the mountains located at the north of the Langyang Rift Valley (Ho, 1975, 1988). The rift valley is caused by the subsidence of the Eurasian Plate, which is located to the north of the island (Figs. 1.1, 1.2 and 1.3) (Teng, 1996a). The Xueshan Range is mainly composed of the low-grade metamorphic rocks (Palaeogene-Miocene), these bed rocks originate from the sedimentary rocks of the continental shelf of the Eurasian Plate at the Eastern China Sea area (Fig. 1.2) (Ho, 1975, 1988; Teng, 1990). Because the subduction of the Eurasian Plate beneath the Philippine Sea Plate at the north of the Taiwan Island, the northern part of the Xueshan Range has been subsiding since 1 Ma (Fig. 1.2) (Teng, 1996a). The tectonism in the Xueshan Rang is relatively complicated, characterized by a southward movement of the subsiding/uplifting boundary (Fig. 1.2) (Teng, 1996a), that while the north section undergoes subsidence, the uplifts are undergoing in the central and southern sections. The highest elevation of the Xueshan Range is about 3,886 m asl with average uplift rates ranging from 4 to 7 mm/yr (Fig. 1.3 and Table. 1.1).

Table 1.1 The uplift rate observes and estimations in Taiwan

source	uplift rate (mm/yr)	study site	time span
Peng et al. (1977)	5 ± 0.7	Henchung Peninsula, Tainan	<9 ka
Liu (1982)	4.2 - 6.8	Backbone Range	3-0.5 Ma
Jahn et al. (1986)	3 - 4	Backbone Range	<3 Ma
Lundberg and Dorsey (1990)	5.9 - 7.5	Coastal Range	<1 Ma
Wang and Burnett (1990)	1.2 - 6.1	Henchung Peninsula	Holocene
Chen et al. (1991)	5 - 14	uplifted corals in Coastal Range	Holocene
Liew et al. (1993)	2.5 - 8	elevated shoreline deposits in Coastal Range	Holocene
Hsieh and Knuepfer (2002)	<10	river terraces in Tainan	Holocene
Song et al. (2004)	5.4; 10.9	Holocene marine terraces in Coastal Range	Holocene
Yamaguchi and Ota (2004)	5 - 15	Holocene marine terraces in Coastal Range	<13 ka
Lee et al. (2006)	<1 (a); 4-10 (b)	Backbone Range	6-1 Ma (a); <1 Ma (b)
Ching et al. (2011)	0.2-18.5	whole Taiwan Island (GPS real-time monitoring)	2000-2008

Simplified from Nagel et al., (2018)

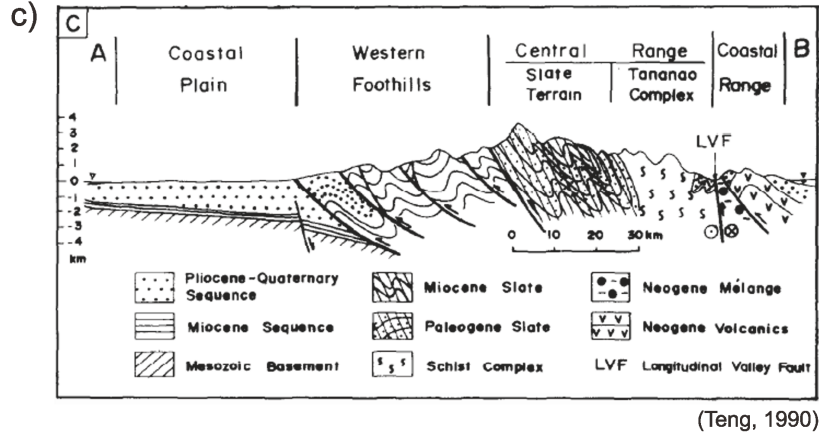
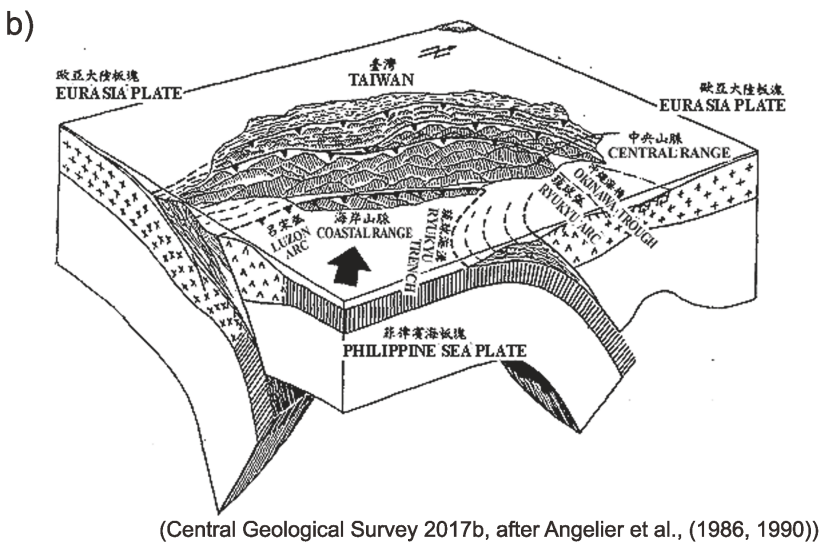
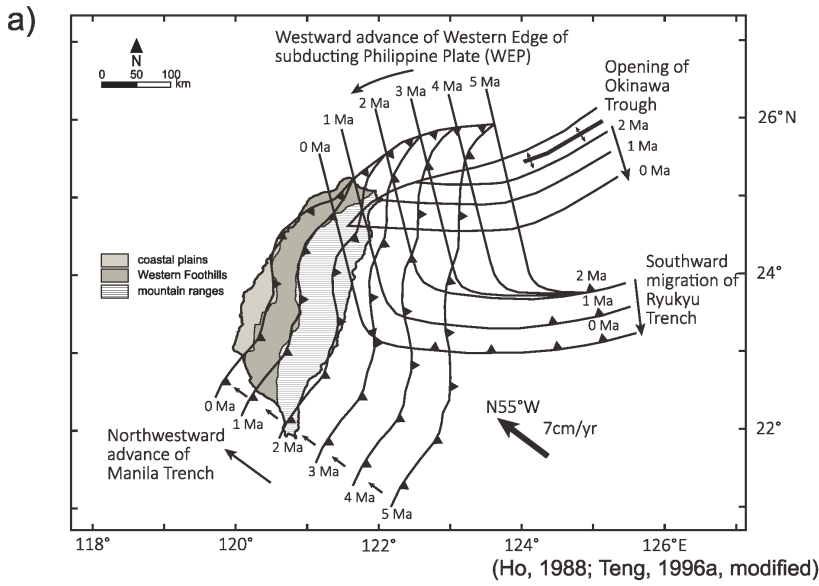


Figure 1.2: The tectonic and geological structure of the Taiwan Island.
 a). the spatial and temporal change of the boundary between convergence and divergence of the Taiwan Island, after Teng (1996a); the geological divisions were simplified after Ho (1988).
 b). 3D (three dimension) model of the plate convergence, subduction model and orogeny of the Taiwan Island (Central Geological Survey 2017b, after Angelier et al., (1986, 1990)).
 c). the E-W cross section of the major geological divisions (including the orogenic belts and the foreland) of the Taiwan Island, after Teng (1990).

The Central Range is the main part of the backbone range, located in the central and southern parts of the island. The Central Range includes the mountains in between the longitudinal valley of Langyang River and the Hualien-Taitung Rift Valley, representing the frontal part of the Eurasian Plate (Figs. 1.1, 1.2 and 1.3). The Central Range is mostly composed of metamorphic rocks (Paleogene-Miocene), with the highest metamorphic grades found in the northeastern (schist, gneiss), and the metamorphic grades gradually decrease toward west and south, so that most bedrocks in these sections are composed of slate and argillite (Ho, 1975, 1988; Teng, 1990) (Fig. 1.2). The genesis of these bed rocks are similar to that of the Xueshan Range originating from the sedimentary rocks of the continental shelf of the Eastern China Sea (Ho, 1975, 1988). The Central Range is uplifting rapidly in general (Table 1.1), except for the parts located at the northeastern boundary with the Xueshan Range (the longitudinal valley of the Langyang River), which are also affected by the subduction of the Eurasian Plate beneath the Philippine Sea Plate (e.g. Ilan area) (Fig. 1.2) (Teng, 1996a). The highest elevation of the Central Range is about 4,000 m asl (Jade Mt., 3952m above sea-level), this elevation is mainly due to rapid uplift with the long-term average rate about 5 mm/yr (Fig. 1.3 and Table 1.1). The low-grade metamorphism of bed rocks also caused their relatively weak resistance to the incision, therefore the exhumation rate is high in the Central Range (ca. 4 to 10 mm/yr) (Dadson et al., 2003).

The western frontal parts of these mountain ranges, which include the mountains with the middle-low elevations (<2500 m asl) (Fig. 1.3), are called “Western Foothills (WF)” in the local terminology (Angelier et al., 1986; Ho, 1975, 1988; Suppe, 1980a) (Fig. 1.2). The WF are assumed to be the boundary between the bedrocks of the Miocene-Pliocene sedimentary rocks and the Quaternary alluviums at the western side of the island (Teng, 1990) (Fig. 1.2). The bedrocks in the WF are mostly composed of sedimentary rocks (sandstones and mudstones) and low-grade metamorphic rocks (argillite and slate). These bedrocks are assumed to have originated from the mountain foreland sedimentary rocks made of the mountain ranges yielded sediments that were subsequently lithified and uplifted (Ho, 1975, 1988) (Fig. 1.2).

The coastal plain is located at the western side of the Western Foothills with low altitude (<200 m asl), which is assumed as the accumulations of non-lithified sediments that have been yielded from the mountain ranges and have been redeposited in the mountain foreland during the late Quaternary time span (Covey, 1986; Liew et al., 2004; Lin and Watts, 2002; Yu and Chou, 2001) (Fig. 1.2).

The Taiwanese sedimentary terraces are located at the mountain foreland of the western coast of the Taiwan Island (Fig. 1.2). The mountain foreland is located beside the backbone ranges in the central part of the island (Angelier et al., 1986; Fisher et al., 2002; Suppe, 1984). The mountain foreland was the depositional space of the sediment yields from the mountain ranges (the mid Neogene metamorphic rocks) (Covey, 1986; Fisher et al., 2002; Ho, 1988; Nagel et al., 2018; Yu and Chou, 2001) (Fig. 1.2). The subsequent tectonism had uplifted

the sediments firstly, and these uplifted sediments were remobilized by fluvial incisions and transportations farther downstream to reach the sea level (Hsieh and Knuepfer, 2001; Teng, 1996b). These huge accumulative sedimentary complexes were subsequently uplifted by the ongoing tectonism, and then the fluvial incision on them formed the sedimentary terrace landforms (Tomita, 1940) located in several places (Fig. 1.2). The incisions had caused the formation of the sedimentary terraces with flat surfaces. These fluvial sediments were cut into terraces by fluvial incisions. The sedimentary terrace landforms are formed by the alternation of deposition and erosion, can be seen as archives for information of environmental changes especially during the Quaternary (Charlton, 2008; Thornbury, 1954). Morphology of these sedimentary terraces is controlled by environmental changes and the corresponded surface processes (Thornbury, 1954). For example, the sea level change took significant effect to the morphology once if the sedimentary terrace landforms are located at the coastal area, because it controlled the spatial-temporal changing of the deposition environments (Reineck, 1986). Analyses of the terraces' sedimentary successions, spatial distribution and depositional ages allow to interpret the morphology and the chronological correlation with other case studies in the similar environmental change settings (Charlton, 2008).

These sedimentary terraces are called "Tableland" tentatively (Figs. 1.2, 1.3 and Table 1.2), featuring their elevations are higher than the surroundings with flat surfaces on the top (Lin, 1957; Lin and Chou, 1974). The tablelands' surfaces were classified formally into a three-stage morphological system as "Lateritic Highlands (LH)", "Lateritic Terraces (LT)" and "Fluvial Terraces (FT)" according to their relative elevations and the weathering degree of the surface materials (Lin, 1957; Tomita, 1953, 1954, 1972) (Fig. 1.2). The tablelands' sedimentary successions have been assumed as late Neogene to Quaternary sedimentary rock strata (i.e. Toukoshan Formation (Tks / Tk) (Chang, 1955a, b; Lin and Chou, 1974)), little has been known about the geochronology due to the methodological restrictions. The recent case studies of the tableland in the intra-montane foreland (e.g. Puli Tableland) showed the morphology of depositional and erosional processes in the last glaciation (marine oxygen isotope stage-2 - MIS 2) to the Holocene time span (Tseng et al., 2016; Tseng et al., 2013) (Table 1.2, Fig. 1.3). The studies in other sedimentary terraces analyzed the tectonic uplift and subsequent erosions on the sedimentary successions to propose the tableland morphological models (Hsieh and Chyi, 2010; Hsieh and Knuepfer, 2001; Ota and Yamaguchi, 2004; Shyu et al., 2006). In addition, the pedogenic properties were studied as an indicator of relative chronology (Tsai et al., 2010), and the dating analyses directly to the surface sediments of the Dadu Tableland and the Pakua Tableland (Horng, 2014; Siame et al., 2012; Tsai et al., 2010; Tseng et al., 2016) (Table 1.1, Fig. 1.3) were also carried out for investigating the geochronology of the tableland sedimentary successions. In summary, the outcomes of these studies led to an overall understanding to the morphological process of the forming of these tablelands and to the assumptions of the relative geochronology. However, the details of each site are not clear so far.

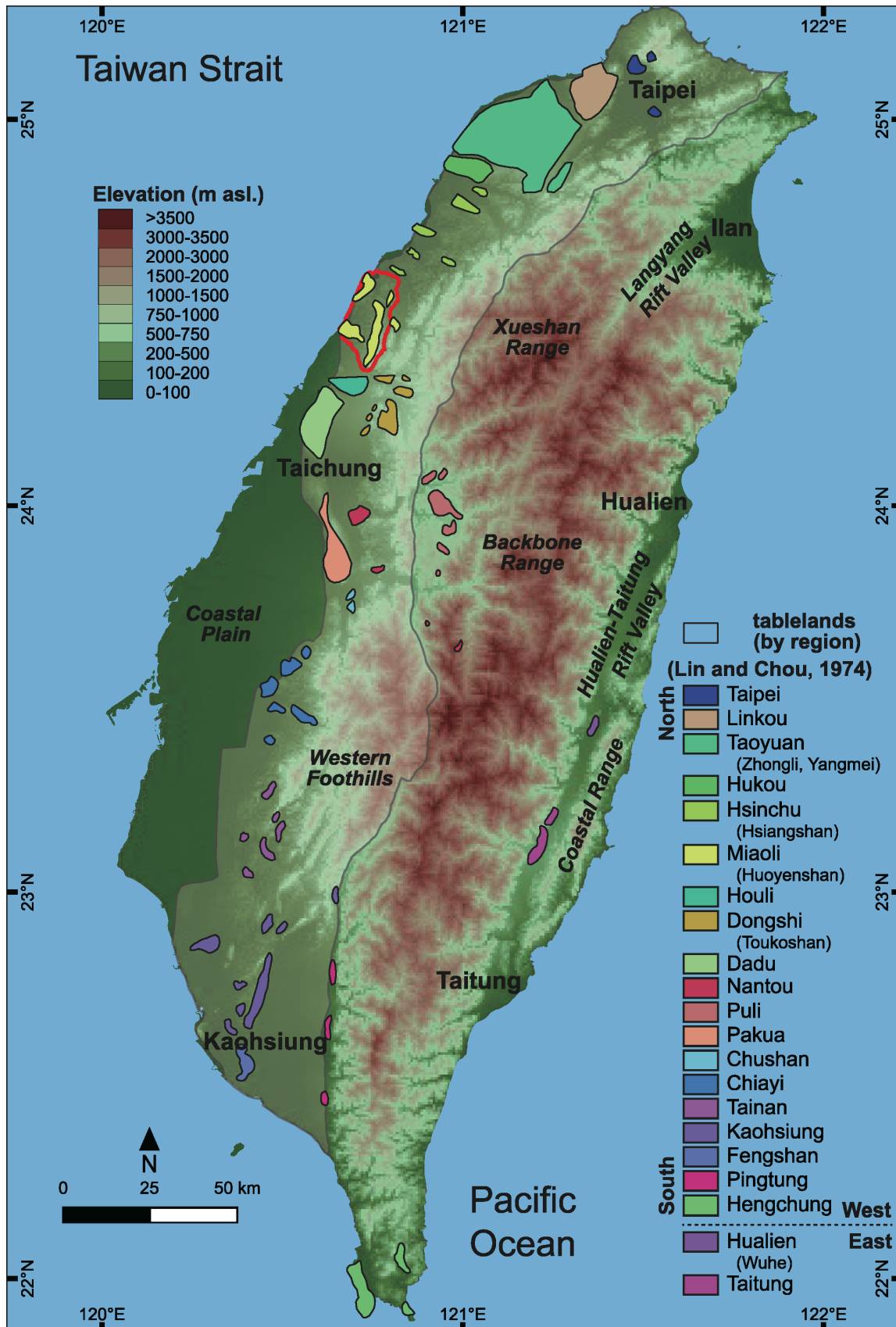


Figure 1.3: Locations of the tablelands in Taiwan, simplified after Lin and Chou (1974). The tablelands were categorized by the traditional geographical divisions in Taiwan. The tablelands are mostly located at the western part of Taiwan. The boundary of the geological division of Western Foothills (WF) was simplified after (Ho, 1988).

Table 1.2 Basic information of the tablelands in Taiwan

area	size (km ²)	high (m asl)	low (m asl)	remark
Taipei	30.2	788	0	Including the terraces in Tatun Volcano
Linkou	139.6	465	1	
Taoyuan	612.2	601	9	Including the terraces in Daxi
Hukou	68.2	310	4	
Hsinchu	61.7	470	1	Including the terraces in Chudong
Miaoli	104.3	566	0	
Houli	42.8	313	105	
Dongshi	69.4	634	181	
Dadu	135.2	311	11	
Pakua	98.8	442	36	
Puli	72.0	1336	362	
Nantou	32.3	1883	103	
Chushan	9.9	527	122	
Chiayi	81.8	490	18	
Tainan	47.2	527	13	
Kaohsiung	126.1	611	8	Including the terraces in Chishan and Meinung
Fengshan	32.2	96	5	
Pingtung	26.5	891	50	
Hengchung	90.5	490	0	
Hualien	10.6	267	69	
Taitung	39.8	540	177	

Reference: Lin and Chou (1974)

On the other hand, other case studies focused on the Quaternary environmental changes and the landform evolutions in Taiwan have worked on different environments and proxies for understanding the overall processes during the environmental changes in the Quaternary time span. The palynological studies for the reconstruction of vegetation and the corresponded climate change models in the mountain lake sediment records (Lee and Liew, 2010; Liew et al., 2006; Liew et al., 1998; Liew and Tseng, 1999) have studied the changes of wet/dry/cold/warm climate conditions in the post-last interglacial time span (Fig. 1.3). The studies for glacial traces and snowline reconstructions (Böse, 2004; Hebenstreit et al., 2011) or from the deposition and the weathering characteristics of the surface sediments in the high mountain areas (Wenske et al., 2011; Wenske et al., 2012) have discussed the existence of glaciers on high mountains and the environmental change model during the glacial time. The climate conditions of these periods caused the different denudation and sediment yielding processes to the present day's settings. The most recent study also has shown the understanding of the overall aeolian dust deposition as the environmental change track (Tsai et al., 2021) of the paleo climate conditions. A detailed study of the deposition environmental change and the deposition ages can give better understanding of the tableland morphology, and these results can also be compared with the studies of other tablelands to discuss fundamental interpretations of Quaternary stratigraphy in the mountain foreland of the Taiwan Island (Figs. 1.2 and 1.3).

The Miaoli Tableland is a representative case of tableland morphology in western Taiwan, it has been chosen as the study area due to the following reasons (Table 1.1 and Fig. 1.3): i.) it is directly located at the vicinity of the coastline of the Taiwan Strait, it is a very sensitive area to Quaternary sea-level change. ii.) it is an example for the study of the tableland uplift according to the foreland tectonics. iii.) the geochronological framework of the sedimentary successions has not been established yet. iv.) the corresponding Quaternary environmental changes were not studied in detail. v.) it has good accessibility to outcrops of the tableland sedimentary successions.

The provenance of topography, sedimentary characteristics, geochronology and the corresponding morphological processes of the Miaoli Tableland were studied initially. Even with the methodological restriction of field observations for the sedimentary successions beneath the surfaces (e.g., the interior of tableland segments, the buried sediments in fluvial plains, active fluvial channels, and estuaries), the strata in the Miaoli Tableland area have been assumed as the depositions on the poorly consolidated continental shelf sedimentary rocks since the end of the Neogene to the late Quaternary (Chang, 1953, 1955a, b; Ho, 1988) (see chapter 2 and 3 for details). The initial tests of numerical dating of the tableland's sediments estimated the LGM (Last Glacial Maximum) and the early Holocene depositional ages of the surface materials (Lin, 1963; Wang and Peng, 1990). However, the geochronology framework of the sedimentary successions has not been established yet. A detailed survey and analysis of the Tableland's sediments and morphology was undertaken by Chang et al. (1998), as the tableland surfaces were grouped into three subgroups by elevations, imbrication of the fluvial sediments and composition of the surface sediments, based on the method proposed by Tomita (1953) and Lin (1957) (see chapter 2 for details). The morphology was interpreted that the Miaoli Tableland was mainly built up by fluvial sediments (i.e. gravels and cobbles) of the (palaeo-) Houlong River and the (palaeo-) Da'an River as alluvial fans. The long-term ongoing uplift caused the diversion of these main river systems. Subsequently developed the local river systems (see Chapter 2 for details). All these factors have controlled the morphology of the forming of the present-day's tableland topography. However, this morphological model had insufficient absolute chronological analyses and thus only the relative chronology was discussed (Chang et al., 1998). Detail discussions regarding to the Quaternary climate changes and their influences on the Miaoli Tableland morphology are scarce so far.

The main questions of this study are set as follows:

1. How to classify the tableland surfaces with a simple protocol that implies concise morphological meaning?
2. Are there regularities of the sedimentary successions? And what is the process to make the difference of them?
3. How old are these sediments?
4. What are the time-space correlations of the tableland morphology processes and how to improve the local stratigraphy with these new findings?

To solve these questions, this study aims to reach four main goals:

1. Implementing the high precision elevation data with an advanced numerical method of morphological mapping provides new categorization of the tableland segments topography by the relative elevation calculations based on the morphology of an alluvial fan palaeo-topography. The new morphological mapping results, instead of the existing subjective categorization results, are integrated with the field investigation records for the discussion of the 3D correlation in between the tableland segments' topography and sedimentary successions.
2. Combining the field investigation records and the public borehole data enables to sketch the spatial distributions of the fluvial sediments (i.e. gravels and cobbles), which is interpreted as the traced factors for a schematic 3D modelling of the remobilization of fluvial sediments with a relative chronological order. The 3D model is used for further interpretations of the sediment erosion, rework, and deposition processes as the key morphological inputs to the landform evolution in the Miaoli Tableland.
3. Establishing the geochronology frameworks of sedimentation processes by using the numerical dating methods (e.g. OSL dating) provides high-precision estimations of the last deposition time and to interpret the morphodynamic model with a clear spatial-temporal sequence. The absolute dating results are combined with the global sea-level change model (Lambeck et al., 2014; Liu et al., 2004; Rabineau et al., 2006; Waelbroeck et al., 2002) to calculate the long-term uplift rates of the Miaoli Tableland.
4. Integrating the morphological, the sedimentological, and the geochronological results into a new approach for 4D modelling of the evolution of a Taiwanese tableland. This initiates an extensive discussion of the local stratigraphy for proposing a revision of the nomenclatures for the Quaternary strata in the Miaoli Tableland that respects a clear historical context and follows the latest international guidelines.

1.2 Structure of the thesis

This thesis used a multi-aspect approach to understand the morphodynamic of the Miaoli Tableland. In chapter 2 the local geographical, geological, and meteorological settings are reviewed, and a briefing of local history is also included. In chapter 3 is the review of historical evolution for the stratigraphical definitions of the Quaternary strata and the deposits in the Miaoli Tableland, with the historical contexts of geoscience traditions, political backgrounds, data accessibility issues and the contemporary developments. The methodology and technical issues are listed in chapter 4 including all the geomorphological, sedimentological, and geochronological methods. Chapter 5 aims to the morphological discussion of the correlation between topography and sedimentary successions of the Miaoli Tableland. Chapter 6 is an experimental application that implemented the public open accessed borehole dataset to analyze the sedimentary succession and to interpret the rework of the fluvial sediment through the Miaoli Tableland area as the trace factor of the morphodynamic is this area. Chapter 7 includes the outcomes of OSL (optically stimulated luminescence) dating of the sediments' last deposition age in the Miaoli Tableland, and the integration of sea-level change that determined the new calculation of uplift-rates. Chapter 8 is the summarizing multi-aspect discussions of the morphological syntheses, the tableland geochronology, and the revision of the stratigraphical nomenclature to fit the field evidence in the Miaoli Tableland. Chapter 9 is the overall conclusion of this study. Chapter 5 and 7 were published in peer review journals, chapter 6 was written in the format for submission to a peer review journal.

Chapter 2. Research area

2.1 Location

The Miaoli Tableland is located in northwestern Taiwan between the margin of the Western Foothills (WF) and the coast of the Taiwan Strait (Figs. 1.2 and 1.3, Table 1.2). There is no specific definition of the boundary of the Miaoli Tableland, traditionally, it is generally the higher relief of sedimentary terraces in the area between the left bank of the Houlong River and the delta of the Daan River (Lin, 1957; Lin and Chou, 1974) (Fig. 2.1). The size of the Miaoli Tableland area is ca. 29 km long and ca. 14 km cross and the area is generally divided as sections of Houlong, the Miaoli City, Sanyi, Tongluo, Tungxiao, Yuanli and Xihu. In this thesis, the boundary of the Miaoli Tableland area (i.e. the study area) is specifically defined as a combination of the slope foets and the thalwegs of the nearest fluvial channels (see 4.2.2 for details) that are located surrounding the higher relief area.

2.2 Topography

The Miaoli Tableland's topography is primary consisting of the sedimentary terraces (i.e. tableland segments), the fluvial valleys (Chang et al., 1998; Lin, 1957; Makiyama, 1937; Ota et al., 2006), and the coastal plains which are located along the coast of the Taiwan Strait (Fig. 1.4 and 2.1).

The tableland segments are mainly distributed in the catchments of the Tungxiao River, the Wumei (Xihu) River and other smaller/local fluvial systems, and these tableland segments are also the water divides in between these catchments. For example, the tableland segments in the northeastern part (e.g. in Houlong, Miaoli City and Xihu) are the divides of the Wumei (Xihu) River, the Nanshi River and the Houlong River, and the tableland segments in the southern part (e.g. in Tungxiao and Yuanli) are the divides of the Fangli River, the Tungxiao River and the Yuanli River (Fig. 2.1). The tableland segment surfaces were identified and mapped since the 20th century (Makiyama, 1934, 1937; Tomita, 1940). Subsequently Lin (1957) mapped the tableland segment surfaces and classified them into three subgroups: the Lateritic Highlands (LH), the Lateritic Terraces (LT) and the Fluvial Terraces (FT). The Lin's classification is based on the method proposed by Tomita (1951; 1953), which is the analysis of the weathering degrees of the surface sediments and their elevations (Figs. 2.1 and 2.2a). Chang et al. (1998) had followed the methods of Lin (1957) and Tomita (1951, 1953 and 1954) to present a revised and more detailed tableland segment surfaces mapping according to the new findings in the field, such as: elevations, the imbrications of the gravels and cobbles and also the weathering degree, distinguished by color, of the surface sediments. However, only the larger tableland segments with identifiable gravel and cobble layer(s) covering the surfaces were included in the Chang et al.'s mapping (Fig. 2.2b). The smaller tableland segments or those without the gravel and cobble layer(s) were excluded from the mapping.

The Lateritic Highlands (LH) are the highest and the oldest subgroup of the tableland segments (Chang et al., 1998; Lin, 1957), which are located at the southeastern part of the study area (Figs. 2.1, 2.2a and 2.2b), these tableland segments were tentatively called “Sanyi Tableland” (Ota et al., 2006). This subgroup consists of the tableland segments with elevations from 250 m to 614 m asl (Fig. 2.1). The elevations of the tableland segment surfaces are gradually decreased (about 2 degrees inclination) northeastward to the left bank of the Wumei (Xihu) River (Fig. 2.1). The Lateritic Terraces (LT) are the tableland segments located in the central and northern parts of the study area (Chang et al., 1998; Lin, 1957), their elevations are mainly between 50 m to 250 m asl, and up to 445 m asl in the upstream area of the Tungxiao River catchment (Figs. 2.1, 2.2a and 2.2b). The larger tableland segments are located at the northwestern and the southwestern areas, and the rest are smaller tableland segments (Fig. 2.2b). The elevations of these ST tableland segment surfaces are gradually decreased toward the coast with westward and northwestward directions (Fig. 2.2b). The Fluvial Terraces include all the modern/active flooding terraces and the plains in the fluvial valley floors (Chang et al., 1998; Lin, 1957), especially in the middle and the downstream areas (Figs. 2.1, 2.2a and 2.2b). The elevations of the Fluvial Terraces (FT) are up to about 150 m asl, which are located at valley floors of the Tungxiao River, the Nanshi River, the Yuanli River, the Fangli River and the Wumei (Xihu) River (Figs. 2.1, 2.2a and 2.2b). An overall pattern was identified that the difference of elevations between the LH and the LT are higher than the differences between the LT and the FT (Chang et al., 1998) (Figs. 2.1 and 2.2b).

The coastal plain shows alluvial sediments that are carried by the fluvial transportations (Chang et al., 1998) and the longshore currents (Huh et al., 2011; Jan et al., 2002; Liao et al., 2008; Wang et al., 2003). The coastal plain has a 30 km long stretch between the Houlong River and the Yuanli River (Fig. 2.1). The coastal plain is ca. 500-1500m wide, and its topographical steepness is ranging from 1° to 3°. The estuaries in the Miaoli Tableland show features of tidal dominated depositional environments (Desjardins et al., 2012; Goodbred and Saito, 2011). The topography of these estuaries are broad tidal flats and sandbars perpendicular to the coastline, for example, the tidal flats area at the estuary of the Houlong River and the Wumei (Xihu) River is enlarged to ca. 800m width in the direction toward the Taiwan Strait (Fig. 2.1).

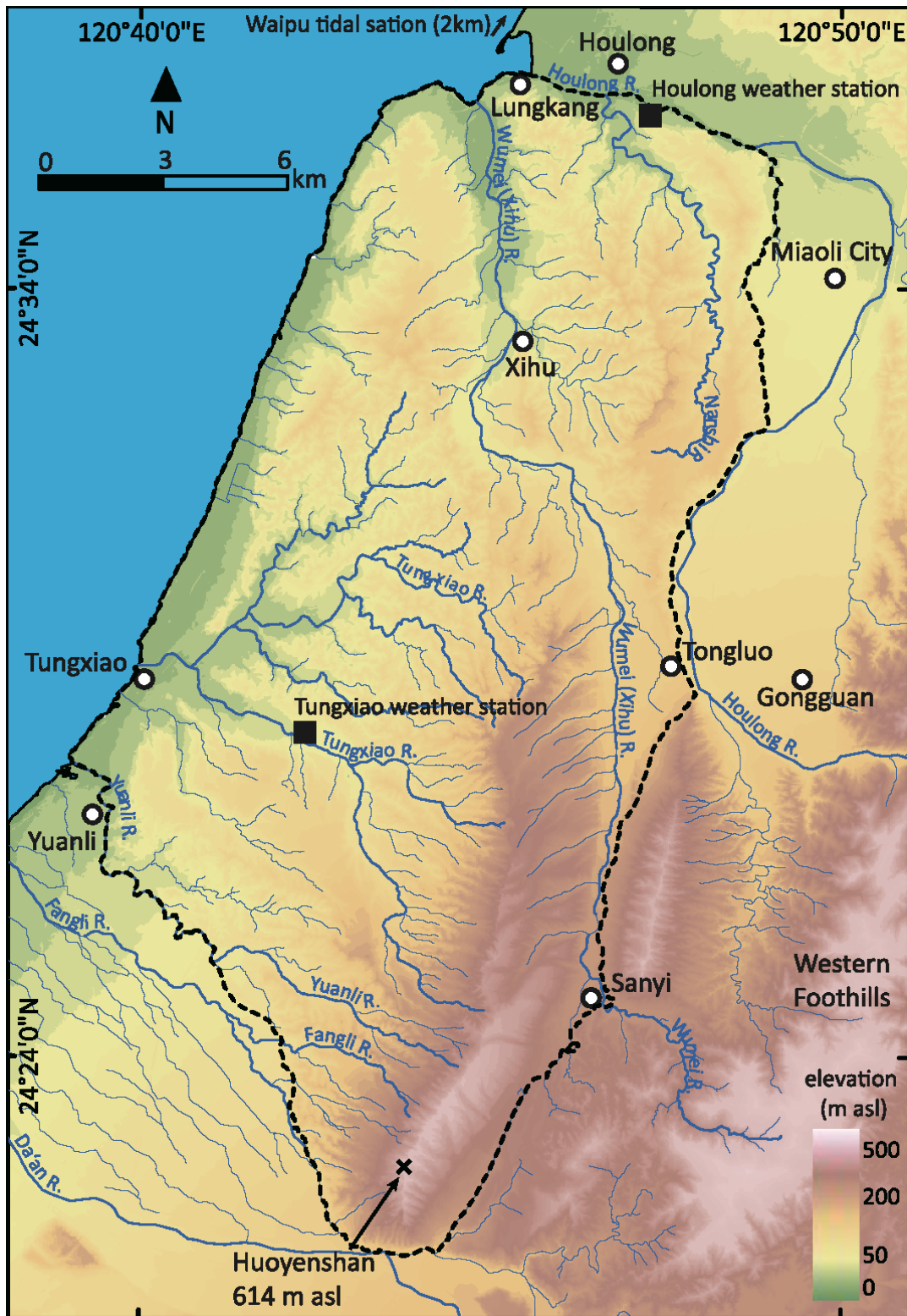
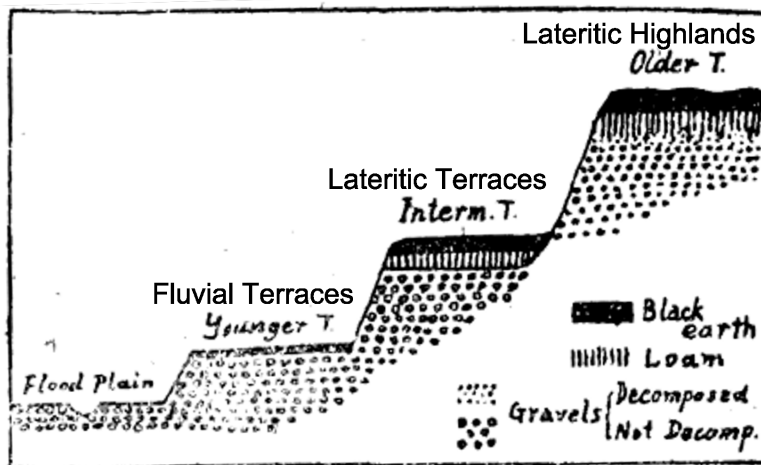


Figure 2.1: The basic map of the Miaoli Tableland. The Miaoli Tableland is located by the coast of the Taiwan Strait in Northwestern Taiwan. The study area is marked by a dashed line. The elevation is higher in its southeastern part, which was tentatively called “Sanyi Tableland” by Ota et al., (2006). The highest point of is located at Huoyenshan (i.e., Fire Mountain). The elevations decrease to the north and west. Two major fluvial systems flow through the study area (the Wumei (Xihu) River and the Tungxiao River). The mainstems of two other rivers forming the boundaries of the Miaoli Tableland from north to east (the Houlong River) and from south to southwest (Da’an River). The digital elevation model (DEM) is taken from the public open-access database (Satellite Survey Center, 2018). The location of weather stations and tidal stations are referenced from the Central Weather Bureau (2022).

a)



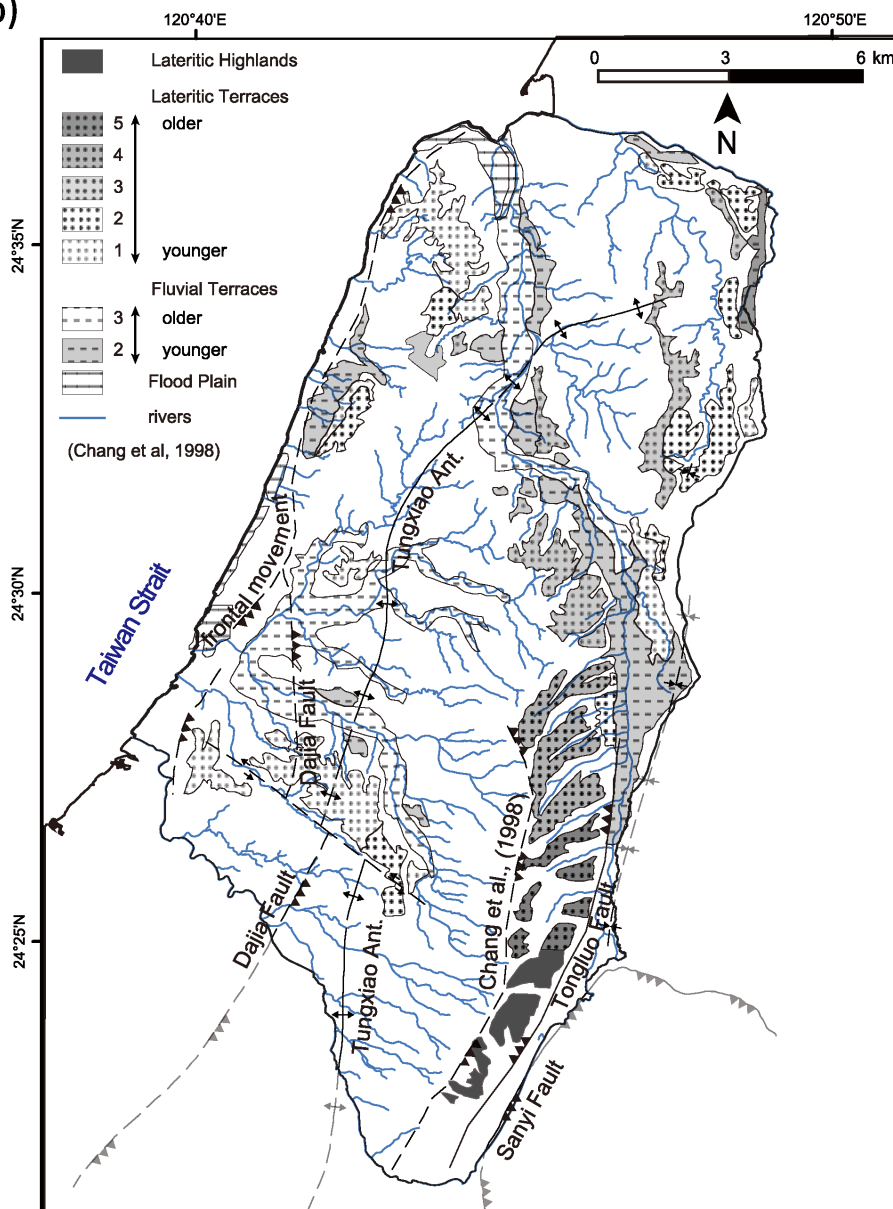
(Tomita, 1954)

Figure 2.2: The morphological models of the Miaoli Tableland.

a) The morphological definitions of the subcategories of sedimentary / fluvial terrace surfaces, according to the relative elevations, the compositions of surface materials and the locations corresponding to the fluvial channels, proposed by Tomita (1951, 1953 and 1954). The profile (after Tomita, 1954) presents the method that has been extensively applied by the subsequent studies for the detailed categorizations of Taiwanese tablelands.

b). The mapping of tableland surfaces and the detailed partitioning of each subcategory, after Chang et al., (1998).

b)



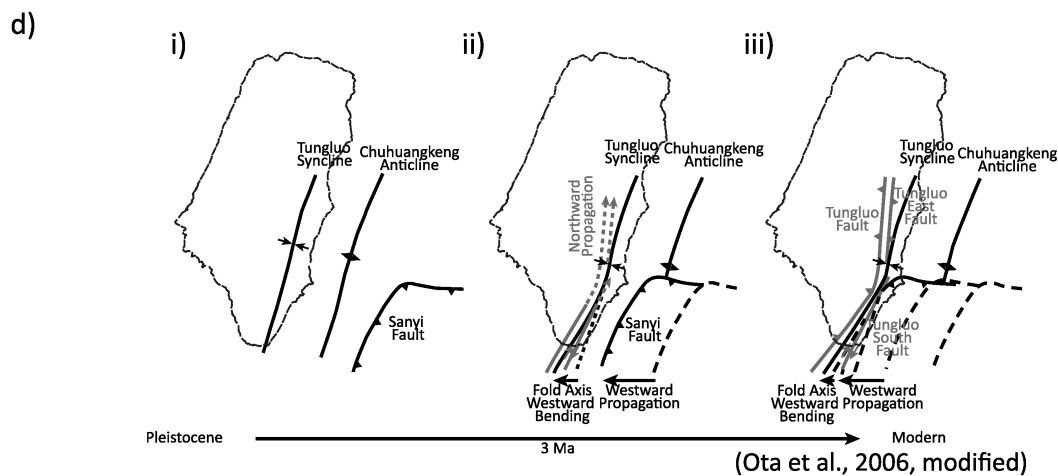
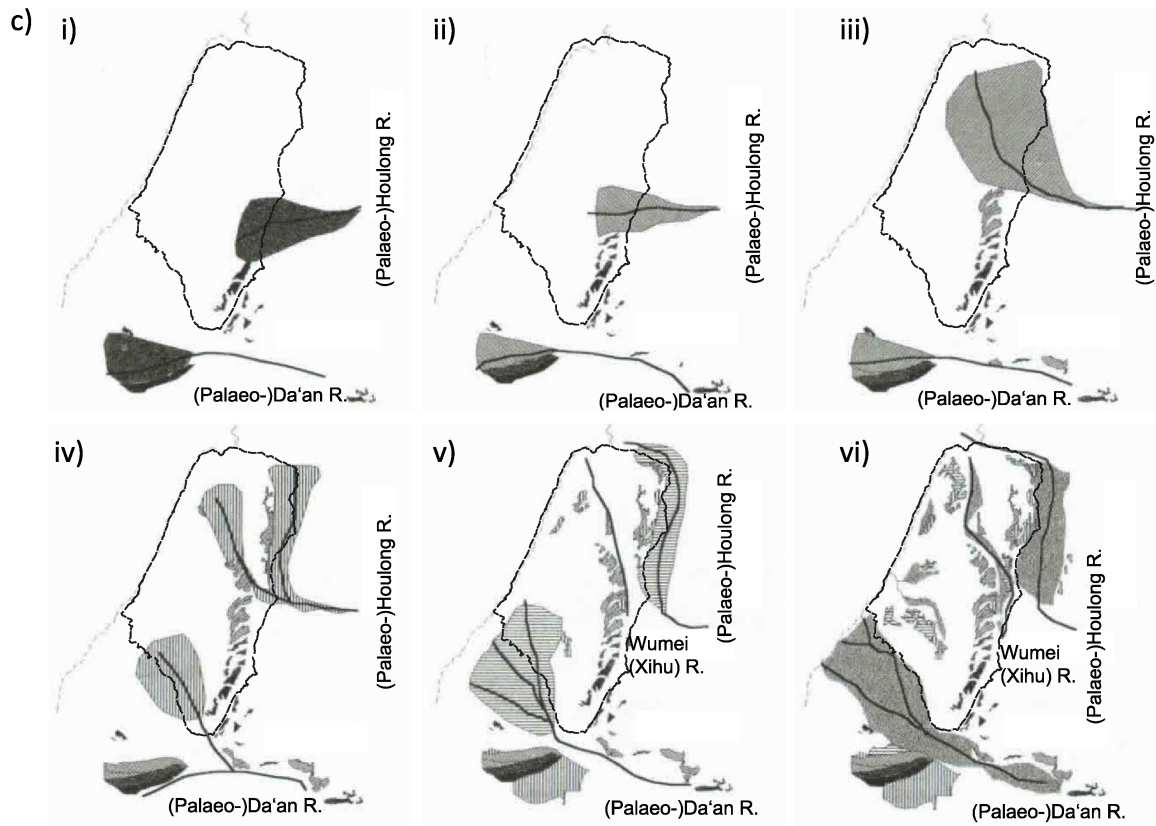


Figure 2.2 (continue): c). The Chang et al. model (1998) of the morphology of the Miaoli Tableland, emphasizing the tectonism and its influence on the diversion of the palaeo rivers' flow path. The (palaeo-) Da'an River and the (palaeo-)Houlong River yielded fluvial sediments, forming the palaeo alluvial fan(s) (i and ii). These palaeo-rivers were subsequently divided after the fan surfaces were uplifted by the thrust faults. The thrust also caused a diversion of the fluvial path, with the branches flew to the Taiwan strait separately, leading to the deposition of alluvial fans to the west and north (iii and iv). The fan surfaces were further dissected, caused by the continuous uplift (v and vi). A relative chronology from Pleistocene to Holocene was given, which based the weathering degrees of the surface materials.

d). The Ota et al.'s model (2006) of the morphology of the Miaoli Tableland, which highlighted the tectonism. The folding of the Tungxiao Anticline caused the formation of the present day's hilly landform in the Tungxiao River catchment. The westward propagation of the Sanyi Fault and the newly formed Tongluo Fault led to the rapid uplift of the alluvial fans to form the LH segments surfaces in the southeast. The northward extension of the Tongluo Fault has been assumed to be a segment of the Tongluo Syncline, due to the vertical displacement in this segment hasn't been identified yet.

2.3 Geology and tectonics

The Miaoli Tableland is located at the mountain foreland that was the main deposition area of the Neogene mountain ranges (Angelier et al., 1986; Ho, 1975, 1988; Suppe, 1980a, b) yielded sediments (Fig. 1.2). Subsequently the ongoing tectonism has uplifted the sedimentary complexes in the frontal part of the mountain foreland (Covey, 1986; Liew et al., 2004; Yu and Chou, 2001), which has caused the long-time scale (i.e., millions of years) regression environmental setting in the Miaoli Tableland area. The sedimentary successions were defined by different scales and aspects of stratigraphy respectively, the most relevant stratigraphical definitions are the Toukoshan Formation (Tks / Tk) (Chang, 1955a, b; Ho, 1975), the Tungxiao/Lungkang Formation (Lk) (Lin, 1963; Makiyama, 1934) and the Quaternary Deposits / Terrace Deposits/Lateritic Terrace Deposits (Chang, 1990; Chang, 1955b; Ho, 1988; Ho, 1994) (Fig. 2.3). (A detail historical review of the stratigraphical definitions in the Miaoli Tableland is presented in chapter 3).

The *Toukoshan Formation* (Tks / Tk Formation) (Chang, 1948a, b, 1953, 1955b; Ho, 1988) is the most broadly used definition to describe the sedimentary successions in the Miaoli Tableland. The thickness of the Toukoshan Formation in the Miaoli Tableland area was estimated for hundreds of meters by geophysical analyses (Yang et al., 2006; Yang et al., 2016; Yue et al., 2005) and the drilling results in the nearby Taichung area (ca. 30km southeast) showed a thickness up to ca. 1600 meter (Chen et al., 2001) (Fig. 2.3). The lower part of the Toukoshan Formation, which consists of the intercalations of shallow marine and tidal-flat sediments, was additionally defined as the Hsiangshan Facies (Hs) (Chang, 1955b) (Fig. 2.3). The Hsiangshan Facies is characterized by sedimentary structures such as cross bedding, ripple marks and aquatic fossil compositions (Chang, 1955b) (Fig. 2.3). The thickness of the Hsiangshan Facies is up to 900m according to the drilling record (Chen et al., 2001). The distribution of the Hsiangshan Facies is mainly in the western and northern part of the study area, where these fine-grained sedimentary layers are exposed (Chang, 1955b; Ho, 1988; Ho, 1994). The middle and upper parts of the Tk Formation are consisted of a thick layering of fluvial sediments and are covered by a ca.100-200 m thick succession of coastal and fluvial sediments (Figs. 1.4 and 2.3). These parts of the Tk Formation were combined and additionally defined as the Huoyenshan Facies (Chang, 1948a, b, 1955b; Ho, 1988) (Fig. 2.3). The distribution of the Huoyenshan facies is in the southern part of the study area (Chang, 1955b; Ho, 1988; Ho, 1994), the thickness of the Huoyenshan facies is up to 600m according to the drilling record (Chen et al., 2001) (Figs. 2.2c and 2.3). A circa. 0.6 to 3 Ma age range was given to the depositions of the Tk Formation (Chang, 1990; Chen et al., 2001; Ota et al., 2006), according to the biochronology analyses (Huang, 1984; Lee et al., 2002). The Tk Formation was assumed that the sedimentary successions had already lithified, and the loose nature of the sediments are interpreted as results of in-situ weathering (Chang, 1994; Ho, 1994).

The *Tungxiao Formation* (Ty / Ts Formation) was initially proposed by Makiyama in the 1930's, according to the field observation results in the Miaoli Tableland area (i.e. Tungxiao, Yuanli, Xihu, Tongluo and Sanyi). The thickness of the sedimentary successions is ca. 400 meters. The fine-grained sediments (clay, silt, sands) are intercalated in the lower and middle part of the succession, a layer of gravels and cobbles (up to tens of meter) in the upper part of the succession, and then a layer of ochre-colored soils covered on the surfaces (Fig. 2.3). The fossils compositions were interpreted that the depositional environments were shallow marine to coastal environments mainly (Makiyama, 1934) (Fig. 2.3). The age of the depositions was unknown for lack of appropriate dating methods by the time. After 1950's this definition has been rarely mentioned, the majority of succeeding studies used Toukoshan Formation (Tks / Tk) (Chang, 1955b) instead of the Tûsyo Formation (Ty / Ts) to describe the strata in the Miaoli Tableland area.

The *Lungkang Formation* (Lk Formation) was proposed to describe the upper most part (ca. 30 meter) of the sedimentary succession exposed in Lungkang village, which is located at the northwest of the study area (Lin, 1963) (Fig. 2.1). The Lk Formation is consisted of a sedimentary succession of depositions of tidal zone, delta, gravel beach, and aeolian sand dune (Lin, 1963) (Fig. 2.3). An early Holocene depositional age range was given based on the test results of the early techniques of radiocarbon dating. Lin interpreted that the Lk Formation is the result of successive changes between transgression and regression phases, that were caused by the eustatic sea level change and the tectonic subsidence during the early to middle Holocene (Lin, 1963) (Fig. 2.3).

Quaternary Deposits, Terrace Deposits and Lateritic Terrace Deposits, all these definitions were provisionally defined to describe the surface sediments composed of reddish / ochre-colored soils, aeolian deposits, dune sands and modern alluvial sediments (Chang, 1990, 1994; Chang, 1955b; Ho, 1988; Ho, 1994) (Fig. 2.3). These definitions were used for describing the surface sediments of the FT, the estuaries, and the coastal plains and some cases of the LT surfaces, especially if the identifiable gravel and cobble layer(s) are missing (Chang, 1990, 1994; Chang et al., 1998; Chang, 1955b; Ho, 1988; Ho, 1994) (Figs. 2.2b, 2.2c and 2.3). The original purposes for these definitions were to classify the sediments that were assumed not to be lithified. Therefore, they were separately defined to avoid misusing of Tk Formation in these cases (Chang, 1955b; Ho, 1975, 1988). Due to lack of the evidence of lithification and the loose nature of these sediments, a late Quaternary time span was assumed for the deposition of all these surface sediments (Chang, 1955b; Ho, 1975, 1988).

In general, the lithology in the Miaoli Tableland is still in debate, particularly for the following remarks:

i). The fluvial gravel and cobble depositions on the tableland segments were studied in detail. According to the field records of Chang et al., (1998), the thickness of the gravel and cobble layer(s) decrease from the southeastern part of the study area (the LH) to the northern and western parts (the LT). The clast-supported gravel and cobble layer(s) are filled with sandy and loamy materials. The gravels and cobbles are mostly

rounded with imbrications from 12 to 80 degree toward northwesterly directions (Chang et al., 1998) (Fig. 2.2b). The gravels and cobbles are deposited as the surface layer in the fluvial valleys (FT), the flood plains (FT), the estuaries, and the coastal plains too. The previous interpretations assumed that these gravels and cobbles were deposited during the most recent rework processes, which took place later than the forming of the gravel and cobble bed(s) of the tableland segments (LH and LT) (Chang et al., 1998). However, studies of the gravels and cobbles depositions are still limited, due to lack of exposures in these locations.

ii). the reddish/ocher-colored fine-grained surface sediments were described as lateritic soils by all these stratigraphical definitions, however, the lateritic characteristics of the surface sediments on the Taiwanese tablelands are still in debate by the differentiated aspects from pedology and geology (Chen et al., 2015; Tsai et al., 2021).

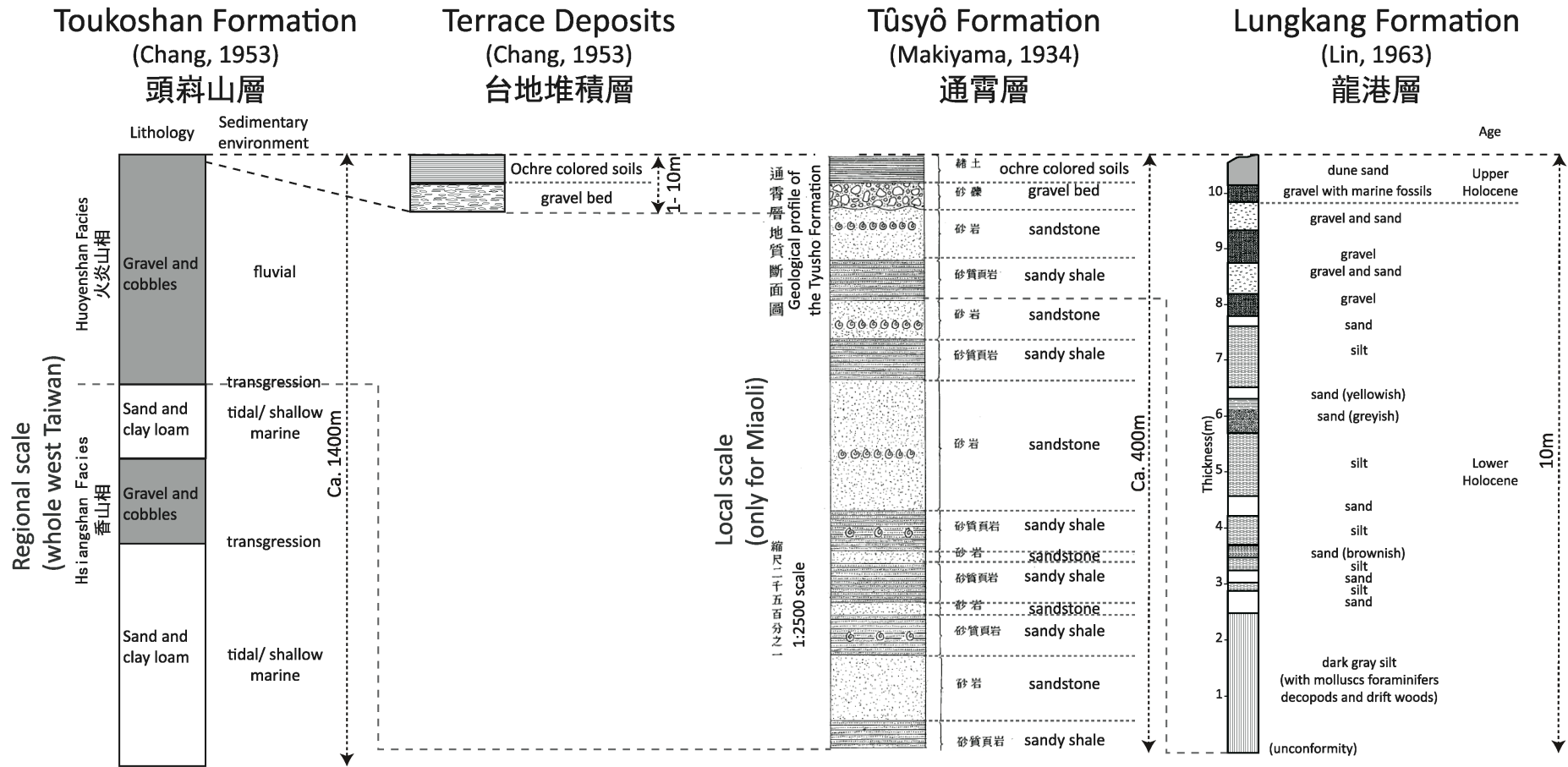


Figure 2.3: The stratigraphy models for the Miaoli Tableland's strata. Four major stratigraphical models and their columns were illustrated and listed with respect to the differentiated scales of thickness. The interpretations among these models were generally identical that the strata were composed of successions of marine-coastal fine-grained sediments, fluvial gravels and cobbles, and a cover layer of fine-grained ochre soils / dune sands.

The identified tectonic features in the Miaoli Tablelands are listed below (Fig. 2.4):

Sanyi Fault

The Sanyi Fault is located at circa 2km southeast outside the boundary of the study area, with a strike direction of N 45° E (Lee, 2000b). This thrust fault is the geological boundary of the Neogene bedrock strata and the Quaternary sedimentary strata (Fig. 1.2) (Lee, 2000b; Yang et al., 2016). This thrust fault belongs to the thrust fault belt that has triggered hazardous earthquakes (Fig. 1.2 and 2.4). For example, the 1935 earthquake was triggered by this fault, and the 1999 earthquake was triggered by the nearby Chelunpu thrust fault, these two faults have been assumed as segments of the tectonic thrust fault belt in the marginal area of the Western Foothills in western Taiwan.

Tongluo Thrust Fault (inferred)

The Tongluo Thrust Fault is located at the eastern margin of the study area, which is very close to the boundary to the Western Foothills (bounded by the Sanyi Fault at two kilometers east). This thrust fault was identified based on the morphological analyses of the linear fractions/displacements of the topography of the Tongluo and Sanyi area (Ota et al., 2006) (Figs. 2.2d and 2.4). There are another two tectonic features near the Tongluo Thrust Fault including the Tongluo East Fault (circa 500m east) (Ota et al., 2006) and an inferred thrust movement identified by the escarpment of the LH at the west (circa 2km west) (Chang et al., 1998) (Figs. 2.2c and 2.4). All these thrusts have a parallel alignment with strike of about N 45 W, the dip angle of these thrusts are about 10 to 15 degrees (Ota et al., 2006). These thrusts can be combined as a joint tectonic system in the southeastern part of the study area.

Tongluo Syncline

This syncline is located at the northeastern part of the study area, which is assumed to be an extending tectonic feature related to the thrust fault at its south (i.e. Tongluo Thrust fault) (Ho, 1994). The syncline has a strike of north to south direction with an asymmetric structure, the west limb is steeper the eastern limb, and dip angle of the both limbs are lower than 10° (Ho, 1994). However, the horizontal bedding of the topping gravel and cobble layer(s) and the surface sediments along the axis areas show that these sediments had deposited after the forming of the syncline (Chang et al., 1998).

Tungxiao Anticline

This anticline is located in the central part of the study area. The anticline has a strike of SSW-NNE direction in its southern and central sections (Chang, 1990, 1994; Ho, 1994). The section located at the north of Tungxiao is the mining area for natural gas, the geological investigation of resources had recorded that this anticline is extended into ca. 3000 meters depth (Chang, 1990). The northern section located at Xihu had been

intercepted by the Futouken Fault at the left bank of the Wumei (Xihu) River, the strike direction of the anticline had changed to E-W direction (Ho, 1994). This anticline has an asymmetry structure so that the east limb is relatively steeper than the west limb, dip angles of the both limbs are between 5° to 15°. The fine-grained marine / costal sedimentary layers are exposed at the axis part of the anticline (Chang, 1990, 1994; Ho, 1994).

Dapingding Fault

This tectonic feature is a sinistral (W-E strike) strike-slip fault, which had intercepted the Dajia Fault and the Tungxiao Anticline at the south of Tungxiao area (Chang, 1994). The forming of this strike-slip fault is assumed to be later than the forming of Dajia Fault and Tungxiao Anticline due to this strike-slip fault had cut off and had made horizontal displacements the other two tectonic features (Chang, 1994).

Fitouken Fault

This is an inferred thrust fault in the northern part of the study area. The southern section of the thrust fault is identified by the surface fraction that has a SSW-NNE strike direction (Chang, 1990). Strike direction of the thrust fault changes to E-W in the north section, however the surface fractions of this section are insignificant, as they are covered by the gravel and cobble layer(s) and the surface sediments (Chang, 1990) (Fig. 2.3).

Beishatun Anticline

This anticline is only exposed on the very northwestern part of the study area. It has a strike of SSW-NNE direction and an asymmetry structure (Chang, 1990). The eastern limb has a gentle dip angle of 6 degree; however, the western limb is much steeper with a dip angle of 16 degree (Chang, 1990).

Dajia/Beishatun Fault (Chang, 1990, 1994) / frontal movement (Shyu et al., 2005)

This thrust fault was assumed to be the youngest thrust movement of the Miaoli Tableland area (Shyu et al., 2005; Yang et al., 2016). It was identified by the linear margin of the tableland segments along the coastal plain. The northward extending section was named "Beishatun Fault"; on the other hand, the southward extending section was named "Dajia Fault" (Chang, 1990, 1994). The marginal thrust movements along the coast of western Taiwan were tentatively called "frontal movement" (Shyu et al., 2005) (Fig. 1.2 and 2.4). The estimations of the uplift rates in Miaoli Tableland are very limited. Previous studies estimated the uplift rates of 1mm/yr according to i). the geochronological data from the tableland sediments in Chushan area (65 km south) (Ota et al., 2002), and ii). the numerical dating results of the marine fossils in the fine-grained sedimentary layers (Wang and Peng, 1990). On the other hand, the modern GPS (Global Positioning System) monitoring data of tectonic movements show that the Miaoli Tableland is stable to slightly subsiding (-1mm/yr) (Ching et al., 2011).

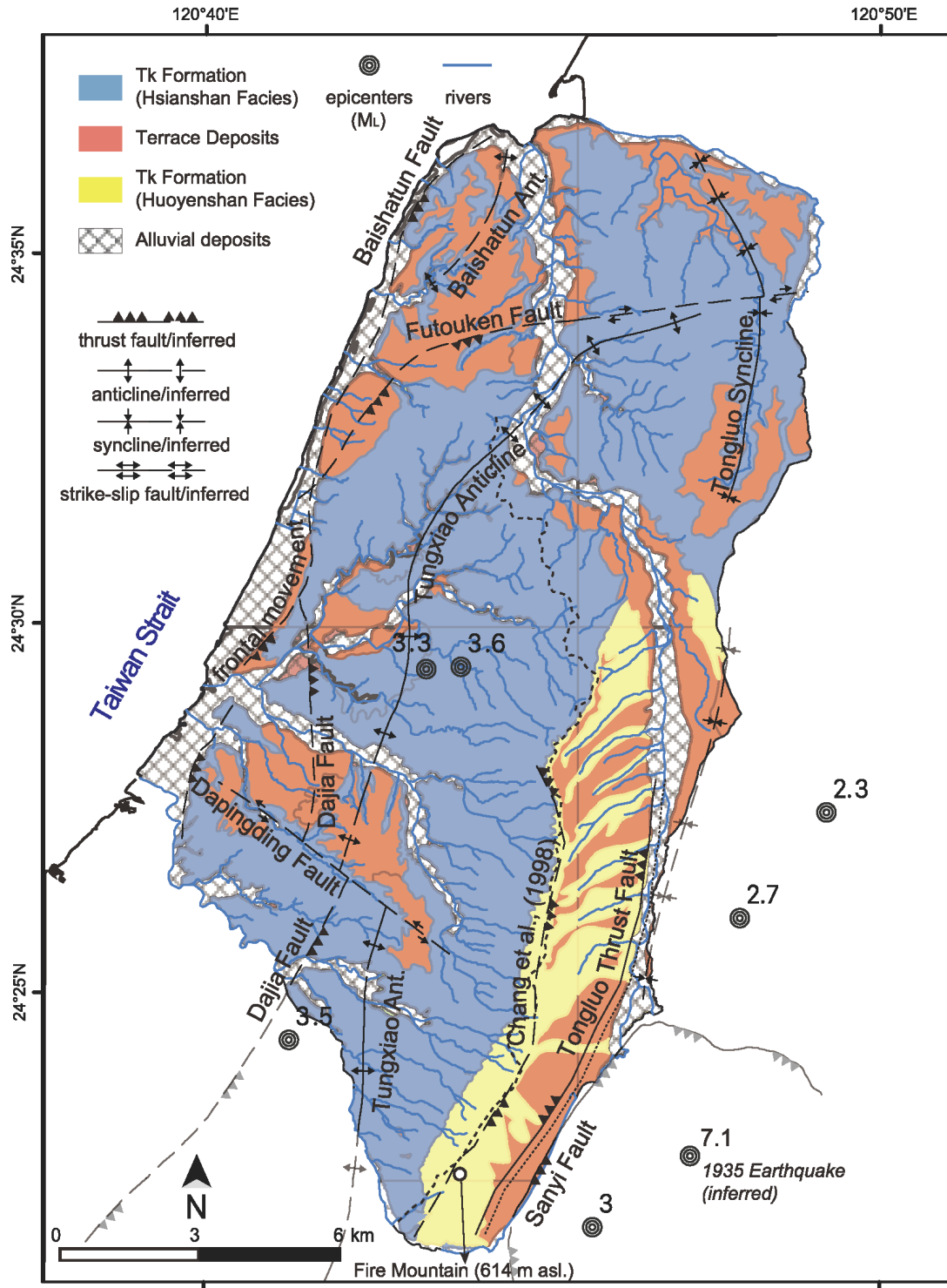


Figure 2.4: The geological features of the Miaoli Tableland. The stratigraphy and tectonic lines were after the local geological maps (Chang, 1990, 1994 and Ho, 1994) and the previous studies of Chang et al., (1998), Ota et al., (2006) and Shyu et al., (2005). Due to the inferred tectonic lines haven't been officially proofed by the Central Geological Survey (CGS), dashed lines were used in the symbology of these tectonic lines. The records of major earthquakes (ML > 2.0) in the Miaoli Tableland and the surrounding areas, including the inferred epicenter of the 1935 earthquake (Hsinchu-Taichung Earthquake), were extracted from the earthquake database of the Central Weather Bureau (2022).

2.4 Climate

In general, the Miaoli Tableland has a typical sub-tropical warm and humid climate (Lai et al., 2007) (Fig. 1.1). The climate statistics from the Central Weather Bureau has collected the temperatures, percipitations, winds and tidal records as follows (Central Weather Bureau, 2019a, b, 2020):

The temperature of the Miaoli Tableland area ranged from 15.3° C to 27.7° C (Tungxiao station, 2011-2019) with an annual average temperature of 22.0° C (Figs. 2.1 and 2.5). The highest temperature reached 37.4° C (17.7.2019) and lowest was 3.5° C (23.1.2014) (Fig. 2.5). The annual precipitation of the Miaoli Tableland area was about 1459.8 mm per year (Tungxiao station, 2010 – 2019) (Figs. 2.1 and 2.5). The precipitations have an uneven distribution with a seasonal change. The precipitations during the winter time (November to February) cover only 15.3% of the annual precipitations in average, however the precipitations during the summer time (June to September) cover 54.7% of the annual precipitations (Fig. 2.5).

The winds of the Miaoli Tableland are mainly influenced by the Eastern Asian Monsoon system (Central Weather Bureau, 2019a; Lai et al., 2007) (Fig. 1.1). The winter monsoon comes from the northeast direction (originating from Russia and Mongolia, and then passing through China, Korea, and Japan) and the summer monsoon comes from the southwest (originating from Indochina and the southern China Sea) (Fig. 1.1). The average wind speed was low (1.6 m/s, Tungxiao station, 2011-2019). Gust winds (32.1 m/s, Tungxiao station 27.9.2016) were frequently happening during the typhoon events (Central Weather Bureau, 2019b, 2020) (Figs. 2.1 and 2.5). The topography has affected the wind speed significantly. For example, in the northern part of the study area, the wind speed was higher during the winter monsoon period (17.4 – 19.3 m/s, Houlong station, 2011-2019); on the other hand, the wind speed in the southern part in the winter monsoon period was lower (13.0 – 14.6 m/s, Tungxiao station, 2011-2019) (Central Weather Bureau, 2019a), due to the southern part is the leeward of the Miaoli Tableland (Figs. 2.1 and 2.5). However, the wind speed records were mostly identical through the whole study area in the summer monsoon period (Figs. 2.1 and 2.5).

The tidal differences of the coast of Miaoli Tableland area are ca. 3.5 meters, with a maximum of 6.0 meters (Waipu station, 120°46'17"E, 24°39'05"N, 2003-2017) (Figs. 2.1 and 2.5). The surges during typhoon events were in average of 4.4 meters (1995-2015), the maximum height of the surge was 17.8 meters (Typhoon Winnie in Aug-1997) (Central Weather Bureau, 2019b, 2020) (Table 2.1 and Fig. 2.5).

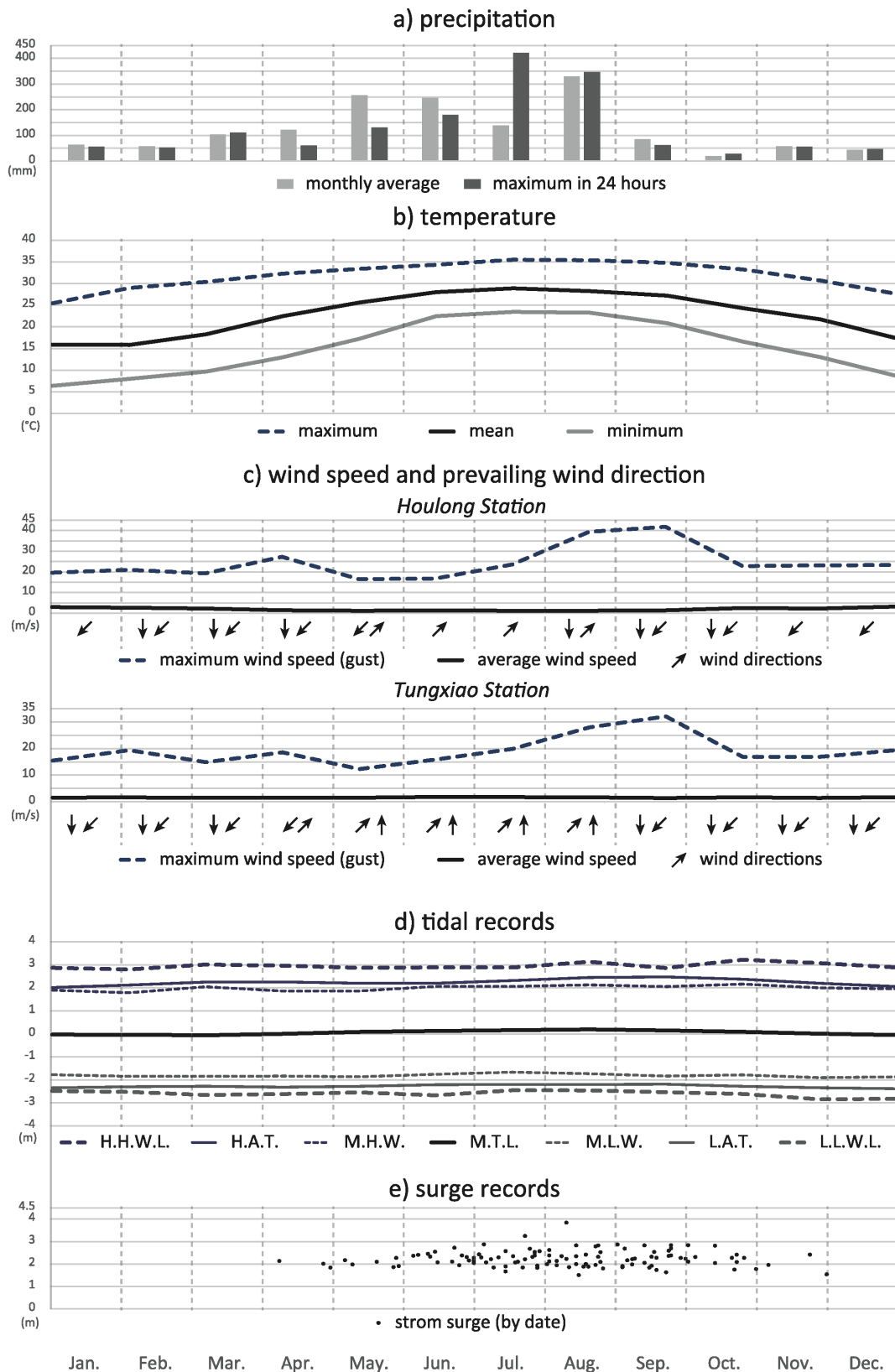


Figure 2.5: The climate statistics of the Miaoli Tableland. The records of the Tungxiao Weather Station were collected from the climate database of the Central Weather Bureau (2022). In order to show landform's affects to the prevailing wind directions and wind speed, wind records of the Houlong Weather Station were included for comparison. The tidal data was collected from the nearest tidal station (the Waipu Station, 2 km north from the Miaoli Tableland), including the tidal statistics and the surge records during storm and typhoon events.

Table 2.1 Records of the severe typhoon events in the Miaoli Tableland (from 2000)

typhoon	year/month	total precipitations (mm)	duration (hr)	average precipitation (mm/day)	Gust wind speed (m/s)
Xangsane (象神)	2000 / 11	165.5	49	81.1	43.3
Toraji (桃芝)	2001 / 7	362.5	82	106.1	27.8
Nari (納莉)	2001 / 9	672.0	154	104.7	27.2
Haitang (海棠)	2005 / 7	187.0	85	52.8	41.9
Matsa (馬莎)	2005 / 8	198.5	71	67.1	21.5
Bilis (碧利斯)	2006 / 7	153.5	72	51.2	30.4
Krosa (柯羅莎)	2007 / 10	234.0	79	71.1	46.4
Kalmaegi (卡玫基)	2008 / 7	186.5	64	69.9	27.4
Sinlaku (辛樂克)	2008 / 9	477.5	127	90.2	30.7
Jangmi (薔蜜)	2008 / 9	211.0	73	69.4	46.1
Morakot (莫拉克)	2009 / 8	278.5	106	63.1	41.3
Saola (蘇拉)	2012 / 8	446.0	91	117.6	33.3
Soulik (蘇力)	2013 / 7	423.0	63	161.1	31.9
Tranmi (潭美)	2013 / 8	214.5	46	111.9	24.6
Kong-Ray (康芮)	2013 / 8	210.0	58	86.9	16.6
Soudelor (蘇迪勒)	2015 / 8	128.5	70	44.8	28.0
Megi (梅姬)	2016 / 9	35.0	67	12.5	32.1
Haitang (海棠)	2017 / 7	23.5	21	26.8	18.1
Nesat (尼莎)	2017 / 7	98.5	50	47.3	19.9
Mitag (米塔)	2019 / 9	20.0	51	9.4	16.4
In-Fa (烟花)	2021 / 6	128.5	62	49.7	13.5

Reference: Central Weather Bureau (2022)

https://rdc28.cwb.gov.tw/TDB/public/warning_typhoon_list/

2.5 The fluvial systems and previous ideas/models of landform evolution developments

The Miaoli Tableland is drained by four main rivers and nine local fluvial systems (Table 2.2). The Houlong River and the Da'an River originating from the Xueshan Range are the main source of yielded fluvial sediments for the Miaoli Tableland (Chang et al., 1998; Teng, 1996b) (Fig. 2.1). The Wumei (Xihu) River originating from the Western Foothills passes the southeastern to the northwestern part of the study area (Fig. 2.1). The Tungxiao River originating from the escarpment between the LH and the LT in the southeastern part of the study area flows toward the Taiwan Strait through the central and western part (Figs. 2.1 and 2.2b). The other nine local fluvial systems (i.e. Yuanli River, Fangli River, Nanshi River, Guogang River and etc.) are all developed in the Miaoli Tableland, with the watersheds' size ranged from 10 - 90 km² (Fig. 2.1 and Table 2.2). The gradients of the main streams range from 0.1° to 0.2°; the tributaries and gullies are steeper with gradients up to 8.0° (Fig. 2.6).

Table 2.2 The fluvial systems in the Miaoli Tableland

name	length (km)	catchment area (km ²)	slope (%)	low (m asl)	high (m asl)	remark
Wumei (Xihu) River / 烏眉(西湖)溪	29.5	109.9	2.19%	0	848	
Tungxiao River / 通霄溪	14.2	88.4	2.46%	0	460	
Fangli River / 房裡溪	13.5	42.4	2.08%	0	407	
Yuanli River / 苑裡溪	15.1	16.1	3.64%	0	438	
Local catchments / 地方水系	up to 4.2	up to 6.08	1.65%	0	94	
Houlong River / 後龍溪	29.0	135.9	0.55%	0	160	down stream section only
Nanshiken River / 南勢坑溪	13.2	23.5	1.08%	2	168	tributary of the Houlong River
Da'an River / 大安溪	17.52	104.68	0.98%	0	172	down stream section only

The fluvial channels of the Wumei River at the LH (Sanyi, Tongluo) and the channels of the Tungxiao River located to the west of the escarpment (Tungxiao, Yuanli) have developed parallel fluvial patterns with linear orientations (Figs. 2.1 and 2.6). On the other hand, the channels at the LT and the rest areas have developed dendritic patterns (in Tungxiao, Xihu) (Figs. 2.1 and 2.6).

The fluvial valleys in the middle and downstream areas are relatively wide (ca. 1km wide) comparing to the size of the active fluvial channels (<10m), which are constrained by the flood plains (FT) mostly (Fig. 2.1). The discharge of the rivers in the Miaoli Tableland has a very significant seasonal difference, as precipitations are mainly happening in summer and autumn, especially during the tropical storms and the typhoon events that provide massive precipitations and trigger subsequent severe floodings (Central Weather Bureau, 2019a, b; The Taiwan Provincial Weather Institution, 1959) (Table 2.1). The floodings happen not only in the main streams but can also happen in the tributaries, such as the case of the flood event in 1959 (The Taiwan Provincial Weather Institution, 1959). The floodings had yielded sediments from the LH to the further downstream areas, which caused that the fluvial channels in the middle- and lower- streams were covered by

gravels and cobbles. This process has resulted in the forming of braided channels in the middle- and lower-streams, only the Nanshi River is an exception that has formed meanders alongside the axis of the Tongluo Anticline.

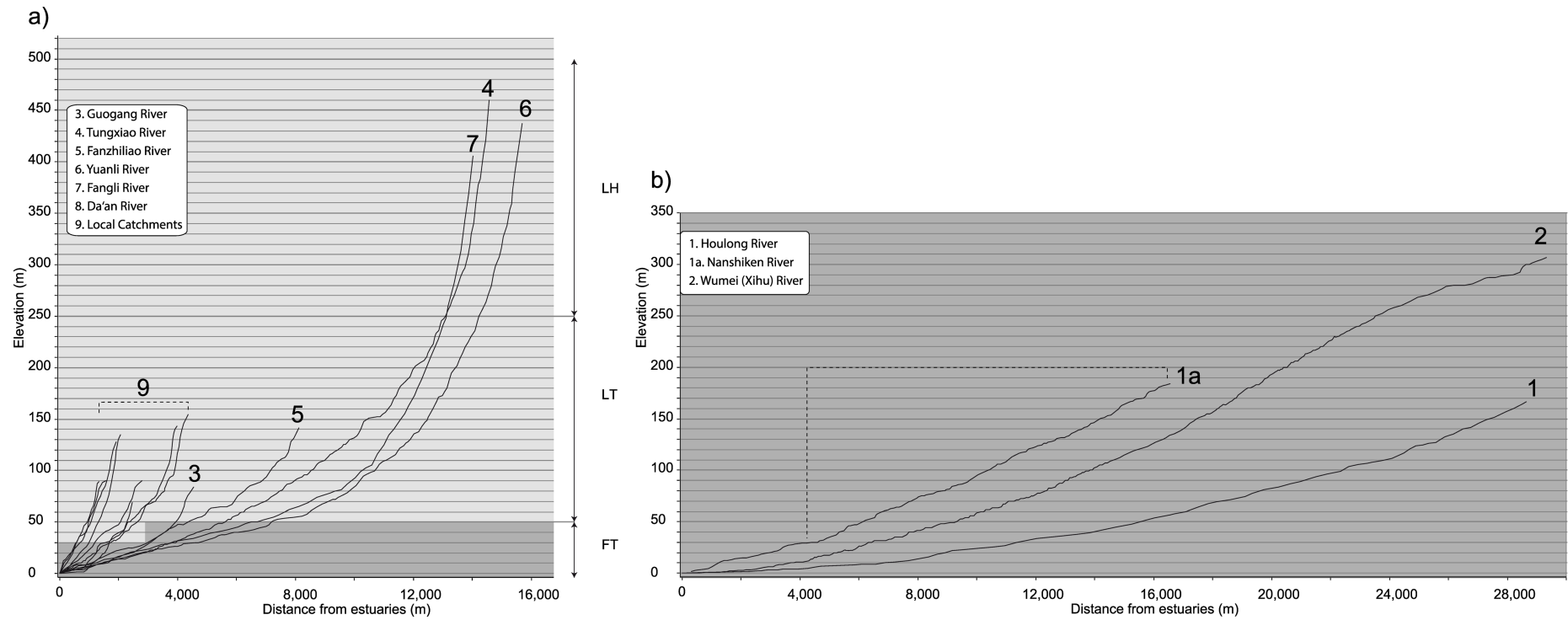


Figure 2.6: The longitudinal profiles of the fluvial systems in the Miaoli Tableland. a). the local rivers that originating in the Miaoli Tableland area. b). the trunk rivers that originating outside the Miaoli Tableland area (in the WF and the Xueshan Range).

The morphological evolution of the Miaoli Tableland was interpreted by two models (Figs. 2.2c and 2.2d):

The first model was proposed by Chang et al. (1998). The fluvial sediment yields of the (palaeo-) Houlong River, (palaeo-) Wumei (Xihu) River and (palaeo-) Da'an River had formed jointed alluvial fans in the foreland basin. These alluvial fans were extended along the palaeo fluvial paths by the continuously yielding of sediments. Subsequently these alluvial fans were uplifted by a thrust, and then the succeeding fluvial incisions resulted in the forming of the tableland segments of the LH (Fig. 2.4). The (palaeo-) Houlong River was cut-off by the uplifting of LH tableland segments in the present day Tongluo area, and its fluvial path had been divided into two separate branches flowing to the Taiwan Strait (Fig. 2.2c). The branch at the west had been converted by the (palaeo-)Wumei (Xihu) River in Tongluo area, which is the downstream section of the present day's Wumei (Xihu) River. The eastern branch has continuously down-cut into the sedimentary successions and formed the fluvial channels of the present-day Houlong River (Fig.2.6). The Tungxiao River catchment was assumed as a huge palaeo-bay of the (palaeo-) Taiwan Strait, due to this area is much lower than the LH tableland segments (Fig.2.1). The LH sediments were yielded by the Tungxiao River and redeposited along the palaeo-fluvial paths as secondary alluvial fans in the palaeo-bay (Fig. 2.3). Ongoing uplift and fluvial incisions have dissected the extended alluvial fans at the north (Wumei R.) and the secondary alluvial fan at the west (Tungxiao R.), and have resulted in the tableland segments of the LT (Chang et al., 1998). A detailed geochronology framework was not established yet, and an early Pliocene to present-day time span was given to this model.

The second model was proposed by Ota et al. (2006), which assumed that the Neogene foldings and thrusts caused differentiated uplifts of the palaeo alluvial fans in the foreland basin (Fig. 2.4). The uplifting at the vicinity of the Tungxiao anticline was more rapid than the surroundings (Fig. 2.4). The gravels and cobbles of the palaeo alluvial fans were reworked from the vicinity of Tungxiao Anticline toward east (the LH segments) and west (the LT segments by the coast) separately. The loose, fine grained sedimentary layers were subsequently exposed in the vicinity of Tungxiao Anticline, they were less resistant to the erosion than the gravels and cobbles (Figs. 2.3 and 2.4). The different resistances of these sedimentary layers resulted in the topographic inversion of a hilly landscape that associated with differential erosion in the perpendicular direction (W-E) of the Tungxiao Anticline. Thus the redeposited gravels and cobbles had formed the cover layer overlain the tableland segments. The subsequent thrust movements of the Tongluo Fault and the Tongluo East Fault had uplifted the LH tableland segments. The latest thrust in the west of the Tongluo Thrust Fault (this tectonic feature was identified by Chang et al., 1998) has uplifted the LH tableland segments even more rapidly, and has caused the tributaries of the Wumei (Xihu) River had been beheaded and had changed their flow directions from west to northeast (Fig. 2.4 and 2.6). It was assumed that the Neogene foldings and thrusts movements began around 3 Ma ago (Ota et al., 2006).

2.6 Human activities and local history

Historically the Miaoli Tableland area was the territory of the aboriginal people (Taokas People / 道卡斯族) before the 17th century. The Taokas People founded tribes that were located at the FTs in the present-day Miaoli-City, Houlong and Tungxiao areas (Chang, 2007) (Fig. 2.1). These Taokas tribes depended on hunter-gathering and extensive agriculture as their economic substance (Huang, 2007). The etymology of Miaoli (苗栗) is originated from the Taokas name of “Pali” (i.e. plain) (Chang, 2007; Huang, 2007). When the European and the Chinese colonists controlled the western and the coastal areas (present-day Houlong and Tungxiao areas) by the end of 17th century, the local name “Pali” was changed into the Chinese pronunciation as Maoli (貓狸) in the beginning (Huang, 2007). In the 18th century, the Qing-Dynasty separated the Chinese settlements and the aboriginals tribes by the Tu-Niu Trench (土牛溝) in the present-day Miaoli-City, Xihu Tungxiao and Yuanli areas as the physical boundary between the Qing-Dynasty territory and the Aboriginal territory (番界) (Chang, 2007; Huang, 2007; Tu, 2007) (Figs. 2.1 and 2.7). The local name Maoli (貓狸) was further changed into Miaoli (苗栗) in the later 19th century (Huang, 2007).

By the end of the 19th century, in order to defend the invasion of the Japanese Empire in 1874 (牡丹社事件), the Qing Dynasty had given up the Tu-Niu Trench and subsequently the Miaoli Tableland area was totally occupied by the Chinese settlers with intensive traditional agriculture developments since then (Huang, 2007; Tu, 2007). The first batch of modernization of the infrastructure developments in the Miaoli Tableland were started since the beginning of the 20th century by the General Government of Taiwan (Cheng, 2007). From the first half of the 20th century to the 1970's, the General Government of Taiwan, the Central Geological Survey (CGS), and the Chinese Petroleum Corporation (CPC) had conducted series of geological investigations for petroleum and natural gas resources in the Miaoli Tableland area for economical purposes (Chi, 2007) (Fig. 1.2).

In general, agricultural land use in Miaoli Tableland is less mechanized, mainly due to its hilly landform (Fig. 2.7) (Liu et al., 2007; Su, 2007). For example, the LH tableland segments surfaces are developed for croplands and small settlements are founded adjacent to the fluvial channels (Liu et al., 2007) (Figs. 2.2b and 2.7). The land uses on the LT tableland segments surfaces are mainly for less-mechanized agricultural (i.e. farms, orchards) and light industry (i.e. factories, brickyards) purposes (Liu et al., 2007; Su, 2007); the FT surfaces are mostly occupied by settlements and less-mechanized agricultural usages (fishery ponds and farms) (Liu et al., 2007; Su, 2007) (Figs. 2.2b and 2.7). In the coastal plain, the majority of the sand dunes were already excavated as fishery ponds or constrained by the coastal levees for defending the surges (Huang, 2007; Su, 2007) (Figs. 2.1 and 2.7).



Figure 2.7: Land use map and the location of the Tu-Niu Trench border in the Miaoli Tableland area. The land use categories were simplified into major categories after National Land Surveying and Mapping Center (2016). The locations of the Tu-Niu Trench and passes were digitized after the historical archive of Ko (2001). The Tu-Niu Trench was the physical boundary that separated the Chinese (at west) and Aborigines (at east) settlements.

Chapter 3. A historical review of the stratigraphic nomenclature problems of the Quaternary depositions in the Miaoli Tableland

3.1 Introduction

The domestic stratigraphic nomenclatures were mainly based on each country's own traditions, the earlier theories and conventional analytical techniques. For example, the stratigraphic nomenclature of Taiwan was originally a compilation of field observation records made by the Japanese geoscientists since the beginning of the 20th century (Chang, 1948a, b; Ho, 1947a, b; Lin, 2020). However, it was totally rewritten from Japanese into Chinese after 1945, due the change of political sovereignty in Taiwan after the Second World War (Chang, 1948a, b; Ho, 1947a, b). The Chinese and the Taiwanese geoscientists had made certain redefinitions of the nomenclature during this period, and then the subsequent evolution of the nomenclature in the latter half of the 20th century was under the Chinese and Taiwanese geoscientists' influences (Chang, 1953, 1955a; Lin, 2020). In fact, the stratigraphic nomenclatures became more and more complicated due to the intention for making more detailed definitions of the strata (Ho, 1990; Lee, 1990). However, the geoscientists mixed both lithostratigraphy and chronostratigraphy methods to invent new stratigraphic definitions, this had caused confusions of the methodological structures and also had made numerous ambiguous statements (Ho, 1990; Lee, 1990). Even though the first version of the International Stratigraphical Guidelines was already published in 1974, the implementation of these guidelines to revise the Taiwanese stratigraphic nomenclatures was initialized not earlier than 2004 (Yuan and Lin, 2009). The procedure of revision is still under discussion, thus the current stratigraphical nomenclatures used in Taiwan has kept the original definitions from the middle to later- 20th century archives.

The reviewing of the stratigraphic nomenclatures of the Miaoli Tableland's strata included the historical literatures from the first modernized geological record published in 1897 to the present day. The sources of data are the online data archive of the Central Geological Survey; the bibliotheca of National Taiwan University (NTU), National Kaohsiung Normal University and Freie Universität Berlin; and the official website of the official journal of the Geological Society of China "Geological Review, -地質論評". The investigation reports, research articles and geological maps (including the explanation manual) were written in Japanese, Chinese and English. For the texts that were written in bilingual versions, the English version was chosen. This study did not use any unauthorized data (i.e. theses, personal communications, unpublished materials, non-peer reviewed second hand reports) or access to the data sets by illegal measurements. A statement of the proposed revision of the stratigraphic nomenclatures of the Miaoli Tableland's strata according to the International Stratigraphical Guidelines is given in chapter 8.6 of this thesis.

3.2 Historical evolution of the stratigraphic nomenclatures of the Miaoli Tableland's strata

This chapter reviews the historical evolution of the stratigraphic nomenclatures of the Miaoli Tableland's strata by three Taiwanese historical stages: the Japanese ruling time (1895-1945), the transition from the Japanese system to the Chinese system (1945-1949), and the Republic of China time (1949-present). All local names were written according to the romanization of Chinese / Japanese spellings for consistency through the following text.

3.2.1 The Japanese ruling time (1895-1945)

The modernized geological investigations in Taiwan were started at the beginning of the Japanese ruling of Taiwan time in 1895. The initial investigations were carried out by the governmental side for example the Japanese Imperial Army and the Government-General of Taiwan, and subsequently private enterprises and geoscientists from Japan and the western countries conducted their own investigations for specific purposes (Chang, 1948a, b; Ho, 1947a, b; Lin, 2020). These initial investigations were more focused to analyze the spatial distribution of natural resources, rather than to summarize the stratigraphy of the whole Taiwan Island (Chang, 1948a, b; Ho, 1947a, b).

The first publication was based on the investigation carried out by Ishii in 1897 (recorded in: Yen et al., 1947). Ishii's contribution was to make a direct comparison of the lithological characteristics between Taiwan and Japan, and then gave an initial framework of the stratigraphy of Taiwan. Ishii's interpretation assumed that the strata in Taiwan are mostly lithified, even the unconsolidated sedimentary layers were described as rocks too. The strata in the Miaoli Tableland and the surroundings areas were defined as Neogene sedimentary rocks initially (Chang, 1948b; Ho, 1947b; Yen et al., 1947). Ishii's assumption has been referenced onwards by the succeeding works as an overall precondition that the loose sedimentary layers are tended to be interpreted as weathered bedrocks (Chang, 1948b, 1955b; Ho, 1947b; Ho, 1988).

The succeeding investigations between the 1910s and 1930s were mostly carried out by the Bureau of Productive Industries in the Government-General of Taiwan, this working group had proposed the early versions of stratigraphical nomenclatures for describing the strata in mid-low altitude areas in western Taiwan (Chang, 1948b; Ho, 1947b; Ishizaki, 1942a; Yen et al., 1947). For example, further investigations by other geoscientists provided more detail definitions of the strata in the Miaoli Tableland, such as the contributions of Deguchi in 1910, Ichikawa in 1926, and Tan in 1929 (recorded in: Chang, 1948a, b; Yen et al., 1947) and Oinoue in 1928 (recorded in: Ishizaki, 1942a). Albeit these definitions were slightly changed by the differentiated aspects of each geoscientist, Ishii's interpretation that the sedimentary "rock" strata were equivalent to the late Neogene rock strata in Japan was followed in general. In the 1930s, the working group started to define the stratigraphical nomenclatures in a more detailed sense for the publications of the

geological maps in local scales. Several detailed definitions of the sedimentary succession among the tablelands of western Taiwan were published by Ando in 1930 (recorded in: Ishizaki, 1942b; Yuan and Lin, 2009), Torii and Yoshida in 1931 (recorded in: Ishizaki, 1942a), Makiyama (1934 and 1937), Oizuka in 1936, Nakamura in 1937 and Ooe in 1938 (recorded in: Yen et al., 1947). At the meanwhile, the newly founded Taihoku Imperial University (TIU) had organized a new working group of geoscientists (geological working group, school of science) since 1927. The TIU working group had more focus on academic research of the geological characteristic of Taiwan, rather than to focus on only the economic goals (Chang, 1948b; Ho, 1947b), for example, Tan (1931, 1933 and 1937) and Yabe and Hanzawa (1930) (recorded in: Chang, 1948b; Ishizaki, 1942f; Yen et al., 1947) have analyzed the fossil contents in the sedimentary successions of the tablelands in western Taiwan for interpreting the palaeo sedimentary environments. The succeeding works of Lin (1937), Tomita (1936), the TIU institute of geological study (1936) and Hayasaka (1935) (recorded in: Chang, 1948b; Ishizaki, 1942a, b, d) had further focused on the interpretations of the fluvial sediments (i.e. gravel and cobble beds) on the top of the tablelands' strata. The TIU working group's interpretations were mostly comparable and generally in agreement with the interpretations of the Government-General of Taiwan working group.

The contributions of Hayasaka, Lin, Makiyama, Tan and Torii are the early studies that had directly analyzed the strata in the Miaoli Tableland (tentatively call Miaoli / Byoritzu Hills by that time) and the surrounding areas. Hayasaka, Lin and Tan investigated the thick layering of gravel and cobble beds exposed in Toukoshan / Takazan area (20km southwest from the Miaoli Tableland) (Fig. 2.3, and 2.4), and proposed a new definition "Takazan Gravel Bed (Tz)" to describe these thick layering of gravel and cobble bed(s) (recorded in: Ishizaki, 1942d). Hayasaka carried out detailed fossil content analyses of the samples taken from the surrounding Dongshi / Tosei area (in Taichung, 15km southwest from the Miaoli Tableland) and revised the detail descriptions of the relative chronology of the "Takazan Gravel Bed" (recorded in: Chang, 1948a). Subsequently Torii described the thick layering of gravels and cobbles depositions at the surrounding of Miaoli / Byoritzu and the Dongshi / Tosei areas (20km east from the Miaoli Tableland) as a part of the "Takazan Gravel Bed(s)" (Torii, 1935) (Fig. 1.3, and 2.3).

In the meanwhile, Makiyama carried out detailed investigations of the mineral resources in the Miaoli Tableland area, including the Tongluo / Dora, Tungxiao / Tûsyô, Xihu / Saiko, Yuanli / Enri, and Sanyi / Sansa areas (Figs. 1.2 and 2.1). Makiyama summarized the investigation records and proposed a new specific stratigraphic unit "Tungxiao/ Tûsyô Formation (Ty / Ts)", due to the type locality is in Tungxiao / Tûsyô area (Figs. 2.1, and 2.3), for describing the Miaoli Tableland's strata in the publications of geological maps (Makiyama, 1934, 1937). The Ty / Ts Formation were summarized as a succession with marine/coastal fine-grained sedimentary strata on the base covered by fluvial gravel and cobble bed(s), and a cover layer of "laterite" ochre-colored soils at the surface. Thickness of the Ty / Ts Formation was assumed to be up to

hundreds of meters. However, the geochronological framework of the Ty / Ts Formation was not available yet by the time. On the other hand, the thick layering of the gravel and cobble beds near the Fire Mountain were separately classified as the Takazan Gravel Bed (i.e. Toukoshan Gravel Bed in Chinese), following the interpretations of Lin, Hayasaka and Torii (Ishizaki, 1942b, d) (Fig. 2.3). Makiyama had also identified the ochre-color soils at the surfaces in the other tablelands (e.g. Linkou / Rinkou, Taoyuan / Toyen, Zhongli / Chuleki, Yangmei / Yobai, Hukou / Kokou and Hsinchu / Shinteku) in northwest Taiwan, and a specific term “ocher-color soils” were used to describe this fine-earth cover layer exclusively (recorded in: Ishizaki, 1942e; Yen et al., 1947) (Fig 1.3 and 1.4).

The research and investigations in Taiwan were strongly restricted by the war situation in the 1940's, only very limited works were done by the time. Oinouye had summarized the aforementioned 1910's to 1930's interpretations and had illustrated an early version of the whole Taiwan Island's geological map; in this map Oenoue classified the Miaoli Tableland's strata as late Neogene depositions of gravels and cobbles and fine-grained marine/coastal sediments (recorded in: Chang, 1948b; Yen et al., 1947) (Fig. 2.3).

In summary, during the Japanese ruling time, the descriptions of the Miaoli Tableland's strata, investigated and classified by the TIU working group and the Government-General of Taiwan working group, were basically accordant to each other. The Hayasaka, Lin and Tan's interpretation of “Takazan Gravel Bed” (recorded in: Ishizaki, 1942d) was introduced for describing the thick layering of the gravel and cobble beds at the Fire Mountain (Fig. 2.1 and 2.3). The sedimentary successions of the marine/coastal depositions, the gravel and cobble beds and the ochre-color soils cover layer on the topographical surfaces were classified according to the Makiyama's interpretation (the Tungxiao/ Tûsyô Formation) (Fig. 2.3). The fossil contents were analyzed not only for interpreting the depositional environments but also as the key information for estimating the chronology of the depositions. The assumptions of relative chronology of Neogene were given to the Miaoli Tableland's strata according to the results of biochronology analyses (Ishizaki, 1942f; Makiyama, 1934, 1937).

3.2.2 Transition from the Japanese system to the Chinese system (1945 to 1949)

After Japan surrendered in August 1945, the sovereignty of Taiwan was transferred from a Japanese colony to be a province of the Republic of China (R.O.C.). By the decision of Chiang Kai-Shek / 蔣介石 and the central government of the R.O.C. in Nanjing, China, all Japanese geoscientists and technicians in the Government-General of Taiwan received the command to return to Japan immediately (Ho, 1947b). On the other hand, certain Japanese geoscientists were allowed to stay in the National Taiwan University (NTU / 國立臺灣大學) (which had succeeded the dismissed Taihoku Imperial University, TIU / 臺北帝國大學) for teaching, but their participations in research works were strictly restricted onward (Ho, 1947a). Conversion of the stratigraphical nomenclatures from the Japanese system to the Chinese system was inevitable, the central

government of the R.O.C. had further deployed Chinese technicians and geoscientists to succeed the ongoing Japanese works in Taiwan since 1945. In fact only very limited new studies of stratigraphy were performed and published at the time, most of these publications were the introductions and reviews of the outcomes during the Japanese ruling time and the direct translations of stratigraphical interpretations for further studies (Chang, 1948a, b; Ho, 1947a, b). These publications were submitted to the official journal of the Society of Chinese Geologists "Geological Reviews / 地質評論", which was based in Nanjing, China at the time.

The Ho's first-hand historical review (1947a, b) had clearly presented overall insights and explanations for the historical developments and the unsolved arguments of stratigraphy in Taiwan, according to the outcomes of the Japanese geoscientists and technicians (Ho, 1947a). Two major arguments for the stratigraphy of the tablelands (Chang, 1948a, b; Ho, 1947a) were summarized, which are related to the stratigraphic nomenclatures used for the Miaoli Tableland's strata:

1. According to the biochronology analyses of the fossil contents, the tablelands' strata were all defined as late-Neogene sedimentary "rocks" (Fig. 1.2).
2. Due to the complicated nature of the tablelands' strata, each technician / geoscientist had used its own terms to describe the strata in each locality independently, therefore, an overall and unified stratigraphic nomenclature was not yet summarized by the time.

Chang had summarized the outcomes between 1897-1944 and had proposed a draft of the revised stratigraphic nomenclatures for the whole Taiwan Island. Chang's revision had introduced the idea for combining all Tertiary-Quaternary strata of the tablelands, which were independently studied and defined by the Japanese geoscientist. This newly invented stratigraphical unit was assumed to be the index stratum for all the tablelands in west Taiwan- the Toukoshan Formation (Chang, 1948a). For instance, Chang had additionally invented a new rank "Facies" as the sub-rank of "Formation", and had downgraded the Takazan Gravel bed and the Ty / Ts Formation into this new rank. The gravel and cobble beds, which were defined as the Takazan Gravel Bed and upper section of the Ty / Ts Formation previously, were combined and redefined as the "Huoyenshan Facies" (Fig. 2.3). The marine / coastal fine-grain sedimentary layers in the middle to lower sections of the Ty / Ts Formation were combined and redefined as the "Hsiangshan Facies", redefined from the Hsiangshan Formation that defined by Torii and Yoshida in 1931 (recorded in: Ishizaki, 1942c) (Fig. 2.3). The geographical names were given by the type localities of each unit (Fig. 1.3).

After 1947, the worsening situation of the Chinese Civil War caused that the research works were almost stopped in the R.O.C. In 1948, Chiang Kai-shek and then the minister of education (Chu, Chia-Hua / 朱家驊) had initiated a special operation "rescuing the scholars / 搶救學人", in order to evacuate the faculty members of the Academia Sinica from the Chinese mainland to Taiwan (Huang, 2010). However, this project was a failure,

because most of the geoscientists in the Academia Sinica refused to be evacuated to Taiwan, and they opted to stay in the Chinese mainland to join the new regime People's Republic of China (P.R.C.) (Huang, 2010). Therefore the geoscientists society in the R.O.C. (Taiwan) faced a devastating loss of its participants and knowledges (Huang, 2010).

3.2.3 The Republic of China since 1949

After the Central Government of the R.O.C. moved to Taiwan in 1949, the geoscientists society started to rebuild with very limited resources. The Central Geological Survey (CGS) and the Chinese Petroleum Corporation (CPC) have taken over the outcomes of the Bureau of Productive Industries of the Government-General of Taiwan to proceed further investigations and researches in the Miaoli Tableland area. The CGS has worked on the geological and stratigraphical investigations and the CPC has worked especially on resources investigations of petroleum and natural gas, in order to support military and economic demands. On the other hand, the NTU has carried out further research based on the findings of the TIU for academic purposes.

The first Chinese version of "Taiwan Geological Map" was published in 1953, the map's manual had included detailed descriptions that are mostly extensive statements based on the previous publications in the 1940's. The statements for the tableland's strata in the 1955 publication were mostly briefings for the definitions and spatial distributions of each stratum, however, statements on i). the unsolved arguments by the Japanese ruling time, ii). the detailed explanations for the logics of revisions, and iii). the newly invented nomenclatures were not stated in detail. For example, Chang had proposed a new unit "Terrace Deposits" that was specialized for describing two cases: i). the thin layering and non-inclined gravel and cobble bed(s) on the tablelands' surfaces that were assumed to be the latest sedimentation processes, and ii). the tablelands' cover layer that consisted of the "laterite" ochre/reddish/dark brownish soils. The intention was to make a separation of these cases from the thick layering or inclined gravel and cobble bed(s) of the Huoyenshan Facies of the Toukoshan Formation, which were assumed to be relatively old and lithified already (Fig. 2.3). In addition, the descriptions in the 1955 text had interpreted the relative chronology based on the fossil content analyses during the Japanese ruling time. Although detail and precise chronological analyses were not available due to the limitation of methodological developments by the time. Thus, the detailed statements of the Toukoshan Formation mentioned that this stratum is the combination of thick layering gravel and cobble bed(s) (the Huoyenshan Facies) and marine / coastal fine-grained materials (the Hsiangshan Facies). These two "Facies" represent differentiated depositional environments that were supposed to have been deposited simultaneously (Chang, 1953, 1955b) (Fig. 2.3).

Later, in 1957, the International Committee of Stratigraphy had published the Lexicon of Stratigraphy to record the stratigraphic nomenclatures around the world at the time (Biq et al., 1957). The volume of Taiwan (i.e.

Formosa) was edited by Biq et al. and included all the existing Japanese and Chinese stratigraphic nomenclatures of Taiwan from 1897 to 1957. This lexicon listed more than 20 units that described the strata in the Miaoli Tableland area. These units are all classified as the same rank in the lithostratigraphic hierarchy “Formation”, but were distinguished by varied spatial scales. In fact the lithostratigraphic hierarchy were not well established initially during the Japanese ruling time and the succeeding geoscientists were tended to invent new definitions to describe the strata rather than to revise the existing definitions (Biq et al., 1957). This had led to confusions for using these existing definitions to describe the strata of the Miaoli Tableland.

In the same year 1957, Lin published an overview book of the morphological interpretations for the landforms in the whole Taiwan Island. In this publication Lin had followed Chang’s interpretation of the Tk Formation to describe the strata in the Miaoli Tableland area initially (Lin, 1957). Later in 1963, Lin investigated an outcrop at the coastal area in the Lungkang village (located besides the Houlong River estuary), and Lin proposed a new stratigraphical unit “the Lungkang Formation (Lk Formation)” to describe the uppermost part (10 to 30 meters) of the sedimentary successions of the Tk Formation exclusively (Lin, 1963) (Figs. 2.1, and 2.3). Lin’s intention of investigations was to summarize the Holocene stratigraphy of Taiwan with “Group” rank in the lithostratigraphic hierarchy that included all the Holocene strata of the whole Taiwan Island, and the “Formation” rank was assumed to be applied for the strata of each locality, such as the case study in the Lungkang village (Lin, 1963, 1969). The radiocarbon dating results of the Lk Formation sediments showed that the dune sand cover layer was deposited at the beginning of the Holocene, but the chronology of the middle and lower parts of the Lk Formation were still unknown at the time, due to the limitations of the early radiocarbon dating methods (Lin, 1963, 1969) (Fig. 2.3). Nevertheless, the Lk Formation was rarely mentioned since then, even in the detailed reviews of the general geology of Taiwan, which was published by Lin and Chou in 1974, the strata in the Miaoli Tableland area were described as the Tk Formation, rather than the Lk Formation.

The succeeding versions of the Taiwan Geological Map were extensive works based on the 1950’s version (Ho, 1975, 1988), hence the strata in the Miaoli Tableland were described as the Tk Formation and the Terrace Deposits. In addition, the term “laterite” was still used to describe the ochre / reddish / dark brownish soils of the cover layer on the tableland segment surfaces. Taiwanese pedologists revised the Taiwanese soil taxonomy according to the USGS soil taxonomy, which was published in the 1970’s (Chen et al., 2015), since then the definition of the term “laterite” has evolved to different meanings for pedologists and geologists. However, the geologists have kept the original early-middle 20th century definition of the term “laterite”, which caused potential confusions for the descriptions of the sediments. In 1984, the biostratigraphical and biochronological analyses gave a Pliocene to Pleistocene deposition age to the Tk Formation (Huang, 1984), which was in accordance with to the previous assumptions from the Japanese ruling time (Fig. 2.3).

In the 1990s, Ho (1990) and Lee (1990) raised critiques about the misuse of stratigraphic nomenclatures in Taiwan. These critiques focused on the arguments that the stratigraphy nomenclatures were systematically misused, several cases of the ambiguous and imprecise stratigraphic nomenclatures were discussed, including the Tk Formation. Ho (1990) and Lee (1990) pointed out that the stratigraphical nomenclatures in Taiwan were hard to be comprehended and studied for comparison with other nomenclatures worldwide, they also suggested a revision of the stratigraphic nomenclatures with a clear historical context, and the revision must be accordant to the principles of the International Stratigraphical Guide (Ho, 1990; Lee, 1990). However, these critiques did not successfully raise systematical reviews and revisions of the stratigraphic nomenclatures in Taiwan, the succeeding works mostly kept the early 20th century stratigraphic nomenclatures.

Even in the recent studies (e.g. (Chang, 1990, 1994; Chang et al., 1998; Ho, 1994; Lee, 2000a; Lee 2000b; Ota et al., 2006; Wang and Peng, 1990)) of the stratigraphy and morphology in the Miaoli Tableland area, the interpretations of Chang (1955a, b) and Ho (1988), based on the definition of the Tk Formation, were followed for describing the Miaoli Tableland's strata: For example, the Huoyenshan Facies was used to describe the thick layering of gravel and cobble beds in the Tongluo, Yuanli and Sanyi area; the Hsiangshan Facies was used to describe all the marine / coastal fine grained sediments and the Terrace Deposits was used to describe the thin layering of gravel and cobble beds, and the term "laterite" was used to describe the ochre/ reddish / brownish soils of the cover layer (Fig. 2.3 and 3.1). The Ty / Ts Formation and Lk Formation were totally forgotten by the studies of the Miaoli Tableland area in recent decades.

The Geological Society located in Taipei raised systematical reviews of the misuse problems of the stratigraphic nomenclatures in Taiwan (Lin, 2020; Yuan and Lin, 2009). A proposal for revisions, which referenced the latest version of the International Guideline of the Stratigraphy, was published by Yuan and Lin (2009) initially. The latest review of the historical evolution of the geological map sets and the stratigraphic nomenclatures in Taiwan from 1897 to present mentioned these unsolved arguments (Lin, 2020). However, the reviewing processes are not finished yet, the revision of stratigraphy terms of the Miaoli Tableland's strata is still under discussion.

3.3 The general remarks of the contemporary stratigraphic nomenclature issues

According to the aforementioned historical review for the stratigraphic nomenclatures, the arguments related to the Miaoli Tableland's strata were about the definition of the Tk Formation, including the Huoyenshan Facies and the Hsiangshan Facies. The arguments and remarks for the issues in the stratigraphic nomenclature of the Miaoli Tableland's strata are as follows:

1). ignorance of the existing definitions, pretending to invent new definitions unnecessarily:

the Toukoshan / Takasan Gravel Bed was originally a specific unit only for describing the gravel and cobble bed(s) in the Toukoshan area, and was applied to describe the gravel and cobble bed(s) at the Huoyenshan area, due to the similarity of lithology in these two localities (Torii, 1935) (Fig. 3.1). On the other hand, the sedimentary successions in the Miaoli Tableland area were already summarized in the detailed statements of the Ty / Ts Formation (Makiyama, 1934, 1937). This means that the Tk Formation, Huoyenshan Facies and Hsiangshan Facies are all invented unnecessarily, as these definitions largely overlapped with the existing ones. New field evidence and new insights of stratigraphical syntheses are recommended to be added to the existing definitions rather than to create new ones (Salvador, 1994), or the stratigraphy nomenclatures are becoming too complicated to be comprehended.

2). the definition of the Tk Formation had mixed the concepts of both lithostratigraphy and chronostratigraphy:

The complicated lithological characteristics of the Tk Formation were interpreted as the result of simultaneous depositions in different sedimentary environments (Chang, 1948a, 1955b). This interpretation was actually based on the concept of chronostratigraphy. However, "Formation" is used for lithostratigraphy only (Salvador, 1994), thus to define an independent chronostratigraphy unit is necessary for this instance (Salvador, 1994).

3). the definitions of the Tk Formation, the Huoyenshan Facies and the Hsiangshan Facies were based on the tentative ideas of lithostratigraphy that are no longer agree with the international guideline:

The original ideas of the Tk Formation were to combine all the Pliocene-Pleistocene strata at the frontal area of the Western Foothills and the tablelands, including the Miaoli Tableland area (Chang, 1955b; Ho, 1988). Chang invented a new rank "Facies" to redefine the Toukoshan / Takazan Gravel Bed and the Tungxiao / Tûsyô Formation as sub-categories of the Tk Formation (i.e., the Huoyenshan Facies and the Hsiangshan Facies)(Fig. 2.3). However, the rank "Facies" is a tentative term that is not included in the guidelines of lithostratigraphy (Salvador, 1994). The suitable ranks for the case that combined several strata of different lithological characteristics should be "Group" or "Super Group", the rank "Formation" is recommended to describe the stratum with homogeneous lithology (Ho, 1990; Lee, 1990).

4). the sedimentary succession may have been included by different units due to the ambiguous criteria:

The outcrop in the Huoyenshan area, which contains the sedimentary succession of the thick layering of gravel and cobble bed(s) covered on the fine-grained sedimentary layers, was defined as the type locality for three different stratigraphical units simultaneously (the Tk Formation, the Huoyenshan Facies, and the Terrace Deposits) (Chang, 1955b; Ho, 1988). In practical the gravel and cobble bed(s) in the Miaoli Tableland area were defined as Huoyenshan Facies (the Tk Formation) (Chang, 1990, 1994; Chang et al., 1998; Ho, 1994; Ota et al., 2006) or Terrace Deposits (Chang, 1990, 1994; Ho, 1994) by each geoscientist. The different usages between these two units are depending on the thickness (thick layering for the Huoyenshan Facies, all the rests for the Terrace Deposits) and the localities (the larger tableland segments for the Huoyenshan Facies, all the rests for the Terrace Deposits) (Chang, 1990, 1994; Chang et al., 1998; Ho, 1994) (Fig. 2.4). These ambiguous criteria are very subjective and made confusions for further analyses during field observations.

5). the type localities are not accordant to the geographical naming of the units and unclear spatial context:

According to the statements from Chang (1953, 1955b), the Tk Formation has two type localities in Toukoshan (Taichung), and Huoyenshan (Miaoli); the Huoyenshan Facies has two type localities in Dadu (Taichung) and Huoyenshan (Miaoli); the type locality of the Hsiangshan Facies is far (48km north) from all the other locations. These facts resulted in imprecise definitions of the units and a lack of consistent spatial and morphological context (Fig. 1.3), which did not follow the principle of geographical naming for lithostratigraphy units. The geographical naming of these units should fit to the hierarchy (Ho, 1990; Lee, 1990; Salvador, 1994), for example Toukoshan and Huoyenshan are the local geographical names, but Hsiangshan is a regional geographical name, therefore the naming of these units is reverse to the spatial context (Fig. 1.3).

In summary, because these early 1950's definitions are no longer in agreement with the latest guidelines of lithostratigraphy, a revision must be taken into consideration (Ho, 1990; Lee, 1990) (Fig. 2.3). A suggestion of revision is listed in the Chapter 8.6. It includes the contemporary discoveries of the geological, the geochronological, and the morphological characteristics of the sedimentary successions in the Miaoli Tableland area, and it follows the historical context, and the principles of the International Stratigraphic Guide (Salvador, 1994).

Chapter 4. Methods

4.1 Methodical approaches of the thesis

This study aims to conduct high-resolution multi-data analyses of the geomorphology, sedimentology, and chronology of the Miaoli Tableland, using methods of geomorphological mapping, field observations, grainsize analysis, borehole data interpolations, and luminescence dating. Geomorphological mapping of different topographical units is applied, for identifying the spatial pattern of tableland segments, and a relative elevation-based classification of these tableland segments is proposed. Field observations of sedimentary layers are combined with particle size analyses for defining sub-types of the sedimentary successions and studying depositional environment changes. Borehole data are integrated to interpolate cross sections of the sedimentary successions for interpreting the tableland morphology, particularly focuses on the successive fluvial erosion and deposition processes. Luminescence dating analyses deliver information to establish geochronological framework of the depositions and to acquire the interplay between paleoclimate and sea-level changes. All these results are combined to give a synthesis of the stratigraphy and the topography, and to reconstruct the morphological processes of the late Quaternary landform evolution of the Miaoli Tableland.

4.2 Morphological analyses

4.2.1 Maps and remote sensing data processing

The maps and remote sensing data are used for identification of the landform features. The maps collected in this study include the topographic maps (National Land Surveying and Mapping Center, 2016), geological maps (Central Geological Survey, 2017b), the soil maps (Chen et al., 2015; Taiwan Agricultural Research Institute, 2016), the land use data (National Land Surveying and Mapping Center, 2016), historical maps (Center for GIS RCHSS Academia Sinica, 2017), the seismic records (Central Weather Bureau, 2022), the bathymetry of the Taiwan strait (Jan et al., 2002) and the tableland segments mapping from previous studies (Chang et al., 1998; Lin and Chou, 1974). These maps are provided by the public open-source database from the Taiwanese Government and the Web Map Tile Service (WMTS) in the GIS (geographical information system) (Center for GIS RCHSS Academia Sinica, 2017; National Land Surveying and Mapping Center, 2016). The paper maps were digitized and imported into the GIS. The coordinate systems and projections of all these map datasets are converted to the World Geodetic System 1984 (WGS 84) / Taiwan Datum 1997 (TWD 97) coordinates for consistency. The high-resolution Digital Elevation Model (DEMs) provided from the Taiwanese Government (Satellite Survey Center, 2018) and the Satellite Radar Topography Mission (SRTM) (NASA JPL, 2013) are used for the raster analyses (e.g. Triangulated Irregular Networks, hydrological calculations and slope calculations) in the GIS. Furthermore, the latest version of satellite imagery is also available from the

WMTS service (National Land Surveying and Mapping Center, 2016), which is used to improve the precision of geomorphological mapping results.

A precise topographical boundary of Miaoli Tableland wasn't defined previously, the first step of data processing in this study therefore is to give a precise definition of the study area. The boundary of the study area is defined by a combination of the lower reliefs (i.e. the coastline and the feet of slopes of the terminal tableland segments) that are located at the surrounding of the higher relief (i.e. tableland segments) (Fig. 2.1). In general, the feet of slopes of the terminal tableland segments are easy to identify, except in the southwest (east and north of Yuanli) and the southeast (south of Sanyi) parts of the study area (Fig. 2.1). The thalwegs of the nearest channels are identified for substitution (Fig. 2.1) in these areas. For example, in the southeast part the boundary of the study area is defined as the thalweg of a branch of the Wumei (Xihu) River in the thrust valley of the Tongluo Fault, and the thalweg of the Yuanli River is defined as the boundary of the study area in the southwest part (Fig. 2.1).

4.2.2 Tableland surface mapping

The flat surfaces of the tableland segments are considered as the remaining of the original palaeo-topographic surfaces of the Miaoli Tableland, which are eroded by the fluvial incisions (Chang et al., 1998; Liu et al., 2022; Ota et al., 2006) (Figs. 2.1 and 2.2). The tableland segments are identified by the flat surfaces that are higher than the surroundings but are not located in the direct vicinity of active fluvial channels (Fig. 4.1). However, the numerical definition of tableland segments was not clearly defined previously, due to the former studies were mostly done by hand mapping based on the field observations of individual geoscientists (Chang et al., 1998; Lin, 1957; Lin and Chou, 1974; Ota et al., 2006) (Fig. 2.2). Thus, to give a simple and numerical definition of the tableland segments is the first step of tableland segment surface mapping. According to the morphological studies of the alluvial fans in Taiwan, the gradient of the modern / active alluvial fan surfaces are mostly lower than 7 degrees (Saito and Oguchi, 2005). Long-term deformation and ongoing tilting of the surfaces affected by the active tectonism (Shyu et al., 2005; Yu and Chou, 2001) must be considered too (Fig. 2.4). In addition, the GIS analyses of the previous mapping results show the identified tableland segment surfaces (Chang et al., 1998; Lin and Chou, 1974; Ota et al., 2006) are inclined up to 10 degrees in general (Fig. 2.2). Combining all the information, a gradient of up to 10 degrees is considered as a reasonable threshold for the mapping of tableland segment surfaces (Liu et al., 2022). On the other hand, the size is another criterion for the mapping of tableland segment surfaces. The previous mappings (e.g. Chang et al., 1998 and Lin and Chou, 1974) had generally included the tableland segment surfaces larger than 1 km², and the minimum size had been not defined (Fig. 2.2). However, these smaller tableland segment surfaces should be included, as they are the remaining parts of the eroded tableland segments (Lin and Chou, 1974; Liu et al., 2022; Ota et al., 2006). The minimum size applied in this study is constrained by DEM's resolution, due to the DEM used in this

study is built up by 20m x 20m square units (Satellite Survey Center, 2018), which equals 400 m², all the tableland segment surfaces larger than this size are mapped.

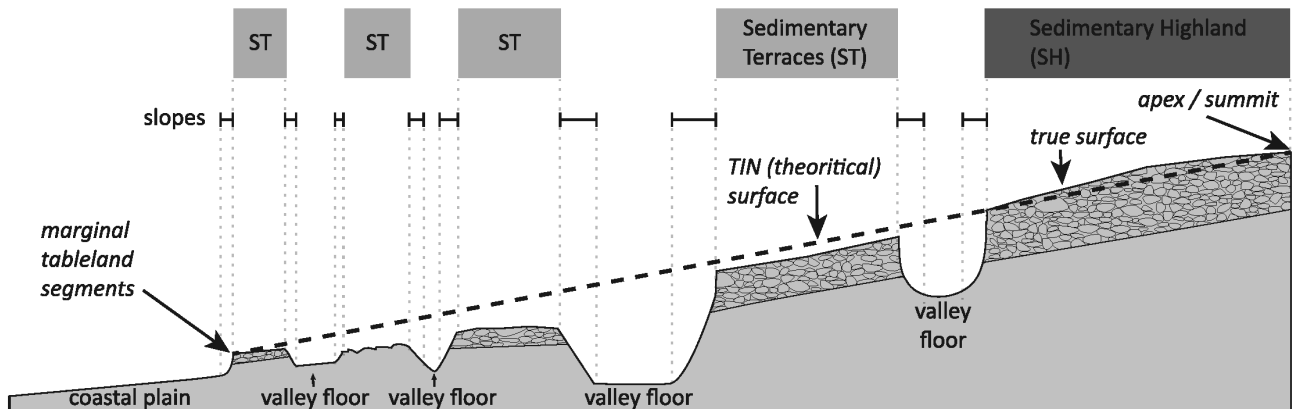


Figure 4.1: The calculation of theoretical linear surfaces and the topographical definitions of landform features in the Miaoli Tableland. The schematical surface profile presents the morphological setting of the Miaoli Tableland from the Sedimentary Highlands to the coast (in E-W direction). The black dashed line represents the “theoretical linear surface” interpolated by the TIN function in the GIS. The apex/summit of this theoretical linear surface is the summit of the Fire Mountain (Huoyenshan), and the margin is the slope of the marginal tableland segments by the coastal plain. The tableland surface classifications are based on the calculation results of the “theoretical linear surface (elevation)” minus the “true surface (elevation)”. The tableland segment surfaces with negative values are classified into the category Sedimentary Highlands (SH); the surfaces with positive values are classified into the category Sedimentary Terraces (ST). Only the tableland segments and remnants are included in this calculation. The slopes, valley floors and coastal plains are all excluded from this calculation.

The detailed mapping of the Miaoli Tableland is processed in the GIS. An adjustment of the “Hillshade” function with the Z-factor of 0.1 is performed on the 20m-resolution DEM (Satellite Survey Center, 2018) in order to enhance the visibility of the tableland segment surfaces. Gradient of the tableland segment surfaces is subsequently calculated in the GIS. The polygons, which marked the tableland segment surfaces, are mapped by hand. Comparing to the automatic mapping function in the GIS, the hand mapping procedure includes the generalization, such as edge smoothing of polygons, by using a simpler approach.

The tableland segment surfaces are identified as landform features which are comprised of i). a gentle flat surface (< 10-degree), ii). the flat surface is higher than the surroundings, and iii). the flat surface is not located in the direct vicinity of active fluvial channels (Fig. 4.1). On the other hand, the flat surfaces in the fluvial valleys, the flood plains of the trunk rivers and the coastal plains are mapped and all these non-tableland segments’ flat surfaces are separately classified as “Alluvial and Coastal Plains (AL)” for the discussions in the following chapters (Fig. 2.1 and 4.1). All the rest surfaces, which are steeper than 10-degree, are defined as “slopes” and they are excluded from the mapping (Fig 4.1).

4.2.3 Classification of tableland surfaces by calculation of the theoretical linear surface

An inferred palaeo-topography of alluvial fans' surface is identified by the 2D (two dimension) mapping result of the spatial distribution of tableland segment surfaces (Liu et al., 2022) (Figs. 2.1 and 2.2). However, due to the landforms are 3D features, interpretations of the vertical dimension (i.e. elevations) must be considered as well (Mather et al., 2017; Saito and Oguchi, 2005). For instance, elevations of the tableland segment surfaces in the Miaoli Tableland are influenced by tectonic thrust movements and subsequent dissection of the palaeo-topography of alluvial fans (Chang et al., 1998) (Figs. 2.2 and 2.4). The traditional classification methods of the fluvial terrace surfaces in Taiwan (Lin, 1957; Tomita, 1953) are based on the weathering degrees of the surface materials and the relative elevations (Fig. 2.2). However, interpretations of relative elevations are given subjectively by the unique perspective of each geoscientist, lacking precise numerical definitions. In order to set a more objective criteria of tableland surface classifications, the approach of theoretical linear surface calculation is provided for a 3D analysis of the relative elevations of the tableland segment surfaces (Fig. 4.1), which is based on the methods applied in the studies of alluvial fans with similar geographical settings (Fontana et al., 2008; Lastochkin et al., 2018; Pierik et al., 2016).

The triangulated irregular network (TIN) was introduced to interpolate palaeo-topography that based on the elevations of the onset alluvial fan surfaces (Volker et al., 2007). The first step is to define the apex of the alluvial fan, which is located at the southeastern part of the study area (i.e. the Fire Mountain). The marginal tableland segment surfaces in the distal areas are defined as the margin of the alluvial fan subsequently (Fig. 2.1). The interpolated-TIN surface represents an inferred palaeo-alluvial fan surface as the "theoretical linear surface" (Fig. 4.1). In the next step, true elevations of the tableland segment surfaces are implied into the calculation of "theoretical linear surface (elevation)" minus "true surface (elevation)" (Fig. 4.1). If the value is positive (the true surface elevation is lower), then the tableland segment surface is assumed to be the redepositions originating from the palaeo alluvial fan. These tableland segments are categorized as the "Sedimentary Terraces (ST)" (Fig. 4.1). On the other hand, if the value is negative (true surface elevation is higher), the tableland segment surface is assumed to be the old, stable, successively uplifted surface that is originated from the palaeo alluvial fan. Due to these tableland segments are higher, they are categorized as the "Sedimentary Highlands (SH)" (Fig. 4.1). This approach allows a topographic related classification of the tableland segments in the Miaoli Tableland, compared to the detailed but subjective traditional classification procedures (Chang et al., 1998; Lin, 1957; Tomita, 1953) (Fig. 2.2).

4.3 Field works

The sampling sites are selected by six steps (Fig. 4.2). First, a total number of ca. 600 potential locations in the Miaoli Tableland are identified by the presence of very steep slopes (>60 degrees) from the DEMs, with an assumption that these sites are outcrops or artificial excavations (Figs. 2.7 and 4.2). The second step is to check the accessibility of all these sites with the topographic maps and the up-to-date satellite images (National Land Surveying and Mapping Center, 2016), the sites with non-accessible conditions are excluded (e.g. private lands, military bases, and other kinds of restricted areas) (Figs. 2.7 and 4.2). In the second step 350 of 600 sites are selected. These 350 selected sites are all compared with the geological maps (Central Geological Survey, 2017b), the soil maps (Taiwan Agricultural Research Institute, 2016), and field records from previous studies (Chang et al., 1998) for recognizing the sedimentary successions (Chang, 1990, 1994; Ho, 1994; Lee, 2000b), and also the tableland segments' morphological status (Fig. 2.2, 2.3 and 4.2). In the third step, the first field observation campaign is carried out to check the physical environment and the vegetation cover of these sites. The outcrops are in unreachable conditions (i.e. located at the opposite site of the fluvial channels without crossing or the actual topography is different from the DEMs) or are covered by dense vegetations are excluded, 120 sites are chosen in this step (Fig. 4.2). In the fourth step, an assessment of representativeness of the sedimentary succession of each site is performed in the second field observation campaign. Only the sites that contain at least two or more sedimentary layers are selected for studying compositions of the sedimentary successions, and the spatial distributions of the different types of sedimentary successions are summarized (Fig. 2.3 and 4.2). In this step, 51 outcrops are chosen, and they are evenly distributed in the study area (Fig. 4.2). In the fifth step, the advanced field works are carried out in these 51 sites, including the detail investigations and sampling in twelve outcrops (see Chapter 5 for the details of the studied outcrops). In ten of these twelve outcrops, the OSL samples are taken additionally in the final step (see Chapter 7 for the details of sampling strategy).

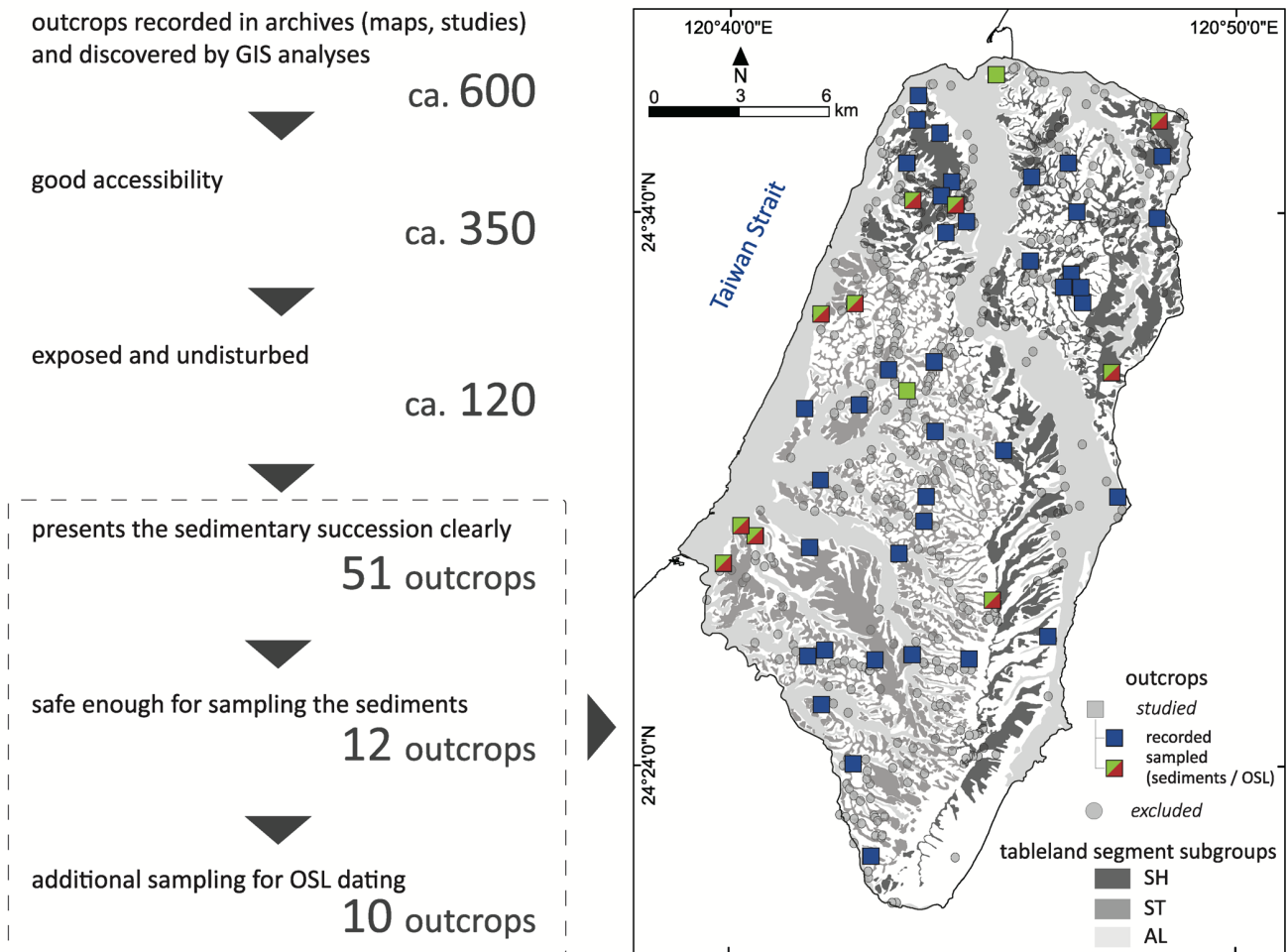


Figure 4.2: The selection procedure of the studied outcrops. The initial raster data (DEMs) analyses show ca. 600 potential sites in the Miaoli Tableland. A three-step selection process is carried out based on accessibility, vegetation cover and disturbances to the sedimentary layers. Finally, 51 outcrops were chosen for studying the sedimentary successions. The twelve sampling outcrops were chosen from these 51 studied outcrops according to the safety concerns. The samples for particle size analyses are taken from these twelve outcrops, and the OSL samples are taken from ten of these twelve outcrops. The map shows the locations of all these studied outcrops and their categories.

The field records describe the sedimentary layers' physical characteristics, including thickness, compositions, weathering degrees, sedimentary structures, and color. The elevations and heights of the outcrops are extracted from the DEMs firstly and are compared with a handheld GPS receiver for calculation of the errors during the field observation campaigns. The sampling for detailed sedimentological and geochronological analyses are carried out for twelve outcrops (Fig. 4.2). These twelve sampling outcrops are chosen according to i). the good accessibility of these sites and ii). the undisturbed sedimentary successions. The outcrops are cleaned before the sampling: ca. 10 to 15 centimeter of the outcrop surface's materials including the plant roots and the colluvial sediments covered on the slope are removed to prevent mixture of different sediments into the samples. Samples for grainsize analyses are taken from each sedimentary layer separately, and the layers more than 3 meters above the slope foot are excluded from sampling due to safety concerns. OSL samples are taken in ten of these twelve outcrops for age determinations of the sediments' last deposition

time (see chapter 7 for details) (Fig. 4.2). For taking the OSL samples, a 5-cm-diameter and 30-cm-long metal cylinder is used as the light-proof container. In addition, ca. 500-600g surrounding matrix materials are taken for gamma-spectroscopy analysis to determine the environmental dose rate. Sampling of the OSL samples focuses on the sediments at the upper and the lower boundaries of the gravel and cobble bed(s) (Liu et al., 2022) (Fig. 2.3, see Chapter 5 and 7 for details discussions of the sedimentary layer CSB). To avoid disturbances of the extra dose attenuation from gravels (Duller, 2008a; Rhodes, 2011), samples are taken by least 30cm from the upper and the lower boundaries of the gravel and cobble bed(s).

4.4 Sedimentological and stratigraphical analyses

The objective of the sedimentological analyses is to figure out the compositions of sedimentary layers for the interpretations of changes to the depositional environments (Fig. 2.3). The particle size composition of each sedimentary layer is studied, the sedimentary successions are identified and compared with the field records of previous studies (Chang et al., 1998; Chang, 1955b; Lin, 1957; Makiyama, 1934, 1937). In addition, the geological maps and the borehole data (Central Geological Survey, 2017a) are combined successively to interpolate a 3D stratigraphical model for interpretations of the morphology of the Miaoli Tableland. This approach opens the possibility of a comparison with case studies in other locations with similar geographical settings (Hanebuth et al., 2013; Ishihara et al., 2012; Pennington et al., 2017; Pickering et al., 2014).

4.4.1 Particle size analyses

Particle size analyses of the sediment samples are performed with a Beckmann-Coulter Laser Particle Size Diffraction analyzer (model: LS-13320), in the laboratory of S3: geochronology in LIAG, Hanover. The samples are sieved with a 2 mm mesh to remove all coarser particles. The sediments are dispersed by adding ammonia solution ($\text{NH}_4(\text{OH})$) to remove the calcite compounds. The samples are set to a rotator for 30 rpm (round per minute) for more than 24 hours to mix the sediments with the solution for homogenizing before measurements.

Each sample is measured five times to reduce the uncertainty caused by laser diffraction (Konert and Vandenberghe, 1997). The samples are additionally measured by an additional run with different measuring sequences. The measurement results of both runs are cross checked with the statistical indexes to validate the reproducibility (reproducing test) (Konert and Vandenberghe, 1997). The result of each sample is presented in a ternary diagram based on the clay-silt-sand compositions. The sedimentary layers are given names separately according to the terminology of soil descriptions from the Food and Agriculture Organization of the United Nations (FAO) (Jahn et al., 2006).

4.4.2 Data processing of the borehole data set

This study uses the open-access borehole data of drilling records of public infrastructure construction projects (Central Geological Survey, 2017a). These data provide information for the spatial distribution of sedimentary layers inside tableland segments and beneath surfaces in fluvial channels, estuaries, and the coastal plain. In these locations, no outcrops are existing (Fig 4.2). The borehole data used in this study are collected from 20 construction projects in the Miaoli Tableland area (Central Geological Survey, 2017a). These selected projects are construction works of the high-speed railway, the motor way, the express way, the electricity network and the power plant in the Tungxiao River's estuary (Central Geological Survey, 2017a) (Fig. 4.3, see Chapter 6 for details). The boreholes of these projects are linear aligned with N-S and W-E directions, they give additional information of the sedimentary layers across all the sub-categories of tableland segments (SH-I, SH-II, ST) also included the AL flat surfaces (Figs. 2.2 and 4.1).

The data of 892 boreholes were evaluated for this study (Central Geological Survey, 2017a). The coordinate systems used for recording the borehole locations are not unified for all the projects. For example, the current standard Taiwan Datum 1997 (TWD97) coordinates and the former standard Taiwan Datum 1967 (TWD67) coordinates had both been used by these projects in the Miaoli Tableland area (Central Geological Survey, 2017a). It is necessary to have a unified coordinate system for all the boreholes therefore the TWD67 coordinates are all converted to the TWD97 coordinates system respectively (Tseng, 1990) (Fig. 4.3). The elevation records of the borehole locations are compared with the elevations extracted from the DEMs, the errors were mostly very minor (less than three meters). If the elevations are apparently different from both datasets (more than three meters), the DEM extracted elevations are taken as the benchmark.

The photos of sediment cores were attached in 80 borehole logs, and the advanced geotechnical tests were proceeded for 658 borehole logs to provide physical characteristics of the sediments for engineering purposes (Central Geological Survey, 2017a). These additional data were combined with the particle size analysis results to interpret compositions of the sedimentary layers and the corresponding coastal and nearshore sedimentary environment changes (Dalrymple and Choi, 2007; Olariu et al., 2012) (Figs. 2.3 and 4.3).

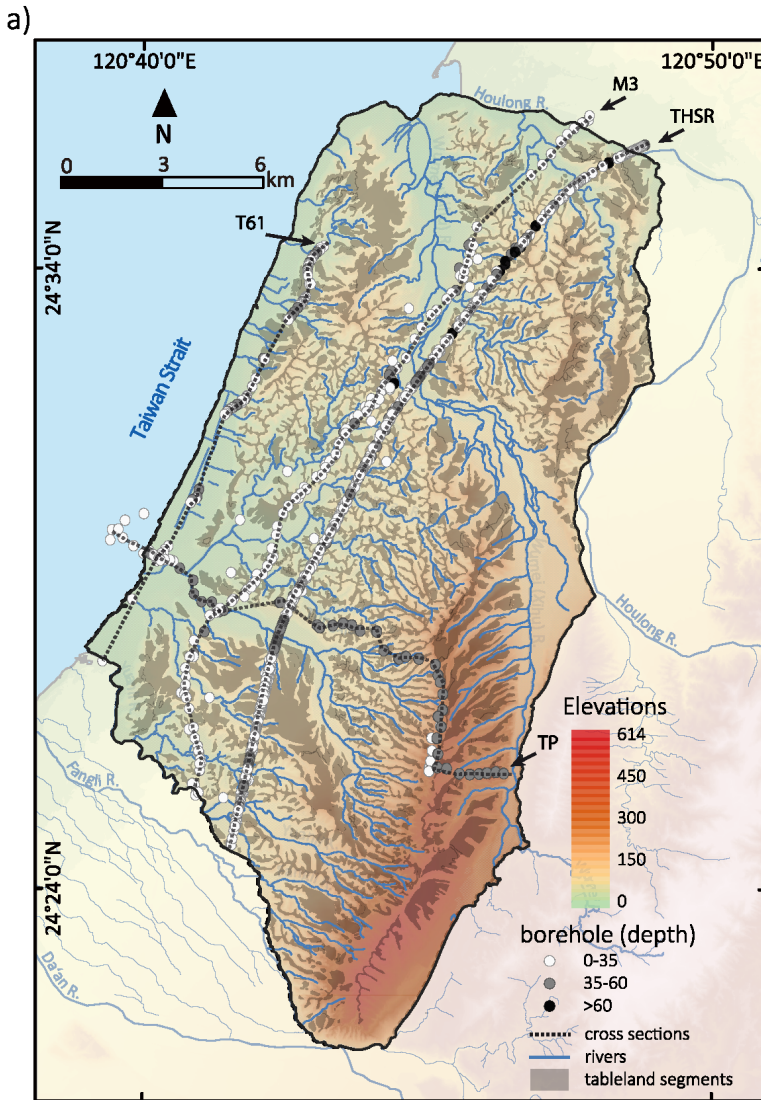
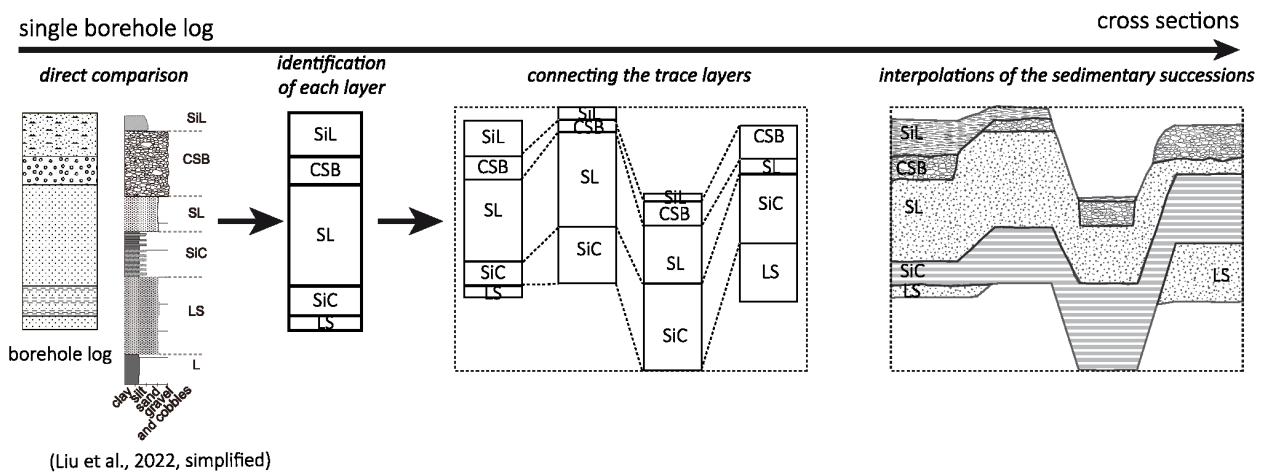


Figure 4.3: Mapping procedures for the cross sections of the Miaoli Tableland that are carried out based on the borehole data.

a). The map presents the locations of borehole logs used in this study. These borehole logs are referenced from four constructions projects and arranged into four cross sections (TP, HSR, M3 and T61). The boreholes have depth for ca. 30 meters mostly.

b). The illustration presents the method of cross section mapping. First the borehole log is directly compared with the sedimentary succession studied by Liu et al., (2022), and then the sedimentary layers are identified according to detail descriptions of the borehole log and the similarity to the descriptions of Liu et al., (2022). The trace sedimentary layers (CSB, coarse sand with stones and boulders (gravels and cobbles) layer; and SiC, alternation of greyish silt loam and yellowish silt loam layers), are applied for connecting the borehole logs. The vacancies in between the borehole logs are directly interpolated.

b) mapping procedure



4.4.3 Cross-section drawing

The cross-sections are drawn from the descriptions of 892 borehole logs in the Miaoli Tableland area (Fig. 4.3). The interpolations of the cross sections are undertaken by high-precision computer drawing, based on the methods implemented in case studies in similar environments such as foreland basins and deltas (Ishihara et al., 2012; Pennington et al., 2017; Tanabe et al., 2003). Four cross sections are built, three in N-S direction and one in E-W direction (Fig. 4.3). The borehole logs obtained in these four cross-sections are around 30 meters deep mainly, which are interpolated to show the spatial correlations of the uppermost 30 meters of sedimentary successions in the Miaoli Tableland area. The spatial correlations among the borehole logs are interpolated according to the similarities of: i). the sediments' physical characteristics, ii). the sedimentary successions, and iii). the reliefs of borehole locations. Interpolations of the sedimentary successions are carried out by the following steps: i). import the basic attributes of each borehole log with a unified coordinate system (TWD-97) and an elevation datum (WGS 84) (Fig. 4.3). ii). identify each sedimentary layer by the comparison with the sedimentary successions that were summarized by the previous studies (Liu et al., 2022) (Figs. 2.2 and 4.3). iii). mark the relevant trace sedimentary layer(s) as indicators to interpolate the spatial correlation of borehole logs that are located in the different parts of the cross sections (Fig. 4.3). For instance, the fluvial sediments (i.e. gravel and cobble bed(s), CSB) are used as the primary trace sedimentary layer; and the intercalation of thin layering of tidal/coastal sediments (SiC) are used as the secondary trace sedimentary layer. iv). combine all four cross sections to build a visualized 3D schematic model of the tableland morphology (Fig. 4.3).

4.5 Geochronological analyses

The luminescence dating is chosen to obtain high-precision age estimations of the depositions in the Miaoli Tableland, because the quartz rich alluvial and aeolian sediments are very suitable materials for this method. The applications of luminescence dating were tested in the case studies of other Taiwanese tablelands and coastal areas, delivering good and robust age estimations within the time span from the last interglacial to present days (Chen et al., 2003b, c; Ho et al., 2017; Ota et al., 2009; Simoes et al., 2007; Wu et al., 2010). A technical difficulty is caused by that the luminescence signals of quartz grains in Taiwan are significantly contaminated with the signals emitted from the intergrown feldspars (i.e. feldspar contaminations), which provide potential overestimations of depositional ages (Duller, 2003). The protocols used in previous studies tested the quartz grains in Taiwan with experimental settings, and these tests delivered reproducible results to conduct good geochronological interpretations (Dörschner et al., 2012; Tseng et al., 2016).

4.5.1 Principles and settings of optically stimulated luminescence (OSL) dating

The stimulated luminescence signals of quartz and feldspar grains are a form of energy that contributed from the absorption of environmental radiation (i.e. equivalent dose, D_e) (Aitken, 1985; Duller, 2008a; Rhodes, 2011) (Fig. 4.4). The luminescence signals are emitted from quartz and feldspar grains by exposure to sun-light or in a high temperature environment (i.e. bleaching effect) (Aitken, 1985) (Fig. 4.4). The D_e steadily accumulates during burial in natural conditions and is easy to reset during transportations, thus the D_e reflects how long the quartz and feldspar grains have been buried since the last deposition (Duller, 2008a; Rhodes, 2011) (Fig. 4.4).

The basic principle of optically stimulated luminescence (OSL) dating is to determine two factors i). the D_e of luminescence signals emitted from quartz or feldspar grains, and ii). the environmental radiation dose rate, measured from the surrounding parental materials. The calculation of the ratio between these two factors gives an estimation of the approximate time span since the grains' last deposition (Aitken, 1985; Duller, 2008a; Rhodes, 2011) (Fig. 4.4). The precision of OSL dating has been assumed to be circa 5% relative to the absolute chronology and no calibration to age estimations is needed (Duller, 2011). On the other hand, a disadvantage of the OSL dating is that its applicational time span is constrained by the capacity of D_e of the grains, for example, a reasonable upper limit of 150Gy (Gray) for the quartz grains has been estimated (Duller, 2003; Duller and Wintle, 2012). This is roughly equivalent to up to 100-120 ka, depending on the variation of environmental dose rates that are influenced by local geographical and geological backgrounds (Rhodes, 2011).

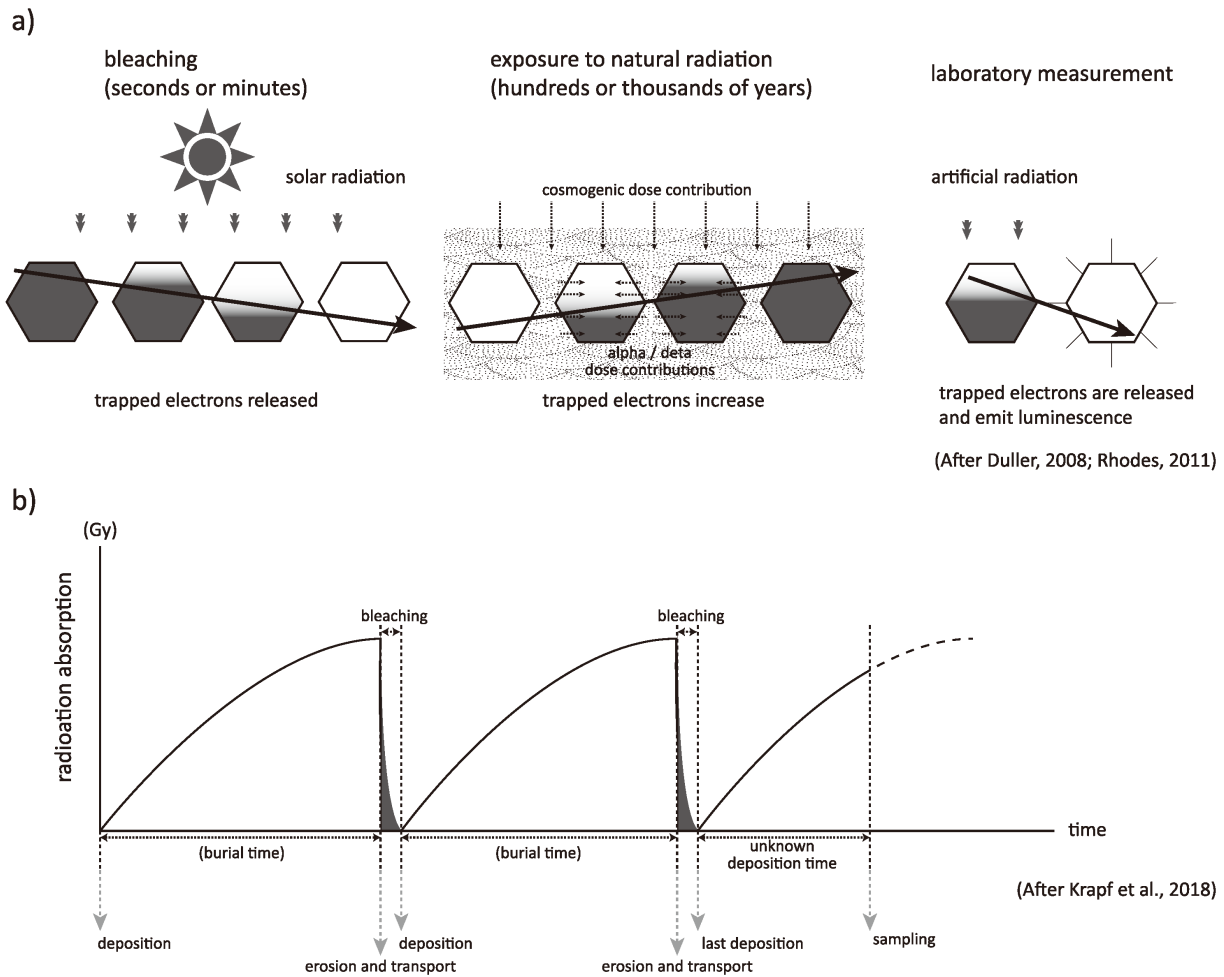


Figure 4.4: The basic principles of optically stimulated luminescence (OSL) dating (after Duller, 2008a and Rhodes, 2011).

a). the solar radiation to the quartz and feldspar grains causes the release of trapped electrons (i.e. bleaching effect). The grains absorb natural radiation after deposition, including the alpha / beta / cosmogenic dose contributions base on the burial time. The trapped electrons are released by the artificial radiation stimulations to the grains, which causes emission of luminescence signals. The intensity of luminescence signals is associated with the absorption of natural radiation (i.e. deposition time).

b). The schematic diagram illustrates the application of OSL dating (after Krapf et al., 2018), which natural radiations are absorbed by quartz and feldspar grains after deposition, the amount of absorptions is determined according to the burial time. The grains are subsequently exposed to sun-light during erosion and transportation, which causes the emission of luminescence signals (i.e. bleaching effect). Thus, the OSL dating could estimate the burial time since the last deposition of the grains.

For older samples, the feldspar-IRSL (infrared stimulated luminescence) dating is considered for application because this method can measure grains with a larger applicational range of up to 300 Gy (Rhodes, 2011). However, the feldspar grains have an unstable luminescence signal, slow-reset behavior and show fading effects on the residual luminescence signal. These physical characteristics significantly affect the precision of the determination of D_e (Duller and Wintle, 2012; Jain et al., 2005; Jain et al., 2004; Rhodes, 2011). On the other hand, the ESR (Electron spin resonance) dating is more time consuming for its measurements, and the experimental settings for measuring samples with different geographical and geological backgrounds are still

under development (Prescott and Hutton, 1994). Therefore the feldspar-IRSL dating and the ESR dating are only used if the samples are not suitable for the quartz-OSL dating (Duller and Wintle, 2012; Jain et al., 2005; Prescott and Hutton, 1994).

All the luminescence dating analyses were carried out in the laboratory of S3-Geochronology in Leibniz Institute for Applied Geophysics in Hanover, Germany. The quartz-OSL dating was applied to give age estimations of the last deposition time of the 20 samples taken from 10 outcrops in the Miaoli Tableland (Fig. 4.2). The laboratory preparations for the OSL samples were finished according to the standardized procedures (Duller, 2008a; Rhodes, 2011) (Fig. 4.5).

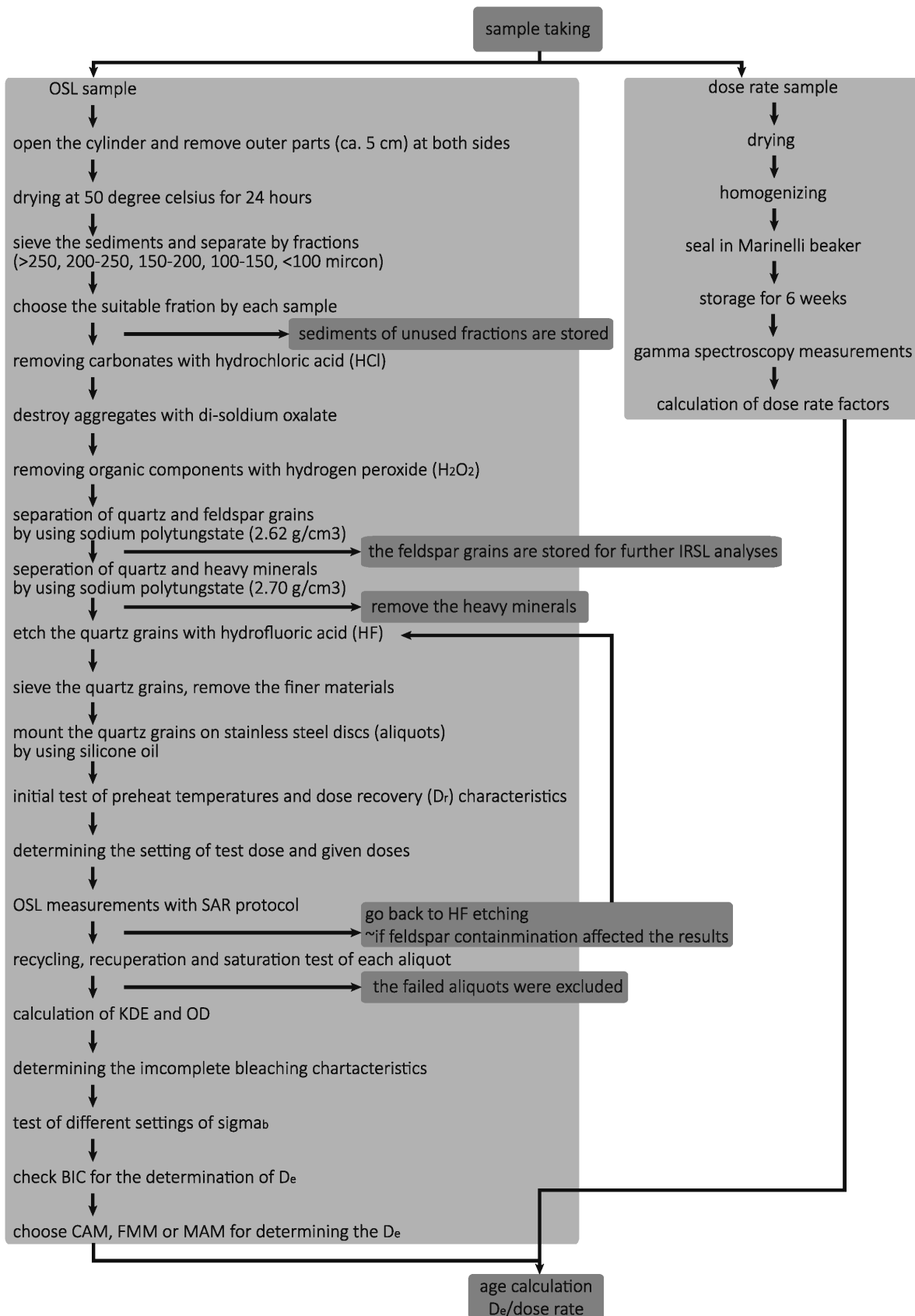


Figure 4.5: The workflow of the OSL dating, from sampling to the final calculation of age estimations of the last deposition time, which includes detailed laboratory procedures and decision-making criteria. The procedures for the OSL measurements are listed on the left side. Information for the dose rate measurements is listed at the right side.

4.5.2 The measurement of environmental dose-rate

The environmental dose is comprised of radiations from the surrounding parental materials (i.e. alpha, beta and gamma radiations) and the cosmic rays (Duller, 2008a; Rhodes, 2011) (Fig. 4.4). The alpha radiation is originated from the Helium atoms, which is mostly negligible because its travel distance is too short (ca. 2 cm) (Duller, 2008a; Rhodes, 2011) (Fig. 4.4). The beta and gamma radiations are emitted from radioactive elements and their isotopes (i.e. Potassium, Uranium chain and Thorium chain) (Duller, 2008a; Rhodes, 2011) which is the main source of the environmental dose (Fig. 4.4). The cosmic rays are radiations that come from sources in the universe (Duller, 2008a; Prescott and Hutton, 1994; Rhodes, 2011) (Fig. 4.4). The absorption of cosmic rays is significantly affected by the depth of the sediments, that is, if the sediments are deeply buried, the cosmic rays' contribution can be very minor (Duller, 2008a; Prescott and Hutton, 1994; Rhodes, 2011). The environmental dose-rate can be measured in the field or in the laboratory, and laboratory measurement is preferred due to better precision and quality control (Duller, 2008a; Rhodes, 2011) (Fig. 4.5). The environmental dose-rate samples, around 700g of parental materials, are separately taken from the OSL samples in the field. For laboratory preparation, the samples are dried for over 24 hours in the oven (at 50 degree Celsius), then sealed in a Marinelli beaker and stored for six weeks to reach the equilibrium state of the radioactive nuclides (Aitken, 1985; Guérin et al., 2011) (Fig. 4.5). The measurement is carried out by using a p-type gamma spectroscopy which analyses the concentration (ppm) of these radioactive elements, the beta dose contribution is calculated by using the conversion parameters for each element (Guérin et al., 2011). The cosmic rays' contribution is determined by the geographical location and depth of the samples. All these dose contributions are finally combined to calculate the environmental dose-rate with respect to the time (Gy/ka) (Aitken, 1985; Guérin et al., 2011; Prescott and Hutton, 1994; Prescott and Stephan, 1982; Rees-Jones, 1995) (Fig. 4.5).

4.5.3 The measurement of equivalent dose by means of the Single-Aliquot-Regenerative dose (SAR) protocol

The measurements of equivalent dose are conducted by using the Single-Aliquot-Regenerative dose (SAR) protocol, which has been widely used for applying the OSL dating to alluvial and aeolian sediments (Murray and Wintle, 2000; Wintle and Murray, 2006) (see Chapter 7). The focus of this study is to establish the geochronological framework of sedimentation processes. The simple SAR protocol with the setting of continuing wavelength - optically stimulated luminescence (CW-OSL) (Murray and Wintle, 2000; Wintle and Murray, 2006) is employed for the measurements (Fig. 4.5). The subsequent adjustments of experimental settings are carried out based on the results of initial test of each sample independently, in order to obtain the best fitting result of the dose regeneration growth curve (Fig. 4.5).

More than 40 aliquots are measured for each sample to prevent random error or biased results that might affect the determination of the D_e . The quality control for measured results included the recycling test, the depletion test and checking the onset of saturation effect (i.e. $2D_0$ test) (Duller, 2003) (Fig. 4.5). The recycling test checks the reproducibility of the luminescence signal by giving the same given dose to the aliquot in multiple runs, if the measured signal intensities are distributed within the error range (10%), then the aliquot passes the test (Fig. 4.5). The recuperation test checks whether extra luminescence signals or residual signals are emitted from the remaining feldspar with the quartz grains on the aliquots, due to these signals could affect reproducibility significantly (Aitken and Smith, 1988). If the majority of aliquots are rejected by the recuperation test, an additional run of etching of the quartz grains to remove the remaining feldspar is considered (Fig. 4.5). The saturation effect occurs when the quartz and feldspar grains had absorbed environmental radiation to their maximum capacity, thus the D_e is no longer increasing respect to burial time (Wintle and Murray, 2006) (Fig. 4.4).

4.5.4 Age model calculations

Determination of D_e for the Miaoli Tableland samples depends on the distributions of records from the aliquots of each sample (Galbraith and Green, 1990; Galbraith and Roberts, 2012) (Figs. 4.5 and 4.6). The statistical analyses applied to determine the D_e values are called age models, the commonly used age models include the central age model (CAM), the finite mixture model (FMM) and the minimum age model (MAM). They were implemented based on different settings of the D_e distributions (Galbraith and Green, 1990; Galbraith and Roberts, 2012) (Figs. 4.5 and 4.6). The required minimum number of aliquots for D_e determination is not a fixed threshold, because reliability and robustness are not directly affected by the number of aliquots (Galbraith and Roberts, 2012; Rixhon et al., 2017). Recent methodological developments in the OSL dating of alluvial and aeolian sediments have given a range of thresholds for reliable D_e determinations with less than 30 aliquots (Galbraith and Roberts, 2012; Rixhon et al., 2017).

The D_e determination results can be diverse by using different age models (Fig. 4.6). The criteria for choosing a suitable age model depend on two factors: the D_e distribution and the overdispersion (OD) (Galbraith and Green, 1990; Galbraith and Roberts, 2012; Rixhon et al., 2017) (Fig. 4.6). For the cases with a unimodal distribution of D_e and a relatively low OD, which are most likely well-bleached samples, the CAM with plus/minus 1-sigma error is taken as the suitable age model of D_e determination (Galbraith and Green, 1990) (Fig. 4.6). On the other hand, for the cases with multimodal and highly skewed distributions of D_e and a higher OD, which may be affected by the incomplete bleaching effect (Jain et al., 2004) (Figs. 4.4 and 4.6), the FMM or the MAM is more preferred as the suitable age models of D_e determination (Duller and Wintle, 2012; Galbraith and Roberts, 2012; Jain et al., 2004) (Fig. 4.6).

The CAM age is based on the weighted mean, which is the simplest approach. On the other hand, the FMM calculates the weighted mean of each cluster of D_e , and the cluster with the minimum OD is assumed to be the best D_e determination result (Galbraith and Green, 1990) (Fig. 4.6). The MAM only calculates the cluster with the minimum D_e , which may contain very limited number of aliquots, so it is preferred especially in cases with a highly right-skewed distribution of D_e (the majority of D_e are very low, but with some data points of very high D_e) (Fig. 4.6). Another approach for choosing the suitable age model depends on the BIC (Bayesian Index Count) (Sivia et al., 2004), with the criterion that the age model that has the highest BIC is assumed to be the best result of D_e determination (Galbraith and Roberts, 2012; Sivia et al., 2004). For example, even in the cases with a multimodal or a highly skewed D_e distribution, once if the BIC reported from the CAM is higher than the BIC reported from the MAM or the FMM, the CAM result is taken for the D_e determination in these cases (Galbraith and Roberts, 2012; Sivia et al., 2004) (Fig. 4.6). For all the D_e determination results in this study, a ± 1 -sigma error is given, which includes the random error from the TL/OSL reader during its measurement of the luminescence signals (Galbraith and Roberts, 2012).

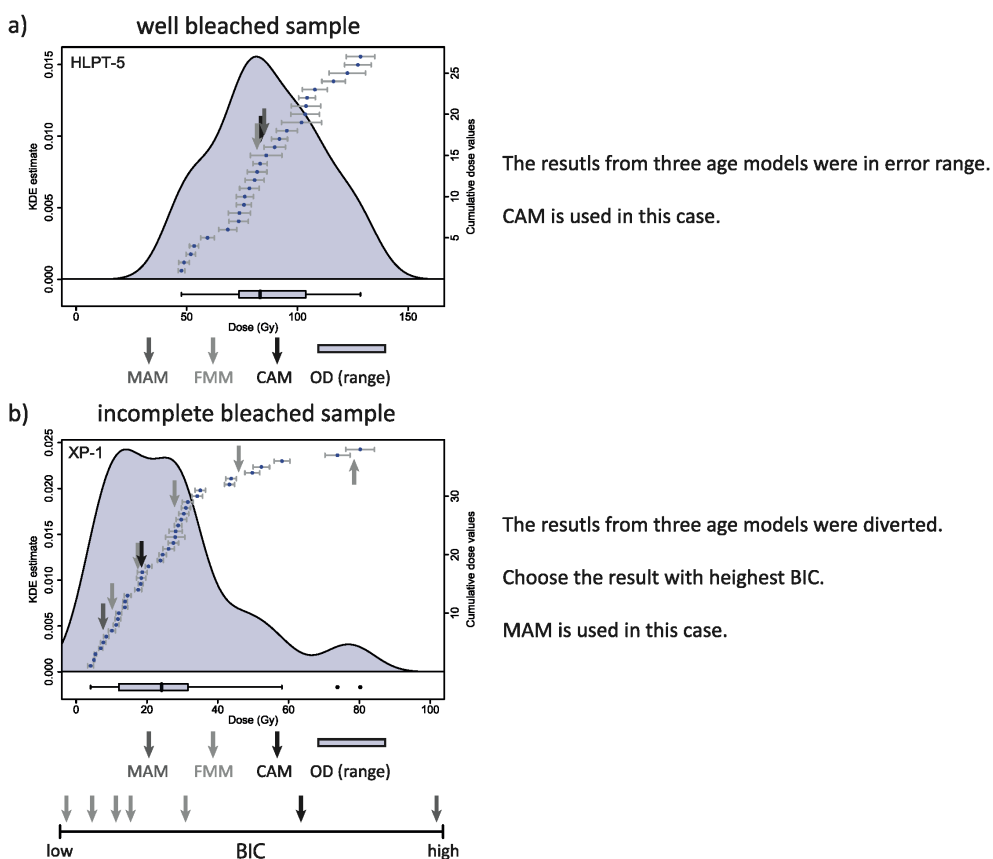


Figure 4.6: The schematic of the age model calculations of the CAM, the MAM and the FMM.

a). an example of the well bleached sample (HLPT-5) with a unimodal distribution of the D_e . The calculations of all age models for this sample are in the error range covered by the OD. Due to the differences among all age models are not significant, the CAM result is used for this sample.

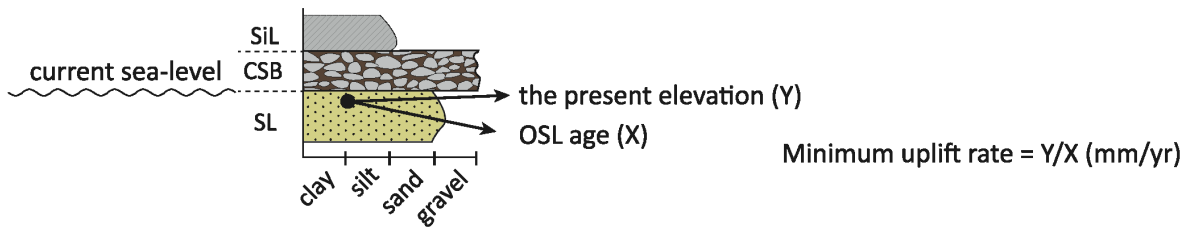
b). an example of an incomplete bleached sample (XP-1), which had a multimodal distribution of the D_e . The calculations of all age models for this sample are different. Totally seven D_e estimations are given from 5 Gy to 82 Gy, one is from the CAM, another one is from the MAM and five are from the FMM. Based on the comparison of BIC in this case, the result of the MAM is used for this sample.

4.5.5 Calculation of the corresponding uplift rates

The age estimations of the tidal/coastal sediments (SL) and the fluvial deposits (CSB) are used to calculate the uplift rates of each outcrop, employing the setting that “the relative elevation in related to the sea-level” divided by “the deposition age” (Muhs et al., 2017; Muhs et al., 2014) (Fig. 4.7). The calculation is based on the premise that the gravel and cobble bed(s) (CSB) were deposited in the near-shore area, these fluvial sediments covered the coastal sediments (SL) and both layers were uplifted subsequently (Figs. 2.4 and 4.7). Because the benchmark for defining the relative elevation greatly affects the calculation results, two benchmarks are applied in the calculation of uplift rates in this study. The first benchmark is to use the present-day sea level height (+/- 0m asl) to estimate the minimum uplift rates (Fig. 4.7). The second benchmark is to use the palaeo sea level heights (from -140 m to +10m, respectively) (Lambeck et al., 2014; Liu et al., 2004; Rabineau et al., 2006; Waelbroeck et al., 2002) depending on the depositional ages of the SL layer, to estimate the maximum uplift rates (Fig. 4.7).

In case if the outcrop doesn't have any dating result, the depositional ages of the identical sedimentary succession from the closest outcrop are referenced for the calculation (Figs. 4.2, and 4.7).

Benchmark I



Benchmark II

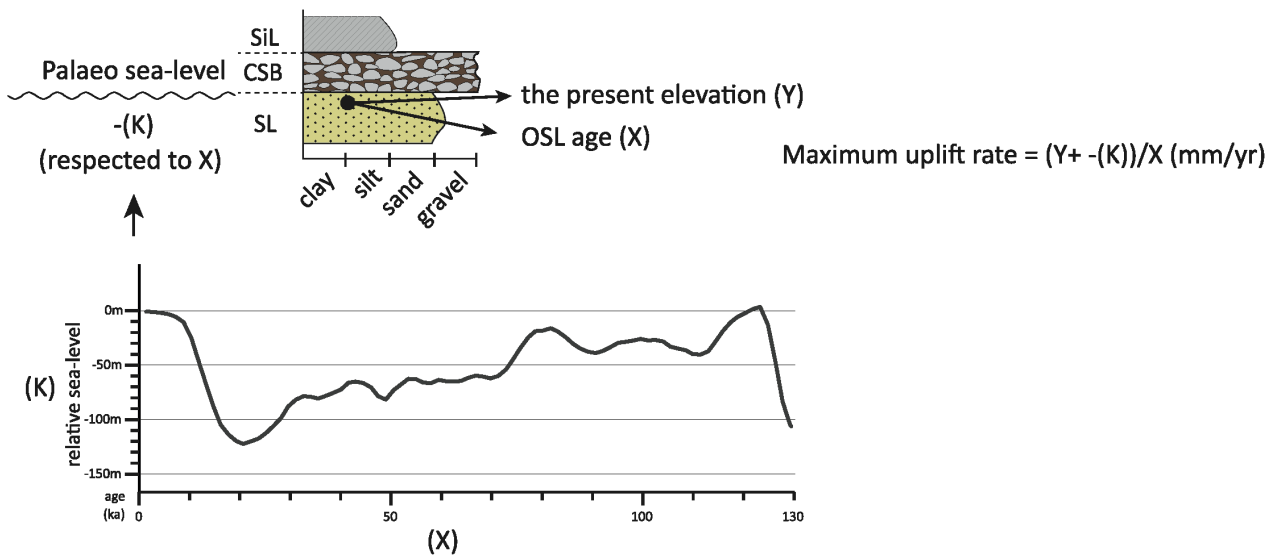


Figure 4.7: The schematic diagram of the concept of uplift rate calculations, based on two different benchmarks.

The benchmark I is to use the current sea-level as the benchmark of elevation, the uplift rates are calculated by dividing the present elevation (Y) by the OSL age (X) of the sample in SL (Sandy Loam) layer. This calculation shows the minimum estimation of uplift rates.

The benchmark II is to use the palaeo sea-level as the benchmark for elevation. The uplift rates are calculated by dividing “the present elevation (Y) plus the difference between the current sea-level and the palaeo sea level (-K)” by “the OSL age (X) of the sample in SL (Sandy Loam) layer”. This calculation shows the maximum estimation of uplift rates. The relative sea-level data are after Lambeck et al., (2014); Liu et al., (2004); Rabineau et al., (2006) and Waelbroeck et al., (2002).

Chapter 5. Paper I — Late Quaternary landform evolution and sedimentary successions in the Miaoli Tableland, northwestern Taiwan

This article presents a morphological analysis of the landform and sedimentary successions in the Miaoli Tableland, which is based on the numerical 3D landform mapping of high precision remote sensing data, field observations, and particle size analyses of sediments. A new landform classification of the tableland surfaces is proposed and discussed in relation to the geographical context. A detailed correlation among the tableland topography, the variation of sedimentary successions and the tectonic input is summarized as a 3D landform evolution model that undergoes processes of spatially differentiated uplifts, fluvial dissections of the palaeo-topography and successive rework processes of fluvial cobbles from the highlands to the coast during the late Quaternary. The field observation records, and a detail study of the sediments' compositions favor an early and rarely used Quaternary stratigraphic code for describing the sedimentary successions in the Miaoli Tableland.

This section has been published in *E&G Quaternary Science Journal* in 2022.

Article information:

Citation: Liu, S.-H., Hebenstreit, R., and Böse, M.: Late Quaternary landform evolution and sedimentary successions in the Miaoli Tableland, northwestern Taiwan, *E&G Quaternary Sci. J.*, 71, 1–22, <https://doi.org/10.5194/egqsj-71-1-2022>, 2022.

Hyperlink: <https://egqsj.copernicus.org/articles/71/1/2022/>

PDF: [pdf \(26252KB\)](#)

DOI: <https://doi.org/10.5194/egqsj-71-1-2022>

Available online at: 18 / Jan / 2022

This work is distributed under the Creative Commons Attribution 4.0 License.

<https://creativecommons.org/licenses/by/4.0/>

E&G Quaternary Sci. J., 71, 1–22, 2022
<https://doi.org/10.5194/egqsj-71-1-2022>
 © Author(s) 2022. This work is distributed under
 the Creative Commons Attribution 4.0 License.



Open Access
E&G Quaternary
 Science
 Journal

Research article

Late Quaternary landform evolution and sedimentary successions in the Miaoli Tableland, northwestern Taiwan

Shih-Hung Liu, Robert Hebenstreit, and Margot Böse

Institute of Geographical Sciences, Department of Earth Sciences, Freie Universität Berlin, 12249 Berlin, Germany

Correspondence: Shih-Hung Liu (liushihhung@zedat.fu-berlin.de)

Relevant dates: Received: 28 April 2021 – Revised: 24 September 2021 – Accepted: 6 December 2021 – Published: 18 January 2022

How to cite: Liu, S.-H., Hebenstreit, R., and Böse, M.: Late Quaternary landform evolution and sedimentary successions in the Miaoli Tableland, northwestern Taiwan, *E&G Quaternary Sci. J.*, 71, 1–22, <https://doi.org/10.5194/egqsj-71-1-2022>, 2022.

Abstract: Elevated Quaternary sedimentary complexes in the western foreland of the central mountain ranges of Taiwan are called tablelands. Their mostly flat surfaces are deeply incised by fluvial processes. The landforms and the fluvial systems in the Miaoli Tableland are investigated by high-resolution terrain analyses based on different datasets. Sediments are described in 51 outcrops and characterized by grain size composition. The outcrops revealed complete or incomplete sequences of the general scheme from bottom to top: sandy tidal–coastal units overlain by gravel- and cobble-rich fluvial deposits always with a fine-grained silt-rich top cover layer influenced by aeolian deposits. All layers are unconsolidated sediments. Three subtypes of this sequence were identified, with respect to the occurrence of the fluvial deposits. The relation of tectonic and erosional processes including the rework of gravels is discussed. The results reveal a tableland surface much more disaggregated than previously mapped, suggesting that individual tableland segments represent remnants of an inferred palaeotopography. The tableland surfaces have been separated into Sedimentary Highlands (SH-I and SH-II) and Sedimentary Terraces (ST) by geometrical properties. The Alluvial and Coastal Plains (AL) represent broad valley bottoms (“box-shaped valleys”) in the dendritic drainage systems below 150 m and the coastal plains. The landforms and predominantly the sediment sequences are discussed in the context of the existing stratigraphical schemes of the Toukoshan Formation and the so far rarely used Lungkang Formation. The latter is recommended as the stratigraphical term for the refined subdivision of the uppermost part of late Quaternary sediments in the Miaoli Tableland.

1 Introduction

Sedimentary terraces are landforms which are formed by deposition, base level change, and subsequent erosion. They provide stratigraphic records and represent archives for changes in sedimentary and erosional processes (Charlton, 2008). The process-inducing environmental factors are climate change, sea-level change, and local tectonism, which

have been studied in various regions worldwide for interpreting the landscape evolution of sedimentary terraces (e.g. Bridgland and Westaway, 2008; Robustelli et al., 2014; Pickering et al., 2014; Mather et al., 2017).

Huge sedimentary complexes are distributed in the western foreland of the Taiwanese mountain ranges (Yu and Chou, 2001; Yang et al., 2006) (Fig. 1a). They are dissected by fluvial incision, thus forming terraces, which are called

2 S.-H. Liu et al.: Late Quaternary landform evolution and sedimentary successions in the Miaoli Tableland

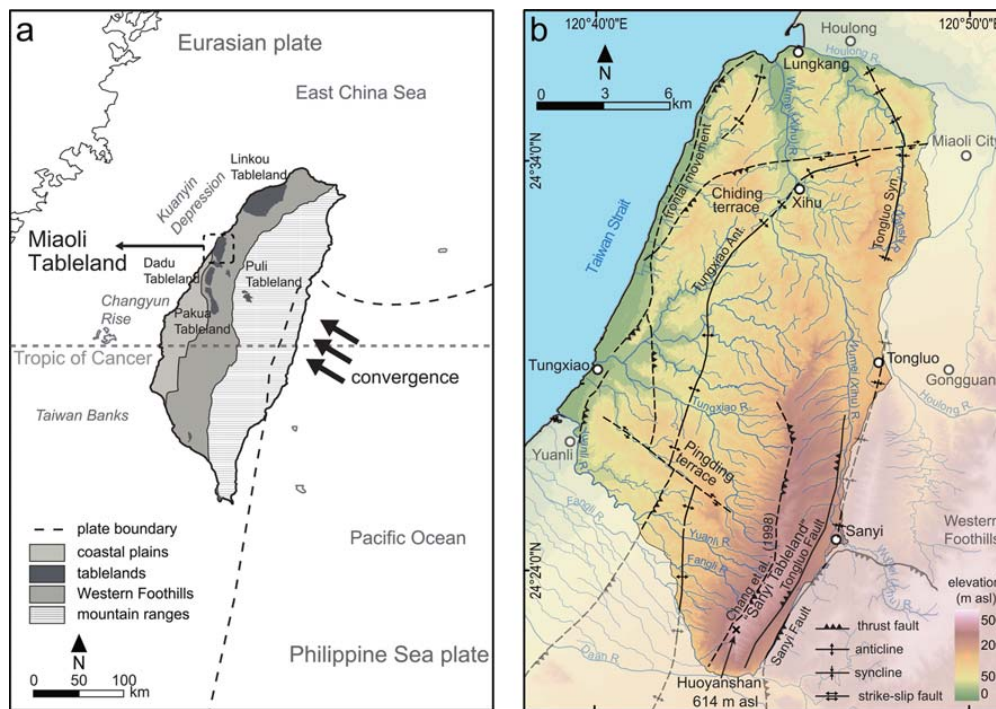


Figure 1. Location of the Miaoli Tableland and other tablelands in Taiwan. Generalized tectonic context after Angelier et al. (1986) and Suppe (1984); geological divisions modified after Ho (1988). (b) Detail map of the study area. Elevation extracted from an open-access digital elevation model (DEM) with 20 m resolution (Satellite Survey Center, 2018); tectonic features adapted from geological maps (Central Geological Survey, 2017); locations of the Tongluo Fault and name of “Sanyi Tableland” by Ota et al. (2006).

“tablelands” by local scientists (Lin, 1957; Teng, 1979; Lin and Chou, 1978; Tomita, 1954; Chang et al., 1998; Tsai et al., 2006, 2010). Landforms similar to the tablelands have been described in the western Pacific area, such as in Japan (Matsu’ura et al., 2014) and Korea (Choi et al., 2009).

However, until now, the detailed formation history of these sedimentary terraces has been widely unclear, even though detailed studies focused on different aspects of the tableland morphology such as the local tectonism (Shyu et al., 2005; Yang et al., 2006; Shih and Yang, 1985), the long-term sedimentation since the Neogene (Teng, 1996b; Teng et al., 2001), or weathering degrees and their corresponding relative chronology of the surface materials (Ota et al., 2002; Shih and Yang, 1985; Tsai et al., 2006). The majority of these studies follow the interpretations that, according to the continuous tectonic uplift since the Pliocene, the age of the tablelands’ sedimentary units ranges from the Pliocene to early Pleistocene (Chang, 1953). Only a few studies included or focused on the late Quaternary sedimentation and surface morphology of the tablelands (Ota et al., 2006; Tseng et al., 2013; Horng, 2014; Chang et al., 1998; Teng et al., 2001; Siame et al., 2012).

The sedimentary sequences represent potentially valuable archives of the Quaternary landscape history of western Taiwan. As the mountainous island is located in a unique position at the Tropic of Cancer between the Asian continent and the western Pacific, these archives may even have implications for the entire region in terms of palaeoclimate and sea-level change. Thus, more detailed morphological studies are required in order to understand the complicated nature of these terraces on the basis of a reconstruction of the process history. This study presents – as a first step – an approach for interpreting morphological processes by the combination of a concise 3D terrain analysis and sedimentological studies by field observation and particle size characterization in a defined research area in northwestern Taiwan, the Miaoli Tableland. A detailed chronology of the sediment sequence is not in the scope of this morphological study.

2 Regional setting

2.1 Tectonic background and erosion rates of the Taiwanese mountain ranges and their foreland

The orogeny of the Taiwanese mountain ranges is caused by the arc-continent collision at the convergence zone of the Eurasian plate and the Philippine Sea plate in the western Pacific (Fig. 1a), which has been active since the Plio-Pleistocene (Suppe, 1984; Angelier et al., 1986; Teng, 1990; Willemin and Knuepfer, 1994; Teng, 1992; Yu and Song, 2000). Today, the mountain ranges of central Taiwan reach an elevation of 3952 m a.s.l. and are composed of Tertiary sedimentary rocks and low-grade metamorphic rocks at the western limb. Their westernmost part, a 10–20 km wide frontal belt has been called the “Western Foothills” (WF) (Fig. 1a) (Ho, 1988; Pelletier and Stephan, 1986) and has a general height below 2500 m a.s.l. The western foreland of the mountain ranges is a Neogene basin (Yang et al., 2006). The basin depositions have been interpreted as a succession of Tertiary sedimentary rocks overlain by Quaternary sediments yielded from the mountain ranges (Fig. 1a) (Simoes and Avouac, 2006; Yu and Chou, 2001; Lin and Watts, 2002; Lin et al., 2003; Chen et al., 2001; Ho, 1994; Covey, 1986). However, their precise chronology is not available yet (Ota et al., 2006; Chang et al., 1998; Teng, 1996b; Lin, 1963; Ho, 1994). Parts of these Quaternary sediments have been uplifted to present altitudes with a maximum height of ca. 1000 m a.s.l. Due to the complexity of the tectonism, the long-term uplift rates of the WF and the Neogene basin are still unclear (Deffontaines et al., 1997; Shyu et al., 2005; Yang et al., 2016; Teng, 1996a; Ching et al., 2011).

The strong uplift of the island and the subtropical monsoon climate including frequent typhoon events induce erosion rates with an average of 3–6 mm a⁻¹ (Dadson et al., 2003). The precipitation is mainly concentrated during the summer and autumn; on average about two to three typhoons strike Taiwan annually (average 1949–2019) (Central Weather Bureau, 2019). Typhoons often cause extreme precipitation events and floods.

2.2 Quaternary sea-level change in Southeast Asia

The post-Last Glacial Maximum (LGM) sea-level curve of the Taiwan Strait has been established by radiocarbon dating of marine sediments (Liu et al., 2008; Chen and Liu, 1996). However, a pre-LGM sea-level curve is not yet established. The combination with global and regional models that reach back further, especially from the Sunda Shelf (Hanebuth et al., 2011; Shackleton, 2000), shows that the sea level was much lower than today after the end of the Eemian sea-level high stand, with a minimum during the LGM (–120 to –140 m). As the depth of the Taiwan Strait west of the Miaoli Tableland is less than 60 m, it was dry land during most of the Late Pleistocene (Hornig and Huh, 2011; Huh et al., 2011), and the palaeoflow directions of the northwestern Taiwanese

rivers were north to northeast toward the Kuanyin Depression (Huh et al., 2011) (Fig. 1a). After the general Holocene sea-level rise, a short-term high stand during the Mid-Holocene reached +5 m (Liu et al., 2004; Chen and Liu, 1996).

2.3 The tablelands in Taiwan

The uplift, sea-level changes, and the subsequent erosional processes have dissected the foreland sediments. These sedimentary terraces are called “-Ding/-頂” in the local language, i.e. terraces (Chen et al., 2004; Tomita, 1954) or tablelands (Tsai et al., 2010, 2006; Lin, 1957; Teng, 1979; Teng et al., 2001; Shih and Yang, 1985; Lin and Chou, 1978) according to different concepts of the landform evolution, respectively.

Tablelands are mainly distributed in a ca. 5–20 km wide area along the western margin of the WF (Fig. 1a), as well as in mountain basins. In the past, the tableland surfaces were differentiated morphologically and sedimentologically by the following criteria: (1) the lithification degree of the sediments, (2) the driving force of current morphology (fluvial incision/tectonic displacement), (3) the weathering characteristics of the cover sediments (relatively old and intensively weathered substrate/relatively young alluvial deposits), and (4) the elevation of surfaces as a relative chronological index of different morphological stages (Lin, 1957; Tomita, 1953, 1951, 1954). The resulting categories of the tableland surfaces were named “Laterite Highlands” for the higher-elevated quasi-flat surfaces that are covered by reddish, highly weathered sediments; “Laterite Terraces” for the lower-elevated quasi-flat surfaces that are covered by brownish/reddish highly weathered sediments; and “Fluvial Terraces” for the modern fluvial terraces/plains in the immediate vicinity of fluvial paths (Lin, 1957).

In recent decades there have been more detailed studies on the origin and development of the tablelands, e.g. studies on tectonism at the Dadu Tableland and Pakua Tableland (Delcaillau, 2001; Shih and Yang, 1985), the soil development and relative chronology at the Dadu Tableland (Tsai et al., 2010) and Pakua Tableland (Tsai et al., 2006), and the morphology and sediment chronology of the Puli Tableland (Tseng et al., 2013). The depositional environments and biostratigraphy of the sedimentary sequence as well as the morphology corresponding to active tectonism were studied in the Linkou Tableland (Hornig, 2014; Teng et al., 2001) as well as the relative and absolute chronology, erosion, and tectonism of smaller terraces in other regions (Chen et al., 2004; Ota et al., 2009, 2002, 2005; Chen et al., 2003). All these studies gave a frame for an understanding of the tableland formation; however, neither an overall morphological model nor a detailed chronology of the tableland development has been established so far.

In past publications the terms “laterite/lateritic” have been used according to the local context, which describes the reddish/brownish, fine-grained soils on the surfaces. However, the usage of this term has recently been challenged by soil

4 S.-H. Liu et al.: Late Quaternary landform evolution and sedimentary successions in the Miaoli Tableland

studies (Tsai et al., 2010). According to the latest review of the soil taxonomy in Taiwan, these so-called laterite cover sediments on the tablelands have been revised as “Ultisols” or “Oxisols” by their chemical composition, respectively (Chen et al., 2015). To avoid over-interpretation of soil development characteristics and because the pedological factors of the sediments are not the subjects of this study, the following geomorphological descriptive terms are used in this text: “Sedimentary Highlands” (SH) for Laterite Highlands, “Sedimentary Terraces” (ST) for Laterite Terraces, and “Alluvial and Coastal Plains” (AL) for Fluvial Terraces.

2.4 Study area: the Miaoli Tableland

The sedimentary complexes in the Miaoli region are called the Miaoli Tableland (Teng, 1979) or Miaoli Hills (Chang et al., 1998). We prefer the former term because the geological and morphological settings of the area are consistent with the other tablelands in northwestern Taiwan (Lin and Chou, 1978; Teng, 1979). The Miaoli Tableland is located on the northwestern coast of Taiwan between the Houlong River and the Daan River (120°38'10" to 120°48'57" E, 24°36'51" to 24°21'32" N). Both rivers have their source area in the mountain belt and therefore a different hydrological regime than the other rivers in the study area. The Miaoli Tableland covers an area of ca. 283 km². Its topographical surface is characterized by terraces with different elevation levels. The highest elevation is located at the southernmost part at about 614 m a.s.l. This point is called “Huoyanshan/火山山”, also known as “Fire Mountain” (Fig. 1b). A narrow coastal plain forms a 30 km long stretch between the Wumei (Xihu) River and Yuanli River (Fig. 1b). It is composed of alluvial sediments that are carried by the longshore current (Jan et al., 2002; Wang et al., 2003); according to climate statistics from 2003 to 2020, the tidal difference in the shore area of Miaoli is 4–6 m (Central Weather Bureau, 2020).

The study area is mainly drained by the Tungxiao River and the Wumei (Xihu) River as well as other small local catchments (Fig. 1b). However, many of the fluvial paths in the area are artificially constrained by levees for defending from flooding. For example, the flooding which affected the Miaoli region on 7 August 1959 (“八七水災”) was the most severe flooding in the 20th century in Taiwan (The Taiwan Provincial Weather Institution, 1959; Central Weather Bureau, 2019).

The geological maps and the studies of tectonic features exhibit one inferred syncline, two inferred anticlines with low dip angles, and four inferred thrust faults with steep dip angles in the study area (Fig. 1b). These features are almost parallel aligned, striking mainly northeast to southwest (Chang, 1990, 1994; Ho, 1994; Yu et al., 2013; Lin and Watts, 2002; Yu and Chou, 2001; Yang et al., 2016). The coastal area is affected by the tentatively called “frontal movement”, which is assumed to be the youngest thrust movement in the Miaoli area (Shyu et al., 2005). Two ac-

tive thrust faults have been identified at the eastern margin of the Miaoli Tableland (Ota et al., 2006), and an inferred thrust fault at the western fringe of the highlands has been proposed by Chang et al. (1998) (Fig. 1b). There are no direct studies on Quaternary uplift rates in the Miaoli area. Results from the southerly Pakua Tableland, based on radiocarbon dating of different heights of the terrace surfaces, show that it can be assumed to be around 1 mm a⁻¹ (Ota et al., 2002, 2006).

The general formation of the Miaoli Tableland has been explained by two hypotheses. Chang et al. (1998) assumed that the present Sedimentary Highlands and the southwest of the Sedimentary Terraces area (the Pingding terrace, Fig. 1b) represent jointed alluvial fans. The gravels and cobbles, which build up the fans, were yielded from the Houlong, Wumei (Xihu), and Daan (palaeo-)rivers. The rest of the area (the Tungxiao River catchment) was interpreted as a palaeobay, which was subsequently filled with sediments (Appendix A). Following the traditional classification of Lin (1957), Chang et al. (1998) assumed that differentiated uplift and erosion during the late Quaternary have dissected the palaeotopography into terraces. They subdivided the surfaces of the Miaoli Tableland into the three surface elevation levels as Laterite Highlands, Laterite Terraces, and Fluvial Terraces (see Sect. 2.2).

In contrast, Ota et al. (2006) focused on differentiated tectonism in the Miaoli region. They assumed that folding along the Tungxiao Anticline (Fig. 1b) caused uplift in the present ST area. This induced the erosion of the overlying sediments, resulting in a topographic inversion along the anticline. The thrust of the Tongluo Fault (Fig. 1b) caused the uplift of the southern SH (tentatively named the “Sanyi Tableland”). This resulted in the separation of the ST and SH along a distinct topographic escarpment, which subsequently was rapidly eroded eastward causing the beheading of the valleys in the southern SH. Colluvial depositions of gravels and cobbles on the western slope foot of the escarpment exhibit the ongoing erosion (Chen, 1983).

The southeastern SH (former Laterite Highlands) is the most detailed studied part of the Miaoli Tableland. Ota et al. (2006) mapped massive, deeply dissected, and tectonically deformed fluvial terraces here. The strata are inclined > 30° to the east in the Fire Mountain area (Chang, 1994). The inclination is assumed to be affected by the westward thrust of the Sanyi Fault (Yang et al., 2007) (Fig. 1b).

2.5 Former stratigraphical interpretations of the Miaoli Tableland

The stratigraphical interpretations of the sedimentary layers in the study area were proposed in the 1930s and redefined in the latter half of the 20th century. The sedimentary layers in the study area were described in different terms as follows.

2.5.1 Toukoshan Formation (Tk Formation)

The Tk Formation is the common term for the Pliocene–Quaternary strata that are exposed along the mountain front of the WF in northern and central Taiwan (Chang, 1990, 1994; Ho, 1994; Lee, 2000; Chen et al., 2001; Chang, 1953). However, information on the dimension and composition of the Tk Formation vary in the available publications. The composition is described as fine-grained sediments in the lower and coarse-grained fluvial sediments in the uppermost sections with a total thickness up to more than 1000 m in central Taiwan (Chang, 1948, 1955; Torii, 1935; Chen et al., 2001). The well-rounded shape of the fluvial gravels and cobbles shows that they might be reworked and transported over certain distances (Teng, 1996b). Some authors described the lower units as already consolidated (Chang, 1955; Ho, 1988; Chang, 1990). Biostratigraphical studies on planktonic foraminifera indicated that the deposition of the Tk Formation started after the end of Olduvai event (Huang, 1984), and a time span of 1.24–0.46 Ma was given by the comparison between the abundance of species and the biozones (Lee et al., 2002).

2.5.2 Tûsyô/Tungxiao/Lungkang Formation (Ts/Lk Formation)

Beside the broadly used term Tk Formation, an older definition of the sediment strata specifically in the Miaoli Tableland is called the Tûsyô Formation (as Ts Formation, according to pronunciations of Japanese of the local name “通霄”). It was proposed by Makiyama (1934, 1937) and renamed in Chinese as the Tungxiao Formation by Chang (1948) to describe the loose, poorly cemented sedimentary layers in the Miaoli Tableland with a sequence from bottom to top of intercalated marine sediments, tidal–coastal layers, gravel and cobble beds, and a surface layer with ocher-coloured soils. In 1963, Lin proposed the term Lungkang Formation (as Lk Formation) for the uppermost 10–15 m of the same succession in the coastal area of the Miaoli Tableland. The only difference between these two definitions is that the cover layer of the Lungkang Formation was interpreted as dune sand (Lin, 1963). The absolute chronology of these strata is uncertain. Makiyama (1934) assumed a late Tertiary deposition according to the composition of fossils by the palaeontological concept at that time. Radiocarbon dating on molluscs gave an early Holocene time span (Lin, 1969). The Ts/Lk Formation has been rarely mentioned by other authors after the 1960s.

2.5.3 “Alluvium Deposits”, “Terrace Deposits”, and “Lateritic Terrace Deposits”

These are different terms for the description of non-cemented deposits on various geographical surfaces (i.e. tablelands, valley floors, flood plains, coastal plains, and estuaries) in the geological maps of the study area (Ota et al., 2006; Chang et al., 1998; Chang, 1990, 1994; Ho, 1994; Chen et al., 2004).

They are composed of gravel, aeolian sands, and a mixture of dusty fine sediments. No direct dating has been proceeded yet. A late Quaternary age was assumed based on the loose, poorly consolidated consistency of the deposits. The thickness of them varies depending to the palaeotopography; it reaches a maximum of about 20 m (Chang, 1990; Ho, 1994).

3 Material and methods

3.1 Terrain analyses

Systematic terrain analyses were undertaken by the combination and integration of 3D and 2D datasets: (1) open-access digital elevation models from the Ministry of the Interior of Taiwan (resolution 20 m) and the Shuttle Radar Topography Mission (SRTM, resolution 1 arcsec, ca. 80 m) (Satellite Survey Center, 2018; NASA JPL, 2013), (2) aerial photos and satellite imagery from the open-access Web Map Tile Service in a geographical information system (GIS) (Center for GIS RCHSS Academia Sinica, 2017; National Land Surveying and Mapping Center, 2016), (3) published topographic maps at a 1 : 25 000 scale accessible online (National Land Surveying and Mapping Center, 2016), and (4) geological maps of Taiwan (1 : 50 000) accessible online (Central Geological Survey, 2017).

For the identification and classification of different topographical landforms, we merged the information of absolute and relative elevation with the terrain steepness by applying automatic functions of the GIS software and manual mapping. The aim is to distinguish between the present fluvial paths, tableland surfaces, modern fluvial plains, and coastal plains as well as the slopes in between (Fig. 2).

Four terrain categories were defined:

- The category “fluvial paths” was derived from a calculation using the “Arc Hydro Tools” function in the GIS programme compared with the topographic maps and the aerial photos. The fluvial paths were mapped as line features, whilst other categories were mapped as surface features (polygons).
- The category “tableland” was defined as a quasi-flat surface with the following criteria: (1) the steepness is lower than 10°; (2) it is larger than 400 m² (1 pixel in the DEM); and (3) the flat surface is not in the direct vicinity of a flow path (Fig. 2). The steepness threshold was adapted from the study of Saito and Oguchi (2005), in which they proceeded the terrain analysis of 690 alluvial fans in Japan, Taiwan, and the Philippines. All fans show a terrain steepness lower than 7°; the majority of them have one less than 5°, including all 71 studied alluvial fans in this context in Taiwan (Saito and Oguchi, 2005). The edges of the tableland segments were determined by hand mapping. Comparing the direct raster to polygon conversion, it has concisely performed the noise reduction and the edge-smoothing pro-

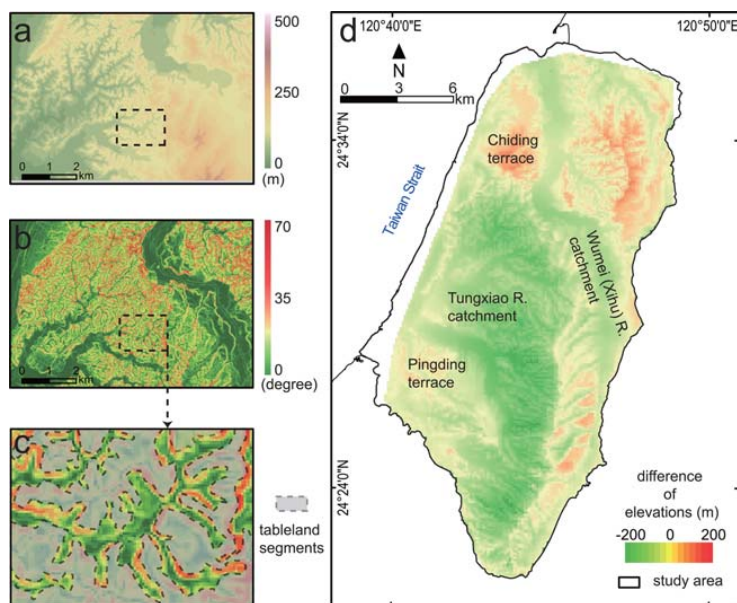


Figure 2. Mapping of the tableland segments. (a) The original digital elevation models (Satellite Survey Center, 2018). (b) Surface steepness was subsequently calculated by an ArcGIS function (slope). (c) An example of hand mapping of the tableland segments in GIS. The tableland segments were recognized by the gentle terrace surfaces. (d) Results of the calculation of relative surface elevations: negative values represent DEM elevations lower than the theoretical linear surface and vice versa. The spatial distribution of negative and positive values shows a clear separation at the divide of the Wumei (Xihu) River and the Tungxiao River catchments and at the southern margin of the Chiding terrace.

cedures. For a normalization of the general surface inclination of the Miaoli Tableland from the southeast to northwest, we calculated a theoretical linear-trend surface from the highest point of the terrain to the distal edge of the tableland surfaces, adapting the method of Volker et al. (2007), by using a triangulated irregular network (TIN) interpolation into a raster. Tableland areas above and below this theoretical linear-trend surface were defined as Sedimentary Highlands (SH) and Sedimentary Terraces (ST), respectively (Fig. 2d).

- Quasi-flat surfaces (less than 5°) in the immediate vicinity of the fluvial paths (e.g. valley floors) were defined as “modern fluvial plains”. The “coastal plains” were defined as the plains which have a steepness less than 5° and an elevation lower than 30 m a.s.l. along the coast of the Taiwan Strait. The boundary of the plain was marked by the slope foot of the edge of the distal-tableland segments. The modern fluvial plains and the coastal plains were combined and defined as Alluvial and Coastal Plains (AL).
- The category “slopes” was defined for the rest of the surfaces which are steeper than 5° .

3.2 Field observations and sampling

The internal sedimentological composition of the tableland segments was studied to characterize and identify typical layer sequences throughout the study area; 51 field sites were chosen for a detailed description by the following criteria: the sites are (1) easily accessible and provide a good overview of the sedimentary layers, (2) evenly distributed across the study area, and (3) contain more than two visible sedimentary layers for a representative sampling and comparison with other outcrops.

The elevations of the sites were extracted from the DEMs and compared with a handheld GPS receiver in the field. The sedimentary layers in the outcrops were recorded by standard characteristics: shape of boundaries, thickness, sedimentary structures, texture, particle size, and visible fossil content (Miall, 2014; Vail et al., 1991). The sediment colour was only described in a general way to identify individual layers in the field. A specific determination of soil parameters as well as a detailed facies analysis of individual layers are not in the scope of this study. The sedimentary layers were identified in each field site independently, and then the records were compared to find identical layers and sequences throughout the study area. At 12 selected sites, 41 samples were taken for particle size analyses including 2 samples from modern beach (dune) sand for comparison.

3.3 Particle size measurements

The particle size analyses were conducted with a Beckman Coulter™ LS-13320 laser diffractometer at Section 3: Geochronology of the Leibniz Institute for Applied Geophysics, Hanover, Germany. This technique is well adapted for high-precision measurements of fine-grained particles smaller than 2 mm (Konert and Vandenberghe, 1997; Eshel et al., 2004; Beuselinck et al., 1998). None of the samples contained particles > 2 mm, even including the matrix of the gravel and cobble beds.

The sample preparations and measurements were proceeded as follows: for each sample, ca. 20–50 mg of the sediments was filled into the test tubes and treated with 1 % ammonium hydroxide (NH₄OH) solution, in order to disperse the aggregates of sediments for the subsequent particle size analyses. The test tubes were rotated for 24 h at 30 rpm to mix the solution and sediments. Organic matter was not removed. The particle size was measured five times for each sample to reduce the random error. The results were accepted when the value of polarization intensity differential scattering (> 80 %) and obscuration (< 10 %) passed both criteria. The statistical index of the coefficient of variance mean (< 5 %) and coefficient of variance standard variation (< 5 %) were chosen to evaluate the reproducibility of the results (Konert and Vandenberghe, 1997). The particle size fractions and the texture classifications (Jahn et al., 2006) were correlated for the characterization of sedimentary records.

4 Results

4.1 Terrain analyses – topography of the Miaoli Tableland

The topographical analyses reveal the proportion of different morphological categories in the study area: the tablelands (SH + ST) represent 24.2 % (ca. 68.7 km²); the slopes and gullies represent 44.8 % (ca. 127.2 km²); the fluvial plains represent 24.2 % (ca. 68.9 km²); and coastal plains represent 6.6 % (ca. 18.7 km²) (Fig. 3).

The tableland surfaces are unevenly spread throughout the study area. Their sizes vary from only a few hundred square metres to several square kilometres. The larger tableland segments with widths ranging from ca. 100–1500 m, such as Pingding (ca. 7.0 km²), Chiding (ca. 4.3 km²), and other parts (from 2.0 to 0.5 km²) represent ca. 14 % of the total terrain. However, the high-resolution mapping revealed that the overall spatial pattern of the tableland surface is made up of numerous smaller segments, which are only ca. 40–200 m wide (Fig. 3). They generally represent the water divides between the fluvial paths and are broadly distributed in the study area. Their distribution and shape depend also on different fluvial drainage patterns in the study area.



Figure 3. Results of the terrain analyses and the classification of tableland segments. The Sedimentary Highlands (SH) represent the fluvial terraces, located in the southeastern (SH-I) and northern part (SH-II) divided by the Wumei (Xi) River. The Sedimentary Terraces (ST) are mainly located in the Tungxiao River catchment. The Alluvial and Coastal Plains (AL) represent the flat surfaces beside the fluvial channels. Detailed mapping of drainage patterns and the elevation profiles of the fluvial valleys is presented in Fig. 4.

The differentiation between the SH and ST can be clearly inferred from the relative height between the true elevations and the theoretical linear-trend surface (Fig. 2d). Furthermore, both show different directions of their inclination in general. The SH is composed of tablelands with ca. 2° northwest-inclining surfaces, while the ST tableland surfaces incline ca. 1° to the west (Fig. 3).

The topographical divide between the ST and the SH is represented by a continuous, west-facing escarpment bending from the southeast to the northwest. The steepness of the slope is about 30° and more. Its relative height is ca. 130–200 m in the south, decreasing northwestward to about 30 m.

4.1.1 The Sedimentary Highlands (SH)

The Sedimentary Highlands (SH) are located in the east and the north of the study area. They were divided into two subgroups by their surface elevation and their location with respect to the Wumei (Xihu) River. The area south of the Wumei (Xihu) River with elevations of about 250 to 614 m a.s.l. is named SH-I. These tableland surfaces are dissected to a minor degree and incline quasi-continuously northward to the left bank of the Wumei (Xihu) River (Fig. 3). The fluvial paths incised in the SH-I segments flow to the northeast. They are tributaries of the Wumei (Xihu) River and show a parallel pattern. The tableland in the northern and the northwestern part of the study area with elevations between 30 and 250 m a.s.l. is classified as SH-II (Fig. 3). The tableland segments are separated by the Wumei (Xihu) River into a western and an eastern part. The western part has larger coherent tableland surfaces, i.e. the tableland segment in Chiding, which is here the topographical divide between the Wumei (Xihu) River and the Taiwan Strait. The eastern SH-II is well dissected, and the remaining tableland segments are the interfluvies between the tributaries of the Wumei (Xihu) River, the Nanshi River, and the Houlong River (Fig. 3). The fluvial paths between the SH-II segments are mainly below 150 m a.s.l. and have formed dendritic drainage patterns. All these streams flow in a western or northwestern direction to join the Wumei (Xihu) River and Houlong River or directly to the coast, respectively.

4.1.2 The Sedimentary Terraces (ST)

The Sedimentary Terraces (ST) are located to the west of the SH-I. They are distributed over the whole Tungxiao River catchment and extend further south to other smaller catchments. The majority of ST is lower than 250 m (the highest point is 445 m a.s.l., located at the boundary to the SH-I) and dropping to ca. 30 m at the distal edge close to the coast (Fig. 3 and Appendix A). The larger tableland segments (i.e. Pingding) are located south of the main stream of the Tungxiao River. The smaller tableland segments make up the bulk of the ST surfaces and can be connected tentatively by a quasi-flat inferred surface through the whole ST area (Fig. 3). Their topographic height is ca. 30 m in the east and decreases westward to ca. 5 m at the distal-tableland segments.

The drainage patterns in the ST are differentiated by the elevation. Streams above 150 m a.s.l. form a parallel drainage pattern similar to the SH-I (Fig. 3). Most of them begin near the topographic escarpment (i.e. western slope of the SH-I), and their flow path gradients vary from 1.0 to 14.0° (Fig. 3). The streams below 150 m a.s.l. in the central and western part of the ST have formed dendritic drainage patterns. The fluvial pattern in the SH-II shows also a dendritic system.

4.1.3 Slopes

The gradient of the slopes ranges from 10 to 66° with a majority of 10 to 26°. The spatial distribution of the gradients clearly shows a pattern in different scales. At an overall scale, the slopes in the north and west are gentler than the slopes in the south and east, while the differences between individual slopes are not so distinct. In the areas of the dendritic drainage patterns, the vertical shape of the slopes tends to be concave; i.e. the upper part of the slope is steeper than its foot. Reversely, in the areas of the parallel drainage patterns, the vertical shape of the slope is more convex (Fig. 4). Thus, the sections of the upper valleys above 150 m are typically V-shaped.

4.1.4 The Alluvial and Coastal Plains (AL)

The Alluvial and Coastal Plains (AL) reach elevations up to 150 m a.s.l. and represent the wide valley floors and the coastal area (Fig. 3). The main streams' flow paths have gradients from 0.1 to 0.2°, whereas the tributaries' flow paths are steeper (up to 8.0°). The majority of them are braided rivers, except the meandering Nanshi River, a tributary to the Houlong River (Fig. 3). The valley width is not consistent. It is up to kilometres in the main streams and ca. 20–100 m in most of the tributaries. Therefore, the AL represents the active fluvial plains as well as the terraces adjacent to the fluvial paths with one or two levels. The relative height of these terraces is < 10 m. Their sizes are constrained by their location and the stream order. The larger ones (> 1 km²) in the vicinity of main streams are up to 2100 m wide; the smaller ones (< 1 km²) in the tributaries are ca. 20–40 m wide (Fig. 3). The AL occurs only in those areas of the SH-II and ST with a dendritic drainage pattern. The valleys are ca. 150–1300 m wide and ca. 20–50 m deep and show relatively narrow flow paths (< 10 m mostly) (Figs. 3 and 4 and Appendix A). In combination with the steep slopes, valley cross sections show a quasi-rectangular transverse profile for which we introduce the term “box-shaped valley”.

The coastal plain has a consistent width of around 500–1000 m, but it widens up to 1500 m in the area of the estuaries. The topographic boundary between the coastal plain and distal-tableland segments can be clearly identified by the slope foot of the tableland segments (Fig. 3).

4.2 Sediment descriptions

The 51 studied outcrops in the Miaoli Tableland are located at the edges of the tableland segments (Fig. 5, Table 1) and provide therefore a vertical insight into their internal composition.

Their height ranges from about 3 to 50 m, and they are characterized by up to six relevant unconsolidated sediment layers (Figs. 5 and 6). However, only two of the outcrops show all layers of the succession (i.e. 001_HLPT and 010_EFB). Only a limited number of layers is exposed in

Table 1. List of studied outcrops.

No.	Name	Latitude	Longitude	Location	Height (m)	Elevation (m a.s.l.)
1	HLPT (Hou-Long Petroleum)	24°35'45.30" N	120°48'24.01" E	SH-II	49	37
2	BTL (Ban-Tian-Liao)	24°35'47.02" N	120°43'38.77" E	SH-II	6	73
3	CSW (Chiuan-Shuei-Wo)	24°35'6.78" N	120°48'28.61" E	SH-II	7	97
5	RSK (Rong-Shu-Keng)	24°34'37.68" N	120°44'23.69" E	SH-II	4	74
6	NBK (Nan-Bei-Keng)	24°34'21.97" N	120°44'6.16" E	SH-II	8	105
7	NCT (Nan-Ching Temple)	24°34'19.24" N	120°43'32.91" E	SH-II	3	71
8	MYK (Ma-Yuan-Keng)	24°34'2.42" N	120°46'48.54" E	SH-II	6	165
9	LG (Long-Gang)	24°34'1.12" N	120°48'21.08" E	SH-II	4	116
10	EFB (Er-Fu Bridge)	24°33'50.55" N	120°44'48.17" E	SH-II	11	28
11	FTK (Fu-Tou-Keng)	24°33'37.89" N	120°44'21.63" E	SH-II	10	107
12	ZW (Zhang-Wo)	24°32'50.93" N	120°46'36.74" E	SH-II	7	68
13	TKD (Tu-Kan-Ding)	24°32'23.29" N	120°42'27.86" E	ST	3	148
15	XP (Xin-Pu)	24°32'8.56" N	120°41'41.95" E	ST	3	10
17	BW (Bei-Wo)	24°31'12.20" N	120°43'3.51" E	ST	6	26
18	DBD (Da-Bi-Dou)	24°30'54.09" N	120°43'14.00" E	ST	8	46
20	GCW (Gu-Cuo-Wo)	24°29'48.64" N	120°44'55.34" E	ST	5	94
22	ZG (Zhu-Gang)	24°28'55.02" N	120°42'8.09" E	ST	20	21
23	XNPW (Xiao-Nan Power Substation)	24°28'17.69" N	120°40'12.99" E	ST	2	29
24	YZS (Yuan-Zih-Shan)	24°27'45.38" N	120°43'15.15" E	ST	6	67
25	JJC (Jin-Ji Company)	24°27'31.52" N	120°39'48.64" E	ST	7	16
26	SLK (Shiau-Lan-Keng)	24°25'45.22" N	120°44'37.25" E	ST	7	227
27	TZK (Tian-Zih-Keng)	24°25'58.22" N	120°41'24.60" E	ST	5	47
28	HDK (Hu-Dong-Kou)	24°34'49.79" N	120°45'48.85" E	SH-II	4	50
29	GJW (Gong-Jiao-Wan)	24°31'14.41" N	120°47'29.54" E	SH-II	7	179
30	TYGC (Tiao-Yan-Gu-Chi)	24°26'51.29" N	120°45'13.33" E	SH-I	5	335
31	XNPWH (Xiao-Nan Power Substation Heights)	24°28'15.05" N	120°40'17.79" E	ST	2	38
32	THST (Dong-He Steelworks)	24°34'13.42" N	120°44'27.13" E	SH-II	3	75
33	SZZ (San-Zuo-Wu)	24°22'14.62" N	120°42'41.03" E	ST	11	177
34	ZNQ (Zhong-Nan Quarry)	24°30'19.62" N	120°41'23.91" E	ST	5	25
35	YCZ (Yu-Cuo-Zhuang)	24°23'59.15" N	120°42'17.68" E	ST	10	118
36	KNS (Keng-Nei South)	24°35'12.39" N	120°46'34.24" E	SH-II	6	50
37	PD (Ping-Ding)	24°28'2.00" N	120°41'0.36" E	ST	7	64
38	JJW (Jie-Jih-Wo)	24°29'6.06" N	120°43'44.16" E	ST	5	70
39	JSS (Jin-Shan South)	24°24'58.39" N	120°41'43.93" E	ST	27	117
40	RGK (Lei-Gong-Keng)	24°32'32.61" N	120°46'53.79" E	SH-II	7	96
41	CHL (Chung-He-Li)	24°35'38.90" N	120°44'16.56" E	SH-II	10	55
42	GGF (Guo-Gang Fossils)	24°36'17.61" N	120°43'49.20" E	SH-II	4	18
43	SLP (Shuei-Liou-Po)	24°25'59.15" N	120°41'42.66" E	ST	10	60
44	NZ (Nan-Zhuang)	24°28'28.28" N	120°43'21.62" E	ST	7	63
45	SFK (Shuang-Fong-Kou)	24°28'43.12" N	120°47'50.39" E	SH-II	6	192
46	SFB (Shuang-Fu Bridge)	24°30'50.62" N	120°42'48.73" E	ST	10	28
47	XBW (Xia-Bei-Wo)	24°31'27.81" N	120°44'4.72" E	ST	10	55
48	CTC (Chih-Tu-Ci)	24°35'3.58" N	120°43'36.15" E	SH-II	4	69
49	HBK (Hong-Beng-Kan)	24°25'49.87" N	120°42'33.61" E	ST	4	121
50	LD (Long-Dong)	24°32'38.91" N	120°46'29.13" E	SH-II	2.5	79
51	LK (Long-Kang)	24°36'37.61" N	120°44'52.69" E	SH-II	9	3
52	NWII (Nan-Wo II)	24°30'5.68" N	120°43'53.50" E	ST	7	57
53	CLK (Che-Lun-Keng)	24°25'51.17" N	120°43'32.89" E	ST	2	157
54	JW (Jiang-Wo)	24°33'3.55" N	120°45'54.91" E	SH-II	10	34
56	IFF (Yi-Fang Farm)	24°32'29.53" N	120°46'52.54" E	SH-II	6	86
57	CTK (Chang-Tan-Keng)	24°26'12.68" N	120°46'19.75" E	SH-I	30	301

Note: 57 outcrops were documented initially, but 6 of them were excluded because of visible disturbances.

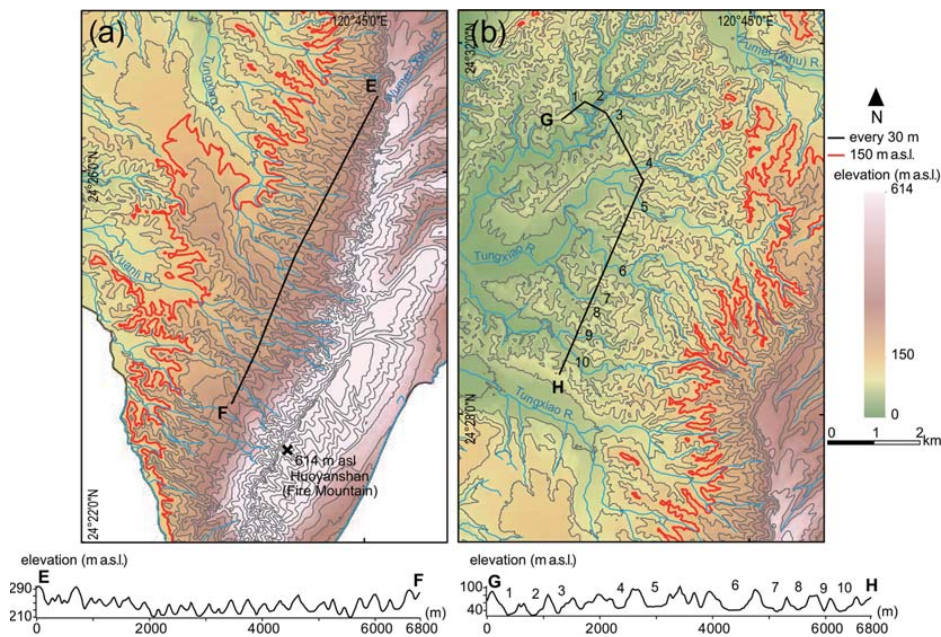


Figure 4. Detail maps of different fluvial drainage patterns in the Sedimentary Terraces (ST) with the respective elevation profiles of the valley cross sections. (a) Parallel patterns near the west-facing topographic escarpment between the SH-I (southeast) and ST (northwest) with valley bottoms mostly higher than 150 m a.s.l. Profile E–F shows the typical V-shaped valley cross sections. (b) Dendritic patterns in the northern ST area, especially with valley bottoms lower than 150 m a.s.l. Profile G–H shows wider and mainly box-shaped valley cross sections.

the rest of the outcrops – in general the upper part of the sequence. The layers were named according to their grain size composition applying the classification of the FAO (Food and Agriculture Organization of the United Nations; Jahn et al., 2006). They are from bottom to top (1) greyish loam (L), (2) loamy sand (LS), (3) alternations between greyish and yellowish silt loam (SiC), (4) sandy loam (SL), (5) gravel and cobble bed (CSB), and (6) silty loamy cover layer (SiL). The results of their respective grain size properties are listed in Table 2 and summarized in Fig. 7.

4.2.1 Greyish loam layer (L)

This layer is exposed only in three outcrops (01_HLPT, 10_EFB, and 025_JJC; Figs. 5 and 6 and Appendix C). They are located in the north of the SH-II and in the west of the ST. The upper 7 m of the layer are visible, but its total thickness is unclear, as the lower boundary is not exposed (Fig. 6). The upper boundary of this layer is even, continuous, and very distinct. Its internal structure is simple and massive; i.e. no bedding or laminae are visible. The sediment is poorly consolidated. However, it is quite sticky and difficult to excavate with hand tools. The grain size proportions range from 39 % to 52 % sand, 37 % to 48 % silt, and 11 % to 15 % clay, based on three samples (Fig. 7). This layer contains abundant mol-

lusc detritus, which is poorly oriented and mixed with the sediments without layering for identifying the palaeoflow direction.

4.2.2 Loamy sand layer (LS)

This layer is exposed in outcrops of the tablelands ST and SH-II ($n = 16$) (Fig. 6 and Appendix C). It is ca. 5–20 m thick. The internal structure of this layer is simple and massive. At some outcrops, thin layers (less than 1 cm) with iron coating are recorded at the upper 50 cm. The sediment is very poorly consolidated and easily to scratch by hand tools. The dominating grain size in the five samples is sand (62 %–88 %). Two of them show a slightly higher content of silt. The clay content is less than 10 % in all samples. The texture is in the range of sand to sandy loam (Fig. 7). This layer's biological content is too low to be distinguished macroscopically.

4.2.3 Alternation of greyish silt loam and yellowish silt loam layers (SiC)

These sediments are exposed in outcrops ($n = 27$; see Fig. 6 and Appendix C) at the tablelands of the ST and SH-II. Their thickness is ca. 10–15 m. The layer is also visible on the tidal flat in outcrop 051_LK during the neap tide. The internal

Table 2. Results of grain size analyses.

Sample ID	Layer	Sand (%)	Silt (%)	Clay (%)	Sediment texture (Jahn et al., 2006)
LK 0-4 sand dune 0-1	Modern beach sand	97.0	1.8	1.2	Sand
LK 0-4 sand dune 0-2	Modern beach sand	97.0	1.9	1.2	Sand
HLPT 0-7	SiL	45.3	43.1	11.6	Loam
NCT0-3	SiL	51.0	37.9	11.1	Loam
XNPW0-2	SiL	46.1	42.7	11.1	Loam
HDK0-4	SiL	34.8	50.2	14.9	Silt loam
TYGC-2	SiL	22.6	57.1	20.3	Silt loam
XP-1	SiL	44.2	39.7	16.2	Loam
XNPWH-2	SiL	43.0	42.2	14.7	Loam
TKD-3	SiL	50.9	36.7	12.4	Loam
JJC-2	SiL	38.8	44.0	17.1	Loam
HLPT 0-6	CSB	37.7	42.3	20.0	Loam
TKD-2	CSB	48.7	34.9	16.4	Loam
HLPT 0-5	SL-b	39.4	41.9	18.7	Loam
NCT0-2	SL-b	44.7	40.0	15.3	Loam
XNPW0-1	SL-b	25.3	53.6	21.1	Silt loam
DBD0-1	SL-b	50.3	42.4	7.3	Loam
XNPWH-1	SL-b	44.3	40.1	15.6	Loam
GJW-2	SL-b	32.8	47.3	19.9	Loam
TKD-1	SL-b	41.6	43.5	14.9	Loam
JJC-1	SL-b	42.3	40.9	16.9	Loam
NCT0-1	SL-y	60.4	29.8	9.8	Sandy loam
HDK0-1	SL-y	79.0	15.9	5.1	Loamy sand
HDK0-2	SL-y	71.3	21.4	7.3	Sandy loam
HDK0-3	SL-y	66.3	23.9	9.8	Sandy loam
LK 0-1	SL-y	89.3	7.7	3.0	Sand
LK 0-2	SL-y	89.9	7.2	2.9	Sand
LK 0-3	SL-y	73.0	19.8	7.2	Sandy loam
THST-1	SL-y	84.0	11.2	4.7	Loamy sand
THST-2	SL-y	56.3	32.4	11.4	Sandy loam
TYGC-1	SL-y	70.8	21.8	7.5	Sandy loam
LK 0-5 yellowish loam	SiC	22.9	68.0	9.2	Silt loam
LK 0-5 greyish silt loam	SiC	8.3	79.7	12.0	Silt loam/silt
HLPT 0-2 001	LS	86.7	10.3	3.0	Sand
HLPT 0-3 001	LS	70.4	25.0	4.7	Sandy loam
HLPT 0-4 upper	LS	85.6	11.4	2.9	Sand
LK 0-6	LS	88.2	8.4	3.4	Sand
LK 0-7	LS	62.4	31.6	6.0	Sandy loam
HLPT 0-1 middle	L	40.5	44.3	15.2	Loam
JJC-A-1	L	39.2	48.0	12.8	Loam
JJC-A-2	L	51.6	37.7	10.7	Loam

structure shows thin beds of (I) the yellowish sandy sediments and (II) greyish clayey and silty sediments (10–100 layers with ca. 5–10 cm thickness of each layer) (Fig. 6). Iron precipitation can be distinguished on the contacts between these thin beds. The sediments are generally poorly consolidated; the greyish sediments are stickier than the yellowish sediments. Silt is the dominating grain size in both sublayers (68 %–80 %), of which the yellowish one has a certain sand content (23 %, Fig. 7). No molluscs or other biological remains are distinguishable in this layer.

4.2.4 Sandy loam layer (SL)

This ca. 10–30 m thick layer is exposed in outcrops across the entire study area ($n = 43$) (Fig. 6 and Appendix C). The upper contact to the overlying gravel and cobble bed (CSB) is continuous and very distinct. However, the contact is difficult to distinguish when the CSB is missing, and this layer is overlain directly by the silty loamy cover layer (SiL) (Fig. 6 and Appendix A). The sedimentary texture of this layer shows significant vertical variations among the outcrops and is therefore subdivided into three categories. (I) The light

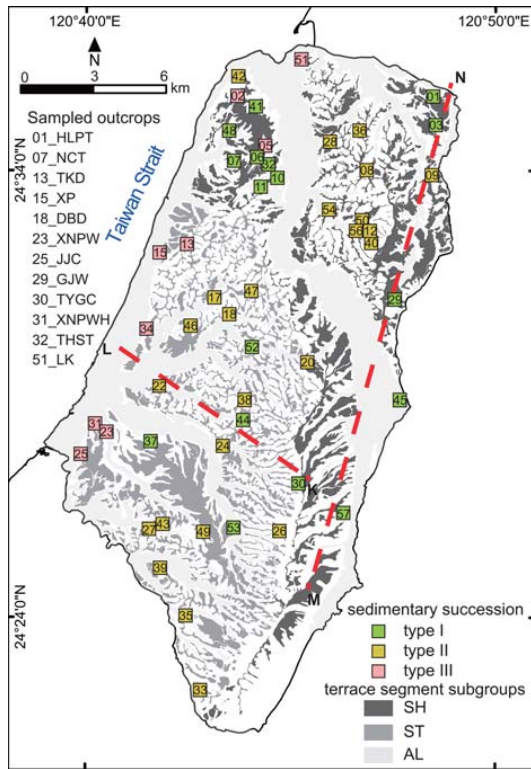


Figure 5. Location of the 51 studied outcrops (see Table 1); 26 outcrops are located in the SH, and 25 outcrops are in the ST. The 12 sampled outcrops for the grain size analyses are listed (see Table 2 for results). For profiles K–L and M–N and sedimentary subtype description, see Fig. 8.

greyish sandy material is in the lower metres (SL-g, not sampled). (II) The yellowish sandy material is in the middle part (ca. 5–10 m), which contains more than 50% and – in two samples – nearly 90% sand (SL-y) (Fig. 7). The upper ca. 1 m consists of brownish sandy loamy substrate (SL-b) with more than 40% silt. The sediments in all three subtypes are very poorly consolidated; only the brownish sediments are stickier. The overall internal structure of SL-g and SL-b is massive. In the SL-y, iron coating in thin beds is visible. Debris of molluscs can be found in this layer; especially outcrop 035_YZS contains abundant detritus of molluscs.

4.2.5 The gravel and cobble bed (CSB)

Gravel and cobble beds are widely distributed in the Miaoli Tableland and exposed in 26 outcrops (Figs. 6 and 7 and Appendix C). Their thickness is varying according to the location: ca. 5–20 m in the SH-II, < 10 m in the ST, and < 2 m in the distal edge of the tableland. The sedimentary structure of the layer is mostly clast-supported but is matrix-supported

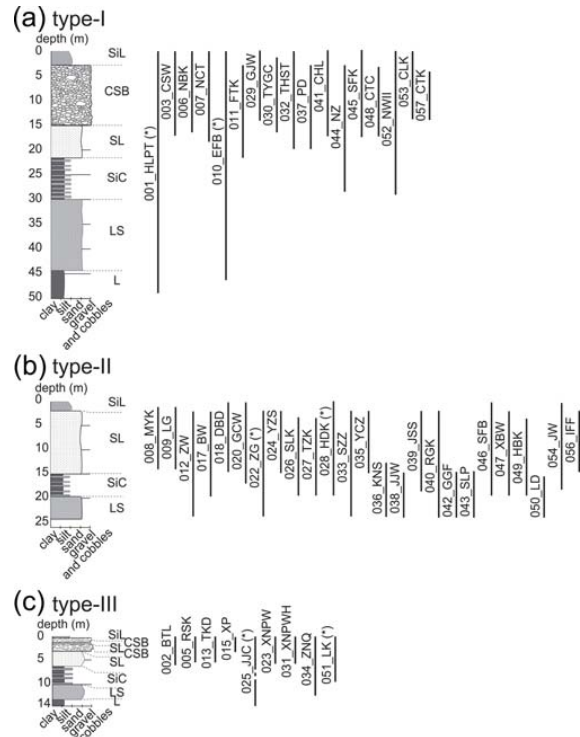


Figure 6. Schematic profiles of different sedimentary successions in the SH-II and ST with the respective outcrop numbers. (a) Type I: complete succession, located mainly in the larger tableland segments. (b) Type II: incomplete succession with the missing gravel and cobble bed (“remnants”), located mainly in the smaller tableland segments. (c) Type III: the succession with one or more thin gravel and cobble bed(s), located in the distal-tableland segments near the coast. Sediment layers are named after the FAO classification (Jahn et al., 2006): L – greyish loam, LS – loamy sand, SiC – alternations of greyish silt loam and yellowish silt loam, SL – sandy loam, CSB – coarse sand with stones and boulders (gravels and cobbles), and SiL – silty loam (cover layer). (*) Vertical lines indicate the relative depth of the outcrops with the respective sediment layers, which are visible in the field. The metrical depth scales are taken from the representative outcrops for each succession type.

in some outcrops at the distal edge of the tableland. Therefore the layer is classified as “coarse sand, with stones and boulders” (CSB) according to Jahn et al. (2006). In the clast-supported outcrops, the gravels are horizontally aligned with the long axes. The imbrication is poor; therefore, a precise analysis of flow directions is not possible. The gravels and cobbles consist of quartzite. Their sizes range from ca. 10 to 40 cm in the SH-II and from < 10 to ca. 30 cm in the ST. The gravels are well-rounded; their sphericity is moderate to platy.

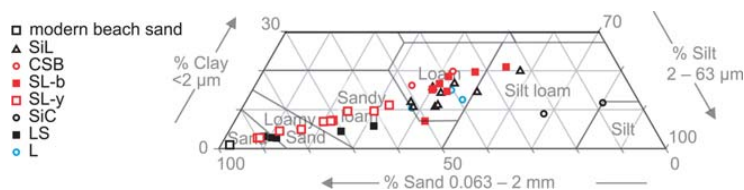


Figure 7. Grain size compositions presented in a combined ternary diagram; the samples were grouped for the respective sediment layers. The sandy loam layer (SL) is subdivided into the lower SL-y and the upper SL-b. The clay content in the samples is relatively constant, while sand and silt change significantly. Sediment nomenclature after Jahn et al. (2006). For detailed grain size distribution curves, see Appendix B.

The matrix material in the two samples taken from outcrops in the distal-tableland area is loamy; it consists of ca. 80 % sand and silt. The CSB in the distal tableland contains biological remains such as roots and wood debris.

The situation in the SH-I is different. Here the gravel and cobble bed is more than 20 m thick, and its elevation above the sea level is higher than in the SH-II and the ST. Its lower boundary is rarely visible. In the southernmost part of the SH-I (i.e. Fire Mountain), the gravel and cobble layer is inclined (estimated to be ca. 30°) to the east, which is in accordance with the records from the geological maps. Unfortunately, they are accessible only in few locations. The two studied outcrops show well-rounded quartz gravels and cobbles from 10–40 cm with poor imbrication.

4.2.6 Silty loamy cover layer (SiL)

The dusty cover layer can be found across the entire study area ($n = 25$) with a thickness from tens of centimetres up to 1.5 m (Fig. 6 and Appendix C). Its lower boundary, especially to the CSB, is very distinct. Its internal structure is simple and massive. It consists of a yellowish to reddish mixture of sand (35 %–51 %) and silt (30 %–44 %); clay occurs at 12 %–20 %. Only two of the nine samples have a silt content higher than 50 % (Fig. 7). The sediment is very loose and contains abundant fresh roots of the modern vegetation.

4.3 Subtypes of the sedimentary succession

The described sedimentary succession is unevenly exposed in the study area. Most outcrops show only a limited number of the layers. However, layers in neighbored outcrops can be recognized and linked over most of the study area. Nevertheless, small variations in the sedimentary succession have been recognized. Three subtypes of the layer assemblage were observed (Figs. 5, 6, and 8 and Appendices A and C): (I) the complete succession, (II) the quasi-complete succession with a missing gravel and cobble layer, and (III) the presence of a thin gravel and cobble bed(s) on the surface (0–3 m).

Type I is widely distributed in larger tableland segments of the SH-II and the ST (Figs. 5 and 8). The outcrops comprise identical sedimentary successions, and the gravel bed (CSB) is getting thinner toward the coast. The complete succession

is exposed with all layers only at two locations (001_HLPT and 010_EFB). However, also the smaller outcrops show an order of the layers, which is in accordance with the complete succession (Figs. 6 and 8).

The sedimentary succession in the SH-I is still unclear. The two studied outcrops contain a very thick gravel and cobble layer (> 20 m mainly). Subjacent sandy substrate is only exposed in outcrop 030_TYGC. Therefore, the sedimentary succession of the SH-I is named “quasi-type I”, because the sedimentary succession below the gravel unit is virtually unknown (Fig. 8).

Type II is found at the smaller tableland segments of the ST and the SH-II (Figs. 5 and 8). The outcrops include all the fine-grained sedimentary layers, but the overlying gravel and cobble layer is missing. In most outcrops in the SH-II, a sequence of LS–SiC–SL–SiL is exposed (Figs. 6 and 8). In contrast, the outcrops in the ST show a relatively thick layer of SL (ca. 20 m or more), while the L, LS, and SiC layers are rarely exposed.

Type III occurs in the ST and the SH-II along the fringe of the distal-tableland segments and at the coast (Figs. 5 and 8) at elevations below 50 m a.s.l. It includes SL, SiC, SiL, and L at the lower part and one or two thin (< 2 m) gravel and cobble bed(s) intercalated with sandy (SL) layers on the upper part to the surface (Figs. 6 and 8). The gravel bed(s) is getting thinner coastward.

Beside the gravel and cobble beds in the tableland segments, gravels and cobbles occur in the AL as well. For example, abundant gravels and cobbles are deposited in most of the fluvial paths especially in tributaries of the Tungxiao River within areas with dendritic drainage patterns (Appendix A). According to the field observations, these gravels and cobbles are composed of quartzite, their shapes are round, but the components are poorly sorted.

5 Discussion

The general topography of the Miaoli Tableland inclines from the highland in the southeast towards the coast in the north and in the west. A clear spatial separation of three main areas can be distinguished: the Sedimentary Highlands in the southeastern part (SH-I) and in the northern part (SH-II) as

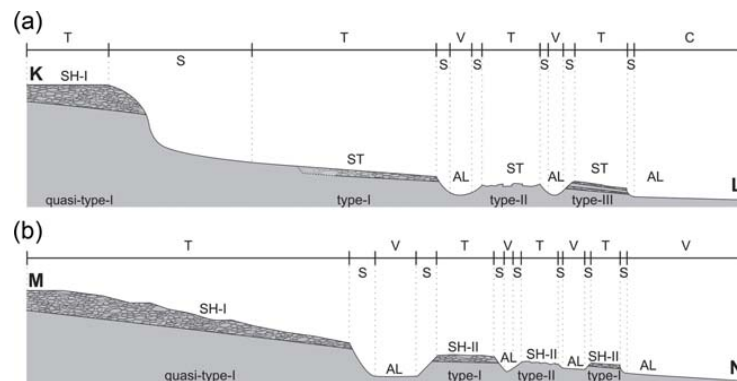


Figure 8. Schematic surface elevation profiles from (a) the highlands to the coastal plain through the SH-I and the ST (K–L) and (b) the highest point (i.e. Fire Mountain) to the Houlong River through the SH-I and the SH-II (M–N). The terrain categories and the corresponding subtypes of the sedimentary succession are marked (T: tableland segment, V: valley floor, C: coastal plain, and S: slope).

well as the Sedimentary Terraces (ST) in the western part. Especially the cliff-like topographic divide between the SH-I and the ST is a distinctive topographic landscape element in the Miaoli Tableland. This elevation-data-based topographical classification agrees in general with previous findings (Chang et al., 1998; Ota et al., 2006). However, the high resolution of the DEMs reveals that the topography of the tableland is much more disaggregated into larger and smaller segments than previously mapped. These segments cover most of the area of the Miaoli Tableland, and their surfaces can be tentatively connected or geometrically interpolated to an inferred palaeotopography in the respective areas (Figs. 2d and 3).

The internal sedimentary succession of the tableland segments is consistent in the SH-II and the ST areas but different in the SH-I. The individual strata of the SH-II and ST appear in the same order. The lower to middle part of the studied sedimentary sequence (L–LS–SiC–SL) represents an intertidal to supratidal deposition sequence, which has been reported by case studies in various locations globally (Goodbred and Saito, 2011; Dalrymple and Choi, 2007; Chen et al., 2014; Olariu et al., 2012; Buatois et al., 2012). This general tidal-dominant environment setting is consistent with the interpretation of the study of molluscs and foraminifera taken from this succession previously (Lee et al., 2002; Lin, 1969), although their stratigraphical context is not clear in detail. It is possibly due to sea-level changes (Shackleton, 2000) and long-term uplift of the Miaoli area (Ota et al., 2006; Yang et al., 2016). The distinct boundaries of each sedimentary layer may result from the interruption of sedimentation or the subsequent erosion, especially during the aforementioned regression periods (Davis, 2012).

Depending on the location, the studied sequence is topped by units of fluvial gravels and cobbles with different thickness. Previously, tablelands were identified by their flat surface and the occurrence of gravels and cobbles on their sur-

face (Chang et al., 1998; Lin and Chou, 1978; Teng, 1979). We found that this is mainly the case for the larger and also some smaller segments, which represent sedimentation type I (Figs. 5 and 8 and Appendix A). On most of the small segments, the gravels and cobbles are missing (type II, Figs. 5 and 8 and Appendix A). However, the inferred palaeotopography implies a formerly continuously distributed gravel and cobble layer in the ST and the SH-II, where the smaller segments represent remnants, from which the gravels and cobbles were eroded. The fact that gravels and cobbles are also accumulated in the channels between segments with missing a gravel and cobble layer supports the idea that they were reworked from higher positions on the ST and the SH-II into the AL. This is new in comparison with Chang et al. (1998) and Ota et al. (2006), who did not assume a continuous gravel and cobble layer in the ST and SH-II area. In the distal segments near the coast, the gravels and cobbles tend to be smaller and occur in several thin layers (type III, Figs. 5 and 8 and Appendix A); thus we assume that the gravels and cobbles are reworked from the nearby sources (i.e. the proximal segments and remnants in the SH-II and ST).

The clast-supported structure and the moderate sorting of the fluvial deposits indicate that the deposition occurred rapidly, assumably during high-precipitation and discharge events. These characteristics are similar to the gravel and cobble beds in the other tablelands in northern Taiwan (Teng, 1996b). Although Chang et al. (1998) measured the cobble imbrication at several locations, we were not able to confirm their results due to the poor conservation of the sampling sites in recent decades. Moreover, the sphericity of the gravels and cobbles in our outcrops hinders the reconstruction of individual transport directions.

Regardless of the occurrence of gravels and cobbles, the whole area is covered by a layer of fine-grained material (SiL), which has been interpreted as the in situ lateritic soil formation before (Chang et al., 1998; Ho, 1988; Chang,

1955). However, the grain size data yielded a high content of fine silt rather than clay in this layer (Fig. 7). The fine silt is typical for aeolian transport (Pye and Zhou, 1989). Therefore, this study follows the assumption of a significant aeolian dust input (Chen et al., 2013; Tsai et al., 2008; Hebenstreit and Böse, 2015) besides the local weathering. Dust transport may also explain the silt enrichment in the upper part of the SL layer.

The whole sedimentary sequence in the SH-II and the ST is in agreement with the descriptions in early sedimentary studies of the Miaoli Tableland, where it has been named the Lungkang (Lk) Formation (Lin, 1963, 1969) or Tūsyō/Tungxiao (Ts) Formation (Chang, 1948; Makiyama, 1934, 1937). This study refers to those definitions because they are based on the descriptions of the uppermost 50–100 m of the succession directly in the study area, although the former studies tended to use the term Toukoshan (Tk) Formation (Chang, 1955), which includes however the whole Plio-Quaternary strata in western Taiwan (Chen et al., 2001; Ota et al., 2006; Lee et al., 2002; Huang, 1984; Tsai et al., 2006; Yang et al., 2016).

Early studies assumed that all fine-grained sediments of the succession are the result of in situ weathered bedrock (Chang, 1955; Ho, 1988). That interpretation might be due to a different usage of the term “bedrock”, which describes in general the underlying beds in the Taiwanese literature. Although the top sediment layers in the Miaoli Tableland are intensively weathered, the loose and not lithified lower sediment units appear unweathered, and the entire sedimentary succession comprises unconsolidated sediments.

The tableland segments are separated by ongoing fluvial incision and backward erosion. Their special layout and morphology follow the fluvial pattern of the respective river catchments, which is dendritic in the SH-II and ST and more parallel in the SH-I. The cross sections of the fluvial channels between the segments are V-shaped above and box-shaped below 150 m a.s.l., respectively. This altitude marks at present the point in the longitudinal river profile where the fluvial morphodynamic changes from linear incision to lateral erosion with gravel accumulation (Charlton, 2008) representing the alluvial plains (AL). The box-shaped valleys are developed in the catchments with the dendritic drainage pattern. The formation of this pattern is supported by the fact that the lithology is basically consistent within the whole study area; thus the flow paths have developed freely, and they are not constrained by the geological or tectonic factors (e.g. the Tungxiao Anticline).

Integrating the results of this study into previous concepts (Chang et al., 1998; Ota et al., 2006), the landscape evolution of the Miaoli Tableland can be summarized as follows:

- Tidal and coastal sediments were deposited in the mountain foreland during periods of different but generally high sea levels in the Taiwan Strait. They are visible as the fine-grained sediments in the present ST and SH-

II areas. These sediments represent the bay sediments in the interpretation of Chang et al. (1998). Whether they were also deposited in the present SH-I area is unknown.

- Subsequently, gravels and cobbles were deposited in the foreland basin in the form of one or several alluvial fans, which made up the present SH-I. Chang et al. (1998) suggested that they covered parts of the coastal sediments in the SH-II area. If they were transported by a single event or by multiple independent events by the Daan River, Wumei (Xihu) River, and Houlong River is also unknown. The terrain of the SH-I was subsequently uplifted along the Tongluo Fault (Ota et al., 2006), and thus the alluvial fans were prevented from further gravel and cobble accumulation.
- The ongoing uplift and the simultaneous incision of the SH-I induced the remobilization of the gravels and cobbles which were transported into the western and northern foreland of the SH-I, where they are accumulated as the present gravel and cobble layers of the SH-II and the ST. Further uplift of the SH-I along the present escarpment between the SH-I and the ST, which was assumed to be an inferred thrust fault (Chang et al., 1998), separated both terrains, stopped the gravel and cobble transport into the ST, and beheaded the valleys of the SH-I. The sediments in the ST area were slightly folded along the Tungxiao Anticline (Ota et al., 2006) during this terrain uplift. The folding may have enhanced the subsequent incision of the ST, where backward erosion is continuing in the upper and steeper channel sections. In this way, the gravels and cobbles are reworked again – from the ST surface into the AL channels and the (coastal) distal-tableland surfaces.
- The result of the rework is a cascade of gravel and cobble transportation in the Miaoli Tableland: previously from the mountains to the Sedimentary Highlands, then to the Sedimentary Terraces, and recently to the Alluvial and the Coastal Plains.

6 Conclusion

This study gives new detailed insights into the surface morphology and the sedimentary sequences of the Miaoli Tableland. The new high-resolution mapping enables the reconstruction of the palaeotopography of the region. The presented classification of tableland segments is thereby inferred from a mathematical calculation and widely independent from a subjective interpretation.

From the newly reconstructed palaeosurfaces in the western and northern part of the tableland we concluded that a quasi-continuous gravel and cobble cover existed not only in the Sedimentary Highlands but also in the Sedimentary Terraces, which is new in comparison with previous interpreta-

tions (Chang et al., 1998; Ota et al., 2006). This means that the Sedimentary Terraces (ST) and the northern Sedimentary Highlands (SH-II) covered originally a wider area than previously mapped (Chang et al., 1998). Our interpretation of cascade-like gravel and cobble rework implies that the main mass of gravels and cobbles was deposited originally in the southern Sedimentary Highlands (SH-I) and was reworked from there to the northern Sedimentary Highlands (SH-II) and the Sedimentary Terraces (ST).

Our sedimentological results suggest that the concept of the Lungkang Formation (Lin, 1963) or the Tûsyô/Tungxiao Formation (Chang, 1948; Makiyama, 1934, 1937) may be considered adequate stratigraphic terms to describe the tidal–fluvial–aeolian sediment succession of the uppermost 50–100 m in the northern and western part (SH-II and ST) of the Miaoli Tableland. Although absolute dating results are not available at this stage of research, the succession may represent one sedimentation cycle, which can be tentatively correlated with the last glacial cycle. Subsequent uplift brought the terrestrial sediments into a position above the Holocene sea-level high stand, provoking incision. The overall tableland morphology exhibits a stepwise sequence of sedimentation, uplift, and erosion in the area.

Fluvial incision created a characteristic drainage network with different patterns, depending on topographical parameters like the altitude and the location in the respective tableland areas but widely independent from the lithology in the Miaoli Tableland. The loose and easily erodible sediments enabled the formation of wide valley cross sections in the alluvial plains, which we tentatively named box-shaped valleys.

This study of terrace landforms in the frontal part of the mountain foreland in Taiwan has highlighted the possibility that a systematical terrain and sediment analysis can reveal new insights into the differentiated landform evolution in the Taiwanese foothills in the future.

Appendix A: Field photos of the Miaoli Tableland



Figure A1. Overview on the Tungxiao River catchment (the ST area) seen from the SH-I terrace (location: $24^{\circ}26'57.92''$ N, $120^{\circ}45'15.42''$ E; facing northwest, 24 October 2018). The tableland segments are dissected by channels of the dendritic fluvial network, visible in the centre of the photo.



Figure A2. Example of type I succession in outcrop 001_HLPT (location: $24^{\circ}35'45.30''$ N, $120^{\circ}48'24.01''$ E; facing west, 3 April 2015). The outcrop is about 49 m high and located on the left bank of the Houlong River. It shows fine-grained coastal sediments in the lower and central part and fluvial gravels and cobbles in the upper part.



Figure A3. Example of type II succession in outcrop 022_ZG (location: 24°28'55.02" N, 120°42'8.09" E; facing west, 8 January 2017). The outcrop is about 20 m high and located in the Tungxiao River catchment. It is excavated by a small creek, which is located between the outcrop and the road in the foreground. It represents the remnant of a tableland segment with fine-grained coastal sediments (greyish sand in the lower part and brownish sand in the upper part). The succession is covered by the silty cover layer (SiL) directly. This cover layer is barely visible between the vegetation in the upper central part of the picture.



Figure A4. Panorama photo of an example of type III succession in outcrop 051_LK (location: 24°36'37.61" N, 120°44'52.69" E; facing southeast, 23 October 2018). The outcrop is about 9 m high and located at the coast between the estuaries of the Houlong River and the Wumei (Xihu) River. It represents the sedimentary succession of the distal-tableland segments as part of the SH-II. The outcrop shows fine-grained sandy sediments covered by gravels and cobbles and modern aeolian sand. The gravels and cobbles appear as a channel infill in the centre of the picture.



Figure A5. A modernized channel in the box-shaped valley in the Tungxiao River catchment (location: 24°27'20.90" N, 120°44'6.72" E; facing west, 25 December 2014). The tableland segments in the background of this photo are classified as the ST. The valley floor is classified as AL; the fluvial channel is constrained by the artificial levees and covered by abundant gravel and cobble depositions.

Appendix B: Grain size distribution curves of all the studied samples

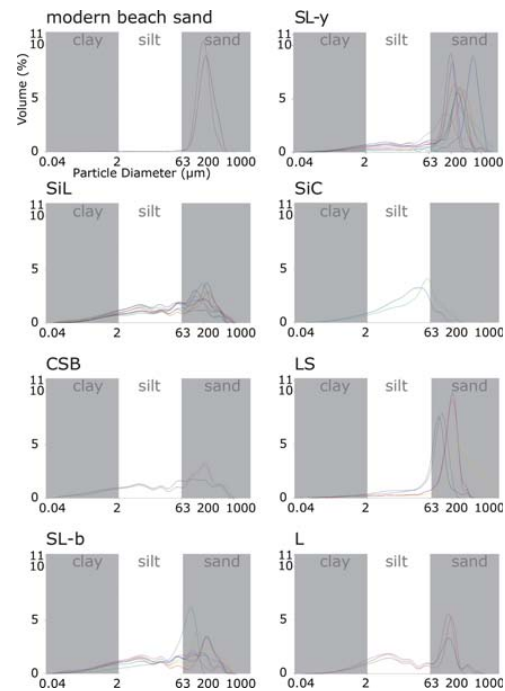


Figure B1. Samples are subgrouped by the corresponding sedimentary layers. Two samples are taken from the modern beach (dune) sand for comparison with the sandy materials in other layers. The grain size fractions are after the Wentworth scale.

Appendix C: Columnar sections and pictures of the outcrops in the Miaoli Tableland

See supplementary data of file 001-HLPT to 057-CTK at <https://doi.org/10.17169/refubium-31813> (Liu et al., 2021).

Data availability. All relevant data used in this study are cited and presented in the text. Supplementary data of file 001-HLPT to 057-CTK are available at <https://doi.org/10.17169/refubium-31813> (Liu et al., 2021).

Author contributions. All authors, SHL, RH, and MB, carried out the conceptualization, methodology, and investigation of this study together. SHL completed the fieldwork and the software and formal analyses, which are in the context of a PhD study programme supervised by MB. SHL and RH carried out the data visualization. This paper was drafted by SHL and revised by RH and MB.

Competing interests. Margot Böse is currently a member of the advisory board of *E&G Quaternary Science Journal*.

Disclaimer. Publisher's note: Copernicus Publications remains neutral with regard to jurisdictional claims in published maps and institutional affiliations.

Acknowledgements. The authors thank Jiun-Chuan Lin, Chia-Han Tseng, and Chia-Hung Jen for their friendly support of the fieldwork and Manfred Frechen for providing the access to the sediment lab. Moreover, we would like to thank Yu-Jia Chiu for the technical support of the base maps in Taiwan. Thanks go to Yan Li and Dirk Wenske for the discussion on the relevant topics and Christopher Lüthgens for the comments during the field observations. Thanks go to Shyh-Jeng Chyi and Lih-Der Ho for the comments during the INQUA Congress 2019. Thanks go to the Jing-Ji company and Chang Chun Petrochemical Co., Ltd Miaoli factory for the assessment of the outcrops. Finally, special thanks go to Li-Chun Xiao for managing the legal issues of open-access data usage for this study and Chu-Pan Lin for supporting the fieldwork.

Financial support. We acknowledge support from the Open Access Publication Initiative of Freie Universität Berlin.

Review statement. This paper was edited by Tony Reimann and reviewed by Toru Tamura and one anonymous referee.

References

- Angelier, J., Barrier, E., and Chu, H. T.: Plate collision and paleostress trajectories in a fold-thrust belt: The foothills of Taiwan, *Tectonophysics*, 125, 161–178, [https://doi.org/10.1016/0040-1951\(86\)90012-0](https://doi.org/10.1016/0040-1951(86)90012-0), 1986.
- Beuselinck, L., Govers, G., Poesen, J., Degraer, G., and Froyen, L.: Grain-size analysis by laser diffractometry: comparison with the sieve-pipette method, *Catena*, 32, 193–208, [https://doi.org/10.1016/S0341-8162\(98\)00051-4](https://doi.org/10.1016/S0341-8162(98)00051-4), 1998.
- Bridgland, D. and Westaway, R.: Climatically controlled river terrace staircases: A worldwide Quaternary phenomenon, *Geomorphology*, 98, 285–315, <https://doi.org/10.1016/j.geomorph.2006.12.032>, 2008.
- Buatois, L. A., Santiago, N., Herrera, M., Plink-Björklund, P., Steel, R. O. N., Espin, M., and Parra, K.: Sedimentological and ichnological signatures of changes in wave, river and tidal influence along a Neogene tropical deltaic shoreline, *Sedimentology*, 59, 1568–1612, <https://doi.org/10.1111/j.1365-3091.2011.01317.x>, 2012.
- Center for GIS RCHSS Academia Sinica: Taiwan Historical Atlas Web Map Tile Service [data set], available at: <http://gis.sinica.edu.tw/tileserver/wmts> (last access: 14 January 2022), 2017.
- Central Geological Survey: National Geological Data Warehouse [data set], available at: <https://gis3.moeacgs.gov.tw/gwh/gsb97-1/sys8/t3/index1.cfm> (last access: 14 January 2022), 2017.
- Central Weather Bureau: Typhoon Data Base [data set], available at: <https://rdc28.cwb.gov.tw/TDB/> (last access: 14 January 2022), 2019.
- Central Weather Bureau: Tidal level statistics [data set], available at: https://www.cwb.gov.tw/V8/C/C/MMC_STAT/sta_tide.html (last access: 14 January 2022), 2020.
- Chang, H.-C.: Baishatun, Central Geological Survey, Geological Map of Taiwan scale 1:50 000, Taipei, Taiwan, available at: <https://twgeoref.moeacgs.gov.tw/GipOpenWeb/wSite/ct?xItem=118492&ctNode=1303&mp=6> (last access: 14 January 2022), 1990.
- Chang, H.-C.: Dajia, Central Geological Survey, Geological Map of Taiwan scale 1:50 000, Taipei, Taiwan, available at: <https://twgeoref.moeacgs.gov.tw/GipOpenWeb/wSite/ct?xItem=118453&ctNode=333&mp=106> (last access: 14 January 2022), 1994.
- Chang, J.-C., Teng, K.-H., and Liu, M.-C.: A Geomorphological Study on River Terraces in Miaoli Hills, *Geogr. Res.*, 29, 97–112, <https://doi.org/10.6234/JGR>, 1998.
- Chang, L.-S.: The revision of stratigraphy categories of Taiwan (continued), *Geological Review*, 13, 291–310, 1948.
- Chang, L.-S.: Geologic map of Taiwan, Geological Survey of Taiwan, Taipei, Taiwan, available at: <https://twgeoref.moeacgs.gov.tw/GipOpenWeb/wSite/ct?xItem=111421&ctNode=217&mp=6> (last access: 14 January 2022), 1953.
- Chang, L.-S.: The strata of Taiwan, *Quarterly Journal of the Taiwan Bank*, 7, 26–49, 1955.
- Charlton, R.: *Fundamentals of fluvial geomorphology*, Routledge, New York, USA, <https://doi.org/10.4324/9780203371084>, 2008.
- Chen, C.-G.: Miaoli County, The soil investigation report of the slopes, Mountain Agricultural Resources Development Bureau,

- Nantou, Taiwan, available at: <https://tssurgo.tari.gov.tw/Tssurgo> (last access: 14 January 2022), 1983.
- Chen, H.-F., Yeh, P.-Y., Song, S.-R., Hsu, S.-C., Yang, T.-N., Wang, Y., Chi, Z., Lee, T.-Q., Chen, M.-T., Cheng, C.-L., Zou, J., and Chang, Y.-P.: The Ti/Al molar ratio as a new proxy for tracing sediment transportation processes and its application in aeolian events and sea level change in East Asia, *J. Asian Earth Sci.*, 73, 31–38, <https://doi.org/10.1016/j.jseaes.2013.04.017>, 2013.
- Chen, S., Steel, R. J., Dixon, J. F., and Osman, A.: Facies and architecture of a tide-dominated segment of the Late Pliocene Orinoco Delta (Morne L'Enfer Formation) SW Trinidad, *Mar. Petrol. Geol.*, 57, 208–232, <https://doi.org/10.1016/j.marpetgeo.2014.05.014>, 2014.
- Chen, W.-S., Ridgway, K. D., Horng, C.-S., Chen, Y.-G., Shea, K.-S., and Yeh, M.-G.: Stratigraphic architecture, magnetostratigraphy, and incised-valley systems of the Pliocene-Pleistocene collisional marine foreland basin of Taiwan, *GSA Bulletin*, 113, 1249–1271, [https://doi.org/10.1130/0016-7606\(2001\)113<1249:SAMAIV>2.0.CO;2](https://doi.org/10.1130/0016-7606(2001)113<1249:SAMAIV>2.0.CO;2), 2001.
- Chen, W.-S., Chen, Y.-G., Shih, R.-C., Liu, T.-K., Huang, N.-W., Lin, C.-C., Sung, S.-H., and Lee, K.-J.: Thrust-related river terrace development in relation to the 1999 Chi-Chi earthquake rupture, Western Foothills, central Taiwan, *J. Asian Earth Sci.*, 21, 473–480, [https://doi.org/10.1016/S1367-9120\(02\)00072-X](https://doi.org/10.1016/S1367-9120(02)00072-X), 2003.
- Chen, Y.-G. and Liu, T.-K.: Sea Level Changes in the Last Several Thousand Years, Penghu Islands, Taiwan Strait, *Quaternary Res.*, 45, 254–262, <https://doi.org/10.1006/qres.1996.0026>, 1996.
- Chen, Y.-G., Shyu, J. B. H., Ota, Y., Chen, W.-S., Hu, J.-C., Tsai, B.-W., and Wang, Y.: Active structures as deduced from geomorphic features: a case in Hsinchu Area, northwestern Taiwan, *Quaternary Int.*, 115–116, 189–199, [https://doi.org/10.1016/S1040-6182\(03\)00107-1](https://doi.org/10.1016/S1040-6182(03)00107-1), 2004.
- Chen, Z.-S., Hseu, Z.-Y., and Tsai, C.-C.: The soils of Taiwan, *World soils book series*, Springer, Dordrecht, <https://doi.org/10.1007/978-94-017-9726-9>, 2015.
- Ching, K.-E., Hsieh, M.-L., Johnson, K. M., Chen, K.-H., Rau, R.-J., and Yang, M.: Modern vertical deformation rates and mountain building in Taiwan from precise leveling and continuous GPS observations, 2000–2008, *J. Geophys. Res.*, 116, B08406, <https://doi.org/10.1029/2011jb008242>, 2011.
- Choi, J. H., Kim, J. W., Murray, A. S., Hong, D. G., Chang, H. W., and Cheong, C.-S.: OSL dating of marine terrace sediments on the southeastern coast of Korea with implications for Quaternary tectonics, *Quatern. Int.*, 199, 3–14, <https://doi.org/10.1016/j.quaint.2008.07.009>, 2009.
- Covey, M.: The Evolution of Foreland Basins to Steady State: Evidence from the Western Taiwan Foreland Basin, in: *Foreland Basins*, Blackwell Publishing Ltd., 77–90, <https://doi.org/10.1002/9781444303810.ch4>, 1986.
- Dadson, S. J., Hovius, N., Chen, H., Dade, W. B., Hsieh, M.-L., Willett, S. D., Hu, J.-C., Horng, M.-J., Chen, M.-C., Stark, C. P., Lague, D., and Lin, J.-C.: Links between erosion, runoff variability and seismicity in the Taiwan orogen, *Nature*, 426, 648–651, <https://doi.org/10.1038/nature02150>, 2003.
- Dalrymple, R. W. and Choi, K.: Morphologic and facies trends through the fluvial–marine transition in tide-dominated depositional systems: A schematic framework for environmental and sequence-stratigraphic interpretation, *Earth-Sci. Rev.*, 81, 135–174, <https://doi.org/10.1016/j.earscirev.2006.10.002>, 2007.
- Davis, R. A.: Tidal Signatures and Their Preservation Potential in Stratigraphic Sequences, in: *Principles of tidal sedimentology*, edited by: Davis, R. A. and Dalrymple, R. W., Springer, Dordrecht, 35–55, https://doi.org/10.1007/978-94-007-0123-6_3, 2012.
- Deffontaines, B., Lacombe, O., Angelier, J., Chu, H. T., Mouthereau, F., Lee, C. T., Deramond, J., Lee, J. F., Yu, M. S., and Liew, P. M.: Quaternary transfer faulting in the Taiwan Foothills: evidence from a multisource approach, *Tectonophysics*, 274, 61–82, [https://doi.org/10.1016/S0040-1951\(96\)00298-3](https://doi.org/10.1016/S0040-1951(96)00298-3), 1997.
- Delcaillau, B.: Geomorphic response to growing fault-related folds: example from the foothills of central Taiwan, *Geodin. Acta*, 14, 265–287, [https://doi.org/10.1016/S0985-3111\(01\)01071-3](https://doi.org/10.1016/S0985-3111(01)01071-3), 2001.
- Eshel, G., Levy, G. J., Mingelgrin, U., and Singer, M. J.: Critical Evaluation of the Use of Laser Diffraction for Particle-Size Distribution Analysis, *Soil Sci. Soc. Am. J.*, 68, 736–743, <https://doi.org/10.2136/sssaj2004.7360>, 2004.
- Goodbred, S. and Saito, Y.: Tide-Dominated Deltas, in: *Principles of tidal sedimentology*, edited by: Davis, R. A. and Dalrymple, R. W., Springer, Dordrecht, 129–149, https://doi.org/10.1007/978-94-007-0123-6_7, 2011.
- Hanebuth, T. J. J., Voris, H. K., Yokoyama, Y., Saito, Y., and Okuno, J. I.: Formation and fate of sedimentary depocentres on Southeast Asia's Sunda Shelf over the past sea-level cycle and biogeographic implications, *Earth-Sci. Rev.*, 104, 92–110, <https://doi.org/10.1016/j.earscirev.2010.09.006>, 2011.
- Hebenstreit, R. and Böse, M.: Quaternary mineral aeolian dust deposits in Taiwan and their potentials as a new archive, XIX INQUA Congress, 27 July–2 August 2015, Nagoya, Japan, available at: https://www.inqua-seqs.org/files/INQUA2015_program_web.pdf (last access: 14 January 2022), 2015.
- Ho, C.-S.: An introduction to the geology of Taiwan: explanatory text of the geologic map of Taiwan, Central Geological Survey, Taipei, Taiwan, available at: <https://twgeoref.moeacgs.gov.tw/GipOpenWeb/wSite/ct?xItem=109139&ctNode=1303&mp=6> (last access: 14 January 2022), 1988.
- Ho, H.-C.: Miaoli, Central Geological Survey, Geological Map of Taiwan scale 1:50 000, Taipei, Taiwan, available at: <https://twgeoref.moeacgs.gov.tw/GipOpenWeb/wSite/ct?xItem=118489&ctNode=1303&mp=6> (last access: 14 January 2022), 1994.
- Horng, C.-S.: Age of the Tananwan Formation in Northern Taiwan: A Reexamination of the Magnetostratigraphy and Calcareous Nannofossil Biostratigraphy, *Terr. Atmos. Ocean. Sci.*, 25, 137–147, [https://doi.org/10.3319/tao.2013.11.05.01\(tt\)](https://doi.org/10.3319/tao.2013.11.05.01(tt)), 2014.
- Horng, C.-S. and Huh, C.-A.: Magnetic properties as tracers for source-to-sink dispersal of sediments: A case study in the Taiwan Strait, *Earth Planet. Sc. Lett.*, 309, 141–152, <https://doi.org/10.1016/j.epsl.2011.07.002>, 2011.
- Huang, T.: Planktic foraminiferal biostratigraphy and datum planes in the Neogene sedimentary sequence in Taiwan, *Palaeogeogr. Palaeoclimatol.*, 46, 97–106, [https://doi.org/10.1016/0031-0182\(84\)90028-2](https://doi.org/10.1016/0031-0182(84)90028-2), 1984.

- Huh, C.-A., Chen, W., Hsu, F.-H., Su, C.-C., Chiu, J.-K., Lin, S., Liu, C.-S., and Huang, B.-J.: Modern (< 100 years) sedimentation in the Taiwan Strait: Rates and source-to-sink pathways elucidated from radionuclides and particle size distribution, *Cont. Shelf Res.*, 31, 47–63, <https://doi.org/10.1016/j.csr.2010.11.002>, 2011.
- Jahn, R., Blume, H. P., Asio, V. B., Spaargaren, O., and Schad, P.: Guidelines for soil description, 4th edn., Food and Agriculture Organization of the United Nations, Rome, ISBN 9251055211, 2006.
- Jan, S., Wang, J., Chern, C.-S., and Chao, S.-Y.: Seasonal variation of the circulation in the Taiwan Strait, *J. Marine Syst.*, 35, 249–268, [https://doi.org/10.1016/S0924-7963\(02\)00130-6](https://doi.org/10.1016/S0924-7963(02)00130-6), 2002.
- Konert, M. and Vandenberghe, J.: Comparison of laser grain size analysis with pipette and sieve analysis: a solution for the underestimation of the clay fraction, *Sedimentology*, 44, 523–535, <https://doi.org/10.1046/j.1365-3091.1997.d01-38.x>, 1997.
- Lee, C.-L., Huang, T., Shieh, K.-S., and Chen, Z.-H.: The chronostratigraphy and sedimentary environments of the Toukoshan Fm. in Beishatun area, Miaoli, Annual Report of Central Geological Survey, MOEA, 1999–2000, 17–20, available at: <https://twgeoref.moeacgs.gov.tw/GipOpenWeb/wSite/ct?xItem=111058&ctNode=1303&mp=6> (last access: 14 January 2022), 2002.
- Lee, J.-F.: Dongshi, Central Geological Survey, Geological Map of Taiwan scale 1:50 000, Taipei, Taiwan, available at: <https://twgeoref.moeacgs.gov.tw/GipOpenWeb/wSite/ct?xItem=118454&ctNode=1303&mp=6> (last access: 14 January 2022), 2000.
- Lin, A. T. and Watts, A. B.: Origin of the West Taiwan basin by orogenic loading and flexure of a rifted continental margin, *J. Geophys. Res.-Sol. Ea.*, 107, ETG 2-1–ETG 2-19, <https://doi.org/10.1029/2001jb000669>, 2002.
- Lin, A. T., Watts, A. B., and Hesselbo, S. P.: Cenozoic stratigraphy and subsidence history of the South China Sea margin in the Taiwan region, *Basin Res.*, 15, 453–478, <https://doi.org/10.1046/j.1365-2117.2003.00215.x>, 2003.
- Lin, C. C.: Geomorphology of Taiwan, The Historical Research Commission of Taiwan Province, Taipei, Taiwan, 1957.
- Lin, C. C.: The Lungkang Formation, lower marine terrace deposits near Miaoli, *Petroleum Geology of Taiwan*, 2, 87–105, 1963.
- Lin, C. C.: Holocene Geology of Taiwan, *Acta Geologica Taiwanica*, 13, 83–126, 1969.
- Lin, C. C. and Chou, J. T.: Geology of Taiwan, Maw Chang Book Co., Ltd., Taipei, Taiwan, 1978.
- Liu, J. P., Milliman, J. D., Gao, S., and Cheng, P.: Holocene development of the Yellow River's subaqueous delta, North Yellow Sea, *Mar. Geol.*, 209, 45–67, <https://doi.org/10.1016/j.margeo.2004.06.009>, 2004.
- Liu, J. P., Liu, C. S., Xu, K. H., Milliman, J. D., Chiu, J. K., Kao, S. J., and Lin, S. W.: Flux and fate of small mountainous rivers derived sediments into the Taiwan Strait, *Mar. Geol.*, 256, 65–76, <https://doi.org/10.1016/j.margeo.2008.09.007>, 2008.
- Liu, S.-H., Böse, M., and Hebenstreit, R.: The columnar sections and pictures of the outcrops in Miaoli Tableland, Refubium – Freie Universität Berlin Repository [data set], <https://doi.org/10.17169/refubium-31813>, 2021.
- Makiyama, T.: Hakusyatou Sheet, Bureau of Productive Industries, Government-General of Taiwan, Explanatory text of the geological map of Taiwan (1:50 000), Tokyo, Japan, available at: <https://twgeoref.moeacgs.gov.tw/GipOpenWeb/wSite/ct?xItem=119130&ctNode=217&mp=6> (last access: 14 January 2022), 1934.
- Makiyama, T.: The topographic and geological map of Tüsyö petroleum field, Bureau of Productive Industries, Government-General of Taiwan, Tokyo, Japan, available at: <https://twgeoref.moeacgs.gov.tw/GipOpenWeb/wSite/ct?xItem=108126&ctNode=1304&mp=104> (last access: 14 January 2022), 1937.
- Mather, A. E., Stokes, M., and Whitfield, E.: River terraces and alluvial fans: The case for an integrated Quaternary fluvial archive, *Quaternary Sci. Rev.*, 166, 74–90, <https://doi.org/10.1016/j.quascirev.2016.09.022>, 2017.
- Matsu'ura, T., Kimura, H., Komatsubara, J., Goto, N., Yanagida, N., Ichikawa, K., and Furusawa, A.: Late Quaternary uplift rate inferred from marine terraces, Shimoka Peninsula, northeastern Japan: A preliminary investigation of the buried shoreline angle, *Geomorphology*, 209, 1–17, <https://doi.org/10.1016/j.geomorph.2013.11.013>, 2014.
- Miall, A. D.: Fluvial Depositional Systems, Springer Geology, Springer International Publishing, Switzerland, 316 pp., <https://doi.org/10.1007/978-3-319-24304-7>, 2014.
- NASA JPL: 1 Arc Second scene N24 E120 [data set], <https://doi.org/10.5067/MEASURES/SRTM/SRTMGL1.003>, 2013.
- National Land Surveying and Mapping Center: Taiwan Map Service [data set], available at: <https://wmts.nlsc.gov.tw/wmts> (last access: 14 January 2022), 2016.
- Olariu, C., Steel, R. J., Dalrymple, R. W., and Gingras, M. K.: Tidal dunes versus tidal bars: The sedimentological and architectural characteristics of compound dunes in a tidal seaway, the lower Baronia Sandstone (Lower Eocene), Ager Basin, Spain, *Sediment. Geol.*, 279, 134–155, <https://doi.org/10.1016/j.sedgeo.2012.07.018>, 2012.
- Ota, Y., Shyu, J. B., Chen, Y.-G., and Hsieh, M.-L.: Deformation and age of fluvial terraces south of the Choushui River, central Taiwan, and their tectonic implications, *Western Pacific Earth Sciences*, 2, 251–260, 2002.
- Ota, Y., Chen, Y.-G., and Chen, W.-S.: Review of paleoseismological and active fault studies in Taiwan in the light of the Chichi earthquake of September 21, 1999, *Tectonophysics*, 408, 63–77, <https://doi.org/10.1016/j.tecto.2005.05.040>, 2005.
- Ota, Y., Lin, Y.-N. N., Chen, Y.-G., Chang, H.-C., and Hung, J.-H.: Newly found Tunglo Active Fault System in the fold and thrust belt in northwestern Taiwan deduced from deformed terraces and its tectonic significance, *Tectonophysics*, 417, 305–323, <https://doi.org/10.1016/j.tecto.2006.02.001>, 2006.
- Ota, Y., Lin, Y.-N. N., Chen, Y.-G., Matsuta, N., Watanuki, T., and Chen, Y.-W.: Touhuanping Fault, an active wrench fault within fold-and-thrust belt in northwestern Taiwan, documented by spatial analysis of fluvial terraces, *Tectonophysics*, 474, 559–570, <https://doi.org/10.1016/j.tecto.2009.04.034>, 2009.
- Pelletier, B. and Stephan, J. F.: Middle miocene deduction and late miocene beginning of collision registered in the hengchun peninsula: Geodynamic implications for the evolution of Taiwan, *Tectonophysics*, 125, 133–160, [https://doi.org/10.1016/0040-1951\(86\)90011-9](https://doi.org/10.1016/0040-1951(86)90011-9), 1986.

- Pickering, J. L., Goodbred, S. L., Reitz, M. D., Hartzog, T. R., Mondal, D. R., and Hossain, M. S.: Late Quaternary sedimentary record and Holocene channel avulsions of the Jamuna and Old Brahmaputra River valleys in the upper Bengal delta plain, *Geomorphology*, 227, 123–136, <https://doi.org/10.1016/j.geomorph.2013.09.021>, 2014.
- Pye, K. and Zhou, L.-P.: Late Pleistocene and Holocene aeolian dust deposition in North China and the Northwest Pacific Ocean, *Palaeogeogr. Palaeoclimatol.*, 73, 11–23, [https://doi.org/10.1016/0031-0182\(89\)90041-2](https://doi.org/10.1016/0031-0182(89)90041-2), 1989.
- Robustelli, G., Ermolli, E. R., Petrosino, P., Jicha, B., Sardella, R., and Donato, P.: Tectonic and climatic control on geomorphological and sedimentary evolution of the Mercure basin, southern Apennines, Italy, *Geomorphology*, 214, 423–435, <https://doi.org/10.1016/j.geomorph.2014.02.026>, 2014.
- Saito, K. and Oguchi, T.: Slope of alluvial fans in humid regions of Japan, Taiwan and the Philippines, *Geomorphology*, 70, 147–162, <https://doi.org/10.1016/j.geomorph.2005.04.006>, 2005.
- Satellite Survey Center: Ministry of the Interior 20 m raster digital elevation model [data set], available at: <https://data.gov.tw/dataset/35430> (last access: 14 January 2022), 2018.
- Shackleton, N. J.: The 100,000-Year Ice-Age Cycle Identified and Found to Lag Temperature, Carbon Dioxide, and Orbital Eccentricity, *Science*, 289, 1897–1902, <https://doi.org/10.1126/science.289.5486.1897>, 2000.
- Shih, T.-T. and Yang, G.-S.: The Active Faults and Geomorphic Surfaces of Pakua Tableland in Taiwan, *Geogr. Res.*, 11, 173–186, 1985.
- Shyu, J. B. H., Sieh, K., Chen, Y.-G., and Liu, C.-S.: Neotectonic architecture of Taiwan and its implications for future large earthquakes, *J. Geophys. Res.*, 110, B08402, <https://doi.org/10.1029/2004jb003251>, 2005.
- Siame, L. L., Chen, R.-F., Derrieux, F., Lee, J.-C., Chang, K.-J., Bourlès, D. L., Braucher, R., Lèanni, L., Kang, C.-C., Chang, C.-P., and Chu, H.-T.: Pleistocene alluvial deposits dating along frontal thrust of Changhua Fault in western Taiwan: The cosmic ray exposure point of view, *J. Asian Earth Sci.*, 51, 1–20, <https://doi.org/10.1016/j.jseaes.2012.02.002>, 2012.
- Simoes, M. and Avouac, J. P.: Investigating the kinematics of mountain building in Taiwan from the spatiotemporal evolution of the foreland basin and western foothills, *J. Geophys. Res.*, 111, B10401, <https://doi.org/10.1029/2005jb004209>, 2006.
- Suppe, J.: Kinematics of arc-continent collision, flipping of subduction, and back-arc spreading near Taiwan, *Memoir of the Geological Society of China*, 6, 131–146, 1984.
- Teng, K.-H.: A Quantitative Study on the Landforms of Lateritic Gravel Tablelands in Northwestern Taiwan, *The College of Chinese Culture Institute of Geography Science Reports*, 3, 113–186, 1979.
- Teng, L. S.: Geotectonic evolution of late Cenozoic arc-continent collision in Taiwan, *Tectonophysics*, 183, 57–76, [https://doi.org/10.1016/0040-1951\(90\)90188-E](https://doi.org/10.1016/0040-1951(90)90188-E), 1990.
- Teng, L.-S.: Geotectonic evolution of Tertiary continental margin basins of Taiwan, *Petroleum Geology of Taiwan*, 27, 1–19, 1992.
- Teng, L. S.: Extensional collapse of the northern Taiwan mountain belt, *Geology*, 24, 949–952, 1996a.
- Teng, L. S.: Geological background of the gravel formations of Taiwan, *Sine-Geotechnics*, 55, 5–24, <https://doi.org/10.30140/SG.199606.0001>, 1996b.
- Teng, L. S., Lee, C., Peng, C.-H., Chen, W.-F., and Chu, C.-J.: Origin and geological evolution of the Taipei basin, northern Taiwan, *Western Pacific Earth Sciences*, 1, 115–142, 2001.
- The Taiwan Provincial Weather Institution: Report on Floods of 7th August, 1959, The Taiwan Provincial Weather Institution, Taipei, Taiwan, available at: <https://photo.cwb.gov.tw/rdcweb/lib/cd/cd02tyrp/typ/1959/6.pdf> (last access: 14 January 2022), 1959.
- Tomita, Y.: On the geomorphological classification of fans in Taiwan (Formosa), *Journal of Geography (Chigaku Zasshi)*, 60, 2–9, 1951.
- Tomita, Y.: The classification of fluvial terraces, *Annals of The Tohoku Geographical Association*, 6, 1–6, <https://doi.org/10.5190/tga1948.6.1>, 1953.
- Tomita, Y.: Surface Geology and Correlation of River Terraces, *Annals of The Tohoku Geographical Association*, 6, 51–58, https://doi.org/10.5190/tga1948.6.4_51, 1954.
- Torii, K.: Tosei Sheet, Bureau of Productive Industries, Government-General of Taiwan, Explanatory text of the geological map of Taiwan (1:50 000), Tokyo, available at: <https://twgeoref.moeacgs.gov.tw/GipOpenWeb/wSite/ct?xItem=104094&ctNode=217&mp=6> (last access: 14 January 2022), 1935.
- Tsai, H., Huang, W.-S., Hseu, Z.-Y., and Chen, Z.-S.: A River Terrace Soil Chronosequence of the Pakua Tableland in Central Taiwan, *Soil Science*, 171, 167–179, <https://doi.org/10.1097/01.ss.0000187376.76767.21>, 2006.
- Tsai, H., Maejima, Y., and Hseu, Z.-Y.: Meteoric ¹⁰Be dating of highly weathered soils from fluvial terraces in Taiwan, *Quaternary Int.*, 188, 185–196, <https://doi.org/10.1016/j.quaint.2007.06.007>, 2008.
- Tsai, H., Hseu, Z.-Y., Huang, S.-T., Huang, W.-S., and Chen, Z.-S.: Pedogenic properties of surface deposits used as evidence for the type of landform formation of the Tadu tableland in central Taiwan, *Geomorphology*, 114, 590–600, <https://doi.org/10.1016/j.geomorph.2009.09.020>, 2010.
- Tseng, C.-H., Wenske, D., Böse, M., Reimann, T., Lüthgens, C., and Frechen, M.: Sedimentary features and ages of fluvial terraces and their implications for geomorphic evolution of the Taomi River catchment: A case study in the Puli Basin, central Taiwan, *J. Asian Earth Sci.*, 62, 759–768, <https://doi.org/10.1016/j.jseaes.2012.11.028>, 2013.
- Vail, P. R., Audemard, F., Bowman, S. A., Eisner, P. N., and Perez-Cruz, C.: The stratigraphic signatures of tectonics, eustasy and sedimentology – an overview, in: *Cycles and Events in Stratigraphy*, edited by: Einsele, G., Ricken, W., and Seilacher, A., Springer-Verlag, Berlin, 617–659, ISBN 3540527842, 1991.
- Volker, H. X., Waskiewicz, T. A., and Ellis, M. A.: A topographic fingerprint to distinguish alluvial fan formative processes, *Geomorphology*, 88, 34–45, <https://doi.org/10.1016/j.geomorph.2006.10.008>, 2007.
- Wang, Y. H., Jan, S., and Wang, D. P.: Transports and tidal current estimates in the Taiwan Strait from shipboard ADCP observations (1999–2001), *Estuar., Coast. Shelf Sci.*, 57, 193–199, [https://doi.org/10.1016/S0272-7714\(02\)00344-X](https://doi.org/10.1016/S0272-7714(02)00344-X), 2003.
- Willemin, J. H. and Knuepfer, P. L. K.: Kinematics of arc-continent collision in the eastern Central Range of Taiwan inferred from geomorphic analysis, *J. Geophys. Res.-Sol. Ea.*, 99, 20267–20280, <https://doi.org/10.1029/94JB00731>, 1994.

- Yang, K.-M., Huang, S.-T., Wu, J.-C., Ting, H.-H., and Mei, W.-W.: Review and New Insights on Foreland Tectonics in Western Taiwan, *Int. Geol. Rev.*, 48, 910–941, <https://doi.org/10.2747/0020-6814.48.10.910>, 2006.
- Yang, K.-M., Huang, S.-T., Jong-Chang, W., Ting, H.-H., Wen-Wei, M., Lee, M., Hsu, H.-H., and Lee, C.-J.: 3D geometry of the Chelungpu thrust system in central Taiwan: Its implications for active tectonics, *Terr. Atmos. Ocean. Sci.*, 18, 143, [https://doi.org/10.3319/TAO.2007.18.2.143\(TCDP\)](https://doi.org/10.3319/TAO.2007.18.2.143(TCDP)), 2007.
- Yang, K.-M., Rau, R.-J., Chang, H.-Y., Hsieh, C.-Y., Ting, H.-H., Huang, S.-T., Wu, J.-C., and Tang, Y.-J.: The role of basement-involved normal faults in the recent tectonics of western Taiwan, *Geol. Mag.*, 153, 1166–1191, <https://doi.org/10.1017/S0016756816000637>, 2016.
- Yu, H.-S. and Chou, Y.-W.: Characteristics and development of the flexural forebulge and basal unconformity of Western Taiwan Foreland Basin, *Tectonophysics*, 333, 277–291, [https://doi.org/10.1016/S0040-1951\(00\)00279-1](https://doi.org/10.1016/S0040-1951(00)00279-1), 2001.
- Yu, H.-S. and Song, G. S.: Submarine physiographic features in Taiwan region and their geological significance, *Journal of the Geological Society of China*, 43, 267–286, 2000.
- Yu, N.-T., Teng, L. S., Chen, W.-S., Yue, L.-F., and Chen, M.-M.: Early post-rift sequence stratigraphy of a Mid-Tertiary rift basin in Taiwan: Insights into a siliciclastic fill-up wedge, *Sediment. Geol.*, 286–287, 39–57, <https://doi.org/10.1016/j.sedgeo.2012.12.009>, 2013.

Chapter 6. An investigation of the Quaternary stratigraphy with borehole data in the Miaoli Tableland

6.1 Introduction, material and methods

6.1.1 Introduction

In recent years the public construction project's borehole records were opened to the public (Central Geological Survey, 2017a), in which the sedimentary successions beneath the surfaces were recorded in detail. In fact, these borehole records have great potential for studying geological characteristics that are not able to be accessed or observed directly in the field. For example, the case studies of Chen et al. (2010) and Yang et al. (2016) had employed the borehole data to create 3D models to interpret the tectonism and the influences on depositions in the mountain foreland in central western Taiwan. These cases made the initial tests of using the borehole data for stratigraphical studies. The Miaoli Tableland in northwestern Taiwan is a representative case that the stratigraphical interpretations and the synthesis of tableland morphology are still under discussion (Chang et al., 1998; Liu et al., 2022; Ota et al., 2006), as data of the sedimentary successions beneath the surface are not available before. This study aims to present a new approach for interpreting tableland morphology by employing the borehole data. These results contribute to explaining the most recent proposed Quaternary stratigraphy interpretations and the morphological synthesis of successive reworking of fluvial sediments in the Miaoli Tableland (Liu et al., 2022) (see chapter 5).

6.1.2 The borehole data set and data coverage

The borehole logs in the Miaoli Tableland are collected from the drilling records of public construction projects (Central Geological Survey, 2017a), such as motorway, high speed railway, express way, high voltage electricity network and power plant (Table 6.1 and Fig. 6.1). The linear alignment of the boreholes is suitable for cross-section mapping. The borehole logs that contained records of artificial filling materials are excluded, due to the sedimentary successions are disturbed.

The boreholes have a depth range from 10 meters to 90 meters (Table 6.2), 232 of 892 boreholes were 10 to 20 m deep, 550 of 892 boreholes were 20 to 40 m deep, 110 of 892 boreholes were 40 to 90 m deep. The descriptions of these borehole logs were documented according to the technical instructions issued by the Central Geological Survey (Central Geological Survey, 2017a; Chen et al., 2010; Yang et al., 2006; Yang et al., 2017) (Table 6.1). The categories of descriptions include the location, elevation, thickness of the sedimentary layers, color of the sediments, particle size, photograph records of the sediment core, ground water table and advanced geophysical test records (e.g. standard penetration test, bulk density test...etc.) (Table 6.2).

Table 6.1 the basic characteristics of the selected borehole logs

cross section	number of boreholes	Depth (<20m)	Depth (20-40m)	Depth (40-60m)	Depth (60-80m)	Depth (>80m)	Data Source	Length (km)	High (m asl)	Low (m asl)	Site / tableland classification	TWD67 Coordinate	TWD97 Coordinate
TP	134	--	35	99	--	--	Central Geological Survey	13.70	447	-19.0	SH-I / ST / AL	14	44
HSR	549	114	398	25	7	5	Central Geological Survey	29.64	142	3.69	SH-II / ST / AL	463	--
M3	141	49	82	10	--	--	Central Geological Survey	27.70	123	5.0	SH-II / ST / AL	110	--
T61	68	6	46	16	--	--	Central Geological Survey	13.98	58	2.0	SH-II / ST / AL	--	65

Table 6.2 The attributions and data coverage of the selected borehole logs

cross section	description of lithology	colour of the sediments	photo records	water table	standard penetration test (SPT)	RQD	advance physical test
TP	133	103	85	119	76	89	59
HSR	549	547	0	528	525	431	460
M3	115	133	0	105	126	105	94
T61	68	65	6	65	68	6	41

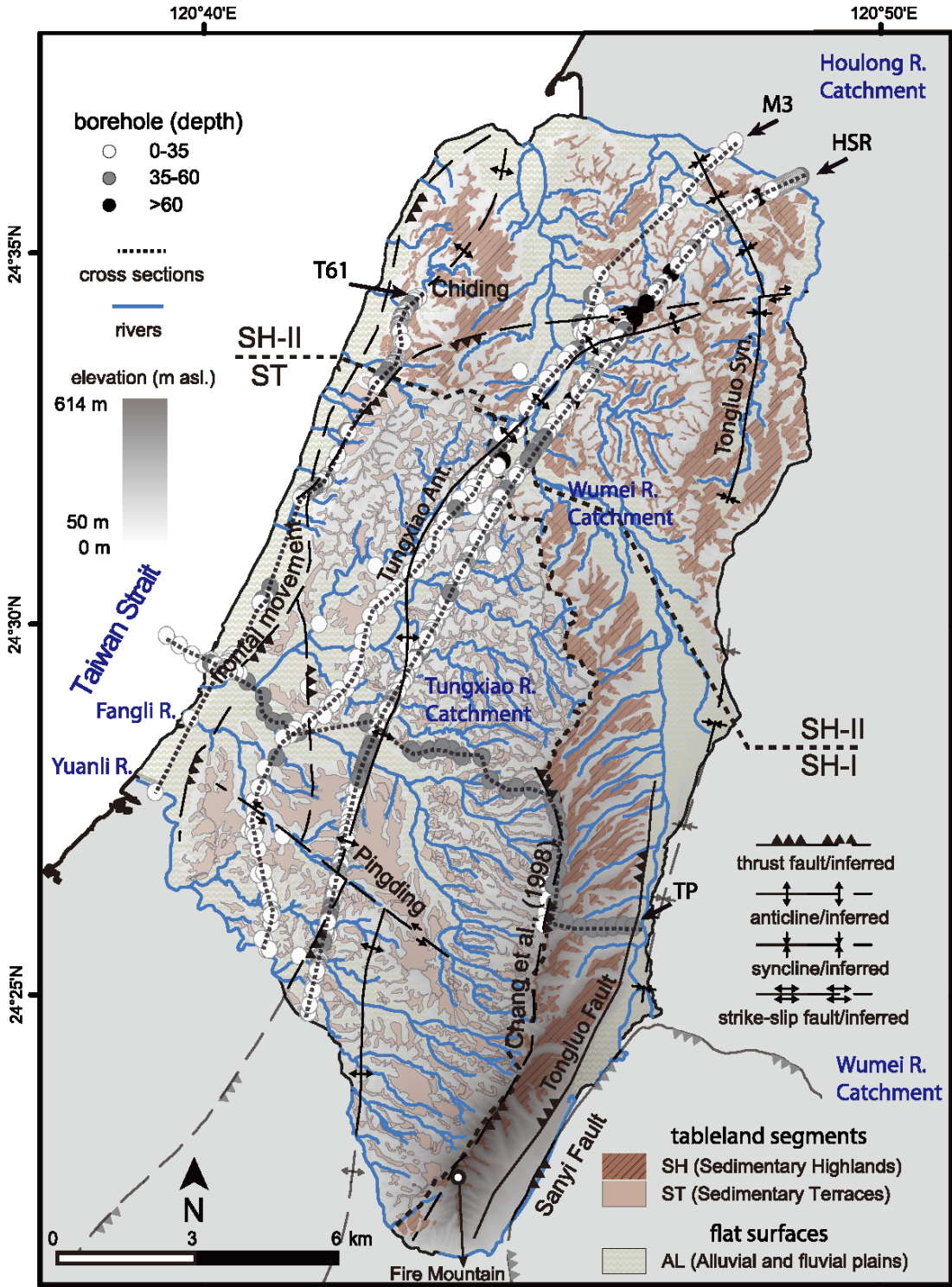


Figure 6.1: Map of the Miaoli Tableland. The elevation data were extracted from the open-access 20m resolution DEM data (Satellite Survey Center, 2018). The tectonic features were simplified from the online database of geological maps (Central Geological Survey, 2017b), and the results of previous studies such as the Tongluo Thrust Fault (Ota et al., 2006), the tentatively called “frontal movement” (Shyu et al., 2005), and an inferred thrust movement identified by a topographical study (Chang et al., 1998). The classifications of the flat surfaces, including the tableland segments, fluvial channels and coastal plains were simplified based on the mapping of Liu et al. (2022) (see chapter 5). The borehole locations were referenced from the coordinates provided by the borehole dataset (Central Geological Survey, 2017a). The depths of the borehole logs were symbolized by greyscale colors. The locations of the four cross-sections were marked by dashed lines that connect the borehole locations of each construction project.

6.1.3 Conversion of coordinates and elevations

The coordinates of borehole locations were recorded with different coordinate systems employed by each construction project. For example, 188 of 892 borehole records were referenced to present-day standard TWD97 coordinates; and 704 of 892 borehole records were referenced to the former standard TWD67 coordinates (Table 6.1). It is necessary to convert all the coordinates into a unified coordinate system, in order to improve the precision of the cross-section mappings. All TWD67 coordinates were converted into TWD97 coordinates using the standard conversion function (Tseng, 1990).

The elevation records of the borehole locations were referenced to the WGS 1984 geoid datum (Central Geological Survey, 2017a). The elevation records are compared with elevations directly extracted from the open-sourced DEM (Satellite Survey Center, 2018) to check potential errors during documentation. The errors between the two datasets are less than +/- 5m for most of the records. In case if the error is significant (i.e. more than 5m), the record from the borehole dataset is adopted, due to the DEM was measured based on elevations after excavations for the constructions.

6.1.4 Cross-section mapping based on the borehole logs

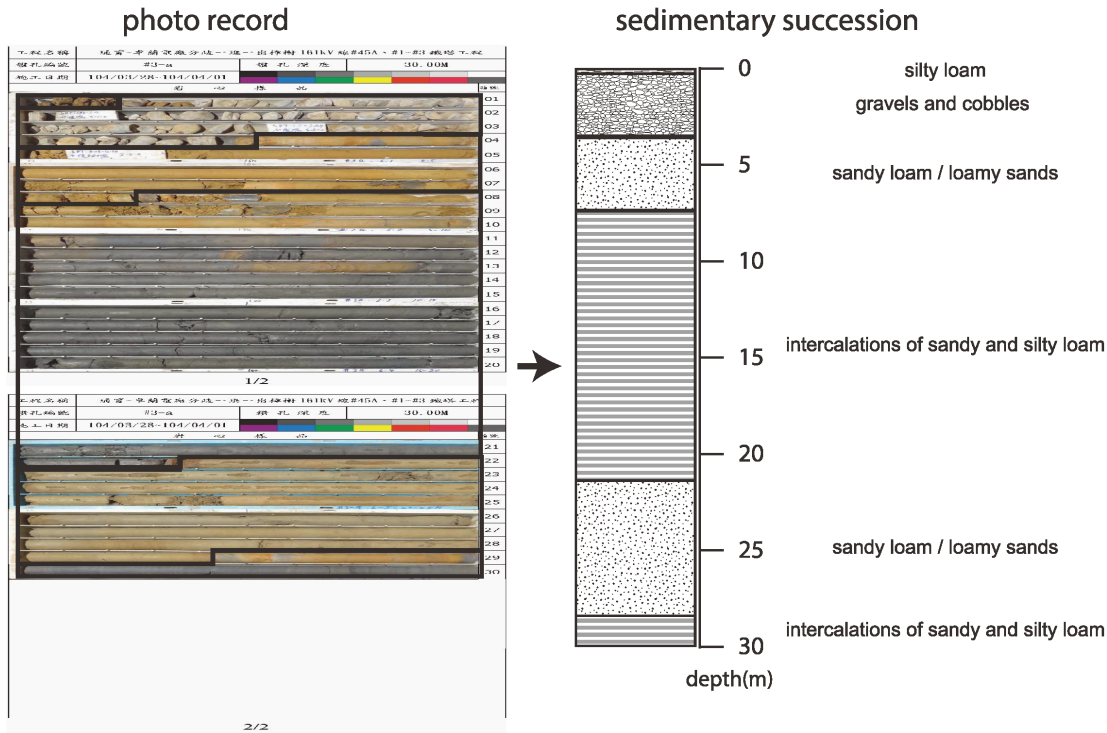
The borehole logs are combined and visualized into four cross-sections to show the sedimentary successions beneath the surface (Table 6.1 and Fig. 6.2). Three cross sections are oriented in north-south direction, and they are distributed in between the central, western and the coastal areas. The other one cross-section is oriented in east to west direction. The mapping of these cross-sections is carried out based on methods employed in the case studies with similar geographical settings (Ishihara et al., 2012; Itoh et al., 2017; Pennington et al., 2017; Pickering et al., 2014):

- 1). The first step is to identify the sedimentary layers for each borehole log independently (Fig. 6.2). Each sediment layer is identified based on the descriptions of particle size compositions, color, and thickness firstly. The sedimentary succession of each borehole log is classified based on similarity to the stratigraphical models of Makiyama (1934,1937), Lin (1963) and Liu et al (2022).
- 2). The interpolations of sedimentary successions are carried out with the borehole logs located in similar landforms within a range of less than 1km. The ground water table records are taken as additional information for identifying the connections between sedimentary successions. These borehole logs are subsequently combined into a cross section to show the overall spatial distributions of sedimentary successions across different landforms (Figs. 6.3, 6.4, 6.5 and 6.6).

3). Two sedimentary layers are selected as the trace layers to make connections among the four cross-sections, based on their relevance to the deposition environment change and tableland morphology (Figs. 6.3, 6.4, 6.5 and 6.6). The first trace layer are the gravel and cobble bed(s) (CSB), which is assumed as field evidence of the successive rework processes of fluvial depositions (Liu et al., 2022) (see chapter 5). The second trace layer is the alternation of greyish silt loam and yellowish silt loam layers (SiC), which is assumed as an indicator of tidal-flat deposition environment prior to the start of the terrestrialization processes in the Miaoli Tableland area (Lin, 1963; Liu et al., 2022; Makiyama, 1934, 1937).

4). The four cross-sections, the tectonic features (Central Geological Survey, 2017b; Ota et al., 2006; Shyu et al., 2005) and the morphological mapping results (Chang et al., 1998; Liu et al., 2022) are combined into a 3D schematic model to interpret a revised morphological synthesis of the Miaoli Tableland. This 3D model is built based on the morphodynamic syntheses of successive erosion – transportation – deposition processes that had remobilized gravels and cobbles from the Sedimentary Highlands (SH-I) and went through north (SH-II) and west (ST) directions to the coast of the Taiwan Strait (Chang et al., 1998; Liu et al., 2022) (see chapter 6.5).

borehole log (cross section TP, name:3a, X:224737; Y:2703465)



borehole log (cross section HSR, name:B4V8-P7, X:222217; Y:2710936)

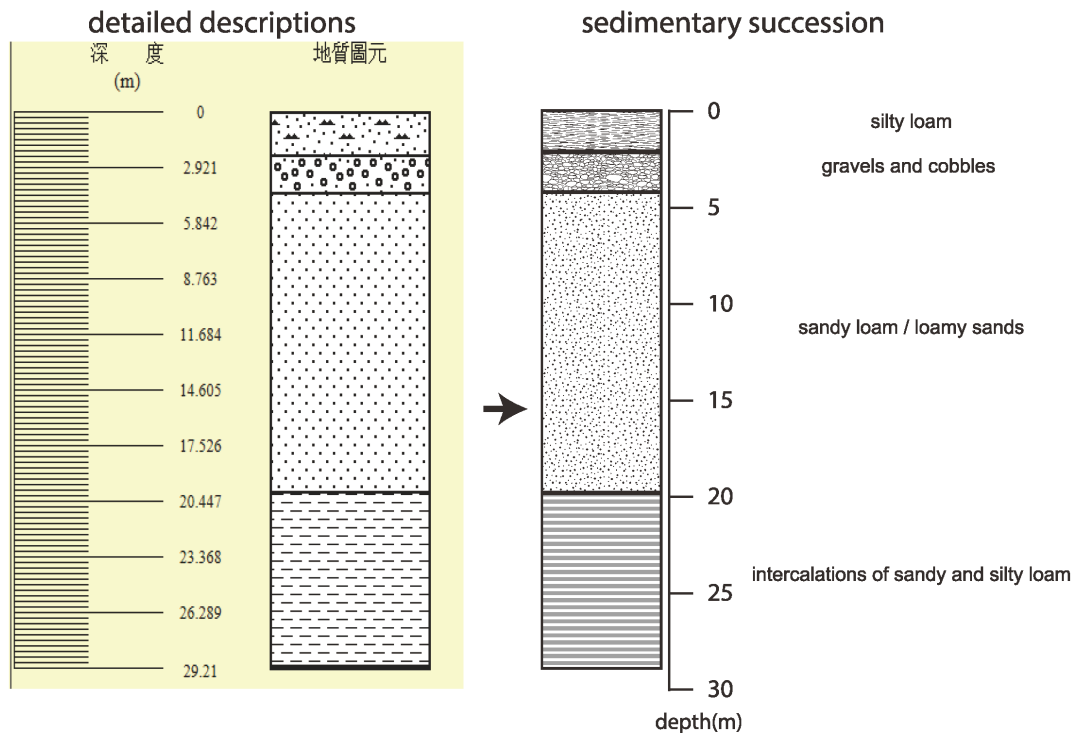


Figure 6.2: Examples of identifying sedimentary layers for a single borehole log according to the photo records and detail descriptions of lithology. Both cases are directly taken from the borehole dataset (Central Geological Survey, 2017a). The definitions of sedimentary layers are referenced from Liu et al. (2022) (see chapter 5), based on the similarity of the lithology and the succession of layers between both datasets. This procedure is undertaken for all the selected borehole logs in this study.

6.2. Results

6.2.1 The cross-section TP (E-W direction)

This cross section is composed of the borehole logs of the high voltage electricity network and the powerplant construction projects (Figs. 6.1 and 6.3). This cross section presents the sedimentary successions in the Miaoli Tableland in east to west direction, including the tableland segments in Sanyi (SH-I) and Tungxiao areas (ST), also the fluvial valley floors, the flood plains, and the estuary (AL) of the Tungxiao River catchment (Fig. 6.1).

The sedimentary successions are formed by fine-grained sedimentary layers in the lower part, a layer of gravel and cobble bed(s) in the middle to upper part and a very thin silty cover layer on the surface in overall. The ground water table is located at a depth of ca. 25-30 meter in the tableland segments and remnants in the upper and middle reaches of the Tungxiao River catchment (Fig. 6.3). Conversely, the ground water table is very close to the surface in the fluvial channel in the lower reach and the estuary of the Tungxiao River catchment (Figs. 6.1, and 6.3).

In summary, the differences in the sedimentary successions are related to the existence and the thickness of the gravel and cobble bed(s). For example, the gravel and cobble bed(s) are recorded as thick layering in the SH-I segments, but are not recorded in the proximal ST segments located at the upper and middle reaches of the Tungxiao River catchment (Figs. 6.1 and 6.3). The thin layering of gravel and cobble bed(s) are recorded in the distal segments (ST), and also in the valley floors and the flood plains (AL) in the lower reach of the Tungxiao River catchment. The thickness of the gravel and cobble bed(s) vary with a spatial pattern, they are thicker in the SH-I segments (> 20 meters) and gradually become thinner toward the lower reach and the estuary areas (about 1 to 15 meters) (Figs. 6.1 and 6.3).

The sedimentary successions in the sedimentary highlands (SH-I) are mostly composed of the sandy deposits (SL) in the deeper part (ca. 30 meter deep) with a brownish or yellowish color; a thick layering of gravel and cobble bed(s) (CSB) in the middle to upper part; and the silty cover layer (SiL) on the surface (Fig. 6.3). In the upper and middle reaches of the Tungxiao River catchment, the sedimentary successions are mostly composed of the intercalation of sandy loam and clay loam layer (SiC) in the lower part and the sandy deposits (SL) with a brownish or yellowish color in the upper part (Fig. 6.3). The gravel and cobble bed(s) are only recorded on the top part of the borehole logs in the distal tableland segments (ST) and become thinner to the lower reach of the Tungxiao River catchment (Fig. 6.3).

The sedimentary successions in the lower reach of the Tungxiao River catchment (including the fluvial valley floors, flood plains and estuary) are composed of the tidal / coastal fine-grained sediment layers (SiC) and a

cover layer of the gravels and cobbles bed(s) (CSB) (Fig. 6.3). The sedimentary successions in the tableland segments show that the gravel and cobble layer(s) become thinner from SH-I to ST, whereas the gravels and cobbles bed(s) in the AL, including the active fluvial channel of lower stream areas, are becoming thicker toward the estuary area (up to 15 meters) (Fig. 6.3).

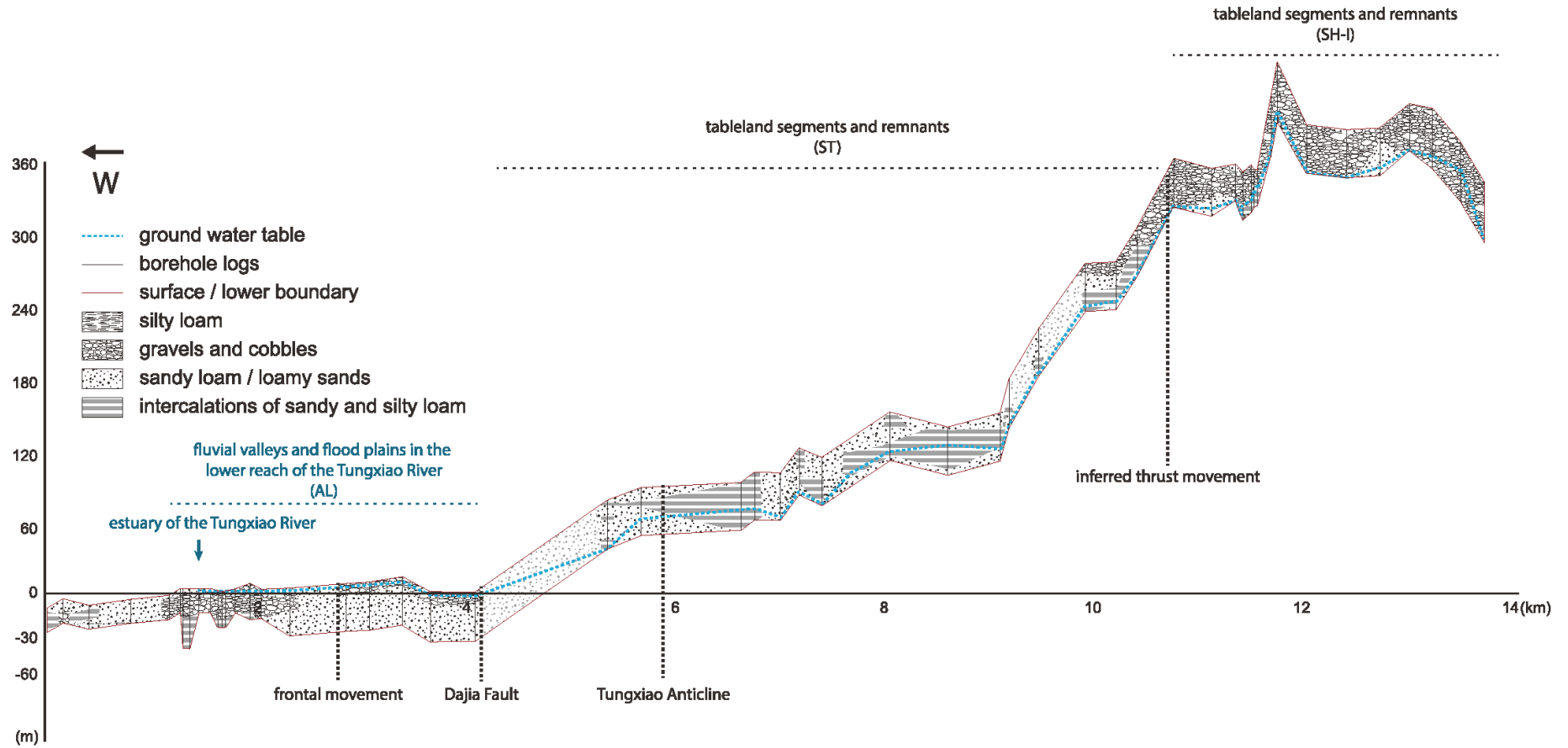


Figure 6.3: The geological cross-section “TP”, shows the distributions of sedimentary successions in the central part of the study area from east to west direction. This cross-section includes the sedimentary successions in the tableland segments of the Sedimentary Highlands (SH-I) in Sanyi area, the remnants (ST) in the middle reach, the fluvial valleys and the estuary (AL) in the lower reach of the Tungxiao River catchment. The vertical scale of this cross-section is exaggerated by 10 times.

6.2.2 The cross-section HSR (N-S direction, proximal area)

This cross-section (Fig. 6.4) is partitioned into five sub-sections as following (from north to south):

The first sub-section (extended from the fluvial valley of Houlong River to the fluvial valley of Nanshi River) (Figs. 6.1 and 6.4a): the tidal / coastal fine-grained sediment layers are recorded in the lower part of the sedimentary successions. The presence and thickness of the gravel and cobble bed(s) in the upper part of the sedimentary successions vary, a spatial correlation with the landforms of the borehole locations is summarized (Figs. 6.1 and 6.4a). For example, a relative thick layering (>10m) of gravel and cobble bed(s) is identified in the valley floors of the Houlong River and the Nanshi River. The relative thin layering (<10m) of the gravel and cobble bed(s) occurs on the very upper part of the sedimentary successions in the tableland segments (SH-II); however, this thin layering of the gravel and cobble bed(s) is rarely recorded in the remnants. Significant vertical displacement of the sedimentary successions is identified next to the slope foots of the distal tableland segments, which is assumed to be related to an unidentified linear structure along the left bank of the Houlong River (Figs. 6.1 and 6.4a). The ground water table records in the segments are located at depth of tens of meters in the sandy loam layer (SL); on the other hand, the ground water table is located on the surface in the fluvial valleys.

In the second sub-section (the Wu-Mei River catchment) (Figs. 6.1 and 6.4b): the sedimentary successions are composed of the tidal / coastal fine-grained sediment layers (SiC, SL) in the lower and middle parts, the gravel and cobble bed(s) (CSB) in the upper part and a silty loamy cover layer (SiL) on the surface. The differences in sedimentary successions are related to the existence and thickness of the gravel and cobble bed(s) (Figs. 6.1 and 6.4b). For example, in the northern part of this sub-section, the sedimentary successions in remnants are composed of the sandy loam layer (SL) and the silty layer (SiL), except the gravel and cobble bed(s) (CSB) (Figs. 6.1 and 6.4b). On the other hand, the borehole logs in the southern part of this sub-section recorded the gravel and cobble bed(s) in the upper part of the sedimentary successions in the tableland segments. The fluvial valleys are covered by gravels and cobbles as well, these gravel and cobble bed(s) in the fluvial valleys are thinner in the tributaries (at north) but become thicker in the mainstream (at south) (Fig. 6.4b). The ground water table records are related to the existence of the gravel and cobble bed(s) too. For example, in the tableland segments and the fluvial channels where a layer of gravel and cobble bed is identified, the ground water table is located at the contact between the sandy loam layer (SL) and the gravel and cobble bed(s) (CSB) (ca. 5 to 15 meters deep). If the gravel and cobble bed(s) are missing (i.e. remnants), the ground water table is located at deeper parts of the sedimentary successions (up to 30m deep). A significant vertical displacement of the sedimentary successions was identified in the vicinity of the Futouken Fault at the tableland segments, which are the topographical height between the tributaries and the mainstream of the Wumei (Xihu) River

(Figs. 6.1 and 6.4b). The sedimentary successions in the southern part are lie higher and thicker than those in the northern part.

The third sub-section (the Tungxiao River catchment) (Figs. 6.1 and 6.4c): The sedimentary successions were mostly consistent with that in the second sub-section (Figs. 6.1, 6.4b and 6.4c). The differences in sedimentary successions are related to the existence of the gravel and cobble bed(s) as well, which show a consistent spatial distribution pattern to that in the second sub-section (Figs. 6.4b and 6.4c). For example, most of the borehole logs in the remnants recorded the intercalations of the tidal/coastal sediment layer (SiC), the sandy loam layer (SL) and a silty loamy cover layer (SiL), except the gravel and cobble bed(s). The gravel and cobble bed(s) (CSB) are only recorded as a cover layer on the intercalation of the tidal / coastal sediment layer (SiC) and the sandy loam layer (SL) in the fluvial valley floors (Figs. 6.1 and 6.4c). The ground water table records in the tableland segments and remnants are mostly located at 5 to 20 meters below the surface. On the other hand, the ground water table recorded in the fluvial valley floors are mostly located at the contact between the gravel and cobble bed(s) and the sandy loam (SL), close to the surface (1 to 5m deep).

The fourth sub-section (the Pingding terrace) (Figs. 6.1 and 6.4d): this sub-section is the largest tableland segment in the Miaoli Tableland, the sedimentary successions are composed of the intercalation of the tidal/coastal sediments layers (SiC) and the sandy loam layer (SL) at the lower to middle part, the gravel and cobble bed(s) (CSB) in the upper part, and then a very thin (less than a meter) silty loamy layer (SiL) at the surface as a cover layer (Figs. 6.1 and 6.4d). The thickness of the gravel and cobble bed(s) (CSB) is consistent across the whole Pingding terrace, for approximately 5-10 meters (Figs. 6.1 and 6.4d). The ground water table records are mostly located close to the contact between the sandy loam layer (SL) and the gravel and cobble bed(s) (CSB) (ca. 5-10 m deep) throughout the whole terrace segment. The record of the ground water table in the gully is located in the lower part of the sandy loam layer (SL), which is more than 20m deep.

The fifth sub-section (the Fangli River and Yuanli River catchments) (Figs. 6.1 and 6.4e): the sedimentary successions recorded in both catchments are consistent with the records in the second (Wumei River) and third (Tungxiao River) sub-sections. The differences of sedimentary successions in this sub-section are related to the landforms of the borehole locations. The gravel and cobble bed(s) are recorded in fluvial valley floors of the Fangli River and the Yuanli River catchments (Figs. 6.1 and 6.4e) by the majority of borehole logs; conversely only a few borehole logs in the tableland segments and remnants record the gravel and cobble bed(s). The sedimentary successions in the tableland segments and remnants are mostly composed of the tidal/coastal sediment layers (SiC and SL), and the SiC and SL layers are directly in contact with the silty loamy layer (SiL) at the surfaces (Figs. 6.1 and 6.4e). The ground water table records in the tableland segments and remnants are located at the contact between the tidal/coastal sediments (SiC) and the sandy loam layer (SL) (about 5 to 15 m deep), while the records of the ground water table in the fluvial valley floors are located close

to the surface. A significant vertical displacement of the sedimentary successions, located in between Dajia Fault and Dapingding Fault, is identified at the topographic divide (i.e. tableland segment) at the north of the Fangli River catchment. The sedimentary successions in the southern part of this sub-section are relatively low in elevation.

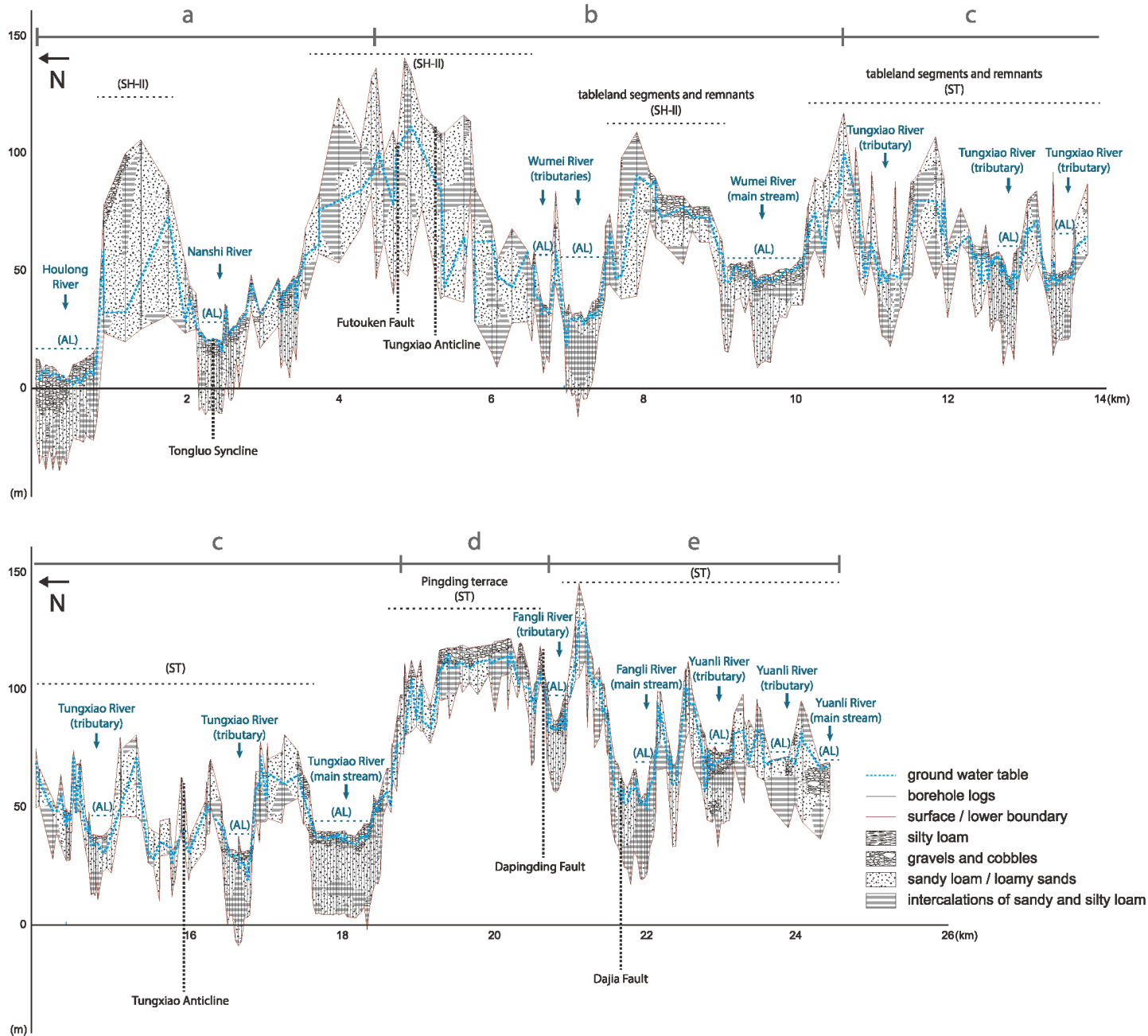


Figure 6.4: The geological cross-section “HSR” shows the distribution of the sedimentary successions in the central part of the study area from north to south. This cross-section is divided into five sub-sections as following.

a). the first sub-section shows the sedimentary successions in the proximal tableland segments and remnants of the SH-II and the fluvial valleys in the lower reach of the Houlong River and the Nanshi River catchments in the Houlong area.

b). the second sub-section shows the sedimentary successions in the proximal tableland segments and remnants of the SH-II and the fluvial valleys in the middle-lower reach of the Wumei (Xihu) River catchment in Xihu area.

c). the third sub-section shows the sedimentary successions in the proximal tableland segments and remnants of the ST and the fluvial valleys in the middle reach of the Tungxiao River catchment in Tungxiao area.

d). the fourth sub-section shows the sedimentary successions in the proximal tableland segment of ST in the Pingding area, which is the largest tableland segment in the study area.

e). the fifth sub-section shows the sedimentary successions in the proximal tableland segments and remnants of ST and the fluvial valley floors in the middle reach of the Yuanli River and Fangli River catchments in the Yuanli area. The vertical scale of this cross section is exaggerated by 10 times.

6.2.3 The cross-section M3 (N-S direction, proximal area)

This cross-section (Fig. 6.5) is located parallel to the west of cross section HSR (Figs. 6.1 and 6.5). The sedimentary successions recorded in this cross section are composed of intercalations of the tidal / coastal sediments (SiC) and the sandy loam layer (SL) in the middle to lower parts, the gravel and cobble bed(s) (CSB) in the upper part, and a silty cover layer (SiL) on the surface (Fig. 6.5).

The sedimentary successions are differentiated according to the landforms of the borehole locations. For example, the larger tableland segments (e.g. Chiding and Pingding) are composed of all the above-mentioned sedimentary layers. The sedimentary successions in the valley floors consist of the tidal / coastal sedimentary layers (SiC) and the sandy loam (SL) in the lower part, and the gravel and cobble bed(s) are in the upper part as the surface layer (Fig. 6.5), which are mostly consistent to the records of the tableland segments. Conversely, the sedimentary successions in the smaller tableland segments and remnants in the SH-II and the ST are composed of the tidal / coastal fine grain sediments that are in direct contact with the silty loamy layer (SiL) of the cover (Fig. 6.5).

The thickness of the gravel and cobble bed(s) are related to the size of the tableland segments and the catchment area of the fluvial channels. For example, the gravel and cobble bed(s) on the larger tableland segments and in the fluvial valley of the mainstream are up to 30 m thick. However, the gravel and cobble bed(s) are relative thinner at the smaller tableland segments and the fluvial valleys of the tributaries (from 5 to 20 m).

The ground water table in the fluvial valley floors and flood plains is mostly located close to the surface, and the records in the tableland segments show that it is close to the contact between the intercalation of the tidal/coastal sediments (SiC) and the sandy loam layer (SL), ranging from ca. 20 to 30 m deep. Significant vertical displacements of sedimentary successions in this cross section are identified in two locations, which are corresponding to the displacements of the intercalations of clay loam and sandy loam layer (SiC). These two locations are: i). the topographical divide in between the Wumei River and Tungxiao River catchments in Xihu area, located at the vicinity of the Futouken Fault, and ii). the topographical divide in between the Tungxiao River and Fangli River catchments in the south of Tungxiao area, located at the south of the Dajia Fault (Fig. 6.5).

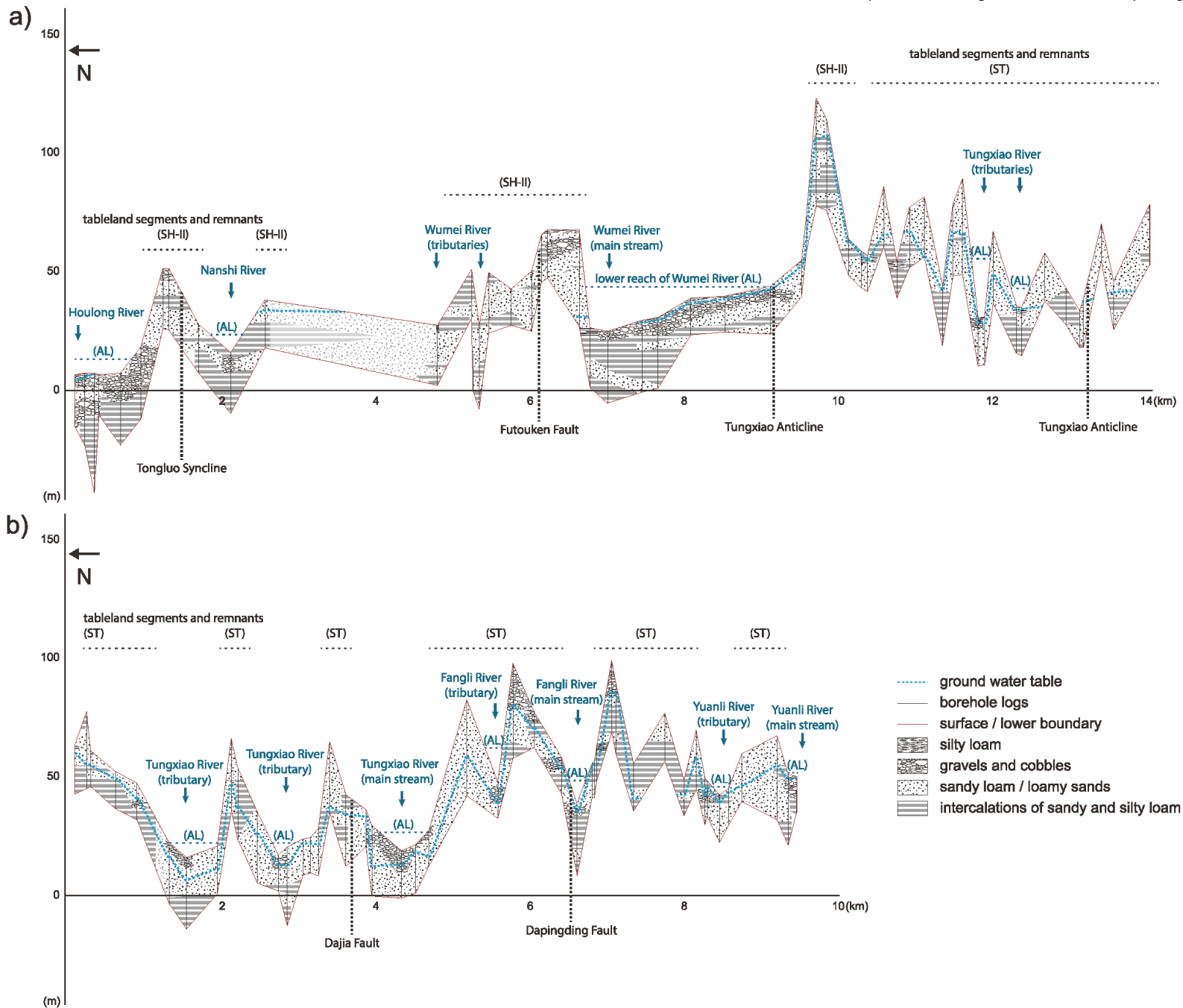


Figure 6.5: The geological cross-section “M3” shows the distribution of sedimentary successions in the central west part of the study area from north to south. This cross-section is divided into two sub-sections.

a). the north sub-section shows the sedimentary successions of the proximal tableland segments and remnants and the fluvial valleys in the lower reaches of the Wumei (Xihu) River and Tungxiao River catchments in Houlong, Xihu and Tungxiao areas.

b). the south section shows the sedimentary successions in the proximal tableland segments and remnants of the ST and the fluvial valley floors in the middle reach of the Yuanli River catchment in Tungxiao and Yuanli areas.

The vertical scale of this cross section is exaggerated by 10 times.

6.2.4 The cross-section T61 (N-S direction, distal and coastal areas)

This cross-section (Figs. 6.1 and 6.6) is located at the west of the study area, it is composed of the borehole logs in: i). the distal tableland segments and remnants (SH-II) at the north of the Tungxiao River catchment, ii). the estuary of the Tungxiao River, and two other estuaries of local fluvial systems south of the Tungxiao River.

The borehole logs in the tableland segments and remnants (SH-II) in the northern part of this cross section record the sedimentary successions that are composed of the fine-grained tidal / coastal sediments (SiC-SL) in the lower part; the fluvial sediments of gravel and cobble bed(s) (CSB) in the middle to upper part; and the silty loamy cover layer (SiL) at the surface (Fig. 6.6). The sedimentary successions in the southern part, such as the borehole logs on the estuaries south of the Tungxiao River, record the gravel and cobble bed(s) (CSB) as the cover layer, which cover the sandy loam layer (SL) in the sedimentary succession.

The gravel and cobble bed(s) (CSB) recorded in the tableland segments (SH-II) are up to ca. 20 m thick. The gravel and cobble bed(s) in the fluvial valleys and estuaries are relatively thin and multilayered, intercalated with the sandy loam (SL) sediments. For example, the sedimentary successions in the Tungxiao River estuary are composed of a cover layer of gravel and cobble bed(s) on the surface and another two to three thin layerings of gravel and cobble bed(s) in the middle to lower part of the sedimentary successions (Fig. 6.6).

The ground water table records are close to the surface (less than 5 meters deep) in all the borehole logs of this cross section, and the depth of ground water table is not affected by the reliefs of borehole locations. A significant vertical displacement of the sedimentary successions is identified by the location of a distal tableland segment north of a local fluvial system located in between the Futouken Fault and the frontal movement (Figs. 6.1 and 6.6), which has caused ca. 50m of displacement according to the elevation of the intercalation of the clay loam and sandy loam layer (SiC) (Fig. 6.6).

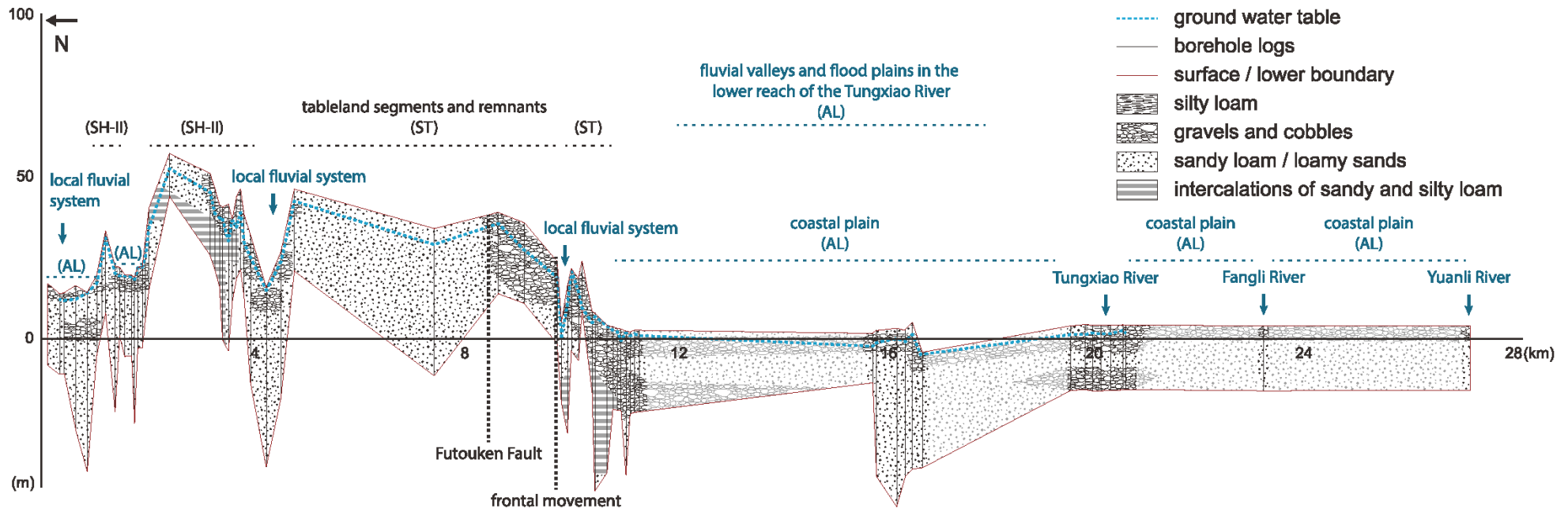


Figure 6.6: The geological cross-section "T-61", shows the distribution of sedimentary successions in the west part of the study area from north to south. The borehole logs of this cross-section are mostly located to the north of the Tungxiao River, which shows the sedimentary successions of the distal tableland segments and remnants of the SH-II in Houlong and Tungxiao areas. The borehole logs at the south of the Tungxiao River show the sedimentary successions in the estuaries of the Tungxiao River and two other local catchments, the interpolation of sedimentary successions in the coastal plain in the south of the Tungxiao River (i.e. Yuanli area) are marked with transparent greyscale symbols. The vertical scale of this cross-section is exaggerated by 10 times.

6.2.5 Remarks of the cross sections

- 1). The sedimentary successions shown in the cross sections are generally consistent with the descriptions of the studied sedimentary succession by Liu et al. (2022) (see chapter 5). The variations of the sedimentary successions are relatively minor and are mostly related to the presence and thickness of the gravels and cobbles bed(s) (CSB) that are in the upper part of the sedimentary successions (Liu et al., 2022) (Figs. 6.3, 6.4, 6.5, and 6.6).
- 2). The locations of the vertical displacements of the sedimentary successions are in accordance with the locations of tectonic features, such as the thrust faults (Chang, 1990, 1994; Ho, 1994; Ota et al., 2006) and the inferred thrust movements studied by Chang et al., (1998) and Shyu et al., (2005) (Fig. 6.1).
- 3). The variations in the depths of the ground water table are related to the landforms of the borehole locations (Fig. 6.3, 6.4, 6.5 and 6.6). The ground water tables are mostly located at the sandy loam layer in the tableland segments and remnants (from 5 to 30m deep). On the other hand, the ground water table is located very close to the surface in the fluvial valley floors, the estuaries, and the coastal plains.
- 4). The gravel and cobble bed(s) recorded in the sedimentary highlands (SH-I) in the cross-section TP are much thinner (<40m) than the those exposed in the Fire Mountain (more than hundreds of meters). The sediments beneath the gravel and cobble bed(s) in the SH-I tableland segments are identified as coastal sediments (i.e. the yellowish sandy loam, assumed to be the SL layer) (Fig. 6.3).
- 5). The thickness of the gravel and cobble bed(s) are related to the landforms of the borehole locations. The gravel and cobble bed(s) in the tableland segments become thinner from the SH-I tableland segments to the proximal tableland segments in the SH-II and the ST, and the distal tableland segments in the SH-II and the ST (Figs. 6.3, 6.4, and 6.5). Conversely, the gravel and cobble bed(s) become thicker in the fluvial valley of the mainstreams and the estuaries.
- 6). The active fluvial gravels and cobbles are deposited in the fluvial valley floors and the estuaries. These multi-layered gravel and cobble bed(s) are intercalated with the sandy loam sediments (SL) in the upper part of the sedimentary successions (Figs. 6.3, and 6.6).

6.3. Discussion

6.3.1 The sedimentary successions

The sedimentary successions recorded in the borehole logs are consistent with the field observations stated by Liu et al. (2022) (Figs. 6.3, 6.4, 6.5, and 6.6). The variations of the sedimentary successions recorded in the borehole logs are related to the landforms, and this correlation is consistent with the stratigraphical and morphodynamic interpretations of Liu et al. (2022) as well (see chapter 5). For example, the sedimentary successions in the tableland segments, with the tidal / coastal sediments in the central and lower part, the gravel and cobble layer(s) in the upper part and a silty loamy cover layer, fit to the description of type-I sedimentary succession of Liu et al. (2022) (Figs. 6.3, 6.4, 6.5, and 6.6). The sedimentary successions of the remnants are composed of SiC-SL-SiL without the CSB, which fit the type-II sedimentary succession as described by Liu et al. (2022) (Figs. 6.3, 6.4, 6.5, and 6.6). The sedimentary successions in the fluvial valley floors and estuaries are composed of intercalations of the multi-layered gravel and cobble layer(s) (CSB) and sandy sediments (SL) at the uppermost part, covering the sandy sediments (SL) and the tidal / coastal sediments (SiC) in the middle to lower part. This fits the type-III sedimentary succession as described by Liu et al. (2022) (Figs. 6.3, 6.4, 6.5, and 6.6).

In addition, the depths of the ground water table are also related to the landforms. For example, the ground water table in the tableland segments and the remnants is found at depth of ca. 5 to 30 meters below the surface, mostly within the sandy loam layer (SL). On the other hand, the ground water table in the fluvial valleys and estuaries is located close to the surface (Figs. 6.3, 6.4, 6.5, and 6.6). The depths of the ground water table are constrained by the different impermeability of the sedimentary layers, thus the SL, CSB and SiL layers serve as aquifers, and conversely, the SiC layer serves as an aquitard.

Based on the overall consistency of the sedimentary successions across the four cross sections and the stratigraphical model of Liu et al. (2022) (see chapter 5); and the correlation between variations of the sedimentary successions and the landforms can be inferred that the sedimentary successions in the Miaoli Tableland were originated from a sedimentary package. This sedimentary package is composed of the tidal / coastal fine-grained sediments (SiC-SL) initially, the fluvial sediments yielded from the WF subsequently covered these tidal/coastal sedimentary layers, and then caused the forming of the alluvial fan(s) palaeo-topography. The fluvial incisions into the alluvial fans were caused by uplifting of the sedimentary successions and the low base level during the sea-level low stands. The gravels and cobbles were successively remobilized farther downstream and displayed the present-days variations in the presence and thickness of the gravel and cobble bed(s) (CSB) (Figs. 6.3, 6.4, 6.5, and 6.6).

6.3.2 Tectonism and its influences on the palaeo-topography

The tectonic thrust movements in the Miaoli Tableland are orientated from east to west (Ota et al., 2006; Shyu et al., 2005; Yang et al., 2016), these movements have caused stepwise uplifting of the sedimentary successions (Figs. 6.1 and 6.3), which are in accordance with the significant vertical displacements of sedimentary successions shown on the cross-sections (Figs. 6.1, 6.3, 6.4, 6.5, and 6.6). In addition, the spatial variations of the thickness of the gravel and cobble bed(s) shown on the cross-sections are consistent with the observations by Liu et al (2022) (see chapter 5). For example, the gravel and cobble bed(s) in the tableland segments are significantly thinner than the original sedimentary package (up to hundreds of meters thick) of the gravels and cobbles exposed in the Fire Mountain. The gravel and cobble bed(s) become thinner from the SH-I tableland segments in the Sanyi area (up to 40m) to the proximal tableland segments in the SH-II and the ST (up to 20m) and then to the distal tableland segments in the coastal area in the northwest and west (Figs. 6.1, 6.3, 6.4, 6.5 and 6.6).

On the other hand, it is assumed that the developments of dendritic networks of tributaries in the Tungxiao River catchment (ST) and the Wumei (Xihu) River catchment (SH-II) (Figs. 6.1 and 6.7) are resulted from rapid uplift with homogenous lithological conditions at both limbs of the Tungxiao Anticline. Many cases can also be found in areas with the following geographical/geological characteristics, which are very similar to those of the Miaoli Tableland: i). the basin sediments are uplifted rapidly (Roigé et al., 2017; Whitfield et al., 2013), and ii). the basin sediments are relatively homogenous, with the basins unaffected by complicated tectonism (Itoh et al., 2017; Twidale, 2004).

The tectonism and its influences on the palaeo-topography in the Miaoli Tableland are interpreted as follows:

The movements of the Tongluo Thrust Fault uplifted the palaeo alluvial fan(s) in the foreland firstly (Ota et al., 2006). The (palaeo-)Houlong River was diverted to the northeast subsequently (Chang et al., 1998), the yields of gravels and cobbles from the WF by the (palaeo-)Houlong River (Chang et al., 1998; Teng, 1996b) were successively deposited to the northeastern part of the study area.

The uplift also caused subsequent fluvial incisions that dissected the palaeo-topography of alluvial fan(s) to form the SH-I tableland segments (Fig. 6.1 and 6.7a). Due to their higher elevations and thick layering of the gravel and cobble bed(s), the SH-I tableland segments are assumed to be the origin of the gravels and cobbles, those were remobilized by fluvial processes from there to the downstream areas at the west and northwest, resulted in the forming of the extended alluvial fan(s) (Figs. 6.1, 6.3 and 6.7a). These fluvial sediments formed the gravel and cobble bed(s) on the surface of present-day's proximal tableland segments throughout the ST area and northwest part of the SH-II area (Chang et al., 1998; Chen et al., 2004; Siame et al., 2012; Teng, 1996b; Tsai et al., 2010; Tsai et al., 2006) (Figs. 6.1, 6.3, 6.4 and 6.7).

The second thrust, which is located along the western fringe of the SH-I (Chang et al., 1998), has contributed to higher uplift of the SH-I tableland segments, that caused the overturning of surface inclinations from westward to eastward (Ota et al., 2006), and also the rapid uplift of the extended alluvial fan(s). In addition, the bathymetry of the Taiwan Strait at the near shore area of Miaoli is mostly shallow (not deeper than 40m) (Jan et al., 2002), this shallow bathymetry caused that the locations of the palaeo-rivers' estuaries were far (more than 50 km) from the Miaoli Tableland area during sea-level low stands probably. For example, in the time span since the last glacial cycle, the sea-level was very low for most of the time, except the sea-level high stands such as the Last Interglacial and the early Holocene (Hanebuth et al., 2011; Rabineau et al., 2006; Shackleton, 2000; Waelbroeck et al., 2002). Hence the extended alluvial fan(s) (SH-II and ST) (Chang et al., 1998; Liu et al., 2022; Ota et al., 2006) are assumed to have been located in the middle reaches at that time.

The prolonged low base level has caused fluvial incisions on the extended alluvial fan(s), which caused the formation of the proximal tableland segments (SH-II and ST), and subsequent redepositions of fluvial sediments from the proximal areas to the distal areas (Liu et al., 2022) (see chapter 5 and Figs. 6.1 and 6.7a). The remobilizations of these fluvial sediments took place on a local scale, constrained by the relatively small size of the catchments. The quantities of these reworked fluvial sediments are limited, resulting in the formation of relative thin layering of the gravel and cobble bed(s) in the distal areas of the SH-II and the ST (Figs. 6.1, and 6.7).

The most recent thrust movements (i.e. frontal movement) (Shyu et al., 2005) along the coast have uplifted the sedimentary successions to form the topographic surfaces in the distal areas. Lately the topographic surfaces in the distal areas have been dissected by successive fluvial incisions to form the tableland segments and remnants (SH-II and ST) (Liu et al., 2022) (see chapter 5 and Figs. 6.1 and 6.7).

6.3.3 The forming of the box shaped valleys and redepositions of the gravels and cobbles in the valley floors, flood plains, coastal areas, and estuaries

The incisions on the tableland segments occurred due to surface runoffs during heavy precipitation events, especially typhoons (Central Weather Bureau, 2019b; The Taiwan Provincial Weather Institution, 1959). The gravel and cobble bed(s) are more resistant to the incisions (Chen and Wan, 2004). After the gravel and cobble bed(s) were removed from the tableland segments, rapid lateral erosions subsequently took place on the tidal / coastal fine-grained sediment layers (SL / SiC) during typhoons or heavy precipitation events (Figs. 6.3, 6.6 and 6.7). The gullies and fluvial valleys were widened, which caused the reduction of tableland segments into remnants (Fig. 6.4, 6.5 and 6.7).

The fluvial valleys of the dendritic fluvial patterns developed in the middle to lower reach of the Tungxiao River and Wumei River catchments (the SH-II and the ST) are at least hundreds of meters wide, with a maximum of approximately two kilometers (Fig. 6.1). However, the width of the active fluvial channels in these fluvial valleys are only several tens of meters wide. These very wide fluvial valleys, including the steep slopes of the tableland segments and remnants at both sides altogether, were identified and tentatively called “the box-shaped valleys” (Liu et al., 2022) (see chapter 5), due their iconic box-liked shapes (Figs. 6.1, 6.4, 6.5, and 6.7).

The gravels and cobbles were eroded from the tableland segments during the formation of the box-shaped valleys. These gravels and cobbles have redeposited on the fluvial valley floors in the vicinity initially. The floodings have subsequently remobilized these gravels and cobbles farther to the fluvial valley floors and flood plains at the lower reach and finally reached the estuaries (the AL) (Figs. 6.3, 6.4, 6.5, and 6.6). The redepositions of these gravels and cobbles in the AL are the latest stage of the morphological synthesis of successive reworking of fluvial sediments in the Miaoli Tableland (Liu et al., 2022) (see chapter 5 and Fig. 6.7).

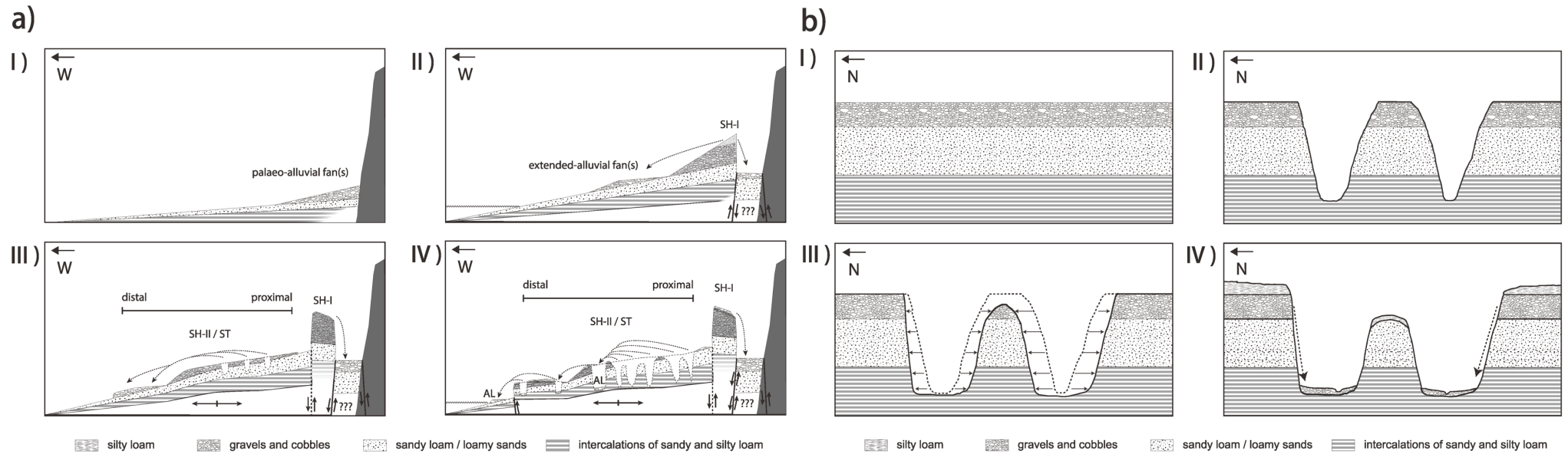


Figure 6.7: a) A schematic sketch of the tableland morphology from east to west. The tableland morphology is related to the tectonism and the phases of erosion and subsequent remobilization of fluvial sediments from the SH-I through the SH-II and the ST to the coast. Visualized as a model with four stages: I). deposition of the palaeo-alluvial fan(s), which are composed of gravels and cobbles from the mountain ranges, covering the fine-grained nearshore / tidal / costal sediments. II). the thrusts of the Tongluo Fault (Ota et al., 2006) uplifted the sedimentary successions of the palaeo-alluvial fan(s), and caused the successive remobilizations of fluvial sediments westward to form the extended alluvial fan(s). III). the inferred tectonic thrusts (Chang et al., 1998) caused more rapid uplifts of the SH-I tableland segments and overturned the surface gradient from westward to eastward. Simultaneously, the extended alluvial fan(s) were dissected by subsequent fluvial incisions caused by marine base-level low stand and the folding of Tungxiao Anticline, resulting in the formation of the proximal tableland segments of the SH-II and ST. These successive erosion processes caused the remobilization of fluvial sediments, and the deposition of relatively thin, multi-layered gravel and cobble bed(s) in the distal areas. IV). the most recent tectonic thrust “frontal movement” (Shyu et al., 2005) caused uplifts of the sedimentary successions in the distal area. Subsequent fluvial incisions led to the formation of the distal tableland segments in the SH-II and ST, and the ongoing redepositions of tableland sediments in the fluvial valleys and the coastal plains (AL).

b). The schematic sketch of the forming of tableland segments, remnants and box-shaped valleys (by north to south direction, in the proximal areas of the SH-II and the ST): I). deposition of the extended alluvial fan(s). II). The fluvial incision of the sedimentary successions of the alluvial fan(s). III). The tableland segments were dissected to form smaller segments and remnants. After the gravel and cobble bed(s) were eroded, lateral erosion took place on the valley slopes. As the costal/tidal sedimentary layers were relatively low resistant to the lateral erosion, the width of fluvial valleys was rapidly enlarged during the floodings and resulted in the forming of the box-shaped valleys. IV). the fluvial sediments redeposited on the fluvial valley floors (AL), and the aeolian silty sediments were accumulated to form the cover layer of the tableland segments and remnants.

Chapter 7. Paper II — Late Quaternary formation of Miaoli Tableland in northwest Taiwan: an interplay of tectonic uplift and fluvial processes dated by OSL

This section presents results of a geochronological analysis of the Miaoli Tableland's quartz rich sediments based on luminescence dating (OSL). New estimations of the tectonic uplift rates based on the OSL ages are proposed in this section. An interplay of tectonic uplifts and fluvial processes in a time span from the post-last interglacial to the Holocene is summarized as a revised synthesis of tableland morphology model of successive redeposition of the fluvial sediments.

This section has been published in *Quaternary Research* in 2022.

Article information:

Citation: Liu, S., Lüthgens, C., Hardt, J., Hebenstreit, R., Böse, M., & Frechen, M. (2023). Late Quaternary formation of the Miaoli Tableland in northwest Taiwan, an interplay of tectonic uplift and fluvial processes dated by OSL. *Quaternary Research*, 112, 128-149. doi:10.1017/qua.2022.52

Hyperlink: <https://www.cambridge.org/core/journals/quaternary-research/article/late-quaternary-formation-of-the-miaoli-tableland-in-northwest-taiwan-an-interplay-of-tectonic-uplift-and-fluvial-processes-dated-by-osl/969C0BD093580A1B066746C480E6B1BF>

PDF: [pdf \(2 mb\)](#)

DOI: <https://doi.org/10.1017/qua.2022.52>


Available online at: 02 / Dec / 2022

This work is distributed under the Creative Commons Attribution 4.0 License.

<https://creativecommons.org/licenses/by/4.0/>

Research Article

Late Quaternary formation of the Miaoli Tableland in northwest Taiwan, an interplay of tectonic uplift and fluvial processes dated by OSL

Shih-Hung Liu^{a*} , Christopher Lüthgens^b, Jacob Hardt^a, Robert Hebenstreit^a, Margot Böse^a and Manfred Frechen^c

^aInstitute of Geographical Sciences, Department of Earth Sciences, Freie Universität Berlin, Berlin, Germany; ^bInstitute of Applied Geology, Department of Civil Engineering and Natural Hazards, University of Natural Resources and Life Sciences, Vienna, Austria and ^cLeibniz Institute for Applied Geophysics, Hanover, Germany

Abstract

The “tablelands” in Taiwan are sedimentary terraces occurring in the foreland basin west of the Neogene mountain ranges. The Miaoli Tableland consists of elevated Late Quaternary sedimentary successions, representing a change from tidal to coastal and fluvial to eolian depositional environments. The present-day morphology is a result of combined processes, including differential tectonic uplift, ongoing fluvial aggradation, and incision. Selected deposits in 10 outcrops were sampled and studied by optical dating. The deposition of fluvial sediments started after the last interglacial (<100 ka) in the southeast of the tablelands. Uplift and sea-level lowering caused a base-level fall, resulting in a stepwise redeposition of the fluvial sediments. Additionally, enhanced remobilization of fluvial sediments occurred during the cold/dry climate during Marine Oxygen Isotope Stages (MIS) 4 and 2. The depositional ages of the coastal sediments enabled the estimation of long-term uplift rates of ca. 0.5 to 3.5 mm/yr. The eolian cover sediments yielded MIS 3 (east) to Holocene ages (west). Our results provide new insight into the interplay of climate, sea-level changes, remobilization of sediments, and tectonism leading to tableland formation during the Late Quaternary.

Keywords: Miaoli Tableland, NW Taiwan, Morphology, Late Quaternary, OSL dating, Fluvial transport, Eolian/fluvial sediments, Paleoclimate, uplift rates

(Received 20 December 2021; accepted 30 August 2022)

INTRODUCTION

The Taiwanese tablelands

The island of Taiwan is located at the convergence zone of the Eurasian and the Philippine Sea plates; it has been continuously uplifted since the late Tertiary (e.g., Suppe, 1981; Teng, 1990; Fig. 1a). The central mountain ranges reach altitudes above 3500 m in several massifs and are built up of pre-Miocene to Pliocene metamorphic rocks (Chang, 1953, 1955a; Ho, 1988). Their western fringes are called the Western Foothills (WF) (Angelier et al., 1986; Ho, 1988).

Tablelands represent characteristic landforms in Taiwan consisting of sedimentary terraces of different altitude, composition, and age. They are distributed mainly in the western mountain foreland (Tomita, 1940; Lin, 1957; Lin and Chou, 1974; Teng, 1996; Fig. 1a), where they are composed of intercalating Quaternary tidal/coastal fine-grained sediments and are covered

by fluvial gravels and cobbles yielded from the central orogenic belt (Lin, 1957; Teng, 1996). Variations in the yield of these coarse-grained sediments have been attributed to climatic changes (Huang et al., 1997; Tseng et al., 2013), that is, glacial and periglacial conditions in the high mountain ranges (Klose, 2006; Hebenstreit et al., 2011) or variable mass-wasting activity in the mountain catchments (Hsieh and Chyi, 2010). Tablelands are also present in an intramountainous basin (Puli Tableland), where they are composed of gravels and cobbles (Teng, 1979; Teng, 1996; Tseng et al., 2013, 2016). The sedimentary successions can reach more than 1000 m in thickness in the western forelands. In central Taiwan, they are ascribed to the Toukoshan Formation (Chang, 1955b; Ho, 1988), which includes the underlying bedrock (Fig. 1c).

The tablelands were tectonically uplifted, partly tilted, and subsequently dissected by fluvial incision, resulting in an irregular topography of the respective tableland surfaces (Hsieh and Knuepfer, 2001; Simoes and Avouac, 2006; Ota et al., 2009; Siame et al., 2012; Fox et al., 2014).

The bathymetry of the Taiwan Strait (Jan et al., 2002) indicates that Pleistocene sea-level lowering during glacial periods resulted in shoreline progradation and emergence of a land bridge (Liu et al., 1998; Hsieh et al., 2006; Bradley et al., 2016; Fig. 1a). The drop in base level also influenced the balance of sedimentation and incision in the Taiwanese mountain foreland.

*Corresponding author at: Institute of Geographical Sciences, Department of Earth Sciences, Freie Universität Berlin, Malteserstraße 74-100, D-13407, Berlin, Germany. E-mail address: Liushihung@zedat.fu-berlin.de (S.-H. Liu).

Cite this article: Liu S-H, Lüthgens C, Hardt J, Hebenstreit R, Böse M, Frechen M (2022). Late Quaternary formation of the Miaoli Tableland in northwest Taiwan, an interplay of tectonic uplift and fluvial processes dated by OSL. *Quaternary Research* 1–22. <https://doi.org/10.1017/qua.2022.52>

© University of Washington. Published by Cambridge University Press, 2022. This is an Open Access article, distributed under the terms of the Creative Commons Attribution licence (<https://creativecommons.org/licenses/by/4.0/>), which permits unrestricted re-use, distribution, and reproduction in any medium, provided the original work is properly cited.

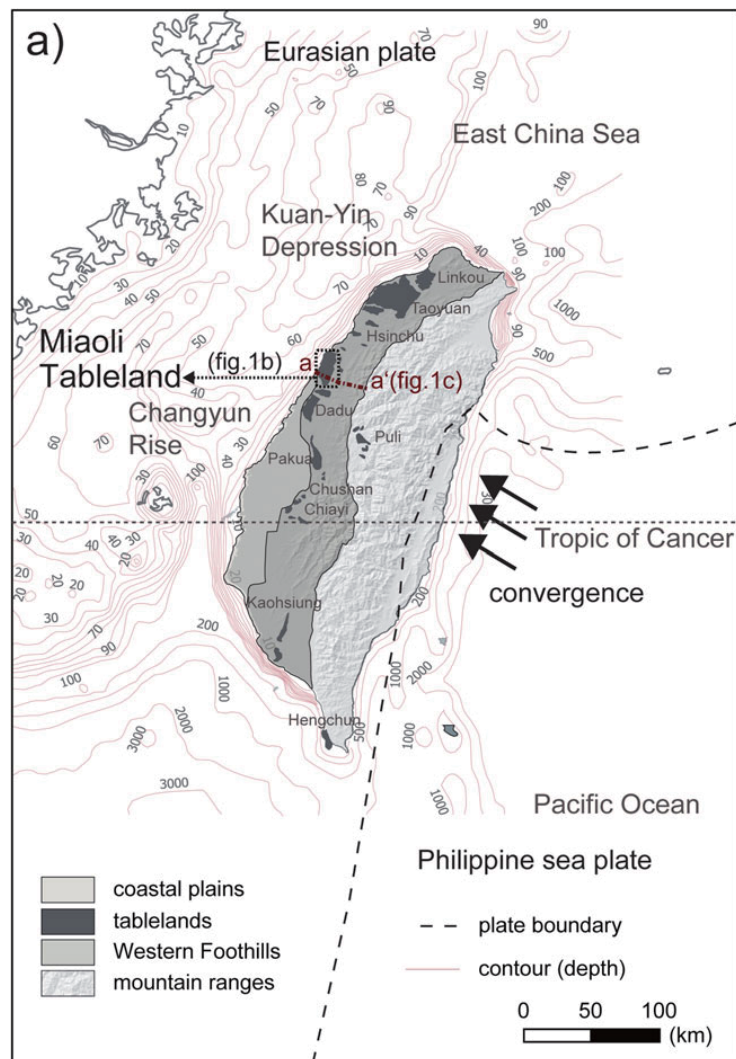


Figure 1. (a) Location of Taiwan and the tablelands in the regional tectonic context (simplified from Suppe [1984], Angelier *et al.* [1986], and Ho [1988]); the bathymetry of the Taiwan Strait was simplified from Jan *et al.* (2002). (b) The Miaoli Tableland and its subdivision into three morphological units from east to west. The elevation data are simplified from the open-access digital elevation model (DEM) with 20 m resolution (Satellite Survey Center, 2018). Tectonic situation based on a simplification of the online database of geologic maps (Central Geological Survey, 2017); the Tung-Luo Thrust Fault was identified by Ota *et al.* (2006); the inferred thrust at the escarpment in between the Sedimentary Highlands located to the west of the Tung-Luo Thrust Fault (SH-I) and Sedimentary Terraces (ST) by Chang *et al.* (1998); the “frontal movement” is simplified from Shyu *et al.* (2005). (c) The underground geologic structure from the Western Foothills (WF) to the Miaoli Tableland and its surrounding area of the WF (simplified from Yang *et al.*, 2016).

Previous interpretations of the tablelands’ chronology were based on proxies such as the lithification characteristics of the sedimentary strata, the degree of weathering of surface sediments and elevation differences. The tablelands were grouped into Lateritic Highlands (oldest), Lateritic Terraces (intermediate), and Fluvial Terraces (youngest) (Tomita, 1951, 1953, 1954; Lin, 1957). Various studies attempted to provide detailed chronological control for the tableland formation by using different dating methods. Radiocarbon dating of tableland surfaces in western-central Taiwan delivered depositional ages younger than 30 ka (Lin, 1969; Hsieh and Knuepfer, 2001; Ota *et al.*, 2002). Electron-spin resonance dating of mollusks in the tableland sediments in southern Taiwan gave depositional age estimates around 140–90 ka (Shih *et al.*, 2002), generally pointing toward deposition during Marine Oxygen Isotope Stage (MIS) 5 (Lisiecki and Raymo, 2005; Cohen *et al.*, 2020). Depth profiles of cosmogenic ^{10}Be on the surfaces the Pakua Tableland and other tablelands in northwest Taiwan delivered ages of up to 300 ka (Tsai *et al.*, 2008; Siame *et al.*, 2012). Luminescence dating

of tableland sediments in north (Hsinchu area) and central (Pakua and Chushan areas) Taiwan yielded Pleistocene ages from 340 ± 66 to 13.5 ± 2.5 ka (Chen *et al.*, 2003a, 2009; Simoes *et al.*, 2007; Ota *et al.*, 2009; Le Béon *et al.*, 2014).

Geomorphological and sedimentological setting of the Miaoli Tableland

The Miaoli Tableland (called “Miaoli Hills” in earlier morphological studies; Chang *et al.*, 1998) is located on the western coast of Taiwan between the Hou-Long River and the Da-An River. To the east it is bounded by the Tung-Luo Thrust Fault (Fig. 1b). The spatial extent of the tableland is about 28 km from north to south and about 14 km from east to west (Fig. 1b). The highest elevations are found at Fire Mountain (614 m above sea level [m asl]) at the southeastern edge of the tableland.

The topography of the Miaoli Tableland is characterized by a deep and narrowly spaced fluvial dissection into numerous segments (Teng, 1979; Chang *et al.*, 1998) and their remnants (Liu

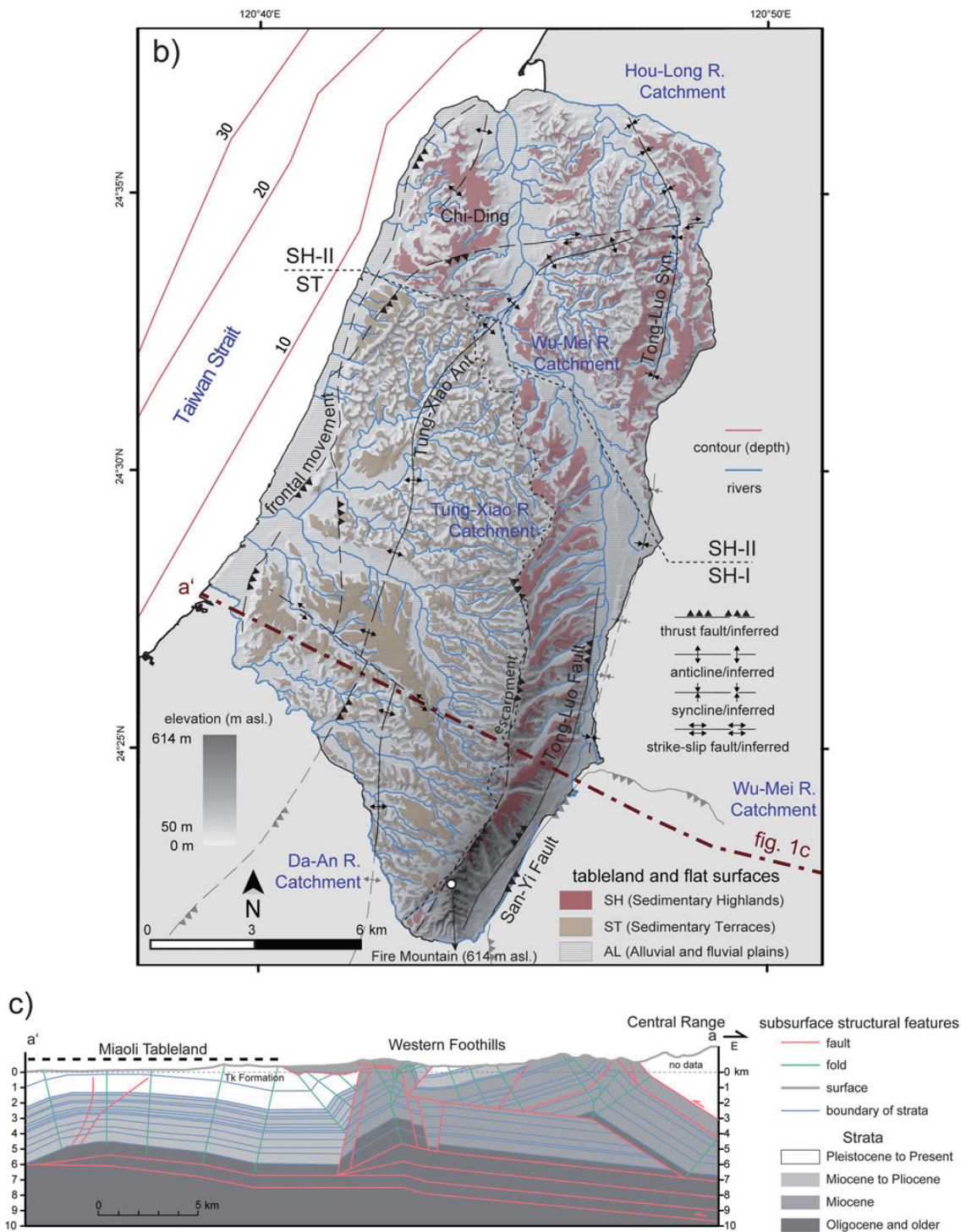


Figure 1. Continued.

et al., 2022). Based on geomorphological studies (Liu *et al.*, 2022), these segments were categorized into three subgroups according to their position relative to one another, elevation, and morphology (Figs. 1b and 2). The Sedimentary Highlands (SH) can be subdivided into SH-I, located to the west of the Tung-Luo Thrust Fault, and SH-II, the northern part on both sides of the

Wu-Mei River (Fig. 1b). The Sedimentary Terraces (ST) are located in the central and southwestern part of the Miaoli Tableland, that is, they are distributed across the whole Tung-Xiao River catchment. Except for the tableland segments and their remnants, all other surfaces below 150 m asl, which are active fluvial plains in the valley floors and coastal plains,

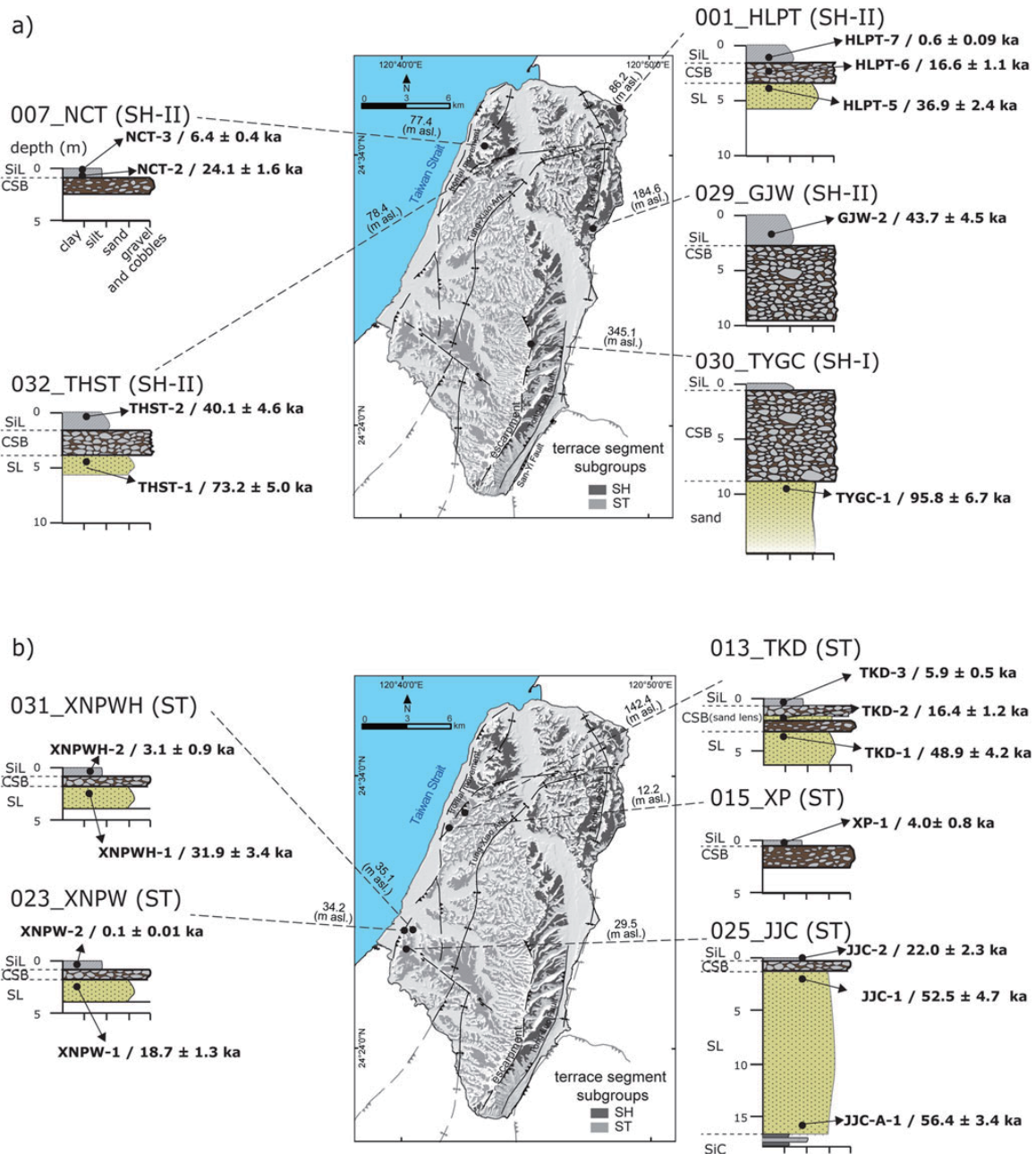


Figure 2. Locations, schematic profiles of the 10 outcrops dated in this study and the derived optically simulated luminescence (OSL) ages (a) in the Sedimentary Highlands (SH-I in the southeast and SH-II in the north and northwest) and (b) the Sedimentary Terraces (ST). The sampling locations for the OSL analyses are highlighted (see Table 2 for detailed information). The nomenclature of the sedimentary units follows Liu *et al.* (2022). SL, sandy loam; CSB, coarse sand with stones and boulders (gravels and cobbles); and SIL, silty loam (cover layer).

are grouped into the Alluvial and Coastal plains (AL) (Fig. 1b). The degree of weathering and colors of surface sediments of the tableland segments have shown a correlation: surfaces of the larger segments are highly weathered with reddish-ocher soils (up to 1.5 m thick); the smaller segments, the remnants, and the downslope surfaces show moderately weathered, light reddish-yellowish soils of normally less than 1 m thickness (Chen, 1983). A similar correlation based on pedological characteristics, relative chronology, and tableland morphology was published for the nearby (12 km south) Dadu Tableland (Tsai et al., 2010) and (30 km south) Pakua Tableland (Siame et al., 2012).

The sedimentary successions within the tableland segments vary between the subgroups (Liu et al., 2022). SH-I, which is the highest and the oldest subgroup according to its degree of weathering, is composed of layers of gravels and cobbles, with an exposed thickness of ca. 300 m on Fire Mountain. In the SH-II and ST segments, which are less elevated and less weathered subgroups of the tableland morphology, the gravels and cobbles are distributed in comparably thin beds with thicknesses of <20 and <10 m, respectively and only <2 m in the distal areas of the tableland.

The non-uniform spatial distribution and the varying thickness of the gravel and cobble beds were interpreted by Liu et al. (2022) as an indicator of redepositions of the gravels and cobbles varying in space and time: a previously continuous distribution of the gravels and cobbles in the form of alluvial fans in the mountain foreland was reconstructed through high-resolution topographic analysis following the interpretation of Chang et al. (1998). After initial uplift, these gravels and cobbles were partly redistributed westward into the present ST area, forming a secondary continuous surface of a thin gravel and cobble bed. Further uplift and fluvial incision also dissected the ST into segments. The gravels and cobbles were thereby eroded from most of the segments, leaving only remnants of material (Liu et al., 2022). The eroded gravels and cobbles were again redeposited farther downstream (Fig. 1b).

The sediments underlying the gravels and cobbles in the SH-II and the ST consist of fine-grained, loose sand and silt. Based on previous investigations in the Miaoli Tableland, they can be described as the Lungkang Formation—a generalized regression succession of tidal/ coastal sediments with an exposed thickness of up to 100 m (Makiyama, 1936, 1937; Lin, 1963). Liu et al. (2022) described the sedimentary succession of the Miaoli Tableland, visible in outcrops, from bottom to top by using the international guidelines of soil descriptions (Jahn et al., 2006): clay loam (L); sandy loam (LS); alternation of sandy loam and clay loam (SiC); and another layer of sandy loam (SL), buried by gravels and cobbles (coarse sand, with stones and boulders; CSB), and a cover layer of silty loam (SiL). The same succession of these layers was observed in broad areas of the SH-II and ST segments. The boundaries in between these sedimentary layers are very distinct (Liu et al., 2022; Supplementary Appendix A), except where the gravel and cobble layer (CSB) is eroded and the silty loam layer (SiL) has direct contact with the sandy loam layer (SL).

The tableland segments were unevenly uplifted. Both the eastern and western margins of the SH-I segments are distinct topographic divides forming escarpments to the neighboring areas (Fig. 1b). A thrust fault has been defined in the eastern escarpment of the Sedimentary Highland area (Ota et al., 2006) and another thrust fault was inferred at the western escarpment (Fig. 1b). The central areas of the SH-II and ST are the location of the Tung-Xiao Anticline. The latest thrust movement (tentatively called “frontal movement” by Shyu et al. [2005]) is located

in the coastal areas (Fig. 1b). It has caused the topographic separation of the tableland segments and the coastal plains (Chang, 1990, 1994; Ho, 1994; Lee, 2000); the precise chronology of the movement is still unclear due to a lack of direct dating results.

The purpose of this study

So far, little is known about the timing of sediment deposition in the Miaoli Tableland, and uplift rates are poorly constrained. An early application of radiocarbon dating on mollusks from the fine-grained tidal sediments resulted in a Holocene age (Lin, 1969), while later radiocarbon dating of the mollusks from the “Kuokang Shell Bed” yielded depositional ages between 45 and 31 ka (Wang and Peng, 1990). Wang and Peng (1990) calculated an average uplift rate of 2 mm/yr on the basis of the vertical displacement of the dated mollusks. Biostratigraphic analyses of the microfossils from the fine-grained tidal sediments of the tableland segments suggested the overall age of the sediments was younger than 2.0 Ma (Lee et al., 2002). However, the stratigraphic context of all three aforementioned age estimations is unclear. Ota et al. (2006) assume an age of the highest terraces in the SH-I (“Sanyi Tableland”) older than 90 ka based on the degree of surface weathering in comparison with other tablelands (Ota et al., 2002).

The age of the gravel and cobble layers (CSB) in the Miaoli Tableland is still unknown, although the timing of their deposition and their uplift is essential for understanding the temporal evolution of the landscape and the formation of the Miaoli Tableland. Therefore, this study focuses on the age determination of the upper layers of the sedimentary succession mainly in the northern part of the Sedimentary Highlands (SH-II) and the Sedimentary Terraces (ST) by means of optically simulated luminescence (OSL). The results are used to infer uplift rates in the respective areas.

The successful application of luminescence dating has been demonstrated in several sedimentary environments and areas in Taiwan to determine the depositional ages of poorly lithified, quartz-rich sediments on Holocene and Pleistocene timescales (e.g., in the tablelands; Chen et al., 2003a, 2009; Chen et al., 2003b; Le Béon et al., 2014) as well as on cover sediments in high mountain areas (Hebenstreit et al., 2006; Wenske et al., 2011, 2012). In general, luminescence dating in Taiwan has proven to be challenging, especially when using quartz as a dosimeter. Quartz signals have been shown to be rather dim, in worst cases even rendering successful dating applications impossible, so feldspar has been used as a dosimeter instead (Ho et al., 2017). Another frequently encountered issue is feldspar contamination of quartz that cannot be eliminated by repeated etching of the quartz separates in the preparation process. As a consequence, Dörschner et al. (2012) compared different approaches to circumvent this issue and tested post-IR-OSL (post-infrared stimulated optically stimulated luminescence) and pulsed-OSL protocols, finally opting for pulsed OSL, an approach later adopted by Tseng et al. (2013). However, Lüthgens et al. (2018) demonstrated that continuous-wavelength OSL (CW-OSL) may also yield reliable luminescence ages, which were confirmed by comparison with feldspar-based luminescence ages as well as radiocarbon dating.

METHODS AND MATERIALS

Basic principles of luminescence dating

All luminescence dating approaches are based on determining a dosimeter’s (e.g., quartz, feldspar mineral grains) last exposure

to daylight. The basic luminescence age calculation is expressed by the equation (Aitken, 1985):

$$\text{Age [in ka]} = D_e [\text{Gy}] / D_r [\text{Gy}^* / \text{ka}]$$

where D_e is the equivalent dose, which is the radiation absorption by the dosimeter during the burial period; D_r is the dose rate of environmental radiation. The radiation dose is given in grays (Gy). Luminescence dating can be applied to quartz grains (OSL) and potassium-rich feldspar grains (infrared stimulated luminescence [IRSL]) (Aitken, 1985). The application range of quartz OSL depends on the physical characteristics of the quartz grains. An applicational maximum D_e is related to the dose saturation characteristics. The most common dose range (saturation limit) empirically observed and confirmed by laboratory and modeling experiments for quartz OSL ranges up to ca. 150 Gy, as stated and summarized in multiple studies (e.g., Jain *et al.*, 2005; Arnold and Roberts, 2011; Chapot *et al.*, 2012; Timar-Gabor and Wintle, 2013), although saturation levels up to 200–300 Gy have also been reported (e.g., Rixhon *et al.*, 2017), corresponding to an age of ca. 200 ka, depending on the dose rate (Rhodes, 2011). On the other hand, feldspar IRSL gives a higher upper age limit for the application range (Rhodes, 2011), even though anomalous fading (athermal signal loss over time) causes unstable luminescence signals (Wintle, 1973; Spooner, 1994; Lamothe *et al.*, 2003). Limitations for the application of luminescence dating techniques may be caused by incomplete bleaching of grains during transport (Cunningham and Wallinga, 2012; Reimann *et al.*, 2012; Gray and Mahan, 2015), as well as the saturation behavior of the grains (Singarayer *et al.*, 2000). All of these issues may lead to inaccurate D_e and age if not detected and corrected for. Being aware of the aforementioned challenges of quartz OSL dating in Taiwan, the luminescence properties of each sample and aliquot were analyzed, especially with regard to the occurrence of feldspar contamination and its potential influence on the measurements. In this study, we applied CW-OSL measurements using a single-aliquot regenerative (SAR) protocol (Murray and Wintle, 2000; Table 1). This setup has been broadly applied for dating alluvial and eolian sediments in various geographic settings (Madsen and Murray, 2009).

Sampling

From the 51 outcrops studied by Liu *et al.* (2022) to establish a model for the sedimentary successions of the Miaoli Tableland, we selected 10 outcrops for OSL sampling (Fig. 2, Table 2), focusing on the stratigraphically important gravel and cobble layer(s) (CSB). As these clast-supported layers are physically hard to sample and also less suitable for luminescence dating, we took 10 samples from the overlying eolian sediment cover layer (SiL) (Liu *et al.*, 2021), 2 samples from the sand lens (TKD-2) and the matrix (HLPT-6) in between the gravels and cobbles (Supplementary Appendix A), and 8 samples from the sandy loam (SL) below the CSB. Because of the often fragmentary nature of terrestrial deposits, we expected hiatuses to occur within our sedimentary record in between the different depositional phases. Thus, we tried to take samples in stratigraphic order (SiC–CSB–SiL) to exclude the poor chronological resolution that might be caused by hiatuses. In addition, the possible depositional age ranges of the CSB were bracketed by the OSL ages of SiC (maximum) and SiL (minimum) as intervals for the sites where no direct sampling of

Table 1. The single-aliquot regenerative (SAR) protocol applied for the quartz-optimally simulated luminescence (OSL) dating.

1. Preheat at 180°C for 10 s, heating rate 5°C/s.
2. Blue-LED stimulation at 125°C for 40 s.
3. Give test dose.
4. Cut-heat at 160°C for 0 s, heating rate 5°C/s.
5. Blue-LED stimulation at 125°C for 40 s.
6. Give a regenerative dose = 0 s; repeat steps 1 to 5.
7. Give four regenerative doses according to the result of initial test and repeat steps 1 to 5.
8. Give a repeated regenerative dose and repeat steps 1 to 5.
Infrared (IR) depletion test
9. Give the same regenerative dose as the test dose in step 3.
10. Preheat at 180°C for 10 s, heating rate 5°C/s.
11. IR diode stimulation at 125°C for 100 s.
12. Repeat steps 2 to 5.

the CSB was possible. The OSL samples were taken from the vicinity (about 20 cm away) of both boundaries of the gravel and cobble layer(s) (Fig. 2, Supplementary Appendix A). Opaque cylinders (e.g., stainless steel or polyvinyl chloride) were used to prevent sunlight bleaching during the sampling, transportation, and storage. The surrounding sediments of the OSL samples were collected for the environmental dose-rate measurements using high-resolution, low-level gamma spectrometry (see “Measurements of Equivalent Dose and Dose Rate” and Table 3).

The outcrops were chosen in areas with respect to the different tableland subgroups (Fig. 2) to develop a chronological frame for the model of a stepwise resedimentation of the gravels and cobbles (Liu *et al.*, 2022). Outcrops 029_GJW and 032_THST are located in the proximal segments of SH-II; outcrop 007_NCT is located at the fringe of the biggest segment (i.e., Chiding, 崎頂) (Figs. 1b and 2a); and outcrop 001_HLPT is located at the fringe of a distal segment of the SH-II. Outcrops 025_JJC, 013_TKD, 023_XNPW, 031_XNPWH, and 015_XP are located at the fringe of the distal segments of the Sedimentary Terraces (ST).

Outcrop 030_TYGC is the only one in the southern Sedimentary Highlands (SH-I) where suitable sediments were accessible for sampling. Here, sandy deposits are exposed below 9-m-thick gravels and cobbles. However, their stratigraphic relationship with the SL layer in the SH-II and ST remains uncertain (Fig. 2a).

In addition, we used a handheld GPS receiver to record coordinates of the outcrops and extracted elevations from the high-precision open-access digital elevation model (DEM) (NASA JPL, 2013; Satellite Survey Center, 2018). Then we calculated the height of each outcrop with an uncertainty of ± 0.75 m (Satellite Survey Center, 2018). We also measured the thickness and depth below surface of each sampled deposit to calculate the elevation of the OSL sampling points. These elevation data were also used for the subsequent calculation of the uplift rates, and related uncertainties were derived from the error range of age estimations.

Sample preparation

The preparation and measurements of the quartz-OSL samples were performed between 2017 and 2018 in the luminescence

Table 2. The basic geographic information and corresponding morphological status of the quartz-optically simulated luminescence (OSL) samples from the Miaoli Tableland.

Sample	Lab ID	Latitude, longitude (WGS84)	Elevation (m)	Depth (m)	Tableland subgroup ^a
HLPT-5	LUM3682	24°35.74'N, 120°48.39'E	84.4	1.7	SH-II
HLPT-6	LUM3683	24°35.74'N, 120°48.39'E	85.0	1.1	SH-II
HLPT-7	LUM3684	24°35.74'N, 120°48.39'E	85.8	0.4	SH-II
NCT-2	LUM3686	24°34.32'N, 120°43.54'E	76.7	0.7	SH-II
NCT-3	LUM3687	24°34.32'N, 120°43.54'E	77.1	0.3	SH-II
XNPW-1	LUM3688	24°28.29'N, 120°40.22'E	33.4	1	ST
XNPW-2	LUM3689	24°28.29'N, 120°40.22'E	33.8	0.4	ST
THST-1	LUM3812_3813	24°34.22'N, 120°44.45'E	75.5	1.5	SH-II
THST-2	LUM3814	24°34.22'N, 120°44.45'E	78.1	0.3	SH-II
XP-1	LUM3815	24°32.13'N, 120°41.68'E	11.5	0.7	ST
XNPWH-1	LUM3816	24°28.25'N, 120°40.29'E	34.1	1	ST
XNPWH-2	LUM3817	24°28.25'N, 120°40.29'E	34.7	0.4	ST
GJW-2	LUM3818	24°31.24'N, 120°47.49'E	184.5	1	SH-II
TYGC-1	LUM3819	24°26.86'N, 120°45.22'E	335.1	10	SH-I
TKD-1	LUM3820	24°32.39'N, 120°42.46'E	141.6	0.8	ST
TKD-2	LUM3821	24°32.39'N, 120°42.46'E	141.3	0.6	ST
TKD-3	LUM3822	24°32.39'N, 120°42.46'E	141.7	0.2	ST
JJC-1	LUM3823	24°27.52'N, 120°39.81'E	28.4	1.1	ST
JJC-2	LUM3824	24°27.52'N, 120°39.81'E	29.1	0.4	ST
JJC-A-1	LUM3825	24°27.52'N, 120°39.81'E	14.3	1.5	ST

^aSH-I, SH-II, Sedimentary Highlands; ST, Sedimentary Terraces.

laboratory at the Leibniz Institute for Applied Geophysics in Hanover, Germany. All laboratory work was done under subdued red-light conditions to prevent the grains from being bleached by artificial light sources. The sediments of both ends of the sampling cylinders were removed, because these grains were possibly bleached during the sampling. The samples were prepared by methods based on Mejdahl and Christiansen (1994) for the extraction of quartz grains: (1) drying of the samples at max. 50°C for 24 h; (2) sieving to separate a suitable grain size, we used the grain-size range of 150–200 µm for the CW-OSL measurements (because all 20 samples contained sufficient amounts of this grain size, it was used for all the samples for the sake of consistency); (3) removal of carbonates by adding HCl (10%); (4) destruction of aggregates by adding sodium oxalate; and (5) removal of organic matter by adding H₂O₂ (30%). Heavy liquid separation was subsequently applied to separate the quartz grains from the other minerals. The quartz grains were then etched with HF solution (40%) for 60 min; this procedure dissolved the remaining feldspar grains and the outer part of quartz grains that were exposed to the alpha radiation (Mejdahl and Christiansen, 1994). A final sieving was carried out after the HF etching step.

Experimental setup

The quartz grains were mounted on stainless steel disks (diameter = 9 mm) and were fixed to an adhesive spot (using silicone oil) of 2 mm diameter at the center of each disk. These 2 mm aliquots

each contained approximately 100 grains (Duller, 2008). Sample NCT-2 was chosen for the evaluation of protocols and dose recovery characteristics (Fig. 3). Dose recovery tests and subsequent measurements were carried out using a Risø TL/OSL reader (model DA-20). The stimulation system was fit with blue LEDs (470 nm) for OSL stimulation and IR LEDs (870 nm) for IRSL stimulation (Bøtter-Jensen et al., 2000, 2010). The luminescence signal detection units were mounted with a Hoya U-340 filter to measure the quartz-OSL signal (Bøtter-Jensen et al., 2000, 2010). The test protocol included an additional stimulation step for the feldspar-IRSL signal to study the feldspar contamination of each aliquot (i.e., depletion test) (Duller, 2003).

Dose recovery tests were conducted with a given dose of 63.5 Gy at preheat temperatures ranging from 180°C to 300°C (tested every 20°C) (Fig. 3). The recovered/given dose ratio showed good (0.9–1.1) results for 160°C and 180°C, but less favorable results at higher preheat temperatures. We set 180°C as the preheat temperature and 160°C as the cut-heat for the subsequent dose recovery tests conducted for all samples to validate the reproducibility of the SAR protocol. Data evaluation was carried out using rejection criteria for recycling of ±10% (Rhodes, 2011) and 5% of the natural signal for recuperation (Murray and Wintle, 2000). The results show that all samples have a recovered/given dose ratio within the range of 0.9 to 1.1, which proves the suitability of the SAR protocol (Fig. 3).

The decay curves of the quartz-OSL signals are fast component-dominated and reach the background rapidly within the first seconds of stimulation (Bailey et al., 1997; Singarayer and Bailey, 2003; Wintle and Murray, 2006; Durcan and Duller,

Table 3. Summary of the dosimetry measurements and calculation of total dose rates.

Sample	Lab ID	Measured water content (%)	Lifetime average water content (%)	²³⁸ U (ppm)	²³² Th (ppm)	K (%)	Beta dose rate (Gy/ka)	Gamma dose rate (Gy/ka)	Cosmic dose rate (Gy/ka)	Total dose rate (Gy/ka)
HLPT-5	LUM3682	10.3	10.8	2.14 ± 0.01	10.76 ± 0.04	1.14 ± 0.01	1.18 ± 0.06	0.89 ± 0.05	0.16 ± 0.02	2.25 ± 0.07
HLPT-6	LUM3683	9.6	10.1	2.15 ± 0.01	11.19 ± 0.04	1.17 ± 0.01	1.22 ± 0.06	0.92 ± 0.05	0.18 ± 0.02	2.34 ± 0.08
HLPT-7	LUM3684	7.4	7.8	2.11 ± 0.01	9.37 ± 0.04	0.97 ± 0.01	1.07 ± 0.06	0.82 ± 0.05	0.20 ± 0.02	2.04 ± 0.08
NCT-2	LUM3686	6.4	6.7	2.19 ± 0.01	10.09 ± 0.03	0.76 ± 0.01	0.96 ± 0.06	0.81 ± 0.05	0.19 ± 0.02	1.97 ± 0.08
NCT-3	LUM3687	2.9	3.1	2.21 ± 0.01	9.65 ± 0.04	0.77 ± 0.01	1.00 ± 0.07	0.83 ± 0.05	0.20 ± 0.02	2.01 ± 0.09
XNPW-1	LUM3688	13.5	14.1	2.43 ± 0.01	12.73 ± 0.04	1.64 ± 0.01	1.53 ± 0.06	1.08 ± 0.04	0.18 ± 0.02	2.80 ± 0.07
XNPW-2	LUM3689	3.3	3.4	2.14 ± 0.01	9.18 ± 0.04	0.94 ± 0.01	1.10 ± 0.06	0.84 ± 0.05	0.19 ± 0.02	2.08 ± 0.08
THST-1	LUM3812_3813	8.5	8.9	1.08 ± 0.01	5.61 ± 0.03	0.87 ± 0.01	0.83 ± 0.05	1.06 ± 0.05	0.17 ± 0.02	1.56 ± 0.07
THST-2	LUM3814	8.5	8.9	1.90 ± 0.01	9.3 ± 0.03	0.98 ± 0.01	1.04 ± 0.06	0.79 ± 0.05	0.20 ± 0.02	2.01 ± 0.08
XP-1	LUM3815	7.4	7.7	2.16 ± 0.01	10.68 ± 0.04	1.1 ± 0.01	1.19 ± 0.06	0.91 ± 0.05	0.19 ± 0.02	2.28 ± 0.08
XNPWH-1	LUM3816	13.6	14.3	1.69 ± 0.01	8.95 ± 0.03	1.25 ± 0.01	1.13 ± 0.05	0.77 ± 0.04	0.18 ± 0.02	2.10 ± 0.07
XNPWH-2	LUM3817	7.7	8.1	1.88 ± 0.01	9.19 ± 0.03	1.17 ± 0.01	1.18 ± 0.06	0.83 ± 0.05	0.19 ± 0.02	2.19 ± 0.08
GJW-2	LUM3818	14.9	15.6	2.52 ± 0.01	12.99 ± 0.04	1 ± 0.01	1.11 ± 0.05	0.94 ± 0.04	0.18 ± 0.02	2.12 ± 0.07
TYGC-1	LUM3819	8.7	9.2	1.43 ± 0.04	6.81 ± 0.08	1.04 ± 0.01	0.98 ± 0.05	0.65 ± 0.05	0.07 ± 0.01	1.82 ± 0.07
TKD-1	LUM3820	9.8	10.3	2.01 ± 0.01	9.82 ± 0.02	1.47 ± 0.01	1.38 ± 0.06	0.92 ± 0.05	0.19 ± 0.02	2.48 ± 0.08
TKD-2	LUM3821	11.7	12.2	2.16 ± 0.01	10.43 ± 0.03	1.05 ± 0.01	1.10 ± 0.05	0.85 ± 0.04	0.19 ± 0.02	2.15 ± 0.07
TKD-3	LUM3822	10.4	11.0	1.95 ± 0.01	8.96 ± 0.03	0.97 ± 0.01	1.01 ± 0.06	0.76 ± 0.05	0.20 ± 0.02	1.94 ± 0.07
JJC-1	LUM3823	14.2	14.9	2.20 ± 0.01	10.96 ± 0.04	1.55 ± 0.01	1.40 ± 0.05	0.96 ± 0.04	0.18 ± 0.02	2.55 ± 0.07
JJC-2	LUM3824	12.3	12.9	2.31 ± 0.01	11.54 ± 0.04	1.56 ± 0.01	1.46 ± 0.06	1.01 ± 0.04	0.19 ± 0.02	2.63 ± 0.07
JJC-A-1	LUM3825	9.3	9.7	2.37 ± 0.01	11.44 ± 0.04	1.8 ± 0.01	1.67 ± 0.06	1.10 ± 0.05	0.17 ± 0.02	2.89 ± 0.08

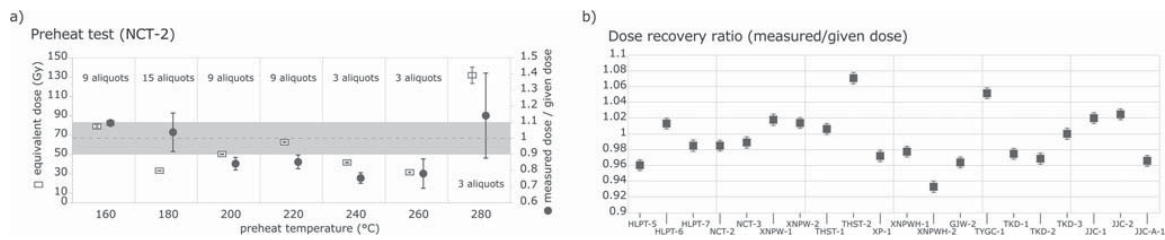


Figure 3. Preheat and dose recovery test of all samples. (a) Results of the preheat and dose recovery tests obtained from the quartz grains of the sample NCT-2; the recycling ratios and equivalent doses were tested in 20°C increments from 160°C to 300°C. (b) The dose recovery test results for all other samples have the same setting of preheat (180°C) and cut-heat temperature (160°C) as for NCT-2. These results were all obtained without a hot-bleaching procedure.

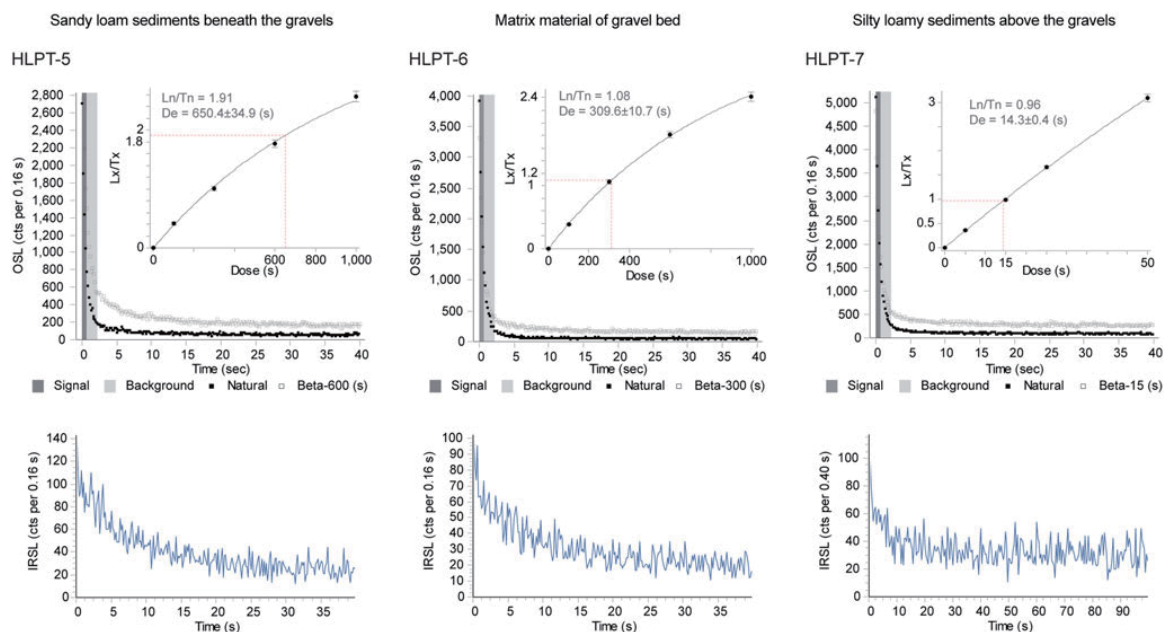


Figure 4. Representative quartz-optically simulated luminescence (OSL) decay curves, single-aliquot regenerative (SAR) growth curves, and feldspar-IRSL signals for samples within and below the gravel and cobble layer (CSB) (see Supplementary Appendix B for the detailed results of all samples). The fast component is clearly dominant; the feldspar-IRSL signals are relatively weak and only contribute to the background noise.

2011). We observed fast component-dominated natural signals for all of the accepted aliquots (Fig. 4). We followed the early background subtraction approach of Cunningham and Wallinga (2010) to set the time intervals for the initial signal (0–0.5 s) and background (0.6–1.5 s) to rule out any influence of medium or slow components on the net signals (Fig. 4). Most of the aliquots show very low recuperation values (<5% of the natural signal), thus the recuperation-caused underestimation of D_e is negligible (Aitken and Smith, 1988; Supplementary Appendix B). The IR depletion was carefully checked for all aliquots (Duller, 2003), and as expected from the results of previous studies, feldspar contamination was also identified in our samples. To test whether the feldspar contamination detected significantly affected the determined doses, we tested all samples and all measured aliquots for a potential correlation between D_e and the IR-depletion ratio (Supplementary Appendix B) (based on the approach of Schmidt et al. [2012]), but although an IR contribution was detected in some aliquots, there is no significant correlation to the D_e ($R^2 < 0.36$) for all samples; thus there is no

clear relationship overall between D_e and feldspar contamination (Supplementary Appendix B). This is corroborated by average IR depletion ratios close to 1 for all samples.

Measurements of equivalent dose and dose rate

For each sample, D_e measurements were performed on at least 40 aliquots (XP-1 and JJC-1). For the majority of the samples, we measured around 42 to 84 aliquots, the maximum amount being 102 aliquots for sample NCT-2 (Table 4). Thus, we collected at least 24 or more aliquots of each sample for the D_e determination, as recommended in relevant studies (Galbraith and Roberts, 2012; Rixhon et al., 2017). The rejection criteria of the recycling ratio and the recuperation ratio were based on the aforementioned tests. In addition, the $2D_0$ test was applied to check whether aliquots were in field saturation (Wintle and Murray, 2006).

For the determination of the environmental dose rate, the sediments were dried at 75°C for more than 24 h to measure their water content (%), and then the sediments were homogenized

Table 4. Results of quartz–optically simulated luminescence (OSL) dating and age estimations.^a

Sample	Lab ID	Grain size (µm)	Aliquot size (mm)	Measured aliquots	Infrared (IR) depletion ratio	Recuperation test ^b	Recycling test ^c	Dose recovery ratio	n for D _e calculations	Overdispersion (%)	D _e (Gy) CAM	age (ka) CAM	D _e (Gy) MAM	Age (ka) MAM ^c
HLP-T5	LUM3682	150–200	2	79	0.95 ± 0.04	79/100%	45/57%	0.96 ± 0.07	27	27.8 ± 3.9	83.0 ± 4.5	36.9 ± 2.4	83.0 ± 10.8	37.0 ± 4.6
HLP-T6	LUM3683	150–200	2	72	0.951 ± 0.05	67/93%	56/78%	1.01 ± 0.02	56	44.0 ± 4.2	39.0 ± 2.3	16.6 ± 1.1	38.9 ± 4.3	16.7 ± 2.0
HLP-T7	LUM3684	150–200	2	54	0.956 ± 0.05	49/91%	46/85%	0.98 ± 0.03	46	51.7 ± 5.4	1.8 ± 0.1	0.9 ± 0.1	1.4 ± 0.2	0.6 ± 0.09
NCT-2	LUM3686	150–200	2	102	0.888 ± 0.04	102/100%	76/75%	0.98 ± 0.03	74	45.5 ± 3.7	47.7 ± 2.5	24.2 ± 1.6	47.7 ± 4.8	23.4 ± 2.8
NCT-3	LUM3687	150–200	2	54	0.948 ± 0.03	53/98%	53/98%	0.98 ± 0.03	53	33.6 ± 3.3	12.8 ± 0.6	6.4 ± 0.4	12.9 ± 1.2	6.4 ± 0.7
XNPW-1	LUM3688	150–200	2	64	0.952 ± 0.04	64/100%	43/67%	1.01 ± 0.02	43	43.5 ± 4.7	52.2 ± 3.4	18.7 ± 1.3	52.2 ± 6.4	18.7 ± 2.4
XNPW-2	LUM3689	150–200	2	48	0.955 ± 0.05	30/63%	28/53%	1.01 ± 0.01	28	56.9 ± 7.8	0.2 ± 0.02	0.1 ± 0.01	0.18 ± 0.03	0.1 ± 0.01
THST-1	LUM3812_3813	150–200	2	84	0.903 ± 0.04	83/99%	55/65%	1.00 ± 0.04	27	25.1 ± 3.5	114.2 ± 5.6	73.2 ± 5.0	114.2 ± 14.7	73.2 ± 9.3
THST-2	LUM3814	150–200	2	42	0.842 ± 0.05	41/98%	25/60%	1.07 ± 0.05	24	52.0 ± 7.6	80.8 ± 8.6	40.1 ± 4.6	74.6 ± 14.1	32.4 ± 7.3
XP-1	LUM3815	150–200	2	40	0.924 ± 0.03	40/100%	38/95%	0.97 ± 0.03	38	72.2 ± 8.3	20.7 ± 2.4	9.0 ± 1.1	9.9 ± 2.2	4.0 ± 0.8
XNPWH-1	LUM3816	150–200	2	42	0.818 ± 0.03	42/100%	24/57%	0.97 ± 0.03	24	50.0 ± 7.3	66.9 ± 6.8	31.9 ± 3.4	66.5 ± 13.5	25.3 ± 6.0
XNPWH-2	LUM3817	150–200	2	42	0.934 ± 0.03	40/95%	32/76%	0.93 ± 0.02	29	67.0 ± 8.9	12.6 ± 1.5	5.8 ± 0.8	6.8 ± 1.9	3.1 ± 0.9
GJW-2	LUM3818	150–200	2	42	0.795 ± 0.03	42/100%	28/62%	0.96 ± 0.02	25	49.0 ± 7.0	92.5 ± 9.1	43.7 ± 4.5	92.5 ± 15.0	39.6 ± 7.2
TYGC-1	LUM3819	150–200	2	42	0.99 ± 0.03	42/100%	30/71%	1.05 ± 0.06	29	30.0 ± 4.1	174.3 ± 9.9	95.8 ± 6.7	174.8 ± 22.5	96.0 ± 12.2
TKD-1	LUM3820	150–200	2	42	0.747 ± 0.03	42/100%	36/86%	0.97 ± 0.03	34	46.3 ± 5.7	121.4 ± 9.7	48.9 ± 4.2	121.4 ± 17.4	44.6 ± 7.3
TKD-2	LUM3821	150–200	2	42	0.938 ± 0.03	42/100%	36/86%	0.96 ± 0.01	36	38.2 ± 4.6	35.2 ± 2.2	16.4 ± 1.2	35.1 ± 4.4	16.4 ± 2.1
TKD-3	LUM3822	150–200	2	42	0.91 ± 0.03	41/98%	40/95%	1.00 ± 0.03	40	42.0 ± 5.4	11.5 ± 0.8	5.9 ± 0.5	11.4 ± 1.5	5.9 ± 0.8
JJC-1	LUM3823	150–200	2	40	0.789 ± 0.04	40/100%	24/60%	1.02 ± 0.03	22	38.7 ± 6.0	134.1 ± 11.2	52.5 ± 4.7	134.2 ± 21.0	52.6 ± 8.0
JJC-2	LUM3824	150–200	2	42	0.852 ± 0.03	42/100%	29/69%	1.02 ± 0.01	29	54.9 ± 7.3	58.0 ± 5.9	22.0 ± 2.3	50.8 ± 10.1	18.3 ± 3.5
JJC-A-1	LUM3825	150–200	2	42	0.753 ± 0.03	42/100%	30/71%	0.96 ± 0.03	29	28.2 ± 3.8	162.4 ± 8.7	56.4 ± 3.4	163.0 ± 20.8	56.4 ± 6.9

^aCAM, central age model; MAM, minimum age model.

^bThe majority of ages are based on the CAM data, except for three samples which are based on the MAM data (Sigma b = 0.45) due to the incomplete bleaching effects.

^cThe MAM ages used in the interpretations are marked in bold.

with a mortar and pestle to break the aggregates of fine-grained sediments and sealed (about 700 g) in a Marinelli beaker for more than 6 weeks to achieve equilibrium between ^{222}Rn and ^{226}Ra (Aitken, 1985; Guérin et al., 2011). The content of naturally occurring radionuclides (decay chains of ^{235}U and ^{232}Th , as well as ^{40}K) was determined by measurements using high-resolution, low-level gamma spectrometry (high-purity p-type germanium detector). The gamma efficiency calibrations were performed by using the reference materials RGK-1, RGU-1, and RTh-1 from IAEA with either 50 or 700 g (depending on the sample amount). The determined radionuclide contents were then included in dose rate calculations using the conversion factors provided by Guérin et al. (2011; Table 3).

Equivalent dose determination and dose-rate and age calculations

We exported the original measured data (e.g., D_e and error of each aliquot) from the Risø-Analyst software (Bøtter-Jensen et al., 2000) and implemented the age model calculations with the R-luminescence package in R Studio (Kreutzer et al., 2012). We first used the central age model (CAM) (Galbraith et al., 1999) to calculate the central dose for all the samples, as well as to determine the corresponding overdispersions (OD) (Galbraith et al., 1999). Kernel density estimate (KDE) plots were generated for the D_e distributions of all samples using the R-luminescence package (Kreutzer et al., 2012).

The acceptance rates of the recuperation test were 91% to 100% for most samples, except for sample XNPW-2 (Table 4), which showed higher recuperation values and only 30 of 48 aliquots (ca. 63%) were accepted following the recuperation test (Table 4). The acceptance rates of the recycling test range from 53% to 98%, and two groups can be differentiated. The group with the higher acceptance ratio (85 to 98%) consists of samples mostly taken from the SiL layers; only two are taken from the CSB layer (TKD-2) and the SL layer (TKD-1) (Table 4). The group of samples with the lower acceptance rate (53% to 78%) are mainly derived from the SL layer. The worst acceptance rate concerning the recycling test (53%) was again observed for sample XNPW-2 (Table 4).

As a result of the additional $2D_0$ test for saturation of the quartz grains, only 13 aliquots in total had to be rejected for the subsequent D_e determination (Wintle and Murray, 2006). They occurred in nine samples (two for HLPT-5, two for NCT-2, one for THST-1, one for THST-2, one for GJW-2, one for TYGC-1, two for TKD-1, two for JJC-1, and one for JJC-A-1).

The skewness of the D_e distributions ranges between -0.42 and 2.59 (Table 4); two samples are slightly left skewed (THST-1 and GJW-2), all other D_e distributions are right skewed (from 0.08 to 2.59). The highly right-skewed samples are XNPWH-2 (2.59), JJC-2 (1.73), XNPW-2 (1.73), TKD-3 (1.5), NCT-3 (1.42), JJC-A-1 (1.42), HLPT-7 (1.3), and XP-1 (1.17), half of these highly right-skewed samples are taken from the SiL layer. The OD values for all samples range between $27.8 \pm 3.9\%$ and $72.2 \pm 8.3\%$ (Table 4). The samples with higher OD values ($>45\%$) are mostly taken from the SiL layer, except samples XNPWH-1 ($50.0 \pm 7.3\%$) and TKD-1 ($46.3 \pm 5.7\%$). While some samples show rather broad, but symmetrical dose distributions, the majority show multimodal or right-skewed distributions (Fig. 5). The corresponding OD values for the samples showing rather symmetrical distributions average about 45%. These are the samples we expect to represent the minimal overdispersion

to be achieved in nature for well-bleached samples from the research area. These multimodal or right-skewed dose distributions may indicate incomplete bleaching prior to burial to be significant for these samples (Stokes et al., 2001). Thus, the residual doses remain, causing a shift toward higher D_e values (Jain et al., 2004). For example, long-lasting or long-distance reworking processes yield a higher bleaching probability than rapid and short-distance (e.g., flooding) reworking processes (Arnold and Roberts, 2009; Gray and Mahan, 2015).

To address the effects of incomplete bleaching in the calculation of the D_e values, we used the three-parameter minimum age model (MAM) (Galbraith et al., 1999) with $\sigma_{\text{MAM}} = 0.45$ as determined to be the average scatter for symmetrical dose distributions, for all samples. The results showed the CAM- and MAM-based ages agreed within error for the large majority of samples, except for three samples: HLPT-7, XP-1, and XNPWH-2 (Table 4). We therefore concluded that incomplete bleaching significantly affected these samples and used the MAM-based (with $\sigma_{\text{MAM}} = 0.45$) D_e values for subsequent age calculation; the CAM-based D_e values were used for age calculation of all other samples. The corresponding ages used for all later interpretation are marked in bold in Table 4.

The dose rate calculations were based on the function comprising dose rate conversion parameters (Rees-Jones, 1995; Guérin et al., 2011) as well as the water content, the beta-dose attenuation (Aitken, 1985; Adamiec and Aitken, 1998), and the cosmic-dose attenuation (Prescott and Stephan, 1982; Prescott and Hutton, 1994). Due to the loss of moisture since the excavation of the sampled outcrops, we estimated the lifetime water content for each sample by adding 5% to the measured water content. The 5% additional water content contributed to a broader error range of the dose rate for ± 0.04 – 0.05 Gy/ka (ca. 2% wider). The depositional ages were calculated with the empirical calculation of the D_e and the dose rate using a spreadsheet (Table 4).

RESULTS

All luminescence samples showed robust results in the pretests, and the SAR protocol we chose yielded accurate D_e estimates for the samples under investigation. Although feldspar contamination was detected for some aliquots, this did not have a systematic effect on the equivalent dose. Sample TYGC-1 showed rather high equivalent doses, with the dose–response curve approaching saturation in that dose range. The resulting age must therefore be handled with care, as it may actually represent a minimum age (Table 4, Supplementary Appendix C). Using the average of scatter expressed as the overdispersion (OD or σ_{MAM}) for the well-bleached samples' (symmetrical) dose distributions as a threshold value, it was possible to identify those samples from the data set that were significantly affected by incomplete bleaching (HLPT-7, XP-1, and XNPWH-2). These three samples showed right-skewed D_e distributions, including some very high data point(s) (Fig. 5, Table 4), and were also characterized by high OD values. To account for the effects of incomplete bleaching, we used the MAM-based D_e values for the age calculation of these three samples, with CAM ages adopted for all other samples (Fig. 5, Table 4). Although the quartz luminescence properties we encountered in this study are not ideal, we carefully investigated the potential influence of feldspar contamination and did not observe any dose dependence with regard to the IR depletion ratio. Average IR depletion ratios for all samples were observed to be close to 1. In addition, all samples showed excellent results in dose recovery experiments. Only one sample was approaching

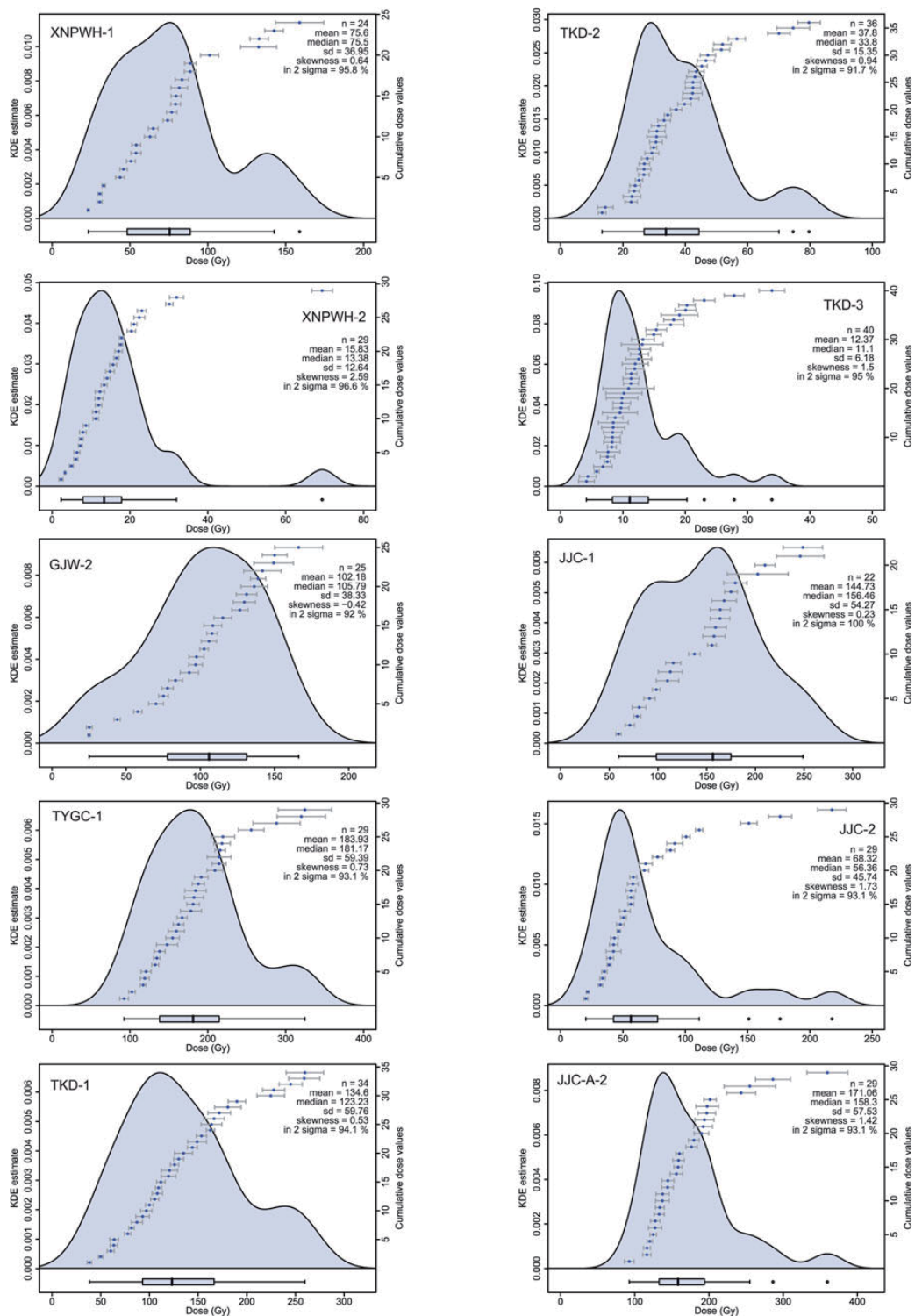


Figure 5. The kernel density estimate (KDE) plots for the D_e distribution of all optically simulated luminescence (OSL) samples. All samples of coastal fine-grained sediments and the matrix sediments of the gravel and cobble layer present symmetrical but relatively broad D_e distributions. Three samples from the uppermost layer (HLPT-7, XP-1, and XNPWH-2), however, present highly right-skewed D_e distributions with some isolated higher data point(s). The high overdispersion values are interpreted to result from incomplete bleaching. To address incomplete bleaching effects, the minimum age model (MAM) was applied to these three samples, and central age model (CAM) ages were used for the other samples.

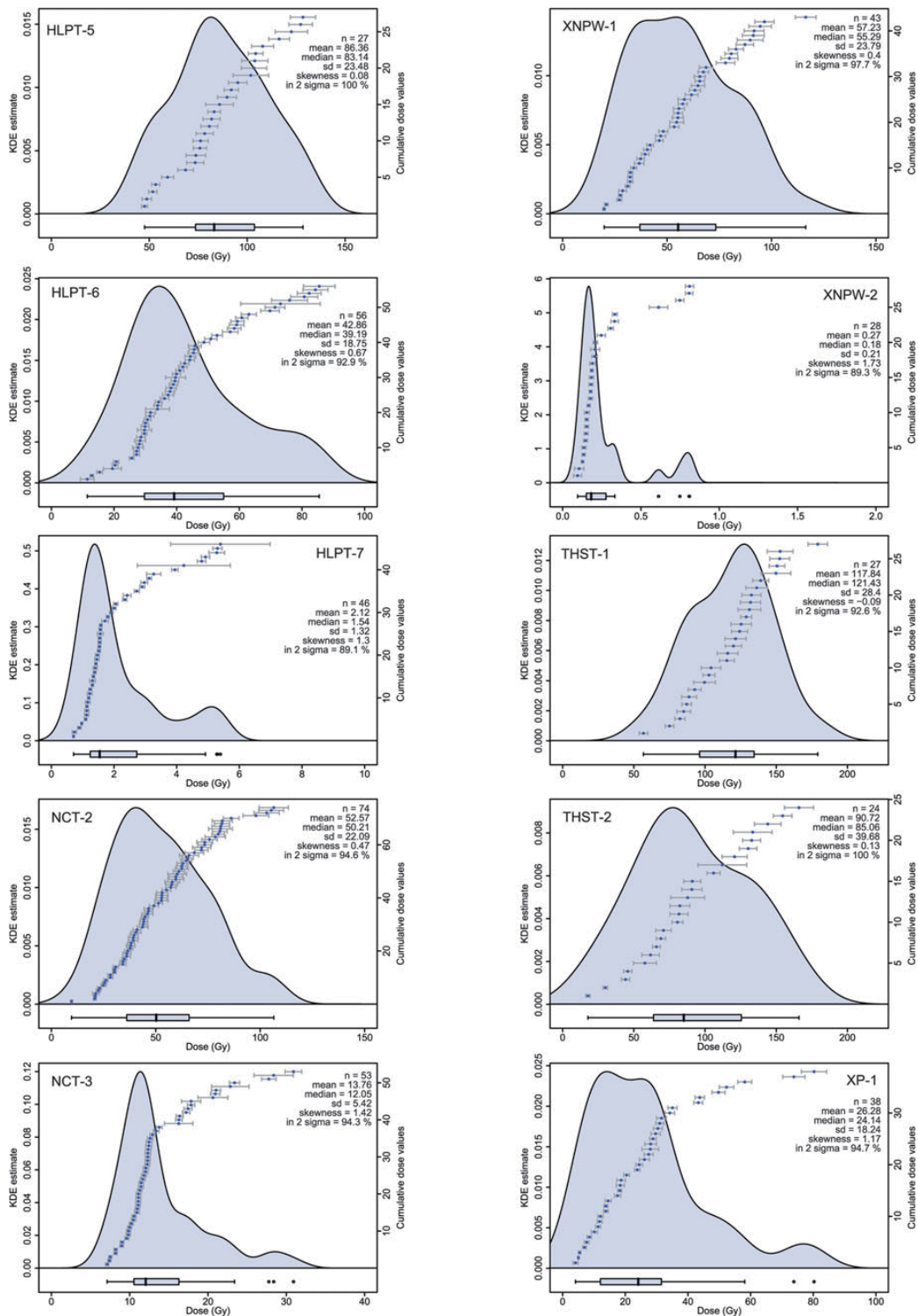


Figure 5. Continued.

signal saturation. We therefore consider our luminescence analyses to provide reliable depositional ages.

The total dose rate ranges from 1.51 ± 0.07 Gy/ka (THST-1) as the minimum and 2.89 ± 0.08 Gy/ka (JJC-A-1) among the 20 studied OSL samples (Table 3). The differences in the cosmic dose contribution among the samples are insignificant, as they only contributed 0.07 ± 0.01 mGy/ka (TYGC-1) to 0.20 ± 0.02 mGy/ka (HLPT-7; THST-2; TKD-3). The beta dose rates are more diverse. They differ from site to site, which is more significant than the difference among the different sedimentary layers in the same site (Table 3). The sites in the distal segments contain higher concentration of radioactive nuclides, and vice versa.

The overall depositional ages of the upper part of sedimentary successions in the Miaoli Tableland from the obtained OSL measurements range from ca. 95.7 ± 6.7 ka (TYGC-1, LUM3819) to ca. 0.1 ± 0.01 ka (XNPW-2, LUM3689).

The results can be categorized tentatively from the post-last interglacial to the Holocene (Figs. 2 and 6, Table 4):

1. post-last interglacial sandy deposits in the SH-I (TYGC-1), $n = 1$;
2. MIS 4 sandy deposits in the proximal segments of the SH-II (THST-1), $n = 1$;
3. MIS 3 to 2 sandy deposits in the distal segments of the SH-II (HLPT-5) and the ST (XNPW-1, XNPWH-1, TKD-1, JJC-1, JJC-A-1), $n = 6$;

4. MIS 3 silty cover layers in the proximal SH-II segments (THST-2, GJW-2), $n = 2$;
5. MIS 2 silty cover layers in the distal segments of the SH-II (NCT-2) and sandy deposits in the ST (JJC-2), $n = 2$;
6. MIS 2 gravel and cobble layer(s) of the SH-II (HLPT-6) and ST (TKD-2), $n = 2$;
7. Holocene silty cover layers in the distal segments of the SH-II (HLPT-7, NCT-3) and ST (XNPW-2, XNPWH-2, XP-1, TKD-3), $n = 6$.

DISCUSSION

OSL ages of the sedimentary units

The numerical ages of the post-last interglacial to modern depositions are presented in stratigraphic order in the respective outcrops (Fig. 2). They generally match the late Pleistocene age estimation of Chang *et al.* (1998) and the radiocarbon dates of mollusks in coastal sediments (sandy deposits) in the distal part of the tableland falling into MIS 3 (Wang and Peng, 1990). Furthermore, our results allow a more detailed chronological framework for the deposition of the coastal and fluvial sediments in the upper layers in the Miaoli Tableland, which agrees with the assumption that the beginning of the deposition of the lower part of the sediment succession occurred during the middle Pleistocene (Ota *et al.*, 2006).

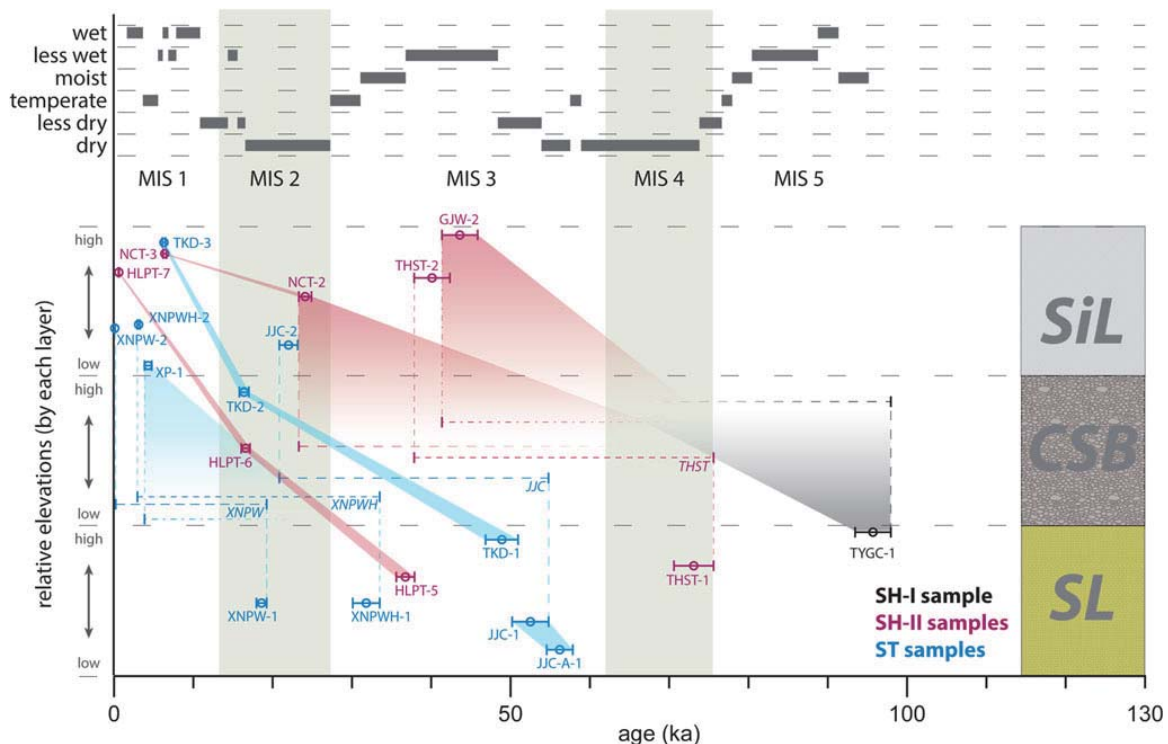


Figure 6. Comparison of the optically simulated luminescence (OSL) ages of the studied sedimentary succession compared with the paleoclimate record after Liew *et al.* (2006). The Marine Oxygen Isotope Stages (MIS) were simplified from the global $\delta^{18}\text{O}$ curve of Lisiecki and Raymo (2005) and Cohen *et al.* (2020). The OSL samples are plotted by the age with uncertainties (x-axis) and relative elevations in the classification of each layer (y-axis). The ages of each outcrop are graphically connected by the colored lines and shadings according to their corresponding tableland segment subcategories (Sedimentary Highlands in the southeast [SH-I], dark gray; in the north and northwest [SH-II], magenta; Sedimentary Terraces [ST], cyan); thus the depositional age of the gravels and cobbles can be tentatively marked with the corresponding intervals by bracketing the ages of the sandy loam (SL) layer (upper limit) and the silty loam layer (SiL) layer (lower limit).

Age of the sandy loam layer (SL)

The SL layer is distributed over the entire area of the Miaoli Tableland. Liu et al. (2022) interpret these sediments as a near-coast (beach) sandy accumulation in the foreland of the WF. The age estimation of sample TYGC-1 in the SH-I was affected by saturation of the quartz grains, even though most of the aliquots passed the $2D_0$ test. Therefore, we took this age estimation (95.7 ± 6.7 ka, TYGC-1) as a minimum age rather than a real depositional age, and we assume the real depositional age for this sandy loamy substrate should be earlier than 100 ka. In this context, we interpret the sampled coastal (beach) sediments as representing the beginning of a post-last interglacial sea-level lowering (Figs. 2a and 6), which resulted in regression in the shallow terrain of the Taiwan Strait (Liu et al., 1998; Jan et al., 2002; Liu et al., 2008).

The age estimation of the SL layer in the proximal segments of the SH-II in outcrop 032_THST (deposited at 73.1 ± 5.0 ka, THST-1) can be related to a further regression at the cold phase that began during the early MIS 4 (Waelbroeck et al., 2002) (Figs. 2b and 7b).

Another group of ages is represented by outcrops 013_TKD (48.9 ± 4.2 ka, TKD-1) and 025_JJC (56.3 ± 3.4 ka, JJC-A-1; 52.5 ± 4.7 ka, JJC-1) (Figs. 2b and 6). The remarkable westward inclination of the SL layer (Liu et al., 2021) in outcrop 025_JJC (Supplementary Appendix A) is mainly influenced by the Tung-Xiao Anticline (Yang et al., 2006, 2016; Figs. 1b and c and 2) and took place after the deposition of the coastal sediments. In contrast, the SL layers of the 023_XNPW and 031_XNPWH outcrops in the immediate vicinity do not show any inclination and were presumably deposited after the tectonic displacement according to their younger ages (31.9 ± 3.4 ka, XNPWH-1; 18.7 ± 1.3 ka, XNPW-1). This also indicates that the anticline was active during a time span around 50–30 ka.

The age in the northern SH-II segments (36.9 ± 2.4 ka, HLPT-5) falls between the aforementioned groups. Overall, the ages of the SL layer indicate that the deposition of coastal (beach) sediments took place over a long period of time during the late MIS 5 to MIS 2 in the area of today's Miaoli Tableland, and the ages are generally getting younger north- and westward (Figs. 2 and 6), implying that the coastline moved northwestward during the last glacial period, which is in agreement with the regression in the Taiwan Strait (Jan et al., 2002). However, local postdepositional remobilization of the highly mobile sand may explain the relatively young age of 18.7 ± 1.3 ka (XNPW-1).

Age of the cover layers (SiL)

Eolian sediments cover large parts of the Miaoli Tableland (Liu et al., 2022); our respective OSL ages range from 43.7 ± 4.5 ka (GJW-2) to 0.1 ± 0.1 ka (XNPWH-2). The depositional ages are consistent in outcrop 029_GJW (43.7 ± 4.5 ka, GJW-2) and outcrop 032_THST (40.1 ± 4.6 ka, THST-2). These samples represent the oldest eolian accumulations in the area, found on the large proximal segments in the SH-II, deposited during MIS 3. In two outcrops in the SH-II and the ST, the sampled eolian sediments were deposited during MIS 2 (24.2 ± 1.6 ka, NCT-2; 22.0 ± 2.3 ka, JJC-2), respectively. The youngest eolian sediments began being deposited on both the distal segments of the SH-II (0.6 ± 0.1 ka, HLPT-7; 6.4 ± 0.4 ka, NCT-3) and the ST (0.1 ± 0.1 ka, XNPW-2; 5.8 ± 0.7 ka, XNPWH-2; 9.1 ± 1.1 ka, XP-1; 5.9 ± 0.5 ka, TKD-3) during the Holocene and continued being deposited until the present day (Fig. 7d, Table 4).

These ages correlate well with the degree of the in situ weathering and pedogenesis in the studied outcrops, which affect the

upper sediment layers on the tableland surfaces (Tsai et al., 2010). We derived the oldest ages from the larger (better-preserved) tableland segments, where the color of the surface substrate appeared to be reddish-ocher (see “Introduction”). Assuming a more or less continuous dust deposition over the study area during the last glacial cycle, the age distribution of the cover layer samples represents the preservation status of the tableland segments.

Similar cover layers or soils with eolian dust input have also been recognized and described in a variety of geomorphological settings and at all altitudes in Taiwan (Hebenstreit, 2016; Tsai et al., 2021), for example, in the Dadu Tableland and the Puli Tableland (Tsai et al., 2010; Tseng et al., 2016), as well as in the mountain ranges, where the ages range from 0.7 ka in the Nanhua Shan (Tsai et al., 2021) to ca. 3–4 ka in the Nanhuta Shan and Hehuan Shan (Hebenstreit et al. 2006, Wenske et al., 2011), and 54.8 ka in the Tachia River catchment (Wenske et al., 2012).

The eolian sediments originate from a mixture of dust brought mainly from the Asian continent (Pye and Zhou, 1989; Chen et al., 2013) until the present (Lin et al., 2007; Hsu et al., 2009) and locally reworked fine-grained sediments (Tsai et al., 2006, 2008, 2010, 2021; Wenske et al., 2012).

Age of the gravel and cobble layers (CSB)

Direct dating results from the gravel and cobble depositions (CSB) are only available for two samples in the SH-II (16.4 ± 1.2 ka, HLPT-6) and ST (16.6 ± 1.1 ka, TKD-2). Therefore, we used bracketing ages from the upper and lower boundary layers to estimate the ages of more CSB layers (Fig. 6).

As the underlying coastal sediments at outcrop 030_TYGC (sample TYGC-1) yielded an age that has to be interpreted as a minimum age $>95.8 \pm 6.7$ ka, we conclude that the deposition of the thick gravels and cobbles of the SH-I is younger than this age. This agrees with Ota et al. (2006), who assume an age older than 90 ka based on the degree of surface weathering of the “Sanyi Tableland” (SH-I). On the other hand, the gravels and cobbles on the proximal segments of the SH-II were deposited before ca. 40 ka, as estimated from the age of the overlying cover layer at outcrops 032_THST and 029_GJW (Figs. 2a and 6). The gravels and cobbles in the Sedimentary Highlands can therefore be related to an early stage of the last glacial cycle, probably to the MIS 4 cold phase (see “Landform Evolution Model”).

The depositional age of the gravels and cobbles in the Sedimentary Terrace (ST) area can be estimated from the under- and overlying layers at the three outcrops 025_JJC, 023_XNPW, and 031_XNPWH, beside the direct age (16.6 ± 1.1 ka, TKD-2). The abovementioned inclination of the subjacent coastal sands (SL layer) at outcrop 025_JJC has affected neither the overlying gravels and cobbles nor the neighboring coastal sands at outcrops 023_XNPW and 031_XNPWH. We can infer that the gravel accumulation in the ST began not earlier than the end of the activity of the Tung-Xiao Anticline at about 30 ka, as indicated by its age in the outcrop XNPWH (31.8 ± 3.4 ka, XNPWH-1). However, in 023_XNPW, the gravels and cobbles must be even younger than the underlying sands (18.6 ± 1.3 ka, XNPW-1). The directly dated gravels and cobbles at outcrop 013_TKD in the northwestern ST confirm this time period. On the other hand, the cover layer at 025_JJC implies an earlier deposition of the gravels and cobbles already before (22.0 ± 2.3 ka, JJC-2) at this location. From our data, we assume a general time frame for the deposition of the ST gravels and cobbles during

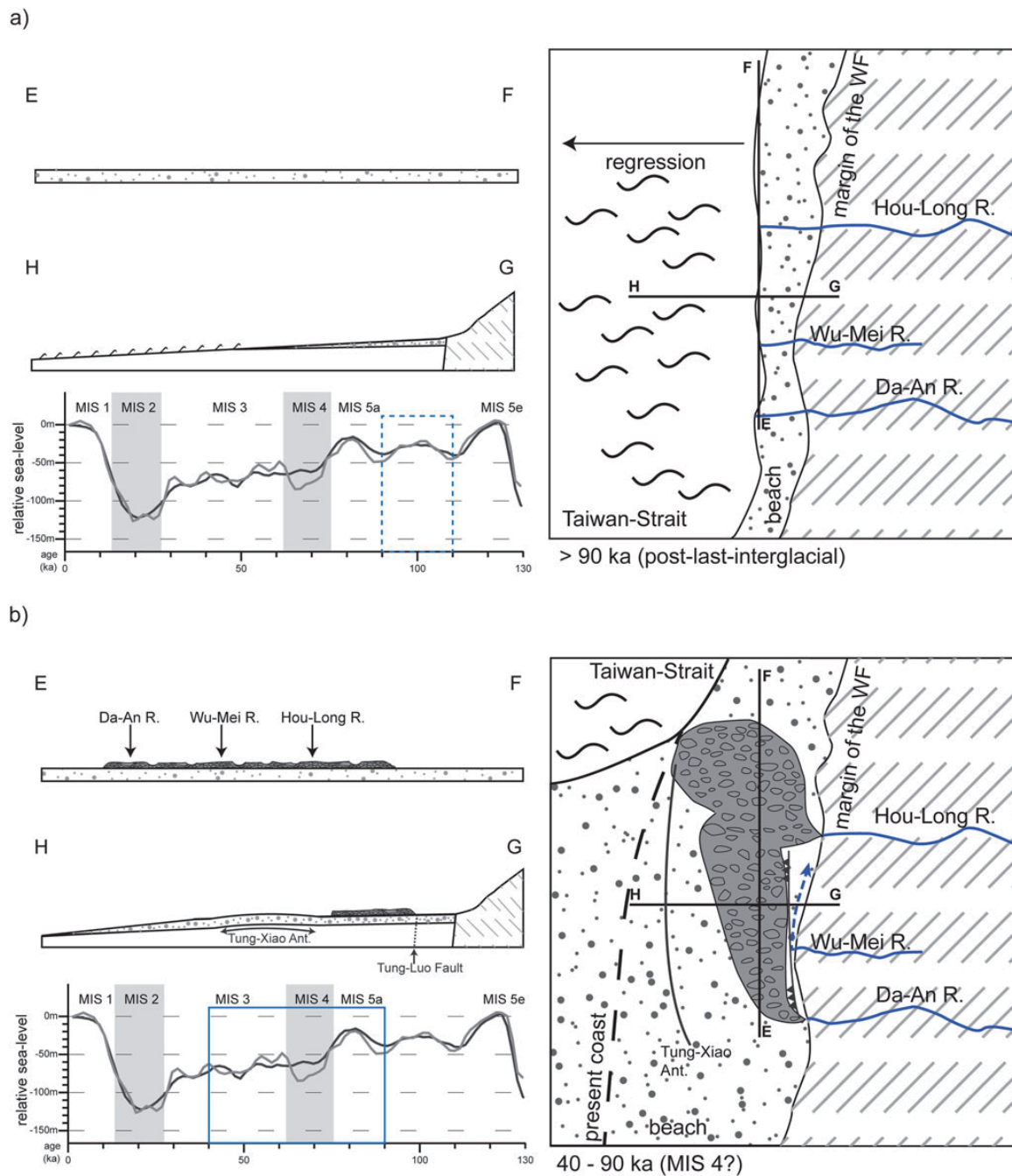


Figure 7. Schematic sketch of a morphological landscape evolution model of the Miaoli Tableland in four time steps (a, b, c, and d). Each step shows a south-north (E–F) and east-west (G–H) profile, a sketch map, and the global sea-level curve simplified from Waelbroeck *et al.* (2002) with the mark of the respective period. The location of the coastlines are referenced from Fig. 1a; the tectonic features after Shyu *et al.* (2005), Ota *et al.* (2006), and Yang *et al.* (2016). For a detailed description see “Landform Evolution Model.” MIS, Marine Oxygen Isotope Stage; SH-I, SH-II, Sedimentary Highlands; ST, Sedimentary Terraces; WF, Western Footwalls.

the MIS 2 cold phase (see “Landform Evolution Model”). However, the special and temporal resolution is not high enough to distinguish between individual gravel and cobble accumulation events.

Uplift rates of the Miaoli area

The Miaoli Tableland does not represent fluvial terraces in a strict sense, although the upper sedimentary units are composed of

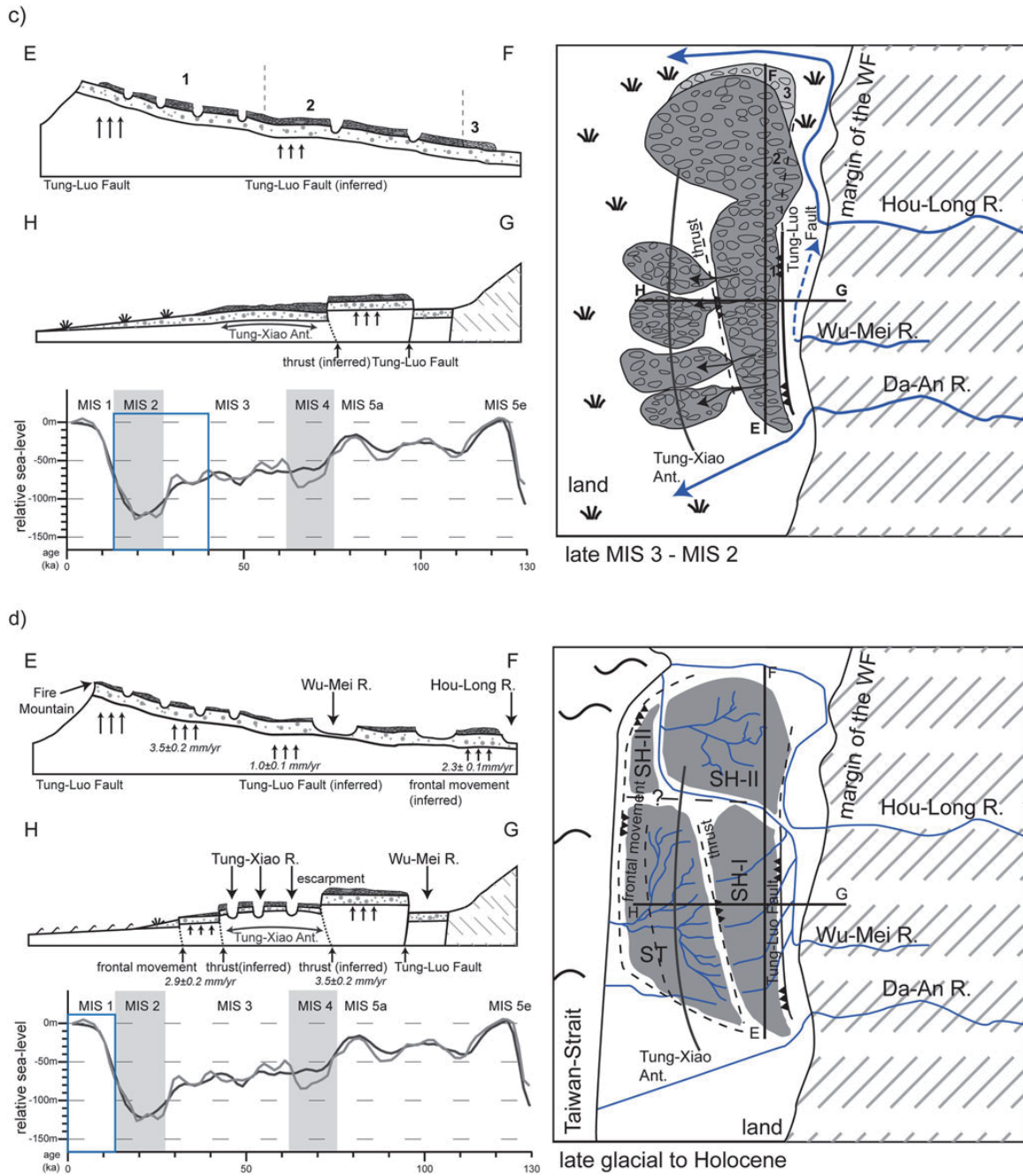


Figure 7. Continued.

fluvial gravels and cobbles and the tableland is dissected by fluvial incision. However, the underlying sediment units represent a sequence of coastal and, in the deeper part, shallow-marine (tidal) sediments (Lin, 1963; Liu et al., 2022). To infer estimates of uplift rates in the area, we calculated the vertical displacement by using the uppermost parts of the coastal sediment (SL layer). A similar approach was taken in southern Taiwan (Chen and Liu, 2000)

and Japan (Matstu'ura et al. 2014), and by Ota and Yamaguchi (2004) with examples from the western Pacific area. Assuming that the coastline in the Taiwan Strait was lower than today at the time of deposition and taking the present coastline as a benchmark, the resulting uplift rates represent minimum values for each outcrop.

The calculations resulted in spatially heterogeneous uplift rates (Fig. 7c and d, Table 5) in the Miaoli Tableland. In the

Table 5. Calculation of the uplift rates.

Outcrop	Tableland subgroup ^a	Optically simulated luminescence (OSL) age of sandy substrate (ka)	Elevation (m)	Minimum uplift rates (mm/yr)
TYGC	SH-I	95.8 ± 6.7	335.1	3.5 ± 0.2
THST	SH-II	73.1 ± 5.0	75.5	1.0 ± 0.1
JJC	ST	52.5 ± 4.7	28.4	0.5 ± 0.1
TKD	ST	48.9 ± 4.2	141.7	2.9 ± 0.2
HLPT	SH-II	36.9 ± 2.4	84.4	2.3 ± 0.1
XNPWH	ST	31.9 ± 3.4	34.1	1.1 ± 0.1

^aSH-I, SH-II, Sedimentary Highlands; ST, Sedimentary Terraces.

Sedimentary Highlands the highest rate is found at outcrop 030_TYGC with 3.5 ± 0.2 mm/yr, reflecting a relatively rapid uplift of the SH-I in the last ca. 100 ka, which is mainly controlled by the Tung-Luo Fault (Fig. 1) in the east (Ota *et al.*, 2006). In the SH-II, the uplift rates are 2.3 ± 0.1 mm/yr at outcrop 001_HLPT and only ca. 1 ± 0.1 mm/yr at outcrop 032_THST.

The uplift rates in the ST area are rather low in the southwestern part. The uplift of 28 and 34 m in the 025_JJC and the 031_XNPWH, respectively, results in an average rate of 0.5–1.1 mm/yr since MIS 2/3. In contrast, the coastal sediments in the outcrop 013_TKD imply an uplift of ca. 142 m in ca. 49 ka at a rate of 2.9 mm/yr, which might be due to the vicinity of the frontal movement at the coastal area (Shyu *et al.*, 2005; Yang *et al.*, 2016).

Our calculated uplift rates are comparable with the previously estimated average of 2 mm/yr for the last 45–30 ka in the Miaoli Tableland (Wang and Peng, 1990), but relatively low compared with rates farther south in the western Taiwan mountain foreland, where Holocene uplift rates of beach and marine sediments of 5–7 mm/yr and 7.7–4.3 ka, respectively, are reported from the Tainan area (Chen and Liu, 2000; Hsieh and Knuepfer, 2001).

The tectonic influence on the morphodynamics in the western Taiwan tablelands is interpreted as a partitioned model (Siame *et al.*, 2012); major tectonic events, rather than continuous processes, might cause the main offsets. For example, the Chi-Chi earthquake in 1999 caused ca. 10 m of vertical offset of the Chelunpu Thrust Fault in the nearby Shi-Gang (ca. 12 km south-east) and Feng-Yuan areas (ca. 17 km south) (Chen *et al.*, 2003a; Yue *et al.*, 2005; Fig. 1a).

Landform evolution model

Combining our results and interpretations, we propose a landform evolution model, integrating the results from Chang *et al.* (1998), Ota *et al.* (2006), and Liu *et al.* (2022), of the Miaoli Tableland in four time slices as follows (Figs. 1b and 7):

1. The lowering of the sea level after the high stand of the last interglacial caused a regression in the western mountain foreland. The upper coastal sediments of the foreland basin in today's SH-I area were accumulated at that time. The deposition of the beach sediments follows the ongoing northward shoreline progradation (Fig. 7a).
2. During the following cold phase (MIS 4 and probably until the beginning of MIS 3), the sea-level lowering shifted the base level to a lower level and farther away from the mountain

front. Cold and wet climate conditions are documented by a vegetation change in the mid-altitude area (1000–3000 m asl) in the mountain ranges (Liew *et al.*, 2006; Fig. 6). Glacial and periglacial conditions prevailed in the upper mountain ranges at that time (Hebenstreit *et al.*, 2006, 2011; Klose, 2006), which resulted in a higher yield of coarse clasts in the rivers. The rivers transported gravels and cobbles from the mountain ranges and the WF into the newly emerged foreland area. They were deposited as alluvial fans that formed the thick gravel and cobble bed of the later Sedimentary Highlands (SH-I and SH-II) (Ota *et al.*, 2006; Liu *et al.*, 2022; Figs. 6 and 7b). These gravels and cobbles were previously interpreted as deposits from multiple sources, such as the Da-An River for the south of the SH-I and the Hou-Long River for the north of the SH-I and the proximal area of the SH-II (Chang *et al.*, 1998; Fig. 1b). We follow this assumption. However, due to the similar lithology in the catchments of the rivers that drain the WF and the mountain ranges, it is difficult to distinguish the origin of gravels and cobbles based on physical properties such as composition, shape, or roundness (Liu *et al.*, 2021, 2022).

Initial uplift took place along the Tung-Luo Fault just after the deposition of the gravels and cobbles, which resulted in a first incision of the Sedimentary Highlands, followed by the activity of the Tung-Xiao Anticline (Fig. 7b).

Eolian sediments subsequently covered the alluvial fans. They have been preserved in the proximal parts of the fans until today; this is also documented in their high degree of weathering. This implies that the larger segments of the present tableland surface are stable and not affected by erosion so far.

3. According to bathymetry (Jan *et al.*, 2002) and current sea-level models (Waelbroeck *et al.*, 2002), the Taiwan Strait was dry and the Miaoli Tableland was far from the paleocoastline (1a and 7c) from MIS 3 to 2.

The ongoing thrusting of the Tung-Luo Fault (Ota *et al.*, 2006) forced the Da-An River to change its fluvial path farther south, which resulted in a cut off of the gravels and cobbles yielded to the paleo-alluvial fan in the present SH-I area. This process tilted the SH-I gravels and induced runoff to the west, which resulted in a deep incision of the SH-I segments, visible in the parallel fluvial pattern (Liu *et al.*, 2022; Fig. 1b). The eroded gravels and cobbles were transported (reworked) to the west, forming secondary fans in the foreland, the present ST area (Fig. 7c). At the same time, the uplift in the northern alluvial fan (the present SH-II) caused initial incision

and a relocation of gravels and cobbles (Liu et al., 2022), which extended the fan to the north (Fig. 7c).

The erodibility of the sediments may have been favored by the cold climatic conditions and the sparse savannah vegetation in the mountain foreland during MIS 2 (Liew et al., 2006). The subsequent increase of precipitation during the late glacial (end of MIS 2) caused accelerated transport of the fluvial gravels and cobbles into the ST area. Reinforced fluvial activity at that time is documented in other locations in Taiwan as well, for example, in the intramountainous basin in Puli (Chen and Liu, 1991; Tseng et al., 2013, 2016).

Finally, the rapid uplift at the inferred thrust (Chang et al., 1998) at the topographic divide between the SH-I and the ST beheaded the valleys in the SH-I and reversed their flow direction from west to east (Ota et al., 2006). This therefore stopped the sediment yield toward the alluvial fans in the ST, where ongoing fluvial incision caused dissection of the topographic surfaces into tableland segments.

4. During the late glacial and the Holocene, sea level was rising rapidly. However, the whole Miaoli Tableland area, including its distal parts, was further uplifted, due to the ongoing frontal movement (Shyu et al., 2005; Fig. 7d). This uplift increased the fluvial incision, which led to the intense dissection of the ST tableland segments forming a dendritic fluvial pattern (Liu et al., 2022) and subsequently caused the deposition of secondarily reworked gravels and cobbles in the present fluvial channels and at the coastal plains (AL) (Fig. 7d).

CONCLUSION

We present detailed and reliable chronological control for the formation of the Miaoli Tableland based on luminescence dating (quartz OSL). The new chronology and the new calculation of long-term uplift rates allow distinguishing between several depositional stages of the coastal, fluvial, and eolian sediments as well as phases of erosion since the last interglacial. They provide a chronological frame for a new landform evolution model proposed by Liu et al. (2022), which describes a stepwise deposition and reworking of fluvial gravels and cobbles during the last glacial period followed by an intense dissection of the tableland segments during the Holocene, representing an interplay of endogenic (tectonic) and exogenic (climatic) forces in the formation of the Miaoli Tableland.

On the other hand, the last glacial OSL ages of the upper coastal sediments (SL layer) suggest that the underlying alternating shallow-marine and coastal sediments (SiC layer) and the lower coastal sediments (LS layer) were accumulated during and before the last interglacial, respectively, and that the beginning of the sedimentary succession dates back to the middle Pleistocene. This time span is in general agreement with previous models (Chang et al., 1998; Ota et al., 2006).

It can be shown that the tectonic activity in the Miaoli Tableland follows a spatiotemporal pattern, beginning in the south-east and progressing to the northwest. It is represented by diverse and moderate long-term uplift rates of ca. 0.5–3.5 mm/yr, which can be clearly correlated to the inferred thrust and bending structures in the area (Chang, 1990, 1994; Ho, 1994; Chang et al., 1998; Lee, 2000; Shyu et al., 2005; Ota et al., 2006) and can be compared with the general uplift rates in the mountain foreland in Taiwan (Chen and Liu, 2000; Hsieh and Knuepfer, 2001).

The combination of high-resolution terrain analyses, detailed sediment description (Liu et al., 2021, 2022), and numerical

dating (this study) provides new insights into the formation of the Taiwanese tablelands. Furthermore, this study demonstrates the capacity of luminescence dating as an efficient tool for a robust chronological control of Quaternary landscape evolution in Taiwan. The outcome of this study is also a further step toward a more detailed Quaternary stratigraphy in Taiwan in the future.

Supplementary Material. The supplementary material for this article can be found at <https://doi.org/10.1017/qua.2022.52>

Acknowledgments. The authors thank Sumiko Tsukamoto and Yan Li for friendly support and access to the laboratory. Thanks to Natacha Gribenski and Dirk Wenske for discussion of the relevant topics. Thanks to Chang Chun Petrochemical Co., Ltd, Miaoli Factory and the Jing-Ji Company for granting access to the outcrops for sampling. Thanks to Chia-Han Tseng for help during the fieldwork. Thanks to Sheng-Hua Li and Ashok Singhvi for comments during the APLED 2018 congress in Beijing. Thanks to the senior editor Derek Booth, the associate editor Barbara Mauz, and the reviewers Magali Rizza, and Bernd Wünnemann for the friendly and constructive comments on this article during the review process.

REFERENCES

- Adamiec, G., Aitken, M.J., 1998. Dose-rate conversion factors: update. *Ancient TL* 16, 37–50.
- Aitken, M.J., 1985. *Thermoluminescence Dating*. Academic Press, Orlando/London.
- Aitken, M.J., Smith, B.W., 1988. Optical dating: recuperation after bleaching. *Quaternary Science Reviews* 7, 387–393.
- Angelier, J., Barrier, E., Chu, H.T., 1986. Plate collision and paleostress trajectories in a fold-thrust belt: the foothills of Taiwan. *Tectonophysics* 125, 161–178.
- Arnold, L.J., Roberts, R.G., 2009. Stochastic modelling of multi-grain equivalent dose (D_e) distributions: implications for OSL dating of sediment mixtures. *Quaternary Geochronology* 4, 204–230.
- Arnold, L. J., Roberts, R. G. 2011. Paper I—Optically stimulated luminescence (OSL) dating of perennially frozen deposits in north-central Siberia: OSL characteristics of quartz grains and methodological considerations regarding their suitability for dating. *Boreas* 40, 389–416.
- Bailey, R.M., Smith, B.W., Rhodes, E.J., 1997. Partial bleaching and the decay form characteristics of quartz OSL. *Radiation Measurements* 27, 123–136.
- Bøtter-Jensen, L., Bulur, E., Duller, G.A.T., Murray, A.S., 2000. Advances in luminescence instrument systems. *Radiation Measurements* 32, 523–528.
- Bøtter-Jensen, L., Thomsen, K.J., Jain, M., 2010. Review of optically stimulated luminescence (OSL) instrumental developments for retrospective dosimetry. *Radiation Measurements* 45, 253–257.
- Bradley, S.L., Milne, G.A., Horton, B.P., Zong, Y., 2016. Modelling sea level data from China and Malay-Thailand to estimate Holocene ice-volume equivalent sea level change. *Quaternary Science Reviews* 137, 54–68.
- Central Geological Survey, 2017. National Geological Data Warehouse. Central Geological Survey, Taipei, Taiwan (accessed September 17, 2022). <https://gis3.moeacgs.gov.tw/gwh/gsb97-1/sys8/t3/index1.cfm>.
- Chang, H.C., 1990. Geological Map of Taiwan—Baishatun. 1:50,000. Central Geological Survey, Taipei, Taiwan.
- Chang, H.C., 1994. Geological Map of Taiwan—Dajia. 1:50,000. Central Geological Survey, Taipei, Taiwan.
- Chang, J.C., Teng, K.H., Liu, M.C., 1998. A Geomorphological Study on River Terraces in Miaoli Hills. *Geographical Research* 29, 97–112.
- Chang, L.S., 1953. *Geologic Map of Taiwan*. Geological Survey of Taiwan, Taipei, Taiwan.
- Chang, L.S., 1955a. The geological history of Taiwan/台灣之地史. *Quarterly Journal of the Taiwan Bank/台灣銀行季刊* 7, 1–7.
- Chang, L.S., 1955b. The strata of Taiwan/台灣之地層. *Quarterly Journal of the Taiwan Bank/台灣銀行季刊* 7, 26–49.
- Chapot, M.S., Roberts, H.M., Duller, G.A.T., Lai, Z.P., 2012. A comparison of natural- and laboratory-generated dose response curves for quartz

- optically stimulated luminescence signals from Chinese loess. *Radiation Measurements* **47**, 1045–1052.
- Chen, C.G., 1983. *The Soil Investigation Report of the Slopes—Miaoli County/山坡地土壤調查報告—苗栗縣*. Mountain Agricultural Resources Development Bureau, Nantou, Taiwan.
- Chen, H.F., Yeh, P.Y., Song, S.R., Hsu, S.C., Yang, T.N., Wang, Y., Chi, Z., *et al.*, 2013. The Ti/Al molar ratio as a new proxy for tracing sediment transportation processes and its application in aeolian events and sea level change in East Asia. *Journal of Asian Earth Sciences* **73**, 31–38.
- Chen, Y.G., Chen, Y.W., Chen, W.S., Lee, K.J., Lee, L.S., Lu, S.T., Lee, Y.H., Watanuki, T., Lin, Y.N.N., 2009. Optical dating of a sedimentary sequence in a trenching site on the source fault of the 1999 Chi-Chi earthquake, Taiwan. *Quaternary International* **199**, 25–33.
- Chen, Y.G., Chen, Y.W., Chen, W.S., Zhang, J.F., Zhao, H., Zhou, L.P., Li, S.H., 2003a. Preliminary results of long-term slip rates of 1999 earthquake fault by luminescence and radiocarbon dating. *Quaternary Science Reviews* **22**, 1213–1221.
- Chen, Y.G., Liu, T.K., 1991. Radiocarbon dates of river terraces along the lower Tahanchi, northern Taiwan: their tectonic and geomorphic implications. *Proceedings of the Geological Society of China* **34**, 337–347.
- Chen, Y.G., Liu, T.K., 2000. Holocene uplift and subsidence along an active tectonic margin southwestern Taiwan. *Quaternary Science Reviews*, **19**, 923–930.
- Chen, Y.W., Chen, Y.G., Murray, A.S., Liu, T.K., Lai, T.C., 2003b. Luminescence dating of neotectonic activity on the southwestern coastal plain, Taiwan. *Quaternary Science Reviews* **22**, 1223–1229.
- Cohen, K.M., Harper, D.A.T., Gibbard, P.L., 2020. *ICS International Chronostratigraphic Chart 2020/03*. International Commission on Stratigraphy, IUGS (accessed September 1, 2020). www.stratigraphy.org.
- Cunningham, A.C., Wallinga, J., 2010. Selection of integration time intervals for quartz OSL decay curves. *Quaternary Geochronology* **5**, 657–666.
- Cunningham, A.C., Wallinga, J., 2012. Realizing the potential of fluvial archives using robust OSL chronologies. *Quaternary Geochronology* **12**, 98–106.
- Dörschner, N., Reimann, T., Wenske, D., Lüthgens, C., Tsukamoto, S., Frechen, M., Böse, M., 2012. Reconstruction of the Holocene coastal development at Fulong Beach in north-eastern Taiwan using optically stimulated luminescence (OSL) dating. *Quaternary International* **263**, 3–13.
- Duller, G.A.T., 2003. Distinguishing quartz and feldspar in single grain luminescence measurements. *Radiation Measurements* **37**, 161–165.
- Duller, G.A.T., 2008. Single-grain optical dating of Quaternary sediments: why aliquot size matters in luminescence dating. *Boreas* **37**, 589–612.
- Durcan, J.A., Duller, G.A.T., 2011. The fast ratio: a rapid measure for testing the dominance of the fast component in the initial OSL signal from quartz. *Radiation Measurements* **46**, 1065–1072.
- Fox, M., Goren, L., May, D.A., Willett, S.D., 2014. Inversion of fluvial channels for paleorock uplift rates in Taiwan. *Journal of Geophysical Research: Earth Surface* **119**, 1853–1875.
- Galbraith, R.F., Roberts, R.G., 2012. Statistical aspects of equivalent dose and error calculation and display in OSL dating: an overview and some recommendations. *Quaternary Geochronology* **11**, 1–27.
- Galbraith, R.F., Roberts, R.G., Laslett, G.M., Yoshida, H., Olley, J.M., 1999. Optical dating of single and multiple grains of quartz from Jinmium rock shelter, northern Australia: part I, experimental design and statistical models. *Archaeometry* **41**, 339–364.
- Gray, H.J., Mahan, S.A., 2015. Variables and potential models for the bleaching of luminescence signals in fluvial environments. *Quaternary International* **362**, 42–49.
- Guérin, G., Mercier, N., Adamiec, G., 2011. Dose-rate conversion factors: Update. *Ancient TL* **29**, 5–8.
- Hebenstreit, R., 2016. Quaternary mineral dust deposits in Taiwan—a new palaeoclimatic archive. Paper presented at DUST 2016—2nd International Conference on Atmospheric Dust (Castellana Marina, Italy, June 12–17, 2016).
- Hebenstreit, R., Böse, M., Murray, A.S., 2006. Late Pleistocene and early Holocene glaciations in Taiwanese mountains. *Quaternary International* **147**, 76–88.
- Hebenstreit, R., Ivy-Ochs, S., Kubik, P.W., Schlüchter, C., Böse, M., 2011. Lateglacial and early Holocene surface exposure ages of glacial boulders in the Taiwanese high mountain range. *Quaternary Science Reviews* **30**, 298–311.
- Ho, C.S., 1988. *An Introduction to the Geology of Taiwan: Explanatory Text of the Geologic Map of Taiwan*. 2nd ed. Central Geological Survey, Ministry of Economic Affairs, Taipei, Taiwan.
- Ho, H.C., 1994. Geological Map of Taiwan—Miaoli. 1:50,000. Central Geological Survey, Taipei, Taiwan.
- Ho, L.D., Lüthgens, C., Wong, Y.C., Yen, J.Y., Chyi, S.J., 2017. Late Holocene cliff-top dune environment in the Hengchun Peninsula of Taiwan: implications for palaeoenvironmental reconstruction. *Journal of Asian Earth Sciences* **148**, 13–30.
- Hsieh, M.L., Chyi, S.J., 2010. Late Quaternary mass-wasting records and formation of fan terraces in the Chen-yeo-lan and Lao-nung catchments, central-southern Taiwan. *Quaternary Science Reviews* **29**, 1399–1418.
- Hsieh, M.L., Knuepfer, P.L.K., 2001. Middle-late Holocene river terraces in the Erhjen River Basin, southwestern Taiwan—implications of river response to climate change and active tectonic uplift. *Geomorphology* **38**, 337–372.
- Hsieh, M.L., Lai, T.H., Wu, L.C., Lu, W.C., Liew, P.M., 2006. Eustatic sea-level change of 11–5 ka in western Taiwan, constrained by radiocarbon dates of core sediments. *Terrestrial, Atmospheric and Oceanic Sciences* **17**, 353–370.
- Hsu, S.C., Liu, S.C., Arimoto, R., Liu, T.H., Huang, Y.T., Tsai, F., Lin, F.J., Kao, S.J., 2009. Dust deposition to the East China Sea and its biogeochemical implications. *Journal of Geophysical Research: Atmospheres* **114**. <http://dx.doi.org/10.1029/2008JD011223>.
- Huang, C.Y., Liew, P.M., Zhao, M., Chang, T.C., Kuo, C.M., Chen, M.T., Wang, C.H., Zheng, L.F., 1997. Deep sea and lake records of the Southeast Asian paleomonsoons for the last 25 thousand years. *Earth and Planetary Science Letters* **146**, 59–72.
- Jahn, R., Blume, H.P., Asio, V.B., Spaargaren, O., Schad, P., 2006. *Guidelines for Soil Description*. 4th ed. Food and Agriculture Organization of the United Nations, Rome.
- Jain, M., Botter-Jensen, L., Murray, A.S., Denby, P., Tsukamoto, S., Gibling, M., 2005. Revisiting TL: dose measurement beyond the OSL range using SAR. *Ancient TL* **23**, 9–24.
- Jain, M., Murray, A.S., Botter-Jensen, L., 2004. Optically stimulated luminescence dating: How significant is incomplete light exposure in fluvial environments? *Quaternaire* **15**, 143–157.
- Jan, S., Wang, J., Chern, C.S., Chao, S.Y., 2002. Seasonal variation of the circulation in the Taiwan Strait. *Journal of Marine Systems* **35**, 249–268.
- Klose, C., 2006. Climate and geomorphology in the uppermost geomorphic belts of the Central Mountain Range, Taiwan. *Quaternary International* **147**, 89–102.
- Kreutzer, S., Schmidt, C., Fuchs, M., Dietze, M., Fischer, M., Fuchs, M., 2012. Introducing an R package for luminescence dating analysis. *Ancient TL* **30**, 1–8.
- Lamothe, M., Auclair, M., Hamzaoui, C., Huot, S., 2003. Towards a prediction of long-term anomalous fading of feldspar IRSL. *Radiation Measurements* **37**, 493–498.
- Le Béon, M., Suppe, J., Jaiswal, M.K., Chen, Y.G., Ustaszewski, M.E., 2014. Deciphering cumulative fault slip vectors from fold scarps: relationships between long-term and coseismic deformations in central Western Taiwan. *Journal of Geophysical Research: Solid Earth* **119**, 5943–5978.
- Lee, C.L., Huang, T., Shieh, K.S., Chen, Z.H., 2002. The chronostratigraphy and sedimentary environments of the Toukoshan Fm. in Beishatun area, Miaoli/苗栗白沙屯地區頭料山層之年代地層與沉積環境. *Annual Report of Central Geological Survey, MOEA 1999 (later half)*—2000, 17–20.
- Lee, J.F., 2000. Geological Map of Taiwan—Dongshi. 1:50,000. Central Geological Survey, Taipei, Taiwan.
- Liew, P.M., Huang, S.Y., Kuo, C.M., 2006. Pollen stratigraphy, vegetation and environment of the last glacial and Holocene—a record from Toushe Basin, central Taiwan. *Quaternary International* **147**, 16–33.
- Lin, C.C., 1957. *Geomorphology of Taiwan*. The Historical Research Commission of Taiwan Province, Taipei, Taiwan.
- Lin, C.C., 1963. The Lungkang Formation, lower marine terrace deposits near Miaoli. *Petroleum Geology of Taiwan* **2**, 87–105.

- Lin, C.C., 1969. Holocene geology of Taiwan. *Acta Geologica Taiwanica* 13, 83–126.
- Lin, C.C., Chou, J.T., 1974. *Geology of Taiwan*. The Historical Research Commission of Taiwan Province, Taichung, Taiwan.
- Lin, C.Y., Wang, Z., Chen, W.N., Chang, S.Y., Chou, C.C.K., Sugimoto, N., Zhao, X., 2007. Long-range transport of Asian dust and air pollutants to Taiwan: observed evidence and model simulation. *Atmospheric Chemistry Physics* 7, 423–434.
- Lisiecki, L.E., Raymo, M.E., 2005. A Pliocene–Pleistocene stack of 57 globally distributed benthic $\delta^{18}\text{O}$ records. *Paleoceanography* 20. <https://doi.org/10.1029/2004PA001071>.
- Liu, J.P., Liu, C.S., Xu, K.H., Milliman, J.D., Chiu, J.K., Kao, S.J., Lin, S.W., 2008. Flux and fate of small mountainous rivers derived sediments into the Taiwan Strait. *Marine Geology* 256, 65–76.
- Liu, S.H., Böse, M., Hebenstreit, R., 2021. The columnar sections and pictures of the outcrops in Miaoli Tableland. Refubium–Freie Universität Berlin Repository. <https://doi.org/10.17169/refubium-31813>.
- Liu, S.H., Hebenstreit, R., Böse, M., 2022. Late Quaternary landforms and sedimentary succession in the Miaoli Tableland, northwestern Taiwan. *E&G Quaternary Science Journal* 71, 1–22.
- Liu, Z., Xia, D., Berne, S., Wang, K., Marsset, T., Tang, Y., Bourillet, J.F., 1998. Tidal deposition systems of China's continental shelf, with special reference to the eastern Bohai Sea. *Marine Geology* 145, 225–253.
- Lüthgens, C., Ho, L.D., Clemenz, N., Chen, J.H., Jen, C.H., Yen, J.Y., Chyi, S.J., 2018. The Holocene paleo-environmental history of the Gangkou River estuary, Hengchun Peninsula, Taiwan. *Terrestrial, Atmospheric and Oceanic Sciences (TAO)* 29, 547–576.
- Madsen, A.T., Murray, A.S., 2009. Optically stimulated luminescence dating of young sediments: a review. *Geomorphology* 109, 3–16.
- Makiyama, T., 1936. *Taiko Sheet*. Bureau of Productive Industries, Government-General of Taiwan, Tokyo.
- Makiyama, T., 1937. *The Topographic and Geological Map of Tüsyö Petroleum Field*. Bureau of Productive Industries, Government-General of Taiwan, Tokyo.
- Matsu'ura, T., Kimura, H., Komatsubara, J., Goto, N., Yanagida, M., Ichikawa, K., Furusawa, A., 2014. Late Quaternary uplift rate inferred from marine terraces, Shimokita Peninsula, northeastern Japan: a preliminary investigation of the buried shoreline angle. *Geomorphology*, 209, 1–17.
- Mejdahl, V., Christiansen, H.H., 1994. Procedures used for luminescence dating of sediments. *Quaternary Science Reviews* 13, 403–406.
- Murray, A.S., Wintle, A.G., 2000. Luminescence dating of quartz using an improved single-aliquot regenerative-dose protocol. *Radiation Measurements* 32, 57–73.
- NASA JPL, 2013. 1 Arc Second Scene N24 E120, NASA EOSDIS Land Processes DAAC. <https://doi.org/10.5067/MEASURES/SRTM/SRTMGL1.003>.
- Ota, Y., Lin, Y.N.N., Chen, Y.G., Chang, H.C., Hung, J.H., 2006. Newly found Tunglo Active Fault System in the fold and thrust belt in northwestern Taiwan deduced from deformed terraces and its tectonic significance. *Tectonophysics* 417, 305–323.
- Ota, Y., Lin, Y.N.N., Chen, Y.G., Matsuta, N., Watanuki, T., Chen, Y.W., 2009. Touhuaping Fault, an active wrench fault within fold-and-thrust belt in northwestern Taiwan, documented by spatial analysis of fluvial terraces. *Tectonophysics* 474, 559–570.
- Ota, Y., Shyu, J.B., Chen, Y.G., Hsieh, M.L., 2002. Deformation and age of fluvial terraces south of the Choushui River, central Taiwan, and their tectonic implications. *Western Pacific Earth Sciences* 2, 251–260.
- Ota, Y., Yamaguchi, M., 2004. Holocene coastal uplift in the western Pacific Rim in the context of late Quaternary uplift. *Quaternary International* 120, 105–117.
- Prescott, J.R., Hutton, J.T., 1994. Cosmic ray contributions to dose rates for luminescence and ESR dating: large depths and long-term time variations. *Radiation Measurements* 23, 497–500.
- Prescott, J.R., Stephan, L.G., 1982. The contribution of cosmic radiation to the environmental dose for thermoluminescence dating. Latitude, altitude and depth dependences. *Pact: Journal of the European Study Group on Physical, Chemical and Mathematical Techniques Applied to Archeology* 6, 17–25.
- Pye, K., Zhou, L.P., 1989. Late Pleistocene and Holocene aeolian dust deposition in North China and the Northwest Pacific Ocean. *Palaeogeography, Palaeoclimatology, Palaeoecology* 73, 11–23.
- Rees-Jones, J., 1995. Optical dating of young sediments using fine-grain quartz. *Ancient TL* 13, 9–14.
- Reimann, T., Thomsen, K.J., Jain, M., Murray, A.S., Frechen, M., 2012. Single-grain dating of young sediments using the pIRIR signal from feldspar. *Quaternary Geochronology* 11, 28–41.
- Rhodes, E.J., 2011. Optically stimulated luminescence dating of sediments over the past 200,000 years. *Annual Review of Earth and Planetary Sciences* 39, 461–488.
- Rixhon, G., Briant, R.M., Cordier, S., Duval, M., Jones, A., Scholz, D., 2017. Revealing the pace of river landscape evolution during the Quaternary: recent developments in numerical dating methods. *Quaternary Science Reviews* 166, 91–113.
- Satellite Survey Center, 2018. Ministry of Interior 20 m Raster Digital Elevation Model. Satellite Survey Center, Taipei, Taiwan (accessed September 17, 2022). <https://data.gov.tw/dataset/35430>.
- Schmidt, S., Tsukamoto, S., Salomon, E., Frechen, M., Hetzel, R., 2012. Optical dating of alluvial deposits at the orogenic front of the andean precordillera (Mendoza, Argentina). *Geochronometria* 39, 62–75.
- Shih, T.S., Sato, H., Ikeya, M., Liew, P.M., Chien, S.H., 2002. Conditions and new extrapolation method for ESR dating of aragonitic mollusk shells in Taiwan. *Advances in ESR Applications* 18, 31–39.
- Shyu, J.B.H., Sieh, K., Chen, Y.G., Liu, C.S., 2005. Neotectonic architecture of Taiwan and its implications for future large earthquakes. *Journal of Geophysical Research* 110.
- Siame, L.L., Chen, R.F., Derrière, F., Lee, J.C., Chang, K.J., Bourlès, D.L., Braucher, R., Léanni, L., Kang, C.C., Chang, C.P., Chu, H.T., 2012. Pleistocene alluvial deposits dating along frontal thrust of Changhua Fault in western Taiwan: the cosmic ray exposure point of view. *Journal of Asian Earth Sciences* 51, 1–20.
- Simoes, M., Avouac, J.P., 2006. Investigating the kinematics of mountain building in Taiwan from the spatiotemporal evolution of the foreland basin and western foothills. *Journal of Geophysical Research: Solid Earth* 111. <https://doi.org/10.1029/2005JB004209>.
- Simoes, M., Avouac, J.P., Chen, Y.G., Singvi, A.K., Wang, C.Y., Jaiswal, M., Chan, Y.C., Bernard, S., 2007. Kinematic analysis of the Pakuashan fault tip fold, west central Taiwan: shortening rate and age of folding inception. *Journal of Geophysical Research: Solid Earth* 112. <https://doi.org/10.1029/2005JB004198>.
- Singarayer, J.S., Bailey, R.M., 2003. Further investigations of the quartz optically stimulated luminescence components using linear modulation. *Radiation Measurements* 37, 451–458.
- Singarayer, J.S., Bailey, R.M., Rhodes, E.J., 2000. Potential of the slow component of quartz OSL for age determination of sedimentary samples. *Radiation Measurements* 32, 873–880.
- Spooner, N.A., 1994. The anomalous fading of infrared-stimulated luminescence from feldspars. *Radiation Measurements* 23, 625–632.
- Stokes, S., Bray, H.E., Blum, M.D., 2001. Optical resetting in large drainage basins: tests of zeroing assumptions using single-aliquot procedures. *Quaternary Science Reviews* 20, 879–885.
- Suppe, J., 1981. Mechanics of mountain building and metamorphism in Taiwan. *Memoir of the Geological Society of China* 4, 67–89.
- Suppe, J., 1984. Kinematics of arc-continent collision, flipping of subduction, and back-arc spreading near Taiwan. *Memoir of the Geological Society of China* 6, 131–146.
- Teng, K.H., 1979. A quantitative study on the landforms of lateritic gravel tablelands in northwestern Taiwan. *The College of Chinese Culture Institute of Geography Science Reports* 3, 113–186.
- Teng, L.S., 1990. Geotectonic evolution of late Cenozoic arc-continent collision in Taiwan. *Tectonophysics* 183, 57–76.
- Teng, L.S., 1996. Geological background of the gravel formations of Taiwan. *Sine-Geotechnics*, 5–24.
- Timar-Gabor, A., Wintle, A.G., 2013. On natural and laboratory generated dose response curves for quartz of different grain sizes from Romanian loess. *Quaternary Geochronology* 18, 34–40.

- Tomita, Y.**, 1940. Terraces in Taiwan/臺灣の段丘に就いて. *Journal of the Taiwan Museum Association/科學の臺灣* **8**, 1–6.
- Tomita, Y.**, 1951. On the geomorphological classification of fans in Taiwan (Formosa)/台灣に於ける扇状地の地形的分類について. *Journal of Geography (Chigaku Zasshi)* **60**, 2–9.
- Tomita, Y.**, 1953. The classification of fluvial terraces 河成段丘の分類に就いて. *Annals of the Tohoku Geographical Association* **6**, 1–6.
- Tomita, Y.**, 1954. Surface geology and correlation of river terraces. *Annals of the Tohoku Geographical Association* **6**, 51–58.
- Tsai, H., Chen, J.H., Huang, W.S., Huang, S.T., Hseu, Z.Y., You, C.F.**, 2021. Aeolian additions of podzolic soils on the high-altitude mountains in central Taiwan—sediment origin and pedological implications. *Geoderma* **383**, 114726.
- Tsai, H., Hseu, Z.Y., Huang, S.T., Huang, W.S., Chen, Z.S.**, 2010. Pedogenic properties of surface deposits used as evidence for the type of landform formation of the Tadu tableland in central Taiwan. *Geomorphology* **114**, 590–600.
- Tsai, H., Huang, W.S., Hseu, Z.Y., Chen, Z.-S.**, 2006. A River Terrace Soil Chronosequence of the Pakua Tableland in central Taiwan. *Soil Science* **171**, 167–179.
- Tsai, H., Maejima, Y., Hseu, Z.Y.**, 2008. Meteoric ¹⁰Be dating of highly weathered soils from fluvial terraces in Taiwan. *Quaternary International* **188**, 185–196.
- Tseng, C.H., Lüthgens, C., Tsukamoto, S., Reimann, T., Frechen, M., Böse, M.**, 2016. Late Pleistocene to Holocene alluvial tableland formation in an intramountainous basin in a tectonically active mountain belt—a case study in the Puli Basin, central Taiwan. *Quaternary Science Reviews* **132**, 26–39.
- Tseng, C.H., Wenske, D., Böse, M., Reimann, T., Lüthgens, C., Frechen, M.**, 2013. Sedimentary features and ages of fluvial terraces and their implications for geomorphic evolution of the Taomi River catchment: a case study in the Puli Basin, central Taiwan. *Journal of Asian Earth Sciences* **62**, 759–768.
- Waelbroeck, C., Labeyrie, L., Michel, E., Duplessy, J.C., McManus, J.F., Lambeck, K., Balbon, E., Labracherie, M.**, 2002. Sea-level and deep water temperature changes derived from benthic foraminifera isotopic records. *Quaternary Science Reviews* **21**, 295–305.
- Wang, C.H., Peng, T.R.**, 1990. Oxygen and carbon isotopic records of mollusks in the Kuokang Shell Bed, Taiwan: implications and applications. *Palaeogeography, Palaeoclimatology, Palaeoecology* **80**, 237–244.
- Wenske, D., Böse, M., Frechen, M., Lüthgens, C.**, 2011. Late Holocene mobilisation of loess-like sediments in Hohuan Shan, high mountains of Taiwan. *Quaternary International* **234**, 174–181.
- Wenske, D., Frechen, M., Böse, M., Reimann, T., Tseng, C.H., Hoelzmann, P.**, 2012. Late Quaternary river terraces in the Central Mountain Range of Taiwan: a study of cover sediments across a terrace section along the Tachia River. *Quaternary International* **263**, 26–36.
- Wintle, A.G.**, 1973. Anomalous fading of thermo-luminescence in mineral samples. *Nature* **245**, 143–144.
- Wintle, A.G., Murray, A.S.**, 2006. A review of quartz optically stimulated luminescence characteristics and their relevance in single-aliquot regeneration dating protocols. *Radiation Measurements* **41**, 369–391.
- Yang, K.M., Huang, S.T., Wu, J.C., Ting, H.H., Mei, W.W.**, 2006. Review and new insights on foreland tectonics in western Taiwan. *International Geology Review* **48**, 910–941.
- Yang, K.M., Rau, R.J., Chang, H.Y., Hsieh, C.Y., Ting, H.H., Huang, S.T., Wu, J.C., Tang, Y.J.**, 2016. The role of basement-involved normal faults in the recent tectonics of western Taiwan. *Geological Magazine* **153**, 1166–1191.
- Yue, L.F., Suppe, J., Hung, J.H.**, 2005. Structural geology of a classic thrust belt earthquake: the 1999 Chi-Chi earthquake Taiwan (Mw=7.6). *Journal of Structural Geology* **27**, 2058–2083.

Chapter 8. Summarizing discussion

This chapter provides a summarized discussion related to the morphology of the Miaoli Tableland:

- i). The consistency of new DTM-based surface mapping and the sedimentary succession in the Miaoli Tableland (see chapter 8.1). This information highlights the correlation between the morphological stages of tableland segments and the sedimentary successions, which is controlled by the erosion and successive redeposition of the sediments. These processes have contributed to the formation of three sub-types of sedimentary successions with distinct spatial distributions.
- ii). A new chronology of the Miaoli Tableland development and the uplift rates (see chapter 8.2), which provide a new insight into the time span of the development of the Miaoli Tableland morphology, and therefore a temporal framework for comparing it with other Taiwanese tablelands. In addition, it allows new interpretations of the uplift rates of the thrusts-induced displacements of the sedimentary successions.
- iii). The aeolian deposition as index of ages of topographic surfaces (see chapter 8.3), which is a key factor for the argument regarding the laterization of the cover layer, as it is also an ongoing phenomenon throughout the Taiwan Island. This also reveals the correlation between erosional processes and the morphological stages, as well as the chronology of the tableland segments.
- iv). Impacts of base-level change to the tableland morphology (see chapter 8.4), which is the controlling factor for the fluvial dissections of the tableland segments and successive depositions of the gravels and cobbles, which resulted in the formation of box-shaped valleys. This also reveals a spatial-temporal pattern of movements from the SH-I to SH-II/ST and further extending to the coast.
- v). The climate impacts on tableland morphology (see chapter 8.5), which reveals that the Quaternary environmental change have affected the surface processes over time. The climate impact is functioned through variations in precipitations, typhoon events and the vegetation cover densities, which is based on late Quaternary climate model of the Taiwan Island.
- vi). A proposal of revision of the stratigraphic model based on the international stratigraphic guidelines (see chapter 8.6). This is the extended outcome of this study, aiming to clarify the ambiguous stratigraphical interpretations of the sedimentary successions in the Miaoli Tableland with a historical review and the new insights obtained from previous discussions.

8.1 Consistency of new DEM-based surface mapping and the sedimentary succession in the Miaoli Tableland

The high-resolution mapping of the Miaoli Tableland segments displays a pattern of an inferred palaeo-topography of alluvial fan(s) covering throughout the study area (Figs. 5.3 and 8.1). This implies a much larger former distribution of the gravel and cobble bed(s) (CSB) compared with the interpretations of previous studies (Chang et al., 1998; Lin, 1957). The field observation records, and the borehole data consistently present the sedimentary successions with the gravel and cobble bed(s) in the very upper part of the larger tableland segments and in the active fluvial valley floors. Conversely, only very limited records in the remnants and the smaller tableland segments present the gravel and cobble bed(s).

The tableland segments' sub-categories are bounded by the thrust faults. These thrust faults caused significant vertical displacements of the sedimentary successions, according to the borehole data interpolations (Figs. 2.4 and 5.3).

The interpolated elevation profile of tableland segments' surfaces is presented in two different shapes (Figs. 4.1, 5.3 and 5.8): i.) a concave shape from east to west direction, including the SH-I tableland segments in the southeast, and the ST tableland segments in the central and west parts (Figs. 2.2, 5.3, 5.8, and 6.7); ii.) a convex shape from south to north, including the SH-I tableland segments in the southeast, and the SH-II tableland segments in the east and northeast (Figs. 5.3 and 5.8). The concave shape is mainly caused by the differentiated uplifts of NE-SW aligned tectonic features, which have divided the palaeo-topography of alluvial fans into different sections (i.e. SH-I, proximal areas of SH-II and ST, distal areas of SH-II and ST). The convex shape is due to the uplift of the Tongluo Fault's south section (Tongluo and Sanyi area), which started earlier, caused larger vertical displacements than in the north section (Miaoli and Houlong area) (Ota et al., 2006).

The borehole data show that the sedimentary successions are mostly consistent throughout the study area, including the records in the tableland segments, remnants, and fluvial valley floors. Variations in the sedimentary successions are only in a minor scale, which is related to the size of the tableland segments and their locations (see chapter 5 and 6). In addition, observations of the fine-grained sediment layers (SL and lower layers) in the distal areas of SH-II and ST indicated that these layers are slightly inclined by the Tungxiao Anticline (with up to 20 degrees of inclination), but the gravel and cobble bed(s) are deposited with horizontal beddings. This reveals that the folding process took place later than the uplift of the SH-I tableland segments (Liu et al., 2023) (Figs. 6.7 and 7.7), and prior to the deposition of the fluvial sediments (CSB layer) in the distal areas (SH-II and ST) (Liu et al., 2023; Liu et al., 2022) (Fig. 7.7, Table 7.4, and Appendix 5C).

The Miaoli Tableland morphology models proposed by Chang et al., (1998) and Liu et al., (2023), which are based on the thrust movements and the variation of sedimentary successions, are supported by the borehole

data interpretations and field observation records. This differs from the interpretation of the “topographic inversion” model provided by Ota et al., (2006) (Fig. 2.2), which assumed the Tungxiao Anticline as the main driving force for the formation of ST tableland segments.

8.2 A new chronology of the Miaoli Tableland development and the uplift rates

The OSL dating in the Miaoli Tableland provides good and robust results. Most quartz grains in the samples are well bleached, which indicates effective reworking processes or transportation over long distances, such is the case by longshore currents, waves, tides, fluvial or aeolian transportation (Fig. 8.1). The good bleaching characteristics have been also recorded by the OSL dating in other study sites in Taiwan, such as beach / aeolian sandy sediments in coastal sand dunes at the northeast coast (Dörschner et al., 2012; Ho et al., 2017) and fluvial sediments, specifically the matrix materials of the gravel and cobble beds on the tableland surfaces in the Puli Basin (Tseng et al., 2016; Tseng et al., 2013).

The quartz-OSL measurements are not applicable for the sediment sample of the SiC layer (alternating tidal and beach sediments) and all other layers in the lower section of the studied sedimentary successions. This is because one sample of the overlying SL layer (upper beach and coastal sediments) shows saturation characteristics, implying that all lower sedimentary layers are out of the range of the dating method (see chapter 7.4.1). The age estimation (ca. 96 ka) of this SL layer sample can only be considered as the minimum of depositional age (Liu et al., 2023) (Fig. 7.6, Table 7.4). This suggests an age range of more than 100 ka for the lower sedimentary layers. The tidal and beach sediments (SiC) must have originated during a sea level high stand. Therefore, it can be interpreted as an approximately Eemian (MIS 5e) age range. The ages of the underlying LS and L layers are still unknown, but their stratigraphical positions suggest the depositions during the Middle Pleistocene or even earlier. This is in general agreement with the assumptions of Ota et al. (2006a) and Chang et al. (1998).

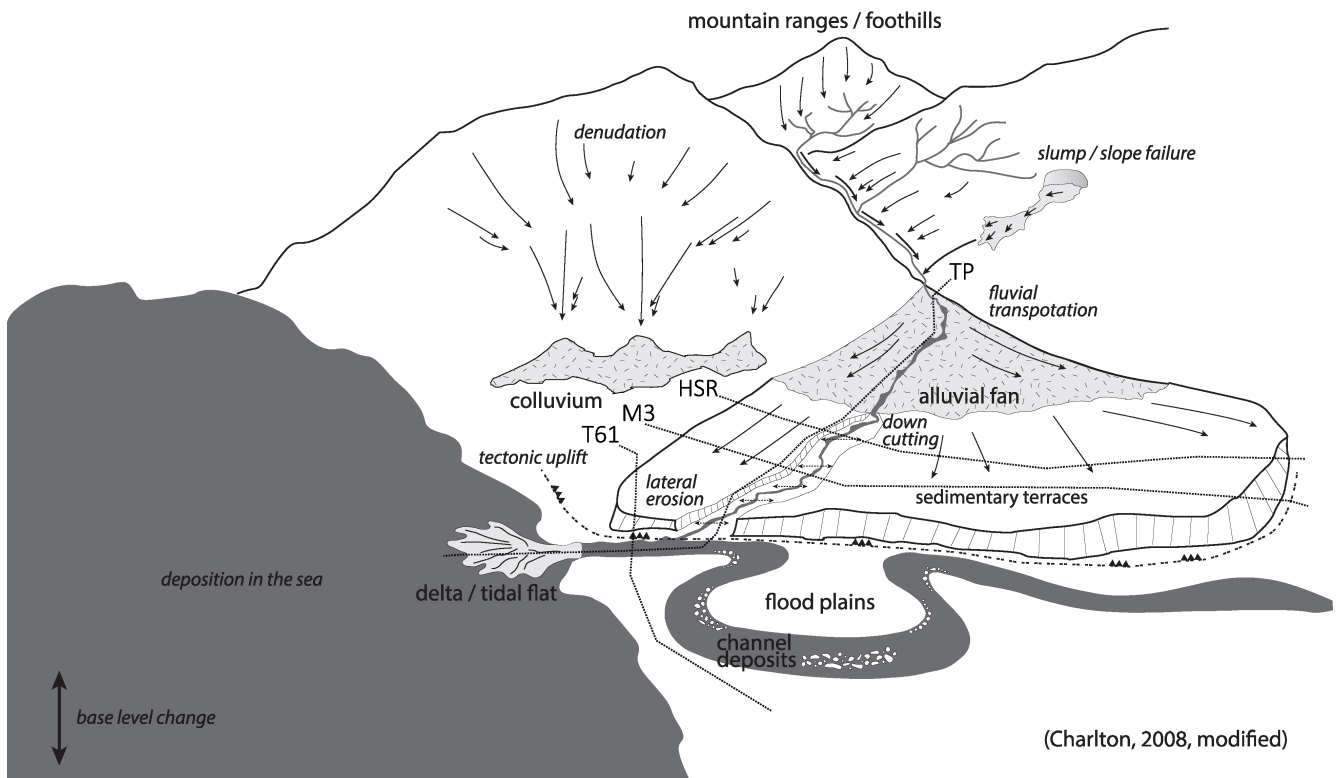


Figure 8.1: The schematic diagram of the morphological settings of the sedimentary terraces (i.e., tablelands) in the mountain foreland, modified after (Charlton, 2008). The Miaoli Tableland is an example of sedimentary terraces that has been formed from the palaeo-topography as alluvial fan(s) in the mountain foreland. The morphology of the Miaoli Tableland is controlled by the interplay of tectonism, base-level change, and subsequent influences of fluvial responses. Locations of the four geological cross-sections interpolated from the borehole data are marked with the dashed lines across the tableland (see figs. 6.3, 6.4, 6.5 and 6.6 for details).

The aggradation of fluvial sediments (gravels and cobbles) and the formation of the paleo-topography of alluvial fan(s) in the Miaoli Tableland area are assumed to have started in the early last interglacial (Liu et al., 2021; Liu et al., 2023) (Figs. 5.8, 6.7 and 7.7). In comparison, the study of the geochronological characteristics of fluvial depositions in other tablelands gave age estimates of deposition ages from ca. 400 ka (Siame et al., 2012; Simoes et al., 2007) to Holocene (Chen et al., 2009), with a clear pattern that the depositions of the tablelands in central and southern Taiwan are mostly older than the tablelands in the central to north (Figs. 1.3 and 8.2). This means that the processes of fluvial depositions have taken place on the uplifted tidal / coastal sediments in the mountain foreland in western Taiwan (Figs. 1.2 and 8.1). According to the age estimations of fluvial gravels and cobbles depositions in the Miaoli Tableland provided by the OSL dating, a temporal and spatial correlation is presented as follows: the gravels and cobbles on the Sedimentary Highlands (SH-I) tableland segments are the oldest deposition (early last interglacial); the gravels and cobbles in the proximal area of the Sedimentary Highlands (SH-II) and the Sedimentary Terraces (ST) tableland segments are successively deposited (probably through MIS4-MIS3), and the gravels and cobbles in the distal SH-II and ST tableland segments are deposited later (MIS 2) (Figs. 7.6, 7.7 and 8.1) (Liu et al., 2023).

Even direct OSL dating analyses are not possible for the active and fresh fluvial gravels and cobbles depositions on the fluvial channels and in the estuaries (Alluvial and Coastal Plains, AL), as the process of remobilization is still going on.

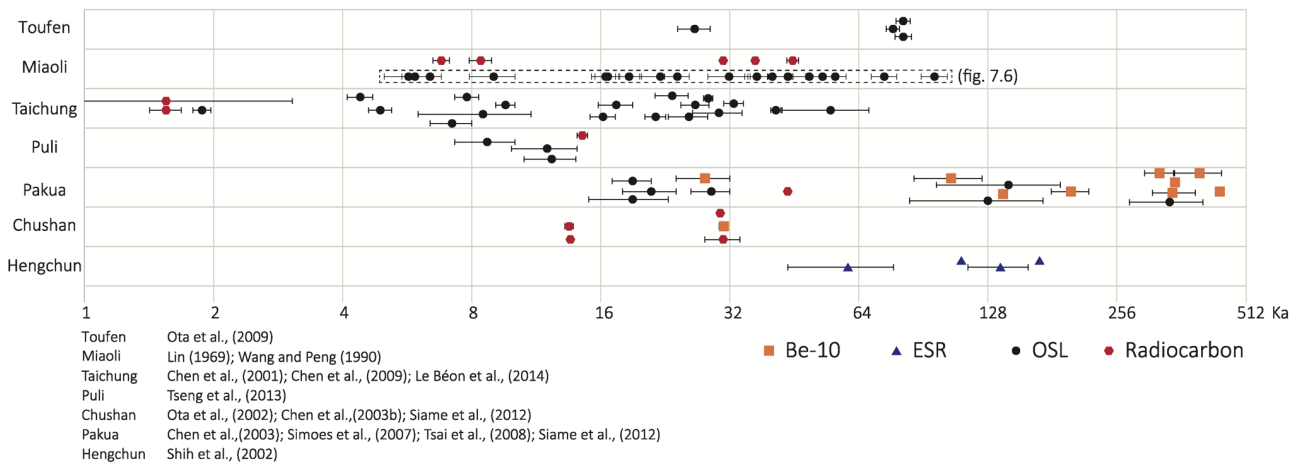


Figure 8.2: The dating results of other tablelands in the mountain foreland of the western Taiwan. The deposition ages including the error range are marked for each study sites, arranged from the north (at top) to the south (at bottom). The dating analyses were carried out with different methods, each marked by the corresponding symbols. The ages (X-axis) are presented on a logarithm scale ranging from 1 ka to 512 ka. The age estimations present a pattern, which shows that the tablelands at the south have older depositional ages and the tablelands in the central to north are relatively younger. The data sources of each study site are annotated in the legend.

The uplift rates can be estimated from the depositional ages of the sandy loam layer (SL) and the gravel and cobble bed(s) (CSB) (Figs. 7.6 and 7.7). The new estimations of the long-term average uplift rates of the Miaoli Tableland, based on the OSL dating results, mostly range from 1 mm/yr to 3 mm/yr (Liu et al., 2023) (Fig. 7.7 and Table 7.5). According to different settings of benchmarks, the maximum estimation for uplift rate is 10 mm/yr (Fig. 4.7). The new estimations of uplift rates (Liu et al., 2023) are consistent with overall uplift rates estimations in other studies in west Taiwan that ranged from 1 to 10 mm/yr (Nagel et al., 2018) (Table 1.1). The new estimations are generally more rapid than the previous assumption of 1mm/yr (Ota et al., 2006; Ota et al., 2002). In addition, the overall uplift of the central and southern part of Taiwan Island has accelerated from 0.5 Ma to present (Fox et al., 2014), which is different from the real time GPS monitoring data that shows slight subsidence in the Miaoli Tableland area (Ching et al., 2011) (Table 1.1). The variance among different estimations of uplift rates and the real time GPS monitoring data offers a possibility that the thrusts may not take place continuously, but rather be mostly stable and only moving during specific tectonic events, which could make significant displacements in a relative short time span. Thus the overall tectonic setting of the Miaoli Tableland area is controlled by ongoing, rapid moving thrust uplifting.

8.3 The aeolian deposition as index of ages of topographic surfaces

The fine-grained (silty), loose, and massive structured sedimentary cover layers have been interpreted as in-situ weathered sediments of Quaternary age (Chang, 1990; Chang, 1955b; Ho, 1988; Ho, 1994) (Fig. 2.3). The weathering degrees of these cover sediments (the silty loam layer, SiL) on the tableland segments (Chang, 1955b; Lin, 1957) were studied for interpreting the relative chronology (Chang et al., 1998; Chen, 1983; Ho, 1994; Tomita, 1953, 1954). For example, the brownish / reddish colored loamy sediments on the tableland segments surfaces were initially described as “Laterite / Lateritic soils” by studies from the Japanese time to the 1950s (Chang, 1955a, b; Tomita, 1940; Yokomitsu et al., 1926) (Figs. 2.3, 5.6 and Appendix 5C). However, the term “Laterite / Lateritic” has been redefined to emphasize the composition of plinthite in the highly-weathered soils lately (United States Department of Agriculture, 1999). Consequently, the latest pedological descriptions of these cover sediments on the tableland segments’ surfaces used the terms Oxisols or Ultisols for more accurate descriptions (Chen et al., 2015). Furthermore, the early last glacial to Holocene time span of depositions (Liu et al., 2023) seems too short for the “laterization” of the SiL layer, especially considering the rapid tectonic uplifting in the study area (Chang, 1955b; Ho, 1988) (Figs. 1.2, 2.2 and Table 1.1).

The varying weathering degrees of the cover sediments in the Miaoli Tableland are correlated to the underlying sedimentary successions and morphological stages of the tableland segments, this is interpreted as an indirect indicator of whether the tableland segments’ surfaces are stabilized (Liu et al., 2021; Liu et al., 2022) (Figs. 2.2, 5.6 and Appendix 5C).

The deposition of aeolian materials occurred on the surface of the gravel and cobble bed(s), which covers the tableland segments. The subsequent in-situ weathering processes formed the highly weathered brownish / reddish silty loam cover layer (SiL) (the subtype-I and subtype-III successions). However, once the tableland segments were rapidly eroded and dissected to form remnants, aeolian materials successively accumulated on the SL layer to form the silty loam cover layer on the remnants (SiL). The tableland segment surfaces of subtype-I and -III successions are supported by a CSB layer, which has relatively high resistance to the erosion. Conversely, the remnant segments’ surfaces are not stable over time, and the in-situ weathering processes could only form a less weathered yellowish silty loam cover layer (SiL) over a shorter period (the subtype-II succession).

The silty loam cover layer (SiL) on the tableland segments in the SH-I and SH-II with the subtype-I sedimentary succession, as well as the larger tableland segments in the distal area of ST and SH-II with the subtype-III sedimentary succession have higher weathering degrees (Fig. 5.6 and Appendix 5C), therefore these tableland segments are assumed to be older than others (Chang et al., 1998; Chen, 1983; Ota et al., 2006) (Figs. 2.2 and 7.6). On the other hand, the silty loam cover layer (SiL) in the smaller tableland segments and the remnants in

the SH-II and ST with the subtype-II sedimentary succession shows lower weathering degrees (Chen, 1983) (Fig. 2.2, 5.6, 6.6 and Appendix 5C), suggesting that the silty loam cover layer (SiL) have been eroded and successively re-accumulated in more recent time (Chang et al., 1998) (Figs. 2.2 and Appendix 5A). The weathering degree and deposition age of the aeolian cover sediments can be regarded as indices for the stabilization of the underlying tableland segments and remnants (Figs. 2.2, 7.2, 7.6, and Appendix 7A).

The aeolian depositions of the silty and dusty materials on the topographical surfaces have also been identified across different study sites throughout the Taiwan Island, such as in the Kenting Peninsula (Huang et al., 2017), in the mountain areas (Tsai et al., 2021; Wenske et al., 2011; Wenske et al., 2012) and the fluvial terraces in the intramountain basin (i.e. Puli Tableland) (Tseng et al., 2016; Tseng et al., 2013).

8.4 Impacts of base-level change to the tableland morphology

The base-level of the fluvial systems is controlled by the interplay of sea-level change and uplift, which has manifested the geomorphic rejuvenation of the fluvial systems in the Miaoli Tableland (Liu et al., 2023) (Figs. 5.8, 6.7, 7.7 and 8.1). The sea-level lowering during the last glacial, the tectonic uplifts caused by the thrust faults and the shallow bathymetry of the Taiwan Strait mean that the Miaoli Tableland was distant from locations where the estuaries of fluvial systems actually were.

The fluvial sediments of the Miaoli Tablelands were yielded from the WF by the Houlong River and the Daan River initially (Figs. 2.1 and 8.1). The uplifting of the SH-I segments by the Tongluo Fault caused the diversions of the Houlong River to the north and the Daan River to the south. Hence, the successive fluvial sediment yielding from the WF has only contributed to the very east and northeast part of the Miaoli Tableland (Fig. 7.7). At the meanwhile, the uplift and the base level lowering during the MIS4 – MIS3 also caused the fluvial dissection of tableland segments and the continuous redeposition of the fluvial sediments, which brought the gravels and cobbles from the SH-I segments to the proximal areas of SH-II and ST firstly (Figs. 8.1 and 8.3). The escarpment at the topographic divide between the SH-I and the ST (Chang et al., 1998) has been identified as the result of subsequent tectonic uplift of the SH-I tableland segments. The rapid uplift of this thrust feature caused the overturning of the surface gradient toward the east, and the existing fluvial channels were beheaded (Ota et al., 2006) (Fig. 8.3), which has significantly restricted the fluvial sediments yielding from the SH-I to the ST.

The base-level was very low during late MIS3 – MIS2, and the tectonic uplift was still ongoing simultaneously, these processes initiated the successive erosion of the sediments from the proximal tableland segments of SH-II and ST, which were subsequently redeposited in the distal areas of SH-II and ST and in the Taiwan Strait (Liu et al., 2023; Liu et al., 2022) (Figs. 5.8, 7.7 and 8.3). Furthermore, due to the relatively small size of the local fluvial catchments in the ST and SH-II areas (< 10 km²), the fluvial sediments in SH-II, ST and AL are mostly

reworked and redeposited on a local scale. The amounts of gravels and cobbles reworked by these fluvial systems are limited, thus the gravel and cobble bed(s) (CSB) in these areas are relatively thin (Liu et al., 2023; Liu et al., 2022) (Figs. 2.1, 2.6, 5.6, 7.7 and Appendix 7A).

The rapid sea-level rise after the MIS2 (during the transition from MIS2 to MIS1) slowed down the downcutting of the SH-II and ST tableland segments, and the lateral erosion in the lower reaches of the channels became the main process for the dissection of tableland segments, and to form the so-called box shaped valleys (Fig. 8.3).

The formation of these box-shaped valleys is related to the influences of tectonic uplift, eustatic sea-level change and varying resistance to erosion among the sedimentary layers (Liu et al., 2023; Liu et al., 2022) (Figs. 2.4, 5.4, 7.7 and 8.1). The lower part of the studied sedimentary successions is composed of unconsolidated sediments, which are low-resistant to erosion especially during the flooding events. Lateral erosion cut the edges of tableland segments and remnants, forming the steep slopes of the fluvial channels (60° to 90°) (Figs. 6.7b and 8.3). These processes have enlarged the fluvial channels and have created very wide valley floors with steep slopes on both sides (Owczarek, 2008; White et al., 2010), which have resulted in the formation of the iconic box-shaped valleys (Figs. 2.6, 5.4, 6.7b and 8.3). These box-shaped valleys will become wider as the lateral erosion will fully dissect the tableland segments, and eventually these box-shaped valleys will be merged to form fluvial plains. The box-shaped valley forming process has progressed from the coastal area toward the middle reaches of the fluvial systems, the present-day boundary between the V-shaped valleys in the upper reaches and the box-shaped valleys in the middle and lower reaches is identified at 150 m asl (Liu et al., 2022) (Figs. 5.4 and 8.1). The box-shaped valley forming process, including i). incisions on the upper stream and the tableland segments, remnants; and ii). the successive depositions in the fluvial valley floors, are still ongoing in the Miaoli Tableland, this 150m asl boundary will probably move further toward higher elevations in the future.

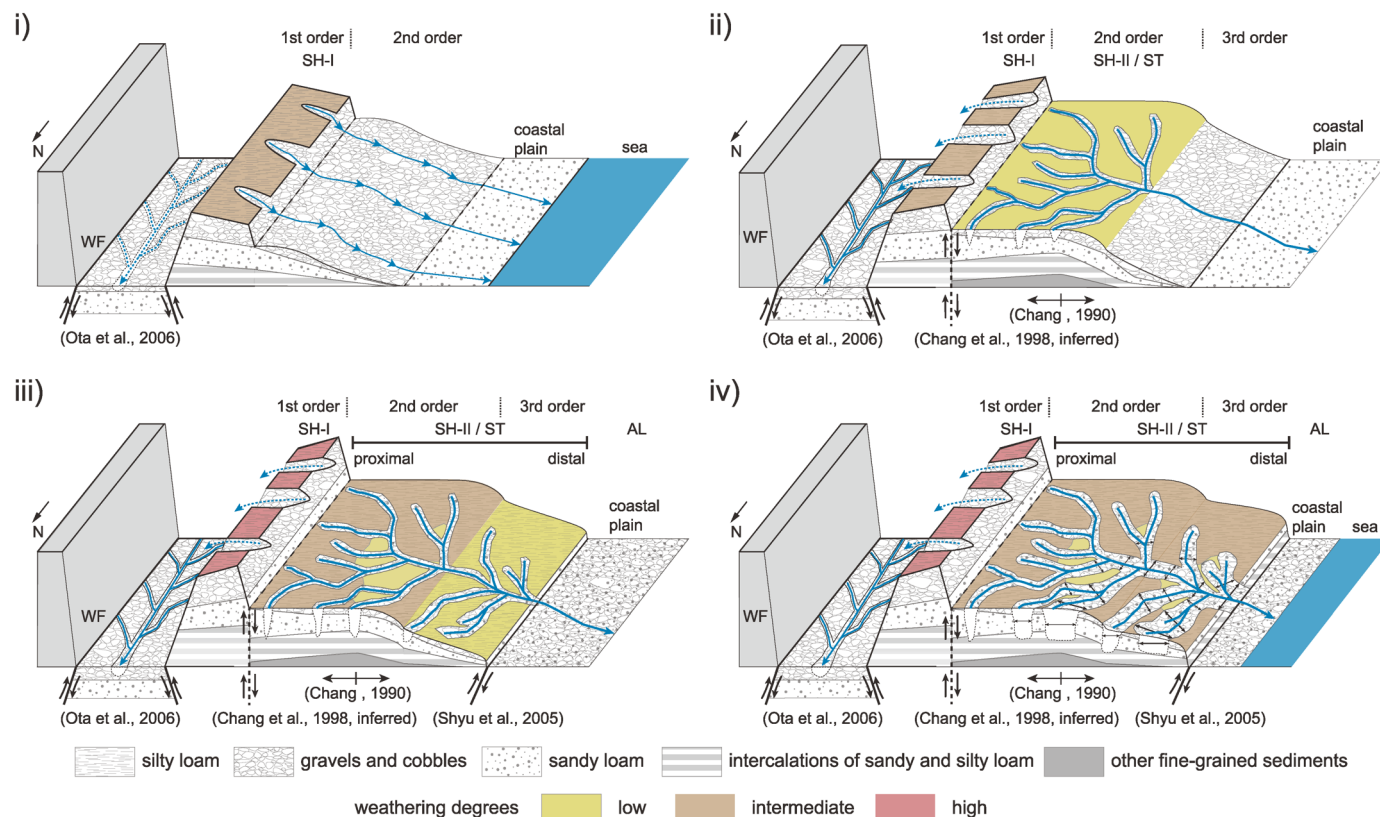


Figure 8.3: The 3D model of the successive redepositions of fluvial sediments in the post-last-interglacial time span in the Miaoli Tableland. i). The fluvial sediments (i.e. the gravels and cobbles) transported from the Western Foothills have been deposited on the sedimentary successions in the foreland basin. They are the 1st order deposition of the gravels and cobbles. The thrust movement of the Tongluo Thrust Fault has uplifted the palaeo-alluvial fan(s). The successive fluvial incisions on the palaeo-alluvial fan(s) surfaces led to the formation of the SH-I tableland segments. The westward redepositions of the gravels and cobbles resulted in the formation of the extended alluvial fan(s) of the 2nd order deposition. ii). The base level lowering, and the folding of the Tungxiao Anticline caused subsequent fluvial incisions on the extended alluvial fan(s), and led to the formation of the tableland segments and remnants in the proximal areas of the SH-II and ST. The gravels and cobbles eroded from these tableland segments were successively redeposited in the distal areas (the 3rd order deposition). iii). The most recent thrust movement (i.e. frontal movement) has uplifted the sedimentary successions in the distal areas (the 3rd deposition). The subsequent fluvial incisions caused the formation of the tableland segments and remnants in the distal areas of the SH-II and ST. The larger tableland segments are more stable, indicating higher weathering degrees of the silty cover layers; conversely, the smaller tableland segments and the remnants are relatively unstable, indicating lower weathering degrees of the silty cover layers. iv). The sea-level rose rapidly after the LGM, therefore the fluvial processes during high discharge events (i.e. flooding / typhoons) caused more rapid lateral erosion onto the slopes of the tableland segments, which are composed of low-resistant fine-grained sedimentary layers. This process has widened the fluvial valleys and has led to the formation of box-shaped valleys, it has also contributed to the active deposition of the gravels and cobbles in the fluvial channels and the coastal plains.

8.5 The climate impacts on tableland morphology

Besides the base-level variations, the changing climatic conditions during the last glacial cycle are assumed to have an additional influence on the differentiated development of the Miaoli Tableland surface as they act as a controlling factor for the composition of the vegetation cover in the landscape and the quantity and the intensity of precipitation, which influences the incision rate of tableland segments and the amount of transported gravels and cobbles. According to the reconstruction of the vegetation composition from pollen records in mid-altitude lake sediments (Liew et al., 2006), the climate conditions in the middle to low altitude areas (e.g., mountain forelands) were generally cooler and dryer during the last glacial period, with short and small warm/wet episodes compared to the present day sub-tropical climate conditions. The abrupt climate changes are recorded at the transitions to: i). the particularly cold MIS 4, ii). the particularly dry MIS 2, and iii). the beginning of the Holocene. Furthermore, the altitudinal vegetation boundaries may have been lowered by more than 1000-1500 m (equals 8-10 °C) in the mountain ranges during colder periods (Liew et al., 2006).

In the present sub-tropical and tropical climate setting of Taiwan, extreme precipitations and flooding are mainly caused by typhoon events (see chapter 2.4, Fig. 2.5). The typhoon events are more frequently and last longer during relatively warm and wet climate conditions (Su et al., 2012; Tu and Chen, 2019; Tu and Chou, 2013). The incision of tableland segments and the reworking of the fluvial sediments in the Miaoli Tableland may therefore be more rapid during these warm and wet climate condition periods, conversely these surface processes may be slower during the relatively dry and cold periods. However, this is in strong contrast to the obtained data of this work, which revealed an increase transport of fluvial gravels during the cooler and dryer MIS 4 and MIS 2 (Liu et al., 2023). This suggests that the climate impact on the tableland evolution and its interplay with the base-level variations and the tectonism is more complex.

The deposition of the SH-I and SH-II gravels and cobbles occurred during the beginning of the last glacial period, and the reworking started assumably at MIS4 and early MIS 3 (Liu et al., 2023, Fig. 7b), which are marked by continuous sea-level lowering and pronounced cold climate conditions (Liew et al., 2006). During the last glacial period, not only the vegetation boundaries, but also the snowline and periglacial belt were depressed, documented in the extent of glaciers and the intensification of mechanical (frost) weathering in the upper mountain ranges (Böse, 2006; Hebenstreit et al., 2006; Hebenstreit et al., 2011; Klose, 2006; Siame et al., 2007; Wenske et al., 2011), which may explain a higher sediment load and transport in the rivers.

The rework of the gravels and cobbles during the pronounced dry phase from MIS3 to MIS2 (Liu et al., 2023, Fig. 7c) may have been favored by the loosened vegetation of a forest steppe instead of woody species as the main composition of vegetation (Liew et al., 2006). In addition, the sea-level descended rapidly at that time, which is correspondent to the drop in base-level of fluvial systems in the Miaoli Tableland area. The erosion

and redeposition processes were more dynamic during this time span that brought the sediments from the proximal area to the distal area of SH-II and ST (Fig. 8.3).

The early Holocene (i.e. the Holocene maximum) was a period of relatively warm and wet subtropical climate conditions in the Taiwan Island (Liew et al., 2006) (Fig. 7.6). Increased fluvial discharge in combination with a sea-level high stand (Liu et al., 2008) may have contributed to the development of the box-shaped valleys. This climate setting is also assumed to be more relevant to the growth of dense vegetation in the mid-lower altitude areas, that have provided protections to the surfaces where the dusty and sandy materials are steadily accumulated as the cover layer, which is recorded by various locations with different morphological settings across the Island (Tsai et al., 2021).

8.6 A proposal of revision of the stratigraphic model based on the international stratigraphic guidelines

The stratigraphical definitions of the fluvial depositions in the mountain foreland and detailed separation of the near shore / coastal / tidal sedimentary layers were first made in the Japanese time (Makiyama, 1934, 1937) (Fig. 2.3). The early versions of geological map in Chinese were subsequently published in 1955 (Chang, 1955a, b), including the redefined stratigraphical nomenclatures of the sedimentary successions of the tablelands in the mountain foreland. The succeeding studies in the late 20th century and the 21st century are mostly based on the 1950s stratigraphical models, rather than the pre-1945 initial nomenclatures. However, the subsequent advancements since the 1950s of the conventional stratigraphic units (i.e., the Tk Formation and the Terrace Deposits / Quaternary Deposits) are no longer in agreement with the current version of principles of lithostratigraphy (see chapter 3) (Murphy et al., 1999; Salvador, 1994). In fact, the purposes of redefinition from Ts Formation to Tk Formation, carried out by Chang in 1950s, are insufficient (Fig. 2.3) (Ho, 1990; Lee, 1990), which caused ambiguous stratigraphic information regarding the following remarks.

1. The geographical naming of the Tk Formation / Huoyenshan Facies / Hsiangshan Facies do not follow the geographical scale of these names. Toukoshan and Huoyenshan are referred to very minor geographical areas (< 10 km²), however, Hsiangshan is referred to a larger geographical area (ca. 20 km²) (Figs. 1.2 and 2.1) (see chapter 3 for details). The choice of geographic names for different ranks of lithostratigraphic units must align with the spatial scale (Ho, 1990; Lee, 1990; Murphy et al., 1999; Salvador, 1994), thus, Hsiangshan should not be used as the geographical name of a subcategory (i.e. Facies) of the Tk Formation.
2. The gravel and cobble bed(s) exposed in Huoyenshan were chosen as the type localities (i.e. standard profile) of the Huoyenshan Facies and the Terrace Deposits simultaneously (Chang, 1953, 1955b; Ho, 1975, 1988) (Figs. 2.3, 5.3, 5.6 and Appendix 5C). However, a standard profile should be defined for a specific lithostratigraphic unit only (Murphy et al., 1999; Salvador, 1994); it should not be defined for two units in order to avoid ambiguous interpretations.
3. According to the descriptions of Chang (1953, 1955b) and Ho (1975, 1988), the type localities of the Tk Formation are located in different places (e.g. Toukoshan, Hsiangshan, Huoyenshan areas); however, all these type localities only exhibit a part of the standard profile of the Tk Formation (Figs. 1.1, 2.3 and Appendix 5A). In fact, the outcrops in Toukoshan and Huoyenshan areas only present the gravel and cobble bed(s). The outcrops in Hsiangshan area only present the fine-grained sedimentary layers (Chang, 1953, 1955b; Ho, 1975, 1988), and the bottom part of the Tk Formation is recorded only in the drilling record in Taichung area (Chen et al., 2001) (Figs. 1.3 and 2.3) (see chapter 3). However, the type locality of a lithostratigraphic unit must be consisted of

the entire succession of the stratum, with a clear, complete and representative outcrop for studying (Murphy et al., 1999; Salvador, 1994). Furthermore, the stratigraphical name of the unit must be corresponded to the geographical name of the type locality (Ho, 1990; Lee, 1990; Murphy et al., 1999; Salvador, 1994), thus the naming of the Tk Formation should be revised if a more representative type locality is determined.

4. The term “Facies” is a tentative lithostratigraphic unit invented by Chang (1953, 1955b), which roughly equals to the lithostratigraphic rank between “Formation” and “Member” (see chapter 3 for details). However, this term is not well-defined and its usage has been mixed with “Member” in the Taiwanese stratigraphic code. In order to follow the international standards for the hierarchy of lithostratigraphy units (Group, Formation, Member, Bed, Flow), the definition of “Huoyenshan Facies” and “Hsiangshan Facies” should be cancelled, and the definition of these units should be revised to fit the appropriate lithostratigraphic rank (i.e. Formation / Member / Bed) by each stratum (Ho, 1990; Lee, 1990; Murphy et al., 1999; Salvador, 1994).

A revision of the stratigraphical nomenclature is proposed, according to the current version of principles of lithostratigraphy. This revision is based on the definitions of the Ts Formation (Makiyama, 1934) and Lk Formation (Lin, 1963), because the field observation records (Liu et al., 2021; Liu et al., 2022) and the borehole records of the sedimentary successions are mostly consistent with these definitions (Figs. 2.3, 5.6, 6.3, 6.4, 7.2 and Appendix 5C).

The original definition of the Ts Formation from Makiyama (1934) could be upgraded into the rank of a “Group” and renamed as the “Miaoli Tableland Group” for two reasons: i). the type locality is located in the Miaoli Tableland area (outcrop 001- HLPT), and ii). the rank “Formation” is applied to describe the stratum with homogeneous lithology, the rank “Group” is intended to describe consistent sedimentary successions that are composed of different lithological facies / beds / strata (Murphy et al., 1999; Salvador, 1994). To subdivide the Miaoli Tableland Group, two stratigraphic units with the corresponding lithostratigraphic rank “Formation” are proposed for the nearshore / tidal / coastal fine-grained sediments (L-LS-SiC-SL) in the lower part of the succession, and the fluvial gravel and cobble bed(s) (CSB) in the upper part of the succession, based on their distinct lithological characteristics and the significantly different sedimentary processes (Figs. 2.3 and 8.4): The succession of fine-grained sedimentary layers, including the massive structured greyish loam (L layer) – the massive structured loamy sand (LS layer) – the alternation of greyish silt loam and yellowish silt loam (SiC layer) – the massive structured sandy loam (SL layer), can be revised as the “Tungxiao Formation”, with type locality located in the Tungxiao River catchment in the Tungxiao Township (Figs. 2.3, 5.6, 8.4, and Appendix 5C). The gravel and cobble bed(s) (CSB layer) can be revised as the “Sanyi-Tongluo Gravel Bed”, with the type locality located at the SH-I tableland segments that are distributed across Sanyi Township and Tongluo

Township (Figs. 2.3, 5.6, 8.4, and Appendix 5C). The aeolian silty loamy cover layer (SiL layer) is not specifically defined, as it is the result of an active depositional process throughout the Taiwan island.

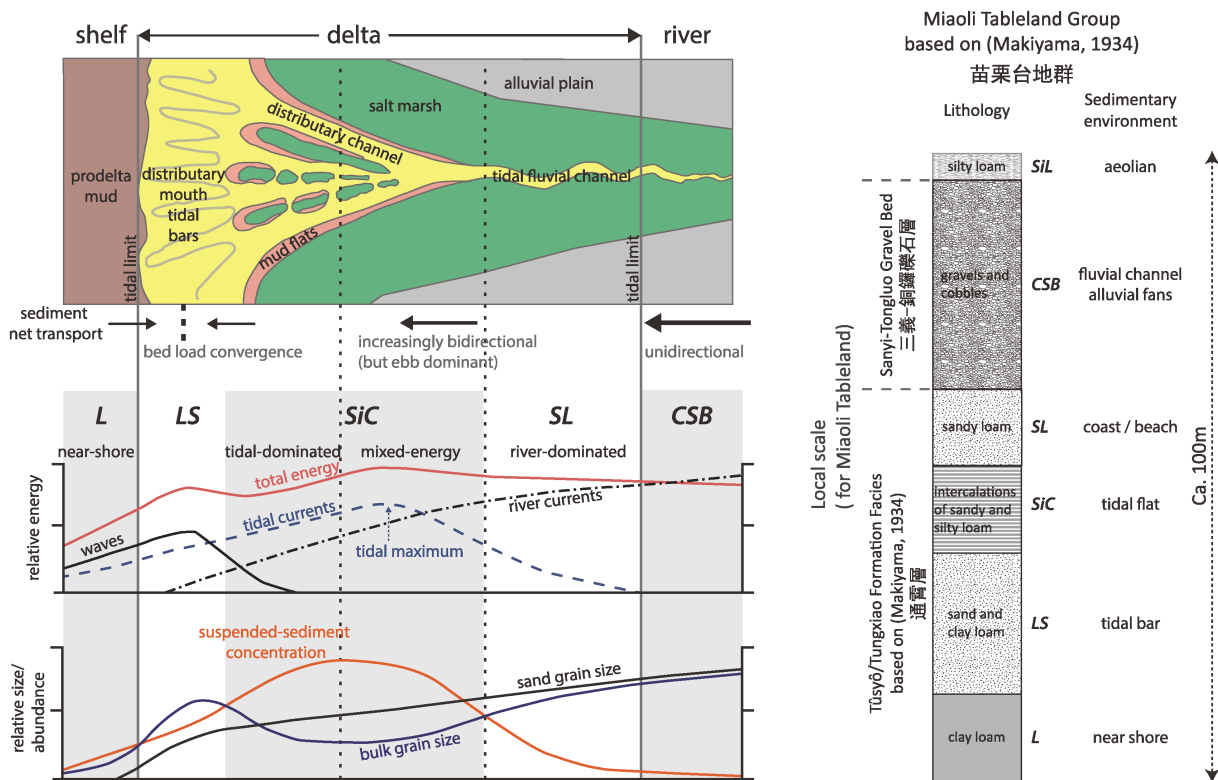


Figure 8.4: The proposed revision of stratigraphy model in Miaoli Tableland aligns with the current version of the principles of lithostratigraphy (Murphy et al., 1999; Salvador, 1994). The model of coastal / tidal sedimentary environments is simplified after Dalrymple et al. (2007). The stratigraphical categorization of the uppermost 100 meters sedimentary succession of the Miaoli Tableland could be revised into three stratigraphical units:

- i). The majority of the sedimentary succession, including the nearshore / tidal / coastal / fluvial sedimentary layers, are combined and upgraded to the “Group” rank and renamed as the Miaoli Tableland Group.
- ii). The fine-grained sedimentary layers in the lower part of the sedimentary succession, which are composed of the near shore / tidal / coastal sedimentary layers (L-LS-SiC-SL layers), are combined and categorized as the Ty / Ts Formation, based on the definition by Makiyama (1934).
- iii). The gravel and cobble bed(s) are independently categorized due to their unique lithology and representativeness for the processes of successive redeposition of fluvial sediments, which is proposed by Liu et al., (2022, 2023). The gravel and cobble bed(s) are named as Sanyi-Tongluo Gravel Bed due to the type localities are exhibited on the tableland segments that are located in Sanyi and Tongluo areas.

The aeolian cover sediments are not specifically categorized as they represent the active dust depositions throughout the Taiwan Island. The schematic diagram of sedimentary successions, legends, nomenclatures do not accurately depict the actual thickness of each sedimentary layer.

Chapter 9. Overall conclusions and outlook

A new 4D landscape evolution model of the Miaoli Tableland is established, including the influencing factors of climate, tectonic and sea-level change during the last glacial cycle, and combining the previous interpretations of Chang et al., (1998) and Ota et al. (2006) (see chapter 5, 6 and 7 for details):

The landscape evolution of Miaoli Tableland began with the deposition of fine-grained sediments (the L-LS-SiC-SL layers) in the foreland basin. The fluvial gravels and cobbles yielded from the Western Foothills (WF) have covered these fine-grained sedimentary layers, forming the palaeo alluvial fan(s) in the southeast of the study area (Sanyi and Tongluo areas), they are identified as the first order of the gravels and cobbles deposition. The ongoing thrust (Ota et al., 2006) has uplifted the sedimentary successions in those areas. The development of fluvial drainage networks on the paleo alluvial fan(s) has begun and subsequently has incised the fan surfaces to form the tableland segments (the SH-I).

The fluvial incisions, coupled with sea-level lowering, have reworked the gravels and cobbles from SH-I tableland segments towards the proximal areas in the north and west subsequently. The aggradation of these redeposited gravels and cobbles has formed the extended alluvial fan(s), identified as the second order of the gravels and cobbles deposition. The successive rapid uplifting of an inferred thrust movement (Chang et al., 1998) caused the overturning of the surface gradient of the SH-I tableland segments from west to east and cut off the fluvial pathways for further yielding of gravels and cobbles to the west. This thrust movement has subsequently coupled with the folding of the Tungxiao Anticline, and the sea level lowering during the MIS 4 and probably continuing until the beginning of MIS3. These processes triggered the rejuvenation of fluvial systems developments on the extended alluvial fan(s). The fluvial incisions have resulted in the formation of the proximal tableland segments (SH-II and ST).

The tableland segments that were incised more rapidly have been dissected to become remnants. Once the gravel and cobble bed(s) (CSB) have been removed, the unstable surfaces of these remnants are featuring relatively lower weathered silty cover layer (SiL), which directly contact the sandy loam layer (SL). Conversely, the deposition of the silty materials on the larger tableland segment surfaces, which are supported by the gravel and cobble bed(s) (CSB), are accumulating, and lasting longer, resulting in highly weathered silty cover layer (SiL) with a brownish/reddish color.

Local fluvial systems remobilized the gravels and cobbles further to the lower reach in the distal areas, which may be attributed to the yielding of gravels and cobbles during the relative cool climate conditions in the MIS 2 (Liew et al., 2006) when the base level was very low, and the loosened vegetation caused less protection of

tableland segment surfaces to erosion. These redeposited gravels and cobbles in the distal areas approximately during the end of MIS 2 are identified as the third order of the gravels and cobbles deposition.

The most recent thrust (Shyu et al., 2005) has uplifted the sedimentary successions and caused the formation of the distal tableland segments (SH-II/ST), as well as contributing to active deposition of gravels and cobbles in the fluvial channels and the estuaries (the AL). The sea level rose rapidly since the end of the MIS2. Subsequently rapid lateral erosions on the low-resistant fine-grained sedimentary layers of the tableland segments (SH-II/ST) resulted in the formation of the box-shaped valleys in the middle and lower reaches of fluvial systems, mostly lower than 150m asl.

This study achieved four main outcomes, serving as a pilot study for a new synthesis of morphological, sedimentological, and geochronological insights to study the correlation of sedimentary successions and landscape developments of the Miaoli Tableland from the post-last interglacial to the present days, with a detailed review of the historical evolution of the stratigraphical nomenclatures and models.

i). The results of OSL dating reveal that the depositional ages of the uppermost part (ca. 100 meters) of tableland's sedimentary succession are mainly within the post-last interglacial time span (Liu et al., 2023). These findings, in fact, revise the chronology control of the Miaoli Tableland morphology, shortening it compared to the previous interpretations of 3Ma (Ota et al., 2006) / Middle Pleistocene (Chang et al., 1998) time spans, which had overestimated the relative chronology of depositions (see chapter 7 for details). The OSL dating of the sedimentary successions also reveals the hiatus of depositions between the fine-grained sediments (SL layer and below) and the gravels and cobbles (CSB layer).

ii). The linear theoretical surface calculation provides a concise and straightforward numerical based approach to defining the sub-groups of the tableland segments (see chapter 5 for details). The boundaries of the Sedimentary Highlands (SH-I, SH-II) and the Sedimentary Terraces (ST) align with the tectonic features (i.e. thrust faults and anticline) (Chang, 1990, 1994; Chang et al., 1998; Ho, 1994; Ota et al., 2006; Shyu et al., 2005). Furthermore, the elevation profile of tableland segment surfaces exhibits a convex shape from the southeast (SH-I) to the northeast (SH-II). These tableland segments are composed with the type-I sedimentary successions that are characterized by full succession with relative thick layering of gravels and cobbles (CSB) and reddish/brownish-colored highly weathered loamy surface materials (SiL), assumed to have been deposited for a longer time (Chang et al., 1998; Chen, 1983). The elevation profile of tableland segments and remnants from the southeast (SH-I) to the north (ST) exhibits a concave shape. The ST tableland segments and remnants are composed mainly of the type-II sedimentary successions, primarily consisting of the fine-grained sedimentary layers (SL layer and below) occasionally with the gravel and cobble bed(s) (CSB layer). They are

covered by the yellowish slightly weathered surface materials (SiL), assumed to have been deposited for a shorter time (Chang et al., 1998; Chen, 1983).

iii). The borehole data analyses exhibit a possibility of studying the spatial distribution of sedimentary layers beneath the surfaces. The interpolated cross-sections show that the vertical displacements of sedimentary successions are parallel aligned (see chapter 6 for details). Their locations are correlated with the identified tectonic features (Chang, 1990, 1994; Ho, 1994; Ota et al., 2006; Shyu et al., 2005) and the topographic escarpment (Chang et al., 1998). The uplift and subsequent erosion control the redeposition processes of the gravels and cobbles, which were started from the southeast (SH-I) through the north (SH-II) and the west (ST), ultimately reaching the fluvial valleys and the estuaries (AL).

iv). A proposal to revise the stratigraphical nomenclatures of the studied sedimentary successions in the Miaoli Tableland is presented, following the principles of the latest version of the International Stratigraphic Guide (Salvador, 1994). The rarely mentioned early definitions, such as the Tyusho Formation (Ty) (Makiyama, 1934, 1937) and the Lungkang Formation (Lk) (Lin, 1963) are reintroduced to describe these sedimentary successions, which rectifies overinterpretations based on the broadly used Toukoshan Formation (Tk) (Chang, 1955b).

There is potential for more works in the future. For example, testing the dating methods with a longer applicational range could provide precise chronology control for the fine-grained sedimentary layers in the lower part of the studied sedimentary successions, offering a better chronological framework to interpret the sedimentary environments changes corresponding to the global sea-level change. This can be a new approach to study an overall morphological model for other Taiwanese tablelands. The outcomes of this study can be further compared with different studies on Quaternary environmental change of sedimentary terraces with similar geographical settings.

References

- Adamic, G., Aitken, M.J.**, 1998. Dose-rate conversion factors: update. *Ancient TL* **16**, 37-50.
- Aitken, M.J.**, 1985. *Thermoluminescence dating*. Academic Press, Orlando/London.
- Aitken, M.J., Smith, B.W.**, 1988. Optical dating: Recuperation after bleaching. *Quaternary Science Reviews* **7**, 387-393.
- Angelier, J., Barrier, E., Chu, H.T.**, 1986. Plate collision and paleostress trajectories in a fold-thrust belt: The foothills of Taiwan. *Tectonophysics* **125**, 161-178.
- Angelier, J., Bergerat, F., Chu, H.-T., Lee, T.-Q.** 1990. Tectonic analysis and the evolution of a curved collision belt: The Hsüehshan Range, Northern Taiwan. *Tectonophysics* **183**, 77-96.
- Arnold, L.J., Roberts, R.G.**, 2009. Stochastic modelling of multi-grain equivalent dose (De) distributions: Implications for OSL dating of sediment mixtures. *Quaternary Geochronology* **4**, 204-230.
- Arnold, L.J., Roberts, R.G.**, 2011. Paper I – Optically stimulated luminescence (OSL) dating of perennially frozen deposits in north-central Siberia: OSL characteristics of quartz grains and methodological considerations regarding their suitability for dating. *Boreas* **40**, 389-416.
- Bailey, R.M., Smith, B.W., Rhodes, E.J.**, 1997. Partial bleaching and the decay form characteristics of quartz OSL. *Radiation Measurements* **27**, 123-136.
- Beuselinck, L., Govers, G., Poesen, J., Degraer, G., Froyen, L.**, 1998. Grain-size analysis by laser diffractometry: comparison with the sieve-pipette method. *CATENA* **32**, 193-208.
- Biq, C., Chang, L.-S., Chen, P.Y., Ho, C.-S., Hsu, T.L., Keng, W.P., Lee, T.H., Pan, C.W., Tan, L.P., Tsan, S.F., Yang, Y.T.**, 1957. *Lexique stratigraphique international. 3. Asie. 4. Taiwan (Formose)*. Congrès Géologique International - Commission de Stratigraphie, Paris.
- Bird, P.**, 2003. An updated digital model of plate boundaries. *Geochemistry, Geophysics, Geosystems* **4**, 1027.
- Böse, M.**, 2004. Traces of glaciation in the high mountains of Taiwan, in: Ehlers, J., Gibbard, P.L. (Eds.), *Developments in Quaternary Sciences*. Elsevier, pp. 347-352.
- Böse, M.**, 2006. Geomorphic altitudinal zonation of the high mountains of Taiwan. *Quaternary International* **147**, 55-61.
- Bøtter-Jensen, L., Bulur, E., Duller, G.A.T., Murray, A.S.**, 2000. Advances in luminescence instrument systems. *Radiation Measurements* **32**, 523-528.
- Bøtter-Jensen, L., Thomsen, K.J., Jain, M.**, 2010. Review of optically stimulated luminescence (OSL) instrumental developments for retrospective dosimetry. *Radiation Measurements* **45**, 253-257.
- Bradley, S.L., Milne, G.A., Horton, B.P., Zong, Y.**, 2016. Modelling sea level data from China and Malay-Thailand to estimate Holocene ice-volume equivalent sea level change. *Quaternary Science Reviews* **137**, 54-68.
- Bridgland, D., Westaway, R.**, 2008. Climatically controlled river terrace staircases: A worldwide Quaternary phenomenon. *Geomorphology* **98**, 285-315.
- Buatois, L.A., Santiago, N., Herrera, M., Plink-Björklund, P., Steel, R.O.N., Espin, M., Parra, K.**, 2012. Sedimentological and ichnological signatures of changes in wave, river and tidal influence along a Neogene tropical deltaic shoreline. *Sedimentology* **59**, 1568-1612.
- Center for GIS RCHSS Academia Sinica**, 2017. Taiwan Historical Atlas Web Map Tile Service, Taipei (accessed 14. 1. 2022). <http://gis.sinica.edu.tw/tileserver/wmts>.
- Central Geological Survey**, 2017a. Engineering Geological Investigation Data Bank. Central Geological Survey, Taipei (accessed 14. 1. 2022). <https://geotech.moeacgs.gov.tw/imoeagis/Home/Map>.
- Central Geological Survey**, 2017b. National Geological Data Warehouse. Central Geological Survey, Taipei. (accessed 17. 9. 2022). <https://gis3.moeacgs.gov.tw/gwh/gsb97-1/sys8/t3/index1.cfm>.
- Central Weather Bureau**, 2019a. CWB Observation Data Inquire System, Taipei. (accessed 14. 1. 2022). <https://e-service.cwb.gov.tw/HistoryDataQuery/index.jsp>.
- Central Weather Bureau**, 2019b. Typhoon Data Base, Taipei. (accessed 14. 1. 2022). <https://rdc28.cwb.gov.tw/TDB/>.

- Central Weather Bureau**, 2020. Tidal level statistics, Taipei. (accessed 14. 1. 2022). https://www.cwb.gov.tw/V8/C/C/MMC_STAT/sta_tide.html.
- Central Weather Bureau**, 2022. Seismological Center, Taipei. (accessed 2. 4. 2022). <https://scweb.cwb.gov.tw/en-US>.
- Chang, H.-C.**, 1990. *Geological Map of Taiwan scale 1:50000 — Baishatun*. Central Geological Survey, Taipei.
- Chang, H.-C.**, 1994. *Geological Map of Taiwan scale 1:50000 — Dajia*. Central Geological Survey, Taipei.
- Chang, J.-C., Teng, K.-H., Liu, M.-C.**, 1998. A Geomorphological Study on River Terraces in Miaoli Hills. *Geographical Research* **29**, 97-112.
- Chang, J.-K.**, 2007. The aboriginal society/ 住民志(下冊): 原住民族群篇 in: Chen, Y.D. (Eds.), *Miaoli County Chronicles (Revised Edition) / 重修苗栗縣志*. Miaoli County Government, Miaoli.
- Chang, L.-S.**, 1948a. The revision of stratigraphy categories of Taiwan (continued) / 台灣地層檢討 (續). *Geological Review / 地質論評* **13**, 291-310.
- Chang, L.-S.**, 1948b. The revision of stratigraphy categories of Taiwan / 台灣地層檢討. *Geological Review / 地質論評* **13**, 185-198.
- Chang, L.-S.**, 1953. *Geologic map of Taiwan*. Geological Survey of Taiwan, Taipei.
- Chang, L.-S.**, 1955a. The geological history of Taiwan / 台灣之地史. *Quarterly Journal of the Taiwan Bank / 台灣銀行季刊* **7**, 1-7.
- Chang, L.-S.**, 1955b. The strata of Taiwan / 台灣之地層. *Quarterly Journal of the Taiwan Bank / 台灣銀行季刊* **7**, 26-49.
- Chapot, M.S., Roberts, H.M., Duller, G.A.T., Lai, Z.P.**, 2012. A comparison of natural- and laboratory-generated dose response curves for quartz optically stimulated luminescence signals from Chinese Loess. *Radiation Measurements* **47**, 1045-1052.
- Charlton, R.**, 2008. *Fundamentals of fluvial geomorphology*. Routledge, New York.
- Chen, C.-G.**, 1983. *The soil investigation report of the slopes — Miaoli County / 山坡地土壤調查報告—苗栗縣*. Mountain Agricultural Resources Development Bureau, Nantou.
- Chen, H., Wan, J.-P.**, 2004. The effect of orientation and shape distribution of gravel on slope angles in central Taiwan. *Engineering Geology* **72**, 19-31.
- Chen, H.-F., Yeh, P.-Y., Song, S.-R., Hsu, S.-C., Yang, T.-N., Wang, Y., Chi, Z., Lee, T.-Q., Chen, M.-T., Cheng, C.-L., Zou, J., Chang, Y.-P.**, 2013. The Ti/Al molar ratio as a new proxy for tracing sediment transportation processes and its application in aeolian events and sea level change in East Asia. *Journal of Asian Earth Sciences* **73**, 31-38.
- Chen, H.-W., Lee, T.-Y., Wu, L.-C.**, 2010. High-resolution sequence stratigraphic analysis of Late Quaternary deposits of the Changhua Coastal Plain in the frontal arc-continent collision belt of Central Taiwan. *Journal of Asian Earth Sciences* **39**, 192-213.
- Chen, S., Steel, R.J., Dixon, J.F., Osman, A.**, 2014. Facies and architecture of a tide-dominated segment of the Late Pliocene Orinoco Delta (Morne L'Enfer Formation) SW Trinidad. *Marine and Petroleum Geology* **57**, 208-232.
- Chen, W.-S., Chen, Y.-G., Shih, R.-C., Liu, T.-K., Huang, N.-W., Lin, C.-C., Sung, S.-H., Lee, K.-J.**, 2003a. Thrust-related river terrace development in relation to the 1999 Chi-Chi earthquake rupture, Western Foothills, central Taiwan. *Journal of Asian Earth Sciences* **21**, 473-480.
- Chen, W.-S., Huang, M.T., Liu, T.-K.**, 1991. Neotectonic significance of the Chimei Fault in the Coastal Range, Eastern Taiwan. *Proceedings of the Geological Society of China* **34**, 43-56.
- Chen, W.-S., Ridgway, K.D., Horng, C.-S., Chen, Y.-G., Shea, K.-S., Yeh, M.-G.**, 2001. Stratigraphic architecture, magnetostratigraphy, and incised-valley systems of the Pliocene-Pleistocene collisional marine foreland basin of Taiwan. *GSA Bulletin* **113**, 1249-1271.
- Chen, Y.-G., Chen, Y.-W., Chen, W.-S., Lee, K.-J., Lee, L.-S., Lu, S.-T., Lee, Y.-H., Watanuki, T., Lin, Y.-N.N.**, 2009. Optical dating of a sedimentary sequence in a trenching site on the source fault of the 1999 Chi-Chi earthquake, Taiwan. *Quaternary International* **199**, 25-33.
- Chen, Y.-G., Chen, Y.-W., Chen, W.-S., Zhang, J.-F., Zhao, H., Zhou, L.-P., Li, S.-H.**, 2003b. Preliminary results of long-term slip rates of 1999 earthquake fault by luminescence and radiocarbon dating. *Quaternary Science Reviews* **22**, 1213-1221.
- Chen, Y.-G., Liu, T.-K.**, 1991. Radiocarbon dates of river terraces along the lower Tahanchi, northern Taiwan: Their tectonic and geomorphic implications. *Proceedings of the Geological Society of China* **34**, 337-347.
- Chen, Y.-G., Liu, T.-K.**, 1996. Sea Level Changes in the Last Several Thousand Years, Penghu Islands, Taiwan Strait. *Quaternary Research* **45**, 254-262.

- Chen, Y.-G., Liu, T.-K.**, 2000. Holocene uplift and subsidence along an active tectonic margin southwestern Taiwan. *Quaternary Science Reviews* **19**, 923-930.
- Chen, Y.-G., Shyu, J.B.H., Ota, Y., Chen, W.-S., Hu, J.-C., Tsai, B.-W., Wang, Y.**, 2004. Active structures as deduced from geomorphic features: a case in Hsinchu Area, northwestern Taiwan. *Quaternary International* **115-116**, 189-199.
- Chen, Y.W., Chen, Y.G., Murray, A.S., Liu, T.K., Lai, T.C.**, 2003c. Luminescence dating of neotectonic activity on the southwestern coastal plain, Taiwan. *Quaternary Science Reviews* **22**, 1223-1229.
- Chen, Z.-S., Hseu, Z.-Y., Tsai, C.-C.**, 2015. *The soils of Taiwan*. Springer, Dordrecht.
- Cheng, C.-H.**, 2007. Infrastructures / 建設志, in: Chen, Y.D. (Eds.), *Miaoli County Chronicles (Revised Edition) / 重修苗栗縣志*. Miaoli County Government, Miaoli, Taiwan.
- Chi, W.-J.**, 2007. Minging and natural resources / 礦業志, in: Chen, Y.D. (Eds.), *Miaoli County Chronicles (Revised Edition) / 重修苗栗縣志*. Miaoli County Government, Miaoli, Taiwan.
- Ching, K.-E., Hsieh, M.-L., Johnson, K.M., Chen, K.-H., Rau, R.-J., Yang, M.**, 2011. Modern vertical deformation rates and mountain building in Taiwan from precise leveling and continuous GPS observations, 2000–2008. *Journal of Geophysical Research* **116**, B08406.
- Choi, J.H., Kim, J.W., Murray, A.S., Hong, D.G., Chang, H.W., Cheong, C.S.**, 2009. OSL dating of marine terrace sediments on the southeastern coast of Korea with implications for Quaternary tectonics. *Quaternary International* **199**, 3-14.
- Cohen, K.M., Harper, D.A.T., Gibbard, P.L.**, 2020. *ICS International Chronostratigraphic Chart 2020/03*. International Commission on Stratigraphy, IUGS.
- Covey, M.**, 1986. The Evolution of Foreland Basins to Steady State: Evidence from the Western Taiwan Foreland Basin, in: Allen, P.A., Homewood, P. (Eds.), *Foreland Basins*. Blackwell Scientific Publications, Oxford, pp. 77-90.
- Cunningham, A.C., Wallinga, J.**, 2010. Selection of integration time intervals for quartz OSL decay curves. *Quaternary Geochronology* **5**, 657-666.
- Cunningham, A.C., Wallinga, J.**, 2012. Realizing the potential of fluvial archives using robust OSL chronologies. *Quaternary Geochronology* **12**, 98-106.
- Dadson, S.J., Hovius, N., Chen, H., Dade, W.B., Hsieh, M.-L., Willett, S.D., Hu, J.-C., Horng, M.-J., Chen, M.-C., Stark, C.P., Lague, D., Lin, J.-C.**, 2003. Links between erosion, runoff variability and seismicity in the Taiwan orogen. *Nature* **426**, 648-651.
- Dalrymple, R.W., Choi, K.**, 2007. Morphologic and facies trends through the fluvial–marine transition in tide-dominated depositional systems: A schematic framework for environmental and sequence-stratigraphic interpretation. *Earth-Science Reviews* **81**, 135-174.
- Davis, R.A.**, 2012. *Principles of tidal sedimentology*. Springer, Dordrecht.
- Deffontaines, B., Lacombe, O., Angelier, J., Chu, H.T., Mouthereau, F., Lee, C.T., Deramond, J., Lee, J.F., Yu, M.S., Liew, P.M.**, 1997. Quaternary transfer faulting in the Taiwan Foothills: evidence from a multisource approach. *Tectonophysics* **274**, 61-82.
- Delcaillau, B.**, 2001. Geomorphic response to growing fault-related folds: example from the foothills of central Taiwan. *Geodinamica Acta* **14**, 265-287.
- Desjardins, P.R., Buatois, L.A., Mángano, M.G.**, 2012. Chapter 18 - Tidal Flats and Subtidal Sand Bodies, in: Knaust, D., Bromley, R.G. (Eds.), *Developments in Sedimentology*. Elsevier, pp. 529-561.
- Dörschner, N., Reimann, T., Wenske, D., Lüthgens, C., Tsukamoto, S., Frechen, M., Böse, M.**, 2012. Reconstruction of the Holocene coastal development at Fulong Beach in north-eastern Taiwan using optically stimulated luminescence (OSL) dating. *Quaternary International* **263**, 3-13.
- Duller, G.A.T.**, 2011. What date is it? Should there be an agreed datum for luminescence ages? *Ancient TL* **29**, 1-3.
- Duller, G.A.T.**, 2003. Distinguishing quartz and feldspar in single grain luminescence measurements. *Radiation Measurements* **37**, 161-165.
- Duller, G.A.T.**, 2008a. *Luminescence Dating: guidelines on using luminescence dating in archaeology*. English Heritage, Swindon.
- Duller, G.A.T.**, 2008b. Single-grain optical dating of Quaternary sediments: why aliquot size matters in luminescence dating. *Boreas* **37**, 589-612.
- Duller, G.A.T., Wintle, A.G.**, 2012. A review of the thermally transferred optically stimulated luminescence signal from quartz for dating sediments. *Quaternary Geochronology* **7**, 6-20.
- Durcan, J.A., Duller, G.A.T.**, 2011. The fast ratio: A rapid measure for testing the dominance of the fast component in the initial OSL signal from quartz. *Radiation Measurements* **46**, 1065-1072.

- Eshel, G., Levy, G.J., Mingelgrin, U., Singer, M.J., 2004. Critical Evaluation of the Use of Laser Diffraction for Particle-Size Distribution Analysis. *Soil Science Society of America Journal* **68**, 736-743.
- Fisher, D.M., Lu, C.Y., Chu, H.T., 2002. Taiwan Slate Belt: Insights into the ductile interior of an arc-continent collision. *Special Paper of the Geological Society of America* **358**, 93-106.
- Fontana, A., Mozzi, P., Bondesan, A., 2008. Alluvial megafans in the Venetian–Friulian Plain (north-eastern Italy): Evidence of sedimentary and erosive phases during Late Pleistocene and Holocene. *Quaternary International* **189**, 71-90.
- Fox, M., Goren, L., May, D.A., Willett, S.D., 2014. Inversion of fluvial channels for paleorock uplift rates in Taiwan. *Journal of Geophysical Research: Earth Surface* **119**, 1853-1875.
- Galbraith, R.F., Green, P.F., 1990. Estimating the component ages in a finite mixture. *International Journal of Radiation Applications and Instrumentation. Part D. Nuclear Tracks and Radiation Measurements* **17**, 197-206.
- Galbraith, R.F., Roberts, R.G., 2012. Statistical aspects of equivalent dose and error calculation and display in OSL dating: An overview and some recommendations. *Quaternary Geochronology* **11**, 1-27.
- Galbraith, R.F., Roberts, R.G., Laslett, G.M., Yoshida, H., Olley, J.M., 1999. Optical dating of single and multiple grains of quartz from Jinmium rock shelter, northern Australia: part I, experimental design and statistical models*. *Archaeometry* **41**, 339-364.
- Goodbred, S., Saito, Y., 2011. Tide-Dominated Deltas, in: Davis, R.A., Dalrymple, R.W. (Eds.), *Principles of Tidal Sedimentology*. Springer, pp. 129-149.
- Gray, H.J., Mahan, S.A., 2015. Variables and potential models for the bleaching of luminescence signals in fluvial environments. *Quaternary International* **362**, 42-49.
- Guérin, G., Mercier, N., Adamiec, G., 2011. Dose-rate conversion factors: Update. *Ancient TL* **29**, 5-8.
- Hanebuth, T.J.J., Mersmeyer, H., Kudrass, H.R., Westphal, H., 2013. Aeolian to shallow-marine shelf architecture off a major desert since the Late Pleistocene (northern Mauritania). *Geomorphology* **203**, 132-147.
- Hanebuth, T.J.J., Voris, H.K., Yokoyama, Y., Saito, Y., Okuno, J.i., 2011. Formation and fate of sedimentary depocentres on Southeast Asia's Sunda Shelf over the past sea-level cycle and biogeographic implications. *Earth-Science Reviews* **104**, 92-110.
- Hebenstreit, R., 2016. Quaternary mineral dust deposits in Taiwan—a new palaeoclimatic archive. Paper presented at DUST 2016 — 2nd International Conference on Atmospheric Dust (Castellaneta Marina, Italy, June 12-17, 2016).
- Hebenstreit, R., Böse, M., 2015. Quaternary mineral aeolian dust deposits in Taiwan and their potentials as a new archive. Paper presented at XIX INQUA Congress (Nagoya, Japan, July 27 - August 2, 2015) (accessed 14.1.2022). https://www.inqua-seqs.org/files/INQUA2015_program_web.pdf.
- Hebenstreit, R., Böse, M., Murray, A., 2006. Late Pleistocene and early Holocene glaciations in Taiwanese mountains. *Quaternary International* **147**, 76-88.
- Hebenstreit, R., Ivy-Ochs, S., Kubik, P.W., Schlüchter, C., Böse, M., 2011. Lateglacial and early Holocene surface exposure ages of glacial boulders in the Taiwanese high mountain range. *Quaternary Science Reviews* **30**, 298-311.
- Ho, C.-S., 1947a. The geological studies of Taiwan for the past fifty years (continued) / 過去五十年內台灣地質之研究 (續) . *Geological Review / 地質論評* **12**, 509-536.
- Ho, C.-S., 1947b. The geological studies of Taiwan for the past fifty years / 過去五十年內台灣地質之研究. *Geological Review / 地質論評* **12**, 397-424.
- Ho, C.-S., 1975. *An Introduction to The Geology Of Taiwan Explanatory Text Of The Geologic Map Of Taiwan*. Central Geological Survey, Taipei.
- Ho, C.-S., 1988. *An introduction to the geology of Taiwan: explanatory text of the geologic map of Taiwan, 2nd ed.* ed. Central Geological Survey, Taipei.
- Ho, C.-S., 1990. The review and discussion of the problems of the stratigraphy in Taiwan with the principles of stratigraphy / 由地層學原理回顧與檢討臺灣的地層問題. *Special Publication of the Central Geological Survey, MOEA. / 經濟部中央地質調查所特刊* **4**, 9-26.
- Ho, H.-C., 1994. *Geological Map of Taiwan scale 1:50000 — Miaoli*. Central Geological Survey, Taipei.
- Ho, L.-D., Lüthgens, C., Wong, Y.-C., Yen, J.-Y., Chyi, S.-J., 2017. Late Holocene cliff-top dune evolution in the Hengchun Peninsula of Taiwan: Implications for palaeoenvironmental reconstruction. *Journal of Asian Earth Sciences* **148**, 13-30.
- Horng, C.-S., 2014. Age of the Tananwan Formation in Northern Taiwan: A Reexamination of the Magnetostratigraphy and Calcareous Nannofossil Biostratigraphy. *Terrestrial, Atmospheric and Oceanic Sciences* **25**, 137-147.

- Horng, C.-S., Huh, C.-A.**, 2011. Magnetic properties as tracers for source-to-sink dispersal of sediments: A case study in the Taiwan Strait. *Earth and Planetary Science Letters* **309**, 141-152.
- Hsieh, M.-L., Chyi, S.-J.**, 2010. Late Quaternary mass-wasting records and formation of fan terraces in the Chen-yeo-lan and Lao-nung catchments, central-southern Taiwan. *Quaternary Science Reviews* **29**, 1399-1418.
- Hsieh, M.-L., Knuepfer, P.L.K.**, 2001. Middle-late Holocene river terraces in the Erhjen River Basin, southwestern Taiwan—implications of river response to climate change and active tectonic uplift. *Geomorphology* **38**, 337-372.
- Hsieh, M.-L., Knuepfer, P.L.K.**, 2002. Synchronicity and morphology of Holocene river terraces in the Southwestern Foothills, Taiwan: A guide to interpreting and correlating erosional river terraces across growing anticlines in: Byrne, T.B., Liu, C.-S. (Eds.), *Geology and Geophysics of an Arc-Continent Collision, Taiwan*. *GSA Special Paper* **358**, 55-74.
- Hsieh, M.-L., Lai, T.-H., Wu, L.-C., Lu, W.-C., Liew, P.-M.**, 2006. Eustatic Sea-Level Change of 11 - 5 ka in Western Taiwan, Constrained by Radiocarbon Dates of Core Sediments. *Terrestrial, Atmospheric and Oceanic Sciences* **17**, 353-370.
- Hsu, S.-C., Liu, S.C., Arimoto, R., Liu, T.-H., Huang, Y.-T., Tsai, F., Lin, F.-J., Kao, S.-J.**, 2009. Dust deposition to the East China Sea and its biogeochemical implications. *Journal of Geophysical Research: Atmospheres* **114**, D15304.
- Huang, C.-Y., Liew, P.-M., Zhao, M., Chang, T.-C., Kuo, C.-M., Chen, M.-T., Wang, C.-H., Zheng, L.-F.**, 1997. Deep sea and lake records of the Southeast Asian paleomonsoons for the last 25 thousand years. *Earth and Planetary Science Letters* **146**, 59-72.
- Huang, L.-A.**, 2010. *Academia Sinica / 朱家驊與中央研究院*. Academia Historica, Taipei.
- Huang, T.**, 1984. Planktic foraminiferal biostratigraphy and datum planes in the Neogene sedimentary sequence in Taiwan. *Palaeogeography, Palaeoclimatology, Palaeoecology* **46**, 97-106.
- Huang, T.-S.**, 2007. Human Geography / 人文地理志 in: Chen, Y.D. (Eds.), *Miaoli County Chronicles (Revised Edition) / 重修苗栗縣志*. Miaoli County Government, Miaoli.
- Huang, W.-S., Jien, S.-H., Huang, S.-T., Tsai, H., Hseu, Z.-Y.**, 2017. Pedogenesis of red soils overlaid coral reef terraces in the Southern Taiwan. *Quaternary International* **441**, 62-76.
- Huh, C.-A., Chen, W., Hsu, F.-H., Su, C.-C., Chiu, J.-K., Lin, S., Liu, C.-S., Huang, B.-J.**, 2011. Modern (<100 years) sedimentation in the Taiwan Strait: Rates and source-to-sink pathways elucidated from radionuclides and particle size distribution. *Continental Shelf Research* **31**, 47-63.
- Hung, T.-Y.**, 2007. Hydraulic engineering / 水利志 in: Chen, Y.D. (Eds.), *Miaoli County Chronicles (Revised Edition) / 重修苗栗縣志*. Miaoli County Government, Miaoli.
- Ishihara, T., Sugai, T., Hachinohe, S.**, 2012. Fluvial response to sea-level changes since the latest Pleistocene in the near-coastal lowland, central Kanto Plain, Japan. *Geomorphology* **147-148**, 49-60.
- Ishizaki, K.**, 1942a. Stratigraphical index of Taiwan (I) / 臺灣の地層名 (I). *Transactions of the natural history society of Formosa / 臺灣博物學會會報* **32**, 51-62.
- Ishizaki, K.**, 1942b. Stratigraphical index of Taiwan (II) / 臺灣の地層名 (II). *Transactions of the natural history society of Formosa / 臺灣博物學會會報* **32**, 147-158.
- Ishizaki, K.**, 1942c. Stratigraphical index of Taiwan (III) / 臺灣の地層名 (III). *Transactions of the natural history society of Formosa / 臺灣博物學會會報* **32**, 180-194.
- Ishizaki, K.**, 1942d. Stratigraphical index of Taiwan (IV) / 臺灣の地層名 (IV). *Transactions of the natural history society of Formosa / 臺灣博物學會會報* **32**, 232-239.
- Ishizaki, K.**, 1942e. Stratigraphical index of Taiwan (V) / 臺灣の地層名 (V). *Transactions of the natural history society of Formosa / 臺灣博物學會會報* **32**, 252-256.
- Ishizaki, K.**, 1942f. Stratigraphical index of Taiwan (VI) / 臺灣の地層名 (VI). *Transactions of the natural history society of Formosa / 臺灣博物學會會報* **32**, 280-282.
- Itoh, N., Hori, K., Takada, M.**, 2017. Latest Pleistocene to Holocene alluvial basin construction: An example from the Nara Basin, central Japan. *Quaternary International* **455**, 102-112.
- Jahn, B.-M., Martineau, F., Peucat, J.J., Cornichet, J.**, 1986. Geochronology of the Tananao Schist Complex, Taiwan, and its regional tectonic significance. *Tectonophysics* **125**, 103-124.
- Jahn, R., Blume, H.P., Asio, V.B., Spaargaren, O., Schad, P.**, 2006. *Guidelines for soil description, 4th edition*. Food and Agriculture Organization of the United Nations, Rome.

- Jain, M., Bøtter-Jensen, L., Murray, A., Denby, P., Tsukamoto, S., Gibling, M., 2005. Revisiting TL: dose measurement beyond the OSL range using SAR. *Ancient TL* **23**, 9-24.
- Jain, M., Murray, A., Botter-Jensen, L., 2004. Optically stimulated luminescence dating: How significant is incomplete light exposure in fluvial environments? *Quaternaire* **15**, 143-157.
- Jan, S., Wang, J., Chern, C.-S., Chao, S.-Y., 2002. Seasonal variation of the circulation in the Taiwan Strait. *Journal of Marine Systems* **35**, 249-268.
- Krapf, C., Werner, M., Questiaux, D., Spooner, N., Williams, F., Dutch, R., 2018. *Optically stimulated luminescence dating revealing new insights into the age of major regolith units of the eastern Musgrave Province, South Australia*. Department for Energy and Mining, South Australia, Adelaide.
- Klose, C., 2006. Climate and geomorphology in the uppermost geomorphic belts of the Central Mountain Range, Taiwan. *Quaternary International* **147**, 89-102.
- Ko, C.-M., 2001. *The Aborigine Landlord: Ethnic Politics and Aborigine Land Rights in Qing Taiwan / 番頭家：清代台灣族群政治與熟番地權*. Institute of Sociology, Academia Sinica, Taipei.
- Konert, M., Vandenberghe, J., 1997. Comparison of laser grain size analysis with pipette and sieve analysis: a solution for the underestimation of the clay fraction. *Sedimentology* **44**, 523-535.
- Kreutzer, S., Schmidt, C., Fuchs, M., Dietze, M., Fischer, M., Fuchs, M., 2012. Introducing an R package for luminescence dating analysis. *Ancient TL* **30**, 1-8.
- Lai, T.-C., Liu, K.-H., Wei, S.-K., Liu, H.-C., Huang, C.-K., Liu, W.-M., 2007. *Physical Geography / 自然地理志* in: Chen, Y.D. (Eds.), *Miaoli County Chronicles (Revised Edition) / 重修苗栗縣志*. Miaoli County Government, Miaoli.
- Lambeck, K., Rouby, H., Purcell, A., Sun, Y., Sambridge, M., 2014. Sea level and global ice volumes from the Last Glacial Maximum to the Holocene. *Proceedings of the National Academy of Sciences USA* **111**, 15296-15303.
- Lamothe, M., Auclair, M., Hamzaoui, C., Huot, S., 2003. Towards a prediction of long-term anomalous fading of feldspar IRSL. *Radiation Measurements* **37**, 493-498.
- Lastochkin, A.N., Zhirov, A.I., Boltramovich, S.F., 2018. System-morphological approach: Another look at morphology research and geomorphological mapping. *Geomorphology* **303**, 486-503.
- Le Béon, M., Suppe, J., Jaiswal, M.K., Chen, Y.-G., Ustaszewski, M.E., 2014. Deciphering cumulative fault slip vectors from fold scarps: Relationships between long-term and coseismic deformations in central Western Taiwan. *Journal of Geophysical Research: Solid Earth* **119**, 5943-5978.
- Lee, C.-L., 2000a. *The chronostratigraphy and sedimentary environments of the Toukoshan Fm. in Beishatun area, Miaoli. / 苗栗白沙屯地區頭嵙山層之年代地層與沉積環境*. Master Thesis of the Department of Earth Sciences, National Central University, Chungli.
- Lee, C.-L., Huang, T., Shieh, K.-S., Chen, Z.-H., 2002. The chronostratigraphy and sedimentary environments of the Toukoshan Fm. in Beishatun area, Miaoli / 苗栗白沙屯地區頭嵙山層之年代地層與沉積環境. *Annual Report of Central Geological Survey, MOEA. 1999 (Later half) - 2000*, 17-20.
- Lee, C.-S., 1990. The analyses of the contemporary issues of the stratigraphy in Taiwan / 臺灣地層問題剖析. *Special Publication of the Central Geological Survey, MOEA. / 經濟部中央地質調查所特刊* **4**, 27-48.
- Lee, C.-Y., Liew, P.-M., 2010. Late Quaternary vegetation and climate changes inferred from a pollen record of Dongyuan Lake in southern Taiwan. *Palaeogeography, Palaeoclimatology, Palaeoecology* **287**, 58-66.
- Lee, J.-F., 2000b. *Geological Map of Taiwan scale 1:50000 — Dongshi*. Central Geological Survey, Taipei.
- Lee, Y.-H., Chen, C.-C., Liu, T.-K., Ho, H.-C., Lu, H.-Y., Lo, W., 2006. Mountain building mechanism in the Southern Central Range of the Taiwan Orogenic Belt – From accretionary wedge deformation to arc-continental collision. *Earth and Planet Science Letters* **252**, 413-422.
- Liao, H.-R., Yu, H.-S., Su, C.-C., 2008. Morphology and sedimentation of sand bodies in the tidal shelf sea of eastern Taiwan Strait. *Marine Geology* **248**, 161-178.
- Liew, P.-M., Huang, S.-Y., Kuo, C.-M., 2006. Pollen stratigraphy, vegetation and environment of the last glacial and Holocene—A record from Toushe Basin, central Taiwan. *Quaternary International* **147**, 16-33.
- Liew, P.-M., Hsieh, M.-L., Shyu, B.H., 2004. An overview of coastal development in a Young Mountain Belt-Taiwan. *Quaternary International* **115-116**, 39-45.

- Liew, P.-M., Kuo, C.-M., Huang, S.-Y., Tseng, M.-H., 1998. Vegetation change and terrestrial carbon storage in eastern Asia during the Last Glacial Maximum as indicated by a new pollen record from central Taiwan. *Global and Planetary Change* **16-17**, 85-94.
- Liew, P.-M., Pirazzoli, P.A., Hsieh, M.-L., Arnold, M., Barousseau, J.P., Fontugne, M., Giresse, P., 1993. Holocene tectonic uplift deduced from elevated shorelines, eastern Coastal Range of Taiwan. *Tectonophysics* **222**, 55-68.
- Liew, P.M., Tseng, M.H., 1999. Climate Events from the Glacial to the Postglacial and Earth Surface Responses in Taiwan. *Science Reports of Tohoku University* **49**, 183-195.
- Lin, A.T., Watts, A.B., 2002. Origin of the West Taiwan basin by orogenic loading and flexure of a rifted continental margin. *Journal of Geophysical Research: Solid Earth* **107**, ETG 2-1-ETG 2-19.
- Lin, A.T., Watts, A.B., Hesselbo, S.P., 2003. Cenozoic stratigraphy and subsidence history of the South China Sea margin in the Taiwan region. *Basin Research* **15**, 453-478.
- Lin, C.-W., 2020. An Introduction to the Practicing Geologists of Taiwan and Their Geological Maps. *Taiwan Mining Industry* **72**, 25-40.
- Lin, C.C., 1957. *Geomorphology of Taiwan*. The Historical Research Commission of Taiwan Province, Taipei.
- Lin, C.C., 1963. The Lungkang Formation, lower marine terrace deposits near Miaoli. *Petroleum Geology of Taiwan* **2**, 87-105.
- Lin, C.C., 1969. Holocene Geology of Taiwan. *Acta Geologica Taiwanica* **13**, 83-126.
- Lin, C.C., Chou, J.T., 1974. *Geology of Taiwan*. The Historical Research Commission of Taiwan Province, Taichung.
- Lin, C.C., Chou, J.T., 1978. *Geology of Taiwan*. Maw Chang Book Co., Ltd., Taipei.
- Lin, C.Y., Wang, Z., Chen, W.N., Chang, S.Y., Chou, C.C.K., Sugimoto, N., Zhao, X., 2007. Long-range transport of Asian dust and air pollutants to Taiwan: observed evidence and model simulation. *Atmospheric Chemistry Physics* **7**, 423-434.
- Lisiecki, L.E., Raymo, M.E., 2005. A Pliocene-Pleistocene stack of 57 globally distributed benthic $\delta^{18}O$ records. *Paleoceanography* **20**, PA1003.
- Liu, T.-K., 1982. Tectonic implication of fission track ages from the Central Range, Taiwan. *Proceedings of the Geological Society of China* **25**, 22-37.
- Liu, J.P., Liu, C.S., Xu, K.H., Milliman, J.D., Chiu, J.K., Kao, S.J., Lin, S.W., 2008. Flux and fate of small mountainous rivers derived sediments into the Taiwan Strait. *Marine Geology* **256**, 65-76.
- Liu, J.P., Milliman, J.D., Gao, S., Cheng, P., 2004. Holocene development of the Yellow River's subaqueous delta, North Yellow Sea. *Marine Geology* **209**, 45-67.
- Liu, S.-H., Hebenstreit, R., Böse, M., 2021. The columnar sections and pictures of the outcrops in Miaoli Tableland. Refubium–Freie Universität Berlin Repository (accessed 31.1.2022). <https://doi.org/10.17169/refubium-31813>.
- Liu, S.-H., Lüthgens, C., Hardt, J., Hebenstreit, R., Böse, M., Frechen, M., 2023. Late Quaternary formation of the Miaoli Tableland in northwest Taiwan, an interplay of tectonic uplift and fluvial processes dated by OSL. *Quaternary Research* **112**, 128-149.
- Liu, S.-H., Hebenstreit, R., Böse, M., 2022. Late Quaternary landform evolution and sedimentary successions in the Miaoli Tableland, northwestern Taiwan. *E&G Quaternary Science Journal* **71**, 1-22.
- Liu, T.-C., Chu, C.-L., Chiang, H.-H., 2007. Agriculture and forestry / 農林志 in: Chen, Y.D. (Eds.), *Miaoli County Chronicles (Revised Edition) / 重修苗栗縣志*. Miaoli County Government, Miaoli.
- Liu, Z., Xia, D., Berne, S., Wang, K., Marsset, T., Tang, Y., Bourillet, J.F., 1998. Tidal deposition systems of China's continental shelf, with special reference to the eastern Bohai Sea. *Marine Geology* **145**, 225-253.
- Lüthgens, C., Ho, L.-D., Clemenz, N., Chen, J.-H., Jen, C.-H., Yen, J.-Y., Chyi, S.-J., 2018. The Holocene paleo-environmental history of the Gangkou River estuary, Hengchun Peninsula, Taiwan. *Terrestrial, Atmospheric and Oceanic Sciences* **29**, 547-576.
- Lundberg, N., Dorsey, R.J., 1990. Rapid Quaternary emergence, uplift, and denudation of the Coastal Range, Eastern Taiwan. *Geology* **18**, 638-641.
- Madsen, A.T., Murray, A.S., 2009. Optically stimulated luminescence dating of young sediments: A review. *Geomorphology* **109**, 3-16.
- Makiyama, T., 1934. *Hakusyatō Sheet, Explanatory text of the geological map of Taiwan (1: 50,000)*. Bureau of Productive Industries, Government-General of Taiwan, Tokyo.
- Makiyama, T., 1936. *Taiko Sheet*. Bureau of Productive Industries, Government-General of Taiwan, Tokyo.
- Makiyama, T., 1937. *The topographic and geological map of Tûsyô petroleum field*. Bureau of Productive Industries, Government-General of Taiwan, Tokyo.

- Mather, A.E., Stokes, M., Whitfield, E.**, 2017. River terraces and alluvial fans: The case for an integrated Quaternary fluvial archive. *Quaternary Science Reviews* **166**, 74-90.
- Matsu'ura, T., Kimura, H., Komatsubara, J., Goto, N., Yanagida, M., Ichikawa, K., Furusawa, A.**, 2014. Late Quaternary uplift rate inferred from marine terraces, Shimokita Peninsula, northeastern Japan: A preliminary investigation of the buried shoreline angle. *Geomorphology* **209**, 1-17.
- Mejdahl, V., Christiansen, H.H.**, 1994. Procedures used for luminescence dating of sediments. *Quaternary Science Reviews* **13**, 403-406.
- Miall, A.D.**, 2014. *Fluvial Depositional Systems*. Springer International Publishing, Switzerland.
- Muhs, D.R., Schweig, E.S., Simmons, K.R., Halley, R.B.**, 2017. Late Quaternary uplift along the North America-Caribbean plate boundary: Evidence from the sea level record of Guantanamo Bay, Cuba. *Quaternary Science Reviews* **178**, 54-76.
- Muhs, D.R., Simmons, K.R., Schumann, R.R., Groves, L.T., DeVogel, S.B., Minor, S.A., Laurel, D.**, 2014. Coastal tectonics on the eastern margin of the Pacific Rim: late Quaternary sea-level history and uplift rates, Channel Islands National Park, California, USA. *Quaternary Science Reviews* **105**, 209-238.
- Murphy, M.A., Salvador, A., Piller, W.E., Aubry, M.P.**, 1999. International stratigraphic guide—an abridged version. *International Subcommission on Stratigraphic Classification of IUGS International Commission on Stratigraphy Special Episodes* **22**, 255-272.
- Murray, A.S., Wintle, A.G.**, 2000. Luminescence dating of quartz using an improved single-aliquot regenerative-dose protocol. *Radiation Measurements* **32**, 57-73.
- Nagel, S., Granjeon, D., Willett, S., Lin, A.T.-S., Castelltort, S.**, 2018. Stratigraphic modeling of the Western Taiwan foreland basin: Sediment flux from a growing mountain range and tectonic implications. *Marine and Petroleum Geology* **96**, 331-347.
- NASA JPL**, 2013. 1 Arc Second scene N24 E120, NASA Shuttle Radar Topography Mission Global 1 arc second. NASA EOSDIS Land Processes DAAC (accessed 14.1.2022). <https://doi.org/10.5067/MEaSURES/SRTM/SRTMGL1.003>.
- National Land Surveying and Mapping Center**, 2016. Taiwan Map Service. National Land Surveying and Mapping Center, Taichung (accessed 14.1.2022). <https://wmts.nlsc.gov.tw/wmts>.
- Olariu, C., Steel, R.J., Dalrymple, R.W., Gingras, M.K.**, 2012. Tidal dunes versus tidal bars: The sedimentological and architectural characteristics of compound dunes in a tidal seaway, the lower Baronia Sandstone (Lower Eocene), Ager Basin, Spain. *Sedimentary Geology* **279**, 134-155.
- Ota, Y., Chen, Y.-G., Chen, W.-S.**, 2005. Review of paleoseismological and active fault studies in Taiwan in the light of the Chichi earthquake of September 21, 1999. *Tectonophysics* **408**, 63-77.
- Ota, Y., Lin, Y.-n.N., Chen, Y.-G., Chang, H.-C., Hung, J.-H.**, 2006. Newly found Tunglo Active Fault System in the fold and thrust belt in northwestern Taiwan deduced from deformed terraces and its tectonic significance. *Tectonophysics* **417**, 305-323.
- Ota, Y., Lin, Y.-N.N., Chen, Y.-G., Matsuta, N., Watanuki, T., Chen, Y.-W.**, 2009. Touhuanping Fault, an active wrench fault within fold-and-thrust belt in northwestern Taiwan, documented by spatial analysis of fluvial terraces. *Tectonophysics* **474**, 559-570.
- Ota, Y., Shyu, J.B., Chen, Y.-G., Hsieh, M.-L.**, 2002. Deformation and age of fluvial terraces south of the Choushui River, central Taiwan, and their tectonic implications. *Western Pacific Earth Sciences* **2**, 251-260.
- Ota, Y., Yamaguchi, M.**, 2004. Holocene coastal uplift in the western Pacific Rim in the context of late Quaternary uplift. *Quaternary International* **120**, 105-117.
- Owczarek, P.**, 2008. Hillslope deposits in gravel-bed rivers and their effects on the evolution of alluvial channel forms: A case study from the Sudetes and Carpathian Mountains. *Geomorphology* **98**, 111-125.
- Pelletier, B., Stephan, J.F.**, 1986. Middle Miocene deduction and late Miocene beginning of collision registered in the Hengchun peninsula: Geodynamic implications for the evolution of Taiwan. *Tectonophysics* **125**, 133-160.
- Peng, T.-H., Li, Y.-H., Wu, F.**, 1977. Tectonic uplift rates of the Taiwan island since the early Holocene. *Memoir of the Geological Society of Taiwan* **2**, 57-69.
- Pennington, B.T., Sturt, F., Wilson, P., Rowland, J., Brown, A.G.**, 2017. The fluvial evolution of the Holocene Nile Delta. *Quaternary Science Reviews* **170**, 212-231.
- Pickering, J.L., Goodbred, S.L., Reitz, M.D., Hartzog, T.R., Mondal, D.R., Hossain, M.S.**, 2014. Late Quaternary sedimentary record and Holocene channel avulsions of the Jamuna and Old Brahmaputra River valleys in the upper Bengal delta plain. *Geomorphology* **227**, 123-136.
- Pierik, H.J., Cohen, K.M., Stouthamer, E.**, 2016. A new GIS approach for reconstructing and mapping dynamic late Holocene coastal plain palaeogeography. *Geomorphology* **270**, 55-70.

- Prescott, J.R., Hutton, J.T.**, 1994. Cosmic ray contributions to dose rates for luminescence and ESR dating: Large depths and long-term time variations. *Radiation Measurements* **23**, 497-500.
- Prescott, J.R., Stephan, L.G.**, 1982. The contribution of cosmic radiation to the environmental dose for thermoluminescence dating. Latitude, altitude and depth dependences. *Pact: Journal of the European Study Group on Physical, Chemical and Mathematical Techniques Applied to Archeology* **6**, 17-25.
- Pye, K., Zhou, L.-P.**, 1989. Late Pleistocene and Holocene aeolian dust deposition in North China and the Northwest Pacific Ocean. *Palaeogeography, Palaeoclimatology, Palaeoecology* **73**, 11-23.
- Rabineau, M., Berné, S., Olivet, J.L., Aslanian, D., Guillocheau, F., Joseph, P.**, 2006. Paleo sea levels reconsidered from direct observation of paleoshoreline position during Glacial Maxima (for the last 500,000 yr). *Earth and Planetary Science Letters* **252**, 119-137.
- Rees-Jones, J.**, 1995. Optical dating of young sediments using fine-grain quartz. *Ancient TL* **13**, 9-14.
- Reimann, T., Thomsen, K.J., Jain, M., Murray, A.S., Frechen, M.**, 2012. Single-grain dating of young sediments using the pIRIR signal from feldspar. *Quaternary Geochronology* **11**, 28-41.
- Reineck, H.E.**, 1986. *Depositional sedimentary environments: with reference to terrigenous clastics, 2., rev. and updated ed. corr. 2. print.* ed. Springer, Berlin u.a.
- Rhodes, E.J.**, 2011. Optically Stimulated Luminescence Dating of Sediments over the Past 200,000 Years. *Annual Review of Earth and Planetary Sciences* **39**, 461-488.
- Rixhon, G., Briant, R.M., Cordier, S., Duval, M., Jones, A., Scholz, D.**, 2017. Revealing the pace of river landscape evolution during the Quaternary: recent developments in numerical dating methods. *Quaternary Science Reviews* **166**, 91-113.
- Robustelli, G., Ermolli, E.R., Petrosino, P., Jicha, B., Sardella, R., Donato, P.**, 2014. Tectonic and climatic control on geomorphological and sedimentary evolution of the Mercure basin, southern Apennines, Italy. *Geomorphology* **214**, 423-435.
- Roigé, M., Gómez-Gras, D., Remacha, E., Boya, S., Viaplana-Muzas, M., Teixell, A.**, 2017. Recycling an uplifted early foreland basin fill: An example from the Jaca basin (Southern Pyrenees, Spain). *Sedimentary Geology* **360**, 1-21.
- Saito, K., Oguchi, T.**, 2005. Slope of alluvial fans in humid regions of Japan, Taiwan and the Philippines. *Geomorphology* **70**, 147-162.
- Salvador, A.**, 1994. *International stratigraphic guide: a guide to stratigraphic classification, terminology, and procedure, 2. ed.* International Subcommittee on Stratigraphic Classification of IUGS International Commission on Stratigraphy and The Geological Society of America, Boulder, Colorado.
- Satellite Survey Center**, 2018. Ministry of Interior 20m raster digital elevation model. Satellite Survey Center, Taipei (accessed 17.9.2022). <https://data.gov.tw/dataset/35430>.
- Schmidt, S., Tsukamoto, S., Salomon, E., Frechen, M., Hetzel, R.**, 2012. Optical dating of alluvial deposits at the orogenic front of the andean precordillera (Mendoza, Argentina). *Geochronometria* **39**, 62-75.
- Shackleton, N.J.**, 2000. The 100,000-Year Ice-Age Cycle Identified and Found to Lag Temperature, Carbon Dioxide, and Orbital Eccentricity. *Science* **289**, 1897-1902.
- Shih, T.-T., Yang, G.-S.**, 1985. The Active Faults and Geomorphic Surfaces of Pakua Tableland in Taiwan. *Geographical Research* **11**, 173-186.
- Shih, T.S., Sato, H., Ikeya, M., Liew, P.M., Chien, S.H.**, 2002. Conditions and New Extrapolation Method for ESR Dating of Aragonitic Mollusk Shells in Taiwan. *Advances in ESR Applications* **18**, 31-39.
- Shyu, J.B.H., Sieh, K., Avouac, J.-P., Chen, W.-S., Chen, Y.-G.**, 2006. Millennial slip rate of the Longitudinal Valley fault from river terraces: Implications for convergence across the active suture of eastern Taiwan. *Journal of Geophysical Research* **111**, B08403.
- Shyu, J.B.H., Sieh, K., Chen, Y.-G., Liu, C.-S.**, 2005. Neotectonic architecture of Taiwan and its implications for future large earthquakes. *Journal of Geophysical Research* **110**, B08402.
- Siame, L., Chu, H.T., Carcaillet, J., Bourlès, D., Braucher, R., Lu, W.C., Angelier, J., Dussouliéz, P.**, 2007. Glacial retreat history of Nanhuta Shan (north-east Taiwan) from preserved glacial features: the cosmic ray exposure perspective. *Quaternary Science Reviews* **26**, 2185-2200.
- Siame, L.L., Chen, R.-F., Derrieux, F., Lee, J.-C., Chang, K.-J., Bourlès, D.L., Braucher, R., Léanni, L., Kang, C.-C., Chang, C.-P., Chu, H.-T.**, 2012. Pleistocene alluvial deposits dating along frontal thrust of Changhua Fault in western Taiwan: The cosmic ray exposure point of view. *Journal of Asian Earth Sciences* **51**, 1-20.
- Simoës, M., Avouac, J.P.**, 2006. Investigating the kinematics of mountain building in Taiwan from the spatiotemporal evolution of the foreland basin and western foothills. *Journal of Geophysical Research* **111**, B10401.

- Simoës, M., Avouac, J.P., Chen, Y.-G., Singhvi, A.K., Wang, C.-Y., Jaiswal, M., Chan, Y.-C., Bernard, S.**, 2007. Kinematic analysis of the Pakuashan fault tip fold, west central Taiwan: Shortening rate and age of folding inception. *Journal of Geophysical Research: Solid Earth* **112**, B03814.
- Singarayer, J.S., Bailey, R.M.**, 2003. Further investigations of the quartz optically stimulated luminescence components using linear modulation. *Radiation Measurements* **37**, 451-458.
- Singarayer, J.S., Bailey, R.M., Rhodes, E.J.**, 2000. Potential of the slow component of quartz OSL for age determination of sedimentary samples. *Radiation Measurements* **32**, 873-880.
- Sivia, D., Burbidge, C., Roberts, R., Bailey, R.**, 2004. A Bayesian Approach to the Evaluation of Equivalent Doses in Sediment Mixtures for Luminescence Dating. *American Institute of Physics Conference Proceedings* **735**, 305-311.
- Song, S.-R., Liu, C.-M., Chen, C.-H., Lo, W.**, 2004. Pumice layers in marine terraces: Implications for tectonic uplift rates on the east and northeast coasts of Taiwan over the last hundreds of years. *Quaternary International* **115-116**, 83-92.
- Spooner, N.A.**, 1994. The anomalous fading of infrared-stimulated luminescence from feldspars. *Radiation Measurements* **23**, 625-632.
- Stokes, S., Bray, H.E., Blum, M.D.**, 2001. Optical resetting in large drainage basins: tests of zeroing assumptions using single-aliquot procedures. *Quaternary Science Reviews* **20**, 879-885.
- Su, M.-H.**, 2007. Fishery and husbandry / 漁牧志 in: Chen, Y.D. (Eds.), *Miaoli County Chronicles (Revised Edition) / 重修苗栗縣志*. Miaoli County Government, Miaoli.
- Su, S.-H., Kuo, H.-C., Hsu, L.-H., Yang, Y.-T.**, 2012. Temporal and Spatial Characteristics of Typhoon Extreme Rainfall in Taiwan. *Journal of the Meteorological Society of Japan* **90**, 721-736.
- Suppe, J.**, 1980a. Imbricated structure of Western Foothills belt, southcentral Taiwan. *Petroleum Geology of Taiwan* **17**, 1-16.
- Suppe, J.**, 1980b. A retrodeformable cross section of northern Taiwan. *Proceedings of the Geological Society of China* **23**, 46-55.
- Suppe, J.**, 1981. Mechanics of mountain building and metamorphism in Taiwan. *Memoir of the Geological Society of China* **4**, 67-89.
- Suppe, J.**, 1984. Kinematics of arc-continent collision, flipping of subduction, and back-arc spreading near Taiwan. *Memoir of the Geological Society of China* **6**, 131-146.
- Taiwan Agricultural Research Institute**, 2016. Soil Storage Supply System. Taiwan Agricultural Research Institute, Taichung (accessed 14.1.2022). <https://tssurgo.tari.gov.tw/Tssurgo/>.
- Tanabe, S., Hori, K., Saito, Y., Haruyama, S., Vu, V.P., Kitamura, A.**, 2003. Song Hong (Red River) delta evolution related to millennium-scale Holocene sea-level changes. *Quaternary Science Reviews* **22**, 2345-2361.
- Teng, K.-H.**, 1979. A Quantitative Study on the Landforms of Lateritic Gravel Tablelands in Northwestern Taiwan. *The College of Chinese Culture Institute of Geography Science Reports* **3**, 113-186.
- Teng, L.S.**, 1992. Geotectonic evolution of Tertiary continental margin basins of Taiwan. *Petroleum Geology of Taiwan* **27**, 1-19.
- Teng, L.S.**, 1990. Geotectonic evolution of late Cenozoic arc-continent collision in Taiwan. *Tectonophysics* **183**, 57-76.
- Teng, L.S.**, 1996a. Extensional collapse of the northern Taiwan mountain belt. *Geology* **24**, 949-952.
- Teng, L.S.**, 1996b. Geological background of the gravel formations of Taiwan. *Sine-Geotechnics* **55**, 5-24.
- Teng, L.S., Lee, C., Peng, C.-H., Chen, W.-F., Chu, C.-J.**, 2001. Origin and geological evolution of the Taipei basin, northern Taiwan. *Western Pacific Earth Sciences* **1**, 115-142.
- The General Bathymetric Chart of the Oceans**, 2022. Imagery reproduced from the GEBCO_2022 Grid, GEBCO Compilation Group (accessed 20. 12. 2022). https://www.gebco.net/data_and_products/gebco_web_services/web_map_service/mapserv?
- The Taiwan Provincial Weather Institution**, 1959. *Report on Floods of 7th August, 1959*. The Taiwan Provincial Weather Institution, Taipei.
- Thornbury, W.D.**, 1954. Principles of Geomorphology. *Soil Science* **78**, 157.
- Timar-Gabor, A., Wintle, A.G.**, 2013. On natural and laboratory generated dose response curves for quartz of different grain sizes from Romanian loess. *Quaternary Geochronology* **18**, 34-40.
- Tomita, Y.**, 1940. Terraces in Taiwan / 臺灣の段丘に就いて. *Journal of the Taiwan museum association / 科學の臺灣* **8**, 1-6.
- Tomita, Y.**, 1951. On the geomorphological classification of fans in Taiwan (Formosa) / 台灣に於ける扇狀地の地形的分類について. *Journal of Geography (Chigaku Zasshi)* **60**, 2-9.

- Tomita, Y.**, 1953. The classification of fluvial terraces / 河成段丘の分類に就いて. *Annals of The Tohoku Geographical Association* **6**, 1-6.
- Tomita, Y.**, 1954. Surface Geology and Correlation of River Terraces. *Annals of The Tohoku Geographical Association* **6**, 51-58.
- Tomita, Y.**, 1972. *Study of the geomorphology of Taiwan*, Kokon Shoin / 古今書院, Tokyo.
- Torii, K.**, 1935. *Tosei Sheet, Explanatory text of the geological map of Taiwan (1: 50,000)*. Bureau of Productive Industries, Government-General of Taiwan, Tokyo.
- Tsai, H., Chen, J.-H., Huang, W.-S., Huang, S.-T., Hseu, Z.-Y., You, C.-F.**, 2021. Aeolian additions of podzolic soils on the high-altitude mountains in central Taiwan-sediment origin and pedological implications. *Geoderma* **383**, 114726.
- Tsai, H., Hseu, Z.-Y., Huang, S.-T., Huang, W.-S., Chen, Z.-S.**, 2010. Pedogenic properties of surface deposits used as evidence for the type of landform formation of the Tadu tableland in central Taiwan. *Geomorphology* **114**, 590-600.
- Tsai, H., Huang, W.-S., Hseu, Z.-Y., Chen, Z.-S.**, 2006. A River Terrace Soil Chronosequence of the Pakua Tableland in Central Taiwan. *Soil Science* **171**, 167-179.
- Tsai, H., Maejima, Y., Hseu, Z.-Y.**, 2008. Meteoric ¹⁰Be dating of highly weathered soils from fluvial terraces in Taiwan. *Quaternary International* **188**, 185-196.
- Tseng, C.-H., Lüthgens, C., Tsukamoto, S., Reimann, T., Frechen, M., Böse, M.**, 2016. Late Pleistocene to Holocene alluvial tableland formation in an intra-mountainous basin in a tectonically active mountain belt — A case study in the Puli Basin, central Taiwan. *Quaternary Science Reviews* **132**, 26-39.
- Tseng, C.-H., Wenske, D., Böse, M., Reimann, T., Lüthgens, C., Frechen, M.**, 2013. Sedimentary features and ages of fluvial terraces and their implications for geomorphic evolution of the Taomi River catchment: A case study in the Puli Basin, central Taiwan. *Journal of Asian Earth Sciences* **62**, 759-768.
- Tseng, C.-L.**, 1990. GPS navigation and positioning. *Photogrammetry and Remote Sensing* **12**, 37-71.
- Tu, C.-M.**, 2007. The Hakka society/ 住民志(上冊): 客家族群篇 in: Chen, Y.D. (Eds.), *Miaoli County Chronicles (Revised Edition) / 重修苗栗縣志*. Miaoli County Government, Miaoli.
- Tu, J.-Y., Chen, J.-M.**, 2019. Large-scale indices for assessing typhoon activity around Taiwan. *International Journal of Climatology* **39**, 921-933.
- Tu, J.-Y., Chou, C.**, 2013. Changes in precipitation frequency and intensity in the vicinity of Taiwan: typhoon versus non-typhoon events. *Environmental Research Letters* **8**, 014023.
- Twidale, C.R.**, 2004. River patterns and their meaning. *Earth-Science Reviews* **67**, 159-218.
- United States Department of Agriculture**, 1999. *Soil taxonomy: A basic system of soil classification for making and interpreting soil surveys*. United States Department of Agriculture Natural Resources Conservation Service, Washington DC.
- Vail, P.R., Audemadede, F., Bowman, S.A., Eisner, P.N., Perez-Cruz, C.**, 1991. The stratigraphic signatures of tectonics, eustacy and sedimentology - an overview, in: Einsele, G., Ricken, W., Seilacher, A. (Eds.), *Cycles and Events in Stratigraphy*. Springer-Verlag, Berlin, pp. 617-659.
- Volker, H.X., Wasklewicz, T.A., Ellis, M.A.**, 2007. A topographic fingerprint to distinguish alluvial fan formative processes. *Geomorphology* **88**, 34-45.
- Waelbroeck, C., Labeyrie, L., Michel, E., Duplessy, J.C., McManus, J.F., Lambeck, K., Balbon, E., Labracherie, M.**, 2002. Sea-level and deep water temperature changes derived from benthic foraminifera isotopic records. *Quaternary Science Reviews* **21**, 295-305.
- Wang, C.-H., Burnett, W.C.**, 1990. Holocene mean uplift rates across an active plate collision boundary in Taiwan. *Bulletin Institute of Earth Sciences, Academia Sinica* **10**, 40.
- Wang, C.-H., Peng, T.-R.**, 1990. Oxygen and carbon isotopic records of mollusks in the Kuokang Shell Bed, Taiwan: implications and applications. *Palaeogeography, Palaeoclimatology, Palaeoecology* **80**, 237-244.
- Wang, Y.H., Jan, S., Wang, D.P.**, 2003. Transports and tidal current estimates in the Taiwan Strait from shipboard ADCP observations (1999–2001). *Estuarine, Coastal and Shelf Science* **57**, 193-199.
- Wenske, D., Böse, M., Frechen, M., Lüthgens, C.**, 2011. Late Holocene mobilisation of loess-like sediments in Hohuan Shan, high mountains of Taiwan. *Quaternary International* **234**, 174-181.
- Wenske, D., Frechen, M., Böse, M., Reimann, T., Tseng, C.-H., Hoelzmann, P.**, 2012. Late Quaternary river terraces in the Central Mountain Range of Taiwan: A study of cover sediments across a terrace section along the Tachia River. *Quaternary International* **263**, 26-36.

- White, J.Q., Pasternack, G.B., Moir, H.J.**, 2010. Valley width variation influences riffle–pool location and persistence on a rapidly incising gravel-bed river. *Geomorphology* **121**, 206-221.
- Whitfield, R.G., Macklin, M.G., Brewer, P.A., Lang, A., Mauz, B., Whitfield, E.**, 2013. The nature, timing and controls of the Quaternary development of the Rio Bergantes, Ebro basin, northeast Spain. *Geomorphology* **196**, 106-121.
- Willemin, J.H., Knuepfer, P.L.K.**, 1994. Kinematics of arc-continent collision in the eastern Central Range of Taiwan inferred from geomorphic analysis. *Journal of Geophysical Research: Solid Earth* **99**, 20267-20280.
- Wintle, A.G.**, 1973. Anomalous Fading of Thermo-luminescence in Mineral Samples. *Nature* **245**, 143-144.
- Wintle, A.G., Murray, A.S.**, 2006. A review of quartz optically stimulated luminescence characteristics and their relevance in single-aliquot regeneration dating protocols. *Radiation Measurements* **41**, 369-391.
- Wu, T.-S., Jaiswal, M.K., Lin, Y.N., Chen, Y.-W., Chen, Y.-G.**, 2010. Residual luminescence in modern debris flow deposits from western Taiwan: A single grain approach. *Journal of Asian Earth Sciences* **38**, 274-282.
- Yamaguchi, M., Ota, Y.**, 2004. Tectonic interpretations of Holocene marine terraces, east coast of Coastal Range, Taiwan. *Quaternary International* **115-116**, 71-81.
- Yang, K.-M., Huang, S.-T., Jong-Chang, W., Ting, H.-H., Wen-Wei, M., Lee, M., Hsu, H.-H., Lee, C.-J.**, 2007. 3D geometry of the Chelungpu thrust system in central Taiwan: Its implications for active tectonics. *Terrestrial, Atmospheric Oceanic Sciences* **18**, 143.
- Yang, K.-M., Huang, S.-T., Wu, J.-C., Ting, H.-H., Mei, W.-W.**, 2006. Review and New Insights on Foreland Tectonics in Western Taiwan. *International Geology Review* **48**, 910-941.
- Yang, K.-M., Rau, R.-J., Chang, H.-Y., Hsieh, C.-Y., Ting, H.-H., Huang, S.-T., Wu, J.-C., Tang, Y.-J.**, 2016. The role of basement-involved normal faults in the recent tectonics of western Taiwan. *Geological Magazine* **153**, 1166-1191.
- Yang, R.J., Liu, J.T., Fan, D., Burr, G.S., Lin, H.-L., Chen, T.-T.**, 2017. Land-sea duel in the late Quaternary at the mouth of a small river with high sediment yield. *Journal of Asian Earth Sciences* **143**, 59-76.
- Yen, T.P., Ho, C.-S., Chen, P.Y.**, 1947. *Bibliography of Geology of Taiwan / 臺灣地質文獻目錄*. Geological Survey, Taiwan Province, Taipei, Republic of China.
- Yokomitsu, Y., Ichikawa, Y., Takahashi, H., Hamamoto, K., Asahi, T.**, 1926. *Map of the Geological Formation and Mineral Distribution of Taiwan*. Bureau of Productive Industries, Government-General of Taiwan, Tokyo.
- Yu, H.-S., Chou, Y.-W.**, 2001. Characteristics and development of the flexural forebulge and basal unconformity of Western Taiwan Foreland Basin. *Tectonophysics* **333**, 277-291.
- Yu, H.-S., Song, G.S.**, 2000. Submarine physiographic features in Taiwan region and their geological significance. *Journal of the Geological Society of China* **43**, 267-286.
- Yu, N.-T., Teng, L.S., Chen, W.-S., Yue, L.-F., Chen, M.-M.**, 2013. Early post-rift sequence stratigraphy of a Mid-Tertiary rift basin in Taiwan: Insights into a siliciclastic fill-up wedge. *Sedimentary Geology* **286-287**, 39-57.
- Yuan, B.D., Lin, A.T.**, 2009. The introduction of the draft for Taiwan Stratigraphic Code / 簡介『中華民國地層命名原則』草案. *Special Publication of the Central Geological Survey, MOEA. / 經濟部中央地質調查所特刊* **22**, 1-11.
- Yue, L.-F., Suppe, J., Hung, J.-H.**, 2005. Structural geology of a classic thrust belt earthquake: the 1999 Chi-Chi earthquake Taiwan (Mw=7.6). *Journal of Structural Geology* **27**, 2058-2083.

Appendix 1: Academic publications and conference contributions

Academic publications

- (1) Kashiwaya, K., **Liu, S.-H.**, Ochiai, S., Lin, J.-C., Hydro-geomorphological changes in an artificial modified lake-catchment system inferred from lacustrine sediments of Ri-Yue Tan (Sun Moon Lake), central Taiwan. (In preparation).
- (2) **Liu, S.-H.**, Lüthgens, C., Hardt, J., Hebenstreit, R., Böse, M., Frechen, M., 2023. Late Quaternary formation of the Miaoli Tableland in northwest Taiwan, an interplay of tectonic uplift and fluvial processes dated by OSL. *Quaternary Research* 112, 128-149.
- (3) **Liu, S.-H.**, Hebenstreit, R., Böse, M., 2022. Late Quaternary landform evolution and sedimentary successions in the Miaoli Tableland, northwestern Taiwan. *E&G Quaternary Science Journal* 71, 1-22.
- (4) **Liu, S.-H.**, Hebenstreit, R., Böse, M., 2021. Late Quaternary landforms and sedimentary succession in the Miaoli Tableland, Northwestern Taiwan. *Refubium–Freie Universität Berlin Repository*. <https://doi.org/10.17169/refubium-31813>.
- (5) Shen, C.-W., **Liu, S.-H.**, Chen, Y.-C., Chiu, Y.-J., Liu, K.-F., 2016. Budget of Landslide-Induced Sediment for the Watersheds in Taiwan– A Case Study in Pre- and Post- Typhoon Morakot Periods, *Journal of Taiwan Agriculture Engineering*, 62(3), 23-42.
- (6) **Liu, S.-H.**, 2013. Sediment characteristic analysis and discussion of environmental change since 16 ka - a case study at Sun-Moon Lake, Taiwan, Diploma Thesis, National Taiwan University, 132pp.

Conference contributions

- (1) **Liu, S.-H.**, Tseng, C.-H., Li, Y., Hebenstreit, R., Böse, M., Frechen, M., 2019. Morphological and geochronological investigations in the Miaoli Tablelands (NW Taiwan). *International Union for Quaternary Research (INQUA) Congress 2019, Dublin, Ireland, 25-31. July. Poster presentation.*
- (2) **Liu, S.-H.**, Li, Y., Hebenstreit, R., Böse, M., Tseng, C.-H., Frechen, M., 2018. Landforms and sedimentary archives of late Quaternary processes in the Miaoli Tablelands, Northwestern Taiwan. *The 5th Asia Pacific Conference on Luminescence and Electron Spin Resonance Dating, Beijing, China, 15-17. October 2018. Oral presentation.*
- (3) **Liu, S.-H.**, Hebenstreit, R., Frechen, M., Tseng, C.-H., Böse, M., 2018. Late Quaternary sedimentary archives and landforms in the Miaoli Tablelands, Northwestern Taiwan. *Central European Conference on Geomorphology and Quaternary Sciences, Giessen, Germany, 23-27. September 2018. Poster presentation.*
- (4) **Liu, S.-H.**, Hebenstreit, R., Frechen, M., Tseng, C.-H., Böse, M., 2017. Landforms and sedimentary archives of late Quaternary processes in the Miaoli Tablelands, Northwestern Taiwan. *European Geosciences Union General Assembly 2018, Vienna, Austria, 8-13. April 2018. Poster presentation.*
- (5) **Liu, S.-H.**, Frechen, M., Hebenstreit, R., Böse, M., 2017. Revising the definition of Quaternary strata in Taiwan, application of a stratigraphical and geochronological approach in the Miaoli Tablelands. *German Conference on Luminescence and Electron Spin Resonance Dating 2017, Schney/Bayreuth, Germany, 27-29. October 2017. Poster presentation.*

Appendix 2: Curriculum Vitae

Shih-Hung Liu

SUMMARY

- Highly motivated **PhD candidate of Geography**, with extensive experiences in designing new models and protocols for managing data and quantitative analyses including conceptual modelling, remote sensing data analyses (raster and vector data), field sensor network design, and landform mapping.
- **Enthusiasm** for GIS (ArcGIS, QGIS) applications, seeking opportunities for environmental engineering, investigation of resources and natural hazard risk assessment in endangered environments.
- Good knowledges of **the historical/geographical background** of Taiwan, Germany (Berlin/Brandenburg), Japan, and China.
- Focusing on the **contemporary geopolitical confrontations** (Corona Pandemic, Russian-Ukrainian War, Energy Crisis) through multi-language data source.

TECHNICAL SKILLS

- Software skills: ArcGIS/QGIS/Adobe Illustrator/Hec-HMS/ERDAS Imagine/R-Studio
- Field and laboratory skills: concise and high-quality field observations planning/ RTK (Real-Time Kinetic Positioning) survey/ ground LiDAR scanning/ ground truth assessments/ ADCP/ weather station and hydrological sensor network design and setup/ laboratory protocol related to luminescence dating and sedimentological analyses
- Languages: Traditional/Simplified Chinese (native), English (proficient), German (intermediate), Japanese (basic).

PROFESSIONAL EXPERIENCE

PhD Candidate @ Freie Universität Berlin, Berlin, Germany

Feb 2017 – Dec 2023

- Independent PhD candidate.
- Invented a specialized mathematical method for concise and high precision geographical mapping to improve the traditional hand mapping and user defined categorization method.
- Invented a new protocol for using huge amounts of borehole data to analyze the landforms and surface processes in 3D.
- Acquired excellent data searching routines for the literatures databases in different countries.
- Extensive experiences in organizing field works, including all the administrative documentary procedures with the local government and connections to the local societies.
- Managed high efficiency workflow of laboratory analyses and completed all the scheduled works under limited lab capacity.

Environmental Engineer (Research Assistant) @ Hydrotech Research Institute, NTU, Taipei, Taiwan

Sep 2014 – Jan 2017

- Managed the research projects for calculation of the 10 years' annual sediment yields, by massive degree raster and vector data analyses of debris production from ca. 32k landslides in more than 100 river catchments of the whole Taiwan island.
- Organized and conducted more than 20 field investigations and the designing of hydrological sensor networks for the water resources with extended potential risk assessments of a reservoir construction project of the Taiwanese Government.
- Established the high precision land use mapping for modelling of the discharge of urban planning projects with Low Impact Development application in the metropolitans and investigated a relevant urban planning case study overseas.
- Managed and participated the quantitative hazard risk assessments for flooding and debris flows, including 3 sites ground LiDAR/UAV surveying of landslides and 2 sites sonar surveying for monitoring capacity changes of fluvial channels.
- Organized 2 workshops for technology transferring of GIS-applications with the government sections of forestry managements, including editing of the technical manual, the teaching materials and the protocols for verification.

Visiting Researcher @ Kanazawa University, Kanazawa, Japan

Mar 2012 – May 2012

- Participated the international research group (organized by 6 countries) of the eastern Asian environmental change models.
- Working independently with the international fellowships overseas.
- Conducted sedimentological analyses and dating (Cs137 and Pb210) analyses with excellent outcomes and translated 2 analyses protocols from English/Japanese to Chinese for the succeeding research projects.
- Joined the activities of local research group for field observations of the natural and cultural landscape conservation projects.

EDUCATION

Freie Universität Berlin @ Berlin, Germany

PhD in Natural Sciences (Dr. rer. nat.)

Feb 2017 – Dec 2023

National Taiwan University @ Taipei, Taiwan

Master of Science in Geography (Physical Geography)

Sep 2011 – Jul 2013

Bachelor of Science in Geography

Sep 2007 – Jul 2011

Appendix 3: Eidesstattliche Erklärung

Eidesstattliche Erklärung

Hiermit erkläre ich, dass ich die vorgelegte Arbeit selbständig verfasst habe und alle in der Arbeit verwendeten Quellen und Hilfsmittel vollständig angegeben sind. Die Beiträge der Mitautoren der wissenschaftlichen Veröffentlichungen und die technische Unterstützung durch andere Mitarbeiter werden in den Danksagungen anerkannt.

Ich erkläre, dass diese Arbeit erstmals und ausschließlich am Fachbereich Geowissenschaften der Freien Universität Berlin angefertigt wurde und ich keinen entsprechenden Doktorgrad an einer anderen Fakultät oder Universität besitze. Der Inhalt der Promotionsordnung ist mir bekannt.

Berlin, 10. 8. 2023

Shih-Hung Liu

Appendix 4: AI-assisted language check disclaimer

I hereby declare that, during the final revision stage of this dissertation, artificial intelligence (AI) tools were introduced to check the language and grammatic proficiencies of its contents.

The tasks conducted by the AI include:

1. Verifying the usage of articles with specific nouns.
2. Confirming the appropriate use of prepositions for clarity of context.
3. Checking the consistency of verb tenses for coherent interpretations.

No AI generated contents, including data, texts, and figures, have been included in this dissertation.

Berlin, 10.3.2024

Shih-Hung Liu